



**HELLENIC REPUBLIC
UNIVERSITY OF IOANNINA
SCHOOL OF ENGINEERING
DEPARTMENT OF MATERIALS SCIENCE
AND ENGINEERING**

**Study of the Graphitic Reinforcement of Hierarchical
Epoxy Matrix Composites**

TSIRKA KIRIAKI
MATERIALS SCIENCE ENGINEER

Thesis for the degree of Doctor of Philosophy

IOANNINA 2019



**ΕΛΛΗΝΙΚΗ ΔΗΜΟΚΡΑΤΙΑ
ΠΑΝΕΠΙΣΤΗΜΙΟ ΙΩΑΝΝΙΝΩΝ
ΠΟΛΥΤΕΧΝΙΚΗ ΣΧΟΛΗ
ΤΜΗΜΑ ΜΗΧΑΝΙΚΩΝ ΕΠΙΣΤΗΜΗΣ ΥΛΙΚΩΝ**

**Μελέτη Γραφικής Ενίσχυσης Ιεραρχικών Σύνθετων Υλικών
με Μήτρα Εποξειδικής Ρητίνης**

**ΤΣΙΡΚΑ ΚΥΡΙΑΚΗ
ΜΗΧΑΝΙΚΟΣ ΕΠΙΣΤΗΜΗΣ ΥΛΙΚΩΝ**

ΔΙΔΑΚΤΟΡΙΚΗ ΔΙΑΤΡΙΒΗ

ΙΩΑΝΝΙΝΑ 2019

Η έγκριση της διδακτορικής διατριβής από το Τμήμα Μηχανικών Επιστήμης Υλικών της Πολυτεχνικής Σχολής του Πανεπιστημίου Ιωαννίνων δεν υποδηλώνει αποδοχή των γνωμών του συγγραφέα Ν. 5343/32, άρθρο 202, παράγραφος 2».

Application date of Ms. Kiriaki Tsirka: 02.11.2012

Appointment date for the three-membered advisory committee: 20.12.2012 & 16.01.2014

Members of the three-membered advisory committee:

Supervisor

Alkiviadis S. Paipetis, Professor at the Dept. of Materials Science and Engineering, School of Engineering, University of Ioannina

Members

Dimitris Gournis, Professor at the Dept. of Materials Science and Engineering, School of Engineering, University of Ioannina

George Papanicolaou, Emeriti Professor at the Department of Mechanical Engineering and Aeronautics School of Engineering, University of Patras

Subject appointment date: 20.12.2012

“Study of the graphitic reinforcement of hierarchical epoxy matrix composites”

Appointment date for the seven-membered advisory committee: 23.01.2019

1. **Alkiviadis S. Paipetis**, Professor at the Dept. of Materials Science and Engineering, School of Engineering, University of Ioannina,
2. **Dimitris Gournis**, Professor at the Dept. of Materials Science and Engineering, School of Engineering, University of Ioannina,
3. **George Papanicolaou**, Emeritus Professor at the Department of Mechanical Engineering and Aeronautics School of Engineering, National Technical University of Athens,
4. **Michael Karakassides**, Professor at the Dept. of Materials Science and Engineering, School of Engineering, University of Ioannina,
5. **Konstantinos Beltsios**, Professor at the Dept. of Materials Science and Engineering, School of Engineering, University of Ioannina,
6. **Pagona Papakonstantinou**, Professor of Advanced Materials, School of Engineering, Engineering Research Institute, University of Ulster,
7. **Nektaria-Marianthi Barkoula**, Associate Professor at the Dept. of Materials Science and Engineering, School of Engineering, University of Ioannina.

The Ph.D. thesis was awarded with grade “EXCELENT” at 06.03.2019.

The Head of the Department

The Secretary of the Department

Alkiviadis Paipetis

Maria Kontou

Ημερομηνία αίτησης της κ. Κυριακής Τσίρκα: 02.11.2012

Ημερομηνία ορισμού Τριμελούς Συμβουλευτικής Επιτροπής: 20.12.2012 & 16.01.2014

Μέλη Τριμελούς Συμβουλευτικής Επιτροπής:

Επιβλέπων

Αλκιβιάδης Παϊπέτης, Καθηγητής του Τμήματος Μηχανικών Επιστήμης Υλικών, της Πολυτεχνικής Σχολής του Πανεπιστημίου Ιωαννίνων

Μέλη

Δημήτρης Γουρνής, Καθηγητής του Τμήματος Μηχανικών Επιστήμης Υλικών, της Πολυτεχνικής Σχολής του Πανεπιστημίου Ιωαννίνων

Γιώργος Παπανικολάου, Καθηγητής του Τμήματος Μηχανολόγων και Αεροναυπηγών Μηχανικών, της Πολυτεχνικής Σχολής του Πανεπιστημίου Πατρών

Ημερομηνία ορισμού θέματος: 20.12.2012

"Μελέτη Γραφικής Ενίσχυσης Ιεραρχικών Σύνθετων Υλικών Με Μήτρα Εποξειδικής Ρητίνης"

Ημερομηνία διορισμού επταμελούς εξεταστικής επιτροπής: 23.01.2019

- 1. Αλκιβιάδης Παϊπέτης**, Καθηγητής του Τμήματος Μηχανικών Επιστήμης Υλικών, της Πολυτεχνικής Σχολής του Πανεπιστημίου Ιωαννίνων,
- 2. Δημήτριος Γουρνής**, Καθηγητής του Τμήματος Μηχανικών Επιστήμης Υλικών, της Πολυτεχνικής Σχολής του Πανεπιστημίου Ιωαννίνων,
- 3. Γεώργιος Παπανικολάου**, Ομότιμος Καθηγητής του Τμήματος Μηχανολόγων και Αεροναυπηγών Μηχανικών, της Πολυτεχνικής Σχολής του Πανεπιστημίου Πατρών,
- 4. Μιχαήλ Καρακασίδης**, Καθηγητής του Τμήματος Μηχανικών Επιστήμης Υλικών, της Πολυτεχνικής Σχολής του Πανεπιστημίου Ιωαννίνων,
- 5. Κωνσταντίνος Μπέλτσιος**, Καθηγητής του Τμήματος Μηχανικών Επιστήμης Υλικών, της Πολυτεχνικής Σχολής του Πανεπιστημίου Ιωαννίνων,
- 6. Παγώνα Παπακωνσταντίνου**, Καθηγήτρια της Πολυτεχνικής Σχολής, του Ερευνητικού Ινστιτούτου, του Πανεπιστημίου του Ulster,
- 7. Νεκταρία-Μαριάνθη Μάρκουλα**, Αναπληρώτρια Καθηγήτρια του Τμήματος Μηχανικών Επιστήμης Υλικών, της Πολυτεχνικής Σχολής του Πανεπιστημίου Ιωαννίνων.

Έγκριση Διδακτορικής Διατριβής με βαθμό «ΑΡΙΣΤΑ» στις 06.03.2019.

Ο πρόεδρος του τμήματος

Η γραμματέας του τμήματος

Αλκιβιάδης Παϊπέτης

Maria Kontou

Καθηγητής

Στο Γιώργο &
στους γονείς μου Δημήτρη και Μαρία.

Abstract

Hierarchical graphitic reinforcements are one of the most promising approaches towards the exploitation of the full capabilities of nanomaterials in advanced Carbon Fiber Reinforced Composites (CFRCs). Nano-engineering of the Carbon Fiber (CF) surfaces, following a biomimetic approach, can lead to the improvement of the structural integrity, as well as impart additional functionalities to the final composites. The structural hierarchy which is ubiquitous in natural systems, such as wood or bones, accounts for some combinations of characteristics which are uncommon in human-made materials, i.e. high stiffness and high strength. A nano-designed architecture of growing interest is the Carbon Nanotube (CNT) “coated” CF, which can entail numerous positive effects including through-thickness and interply matrix reinforcement of CFRCs, while simultaneously enabling or enhancing additional multifunctional characteristics such as electrical and thermal conductivity and strain sensing. Within this context, two of the most widely used approaches for the production of hierarchical reinforcements for CFRPs are the growth of CNTs on CFs by Chemical Vapor Deposition (CVD) techniques and the deposition of CNTs on CFs by wet chemical modifications of their surfaces. However, an easily scalable, economical process has not been presented hitherto.

This thesis aimed at developing an understanding of the interactions of the CNTs with the CFs and the epoxy matrix and to the implementation of this knowledge in order to design and optimise a simple process for the preparation of hierarchical reinforcements with enhanced mechanical and multifunctional properties. A dip coating process, which relied on the wet chemical modification of the surfaces of the CFs and the CNTs, was designed and optimised. This process is promising for use on various applications since it allows for the control of the thickness of the resulting coating by CNTs. The morphology, physicochemical and mechanical properties and Raman strain sensitivity of the hierarchical reinforcements produced by both these methods were investigated. Then, the hierarchical reinforcements were embedded in epoxy matrices, and the interfacial properties of model composites, as well as the residual thermal stresses, were also evaluated. Finally, laminated composites were produced, and their interlaminar properties, as well as their electrical response, were studied.

Περίληψη

Οι ιεραρχικές γραφιτικές ενισχύσεις αποτελούν μια πολλά υποσχόμενη προσέγγιση στον κλάδο των προηγμένων σύνθετων υλικών καθώς παρέχουν τη δυνατότητα της πλήρους εκμετάλλευσης των ιδιοτήτων των νανο-υλικών. Η τροποποίηση των επιφανειών των ινών άνθρακα με νανο-δομές, ακολουθώντας μια βιομημική προσέγγιση, μπορεί να οδηγήσει στη βελτίωση της δομικής ακεραιότητας καθώς και στην εμφάνιση ή ενίσχυση διαφόρων λειτουργικότητων στα τελικά σύνθετα υλικά. Πιο συγκεκριμένα, μια αρχιτεκτονική δομή που προσελκύει αυξανόμενο ερευνητικό ενδιαφέρον είναι οι ιεραρχικές ίνες άνθρακα, δηλαδή ίνες επικαλυμμένες με νανοσωλήνες άνθρακα (ΝΣΑ). Αυτή η δομή προσδίδει πολλαπλά πλεονεκτήματα όπως διαστρωματική ενίσχυση σε ινοπλισμένα σύνθετα υλικά, αυξημένη ηλεκτρική και θερμική αγωγιμότητα καθώς και λειτουργικότητες όπως η ανίχνευση της παραμόρφωσης από το ίδιο το σύνθετο. Δύο από τις πιο γνωστές μεθόδους παρασκευής των ιεραρχικών ενισχύσεων είναι η τεχνική της χημικής εναπόθεσης ατμών και η εναπόθεση ΝΣΑ στην επιφάνεια των ινών άνθρακα μέσω υγρών χημικών τροποποιήσεων. Ωστόσο, έως σήμερα δεν έχει παρουσιαστεί μια εύκολα επεκτάσιμη και συμφέρουσα λύση παρασκευής ιεραρχικών ενισχύσεων.

Η παρούσα διδακτορική διατριβή επιδιώκει την κατανόηση των αλληλεπιδράσεων των ΝΣΑ με τις ίνες άνθρακα και την εποξειδική μήτρα και στην εφαρμογή αυτής της γνώσης για το σχεδιασμό μιας απλής διαδικασίας παρασκευής ιεραρχικών ενισχύσεων με βελτιωμένες μηχανικές ιδιότητες και πολυλειτουργικότητες. Η εργασία ανέπτυξε και βελτιστοποίησε μια απλή μέθοδο χημικής τροποποίησης των επιφανειών των ινών και των ΝΣΑ και εμφάνισε η οποία επιτρέπει τον έλεγχο του πάχους του στρώματος επικάλυψης. Οι ιεραρχικές ενισχύσεις που παράχθηκαν μέσω των δύο παραπάνω μεθόδων μελετήθηκαν ως προς τη μορφολογία, τις φυσικοχημικές και μηχανικές ιδιότητες τους καθώς και την λειτουργικότητα της ανίχνευσης της παραμόρφωσης μέσω της τεχνικής Raman. Έπειτα οι ιεραρχικές ενισχύσεις ενσωματώθηκαν σε εποξειδικές μήτρες και μελετήθηκαν οι διεπιφανειακές ιδιότητες καθώς και οι παραμένουσες τάσεις στις διεπιφάνειες των μοντέλων συνθέτων υλικών. Στο τελικό στάδιο, παρασκευάστηκαν πολυστρωματικά ινοπλισμένα ιεραρχικά σύνθετα υλικά τα οποία αξιολογήθηκαν ως προς τη διαστρωματική αντοχή και τις ηλεκτρικές τους ιδιότητες.

Acknowledgements

During the development of this PhD research, I had the opportunity to collaborate with several remarkable people who significantly contributed to the realisation of this effort, and I would like to dedicate the following paragraphs as an acknowledgement to them.

First and foremost, I would like to express my sincere appreciation and gratitude to my advisor, Alkiviadis Paipetis, Professor and Head of the Dept. of Materials Science and Engineering (MSE) who gave me the opportunity to conduct the following research in the Composite and Smart Materials Laboratory (CSML). I want to kindly thank him for his patience during my early researching steps and his guidance and support through the whole PhD study. I also want to thank him for the scientific discussions as well as the opportunities he offered to me throughout these years.

I also wish to thank Dimitrios Gournis Professor at the MSE, for his participation as a member of the advisory committee, his guidance at crucial points of the synthesis experiments as well as for providing me access to several experimental types of equipment during this research. I would also like to thank George Papanicolaou, Emeritus Professor at the Department of Mechanical Engineering and Aeronautics of the University of Patras, for his participation as a member of the advisory committee support and discussion with regards to composites.

At this point, I want to express my sincere gratitude to Nektaria-Marianthi Barkoula, Associate Professor at the Dept. of MSE, for her scientific advice and our insightful discussions. Her advice and support were always valuable and helpful to me. My sincere appreciation also goes to Pagona Papakonstantinou, Professor of Advanced Materials at the School of Engineering, at the Engineering Research Institute of the University of Ulster, for the fruitful discussions on the subject of advanced hierarchical composites. I would also like to deeply thank Konstantinos Beltsios, Professor at the at the Dept. of MSE, for introducing me to composite materials during my undergraduate studies and for honouring me with his participation to my committee. I also want to thank Michael Karakassides Professor at the Dept. of MSE for his support throughout this research and his participation in my committee.

Lastly, I would like to sincerely thank Alexandros Karantzalis, Assistant Professor at the Dept. of MSE, for introducing me to Scanning Electron Microscopy. I would also like to thank Tiverios Vaimakis, Professor at the Dept. of Chemistry, for his assistance on the Differential Scanning Calorimetry experiments.

I have to express my thanks to my first two companions in this journey, Dr Dimitrios Bekas and PhD candidate Dimitrios Baltzis, for their friendship, support, collaboration and of course their patience. It was a great pleasure and a privilege working with them on a daily basis. I also thank my newer companions who collaborated with me and supported me during the last steps of this journey, PhD candidates Maria Kosarli, Georgios Foteinidis, Anastasia Polymerou, Georgios Karalis, Christos Mitafides, MSc Michaela Konstantinidou and Dr Lazaros Tzounis for the fruitful discussions and collaboration. I would also like to thank Marilena Georgosopoulou, a colleague at the CSML for her support and care during the writing stage of this research.

At this point, I want to thank all the people who worked with me during this research: Vardis Tsouris, Stavroula Spentzou, Vasilios Spais, Marios Skouras, Marina Alantzoglou, Katerina Vlachaki, Anastasios Kaditis, Christos Drougas, for their support and collaboration.

Last but not least, I want to sincerely thank some special people like George for his love, patience, understanding and support, my father Dimitris, my mother Maria, my sister Chrysa and my brother Konstantinos for providing me with everything I needed, for giving me strength and courage to carry on with my personal goals and for making me believe in myself. I would not be here without their support.

The current PhD thesis has been co-financed by the Operational Program "Human Resources Development, Education and Lifelong Learning" and is co-financed by the European Union (European Social Fund) and Greek national funds.



Table of Contents

<i>Chapter 1 Introduction to Carbon Fibres & their Composites</i>	33
1.1 Carbon Fibres and Carbon Fibre Reinforced Composites	35
1.2 Motivation: Hierarchical Composites with Nano-engineered Architectures	36
1.3 Thesis Outline	37
<i>Chapter 2 Overview and State-of-the-art of Hierarchical Carbon Fibre Reinforced Composites</i>	41
2.1 Introduction to Carbon Fibre-Carbon Nanotube reinforced Hierarchical Composites	43
2.1.1. Hierarchical reinforcements produced by Chemical Vapour Deposition (CVD) and their composites	44
2.1.2. Hierarchical reinforcements produced by wet chemical treatments and their composites	61
2.1.3. Hierarchical reinforcements produced by Electrophoretic deposition (EPD) and their composites	71
2.1.4. Recent and advanced techniques for the production of hierarchical reinforcements	79
2.1.4.1. Spraying and electrospraying processes	79
2.1.4.2. The flame method	83
2.1.4.3. Introduction of the CNTs into a polymeric sizing	85
2.1.4.4. Other advanced techniques	87
2.1.5. Comparative studies on the production of hierarchical reinforcements and their composites	88
2.1.6. Functionalities of hierarchical composites	92

Chapter 3 From Carbon Fibres towards Hierarchical Graphitic Reinforcements:

<i>Production routes</i>	97
3.1 Introduction	99
3.2 Materials and Methods related to the CVD process	102
3.2.1. Materials	102
3.2.2. Methods	102
3.2.2.1. The growth of CNTs on the CF surface via CVD	102
3.2.2.2. Microstructural characterisation of the hierarchical reinforcements	103
3.3 Results and discussion related to Hierarchical reinforcements produced via CVD	104
3.3.1. Screening study at the single fibre level	104
3.3.1. Morphological study of CF-CNT tows	105
3.4 Conclusions related to Hierarchical reinforcements produced by CVD	107
3.5 Materials and Methods related to the wet chemical process	108
3.5.1. Materials	108
3.5.2. The oxidation process of the carbon fibres	108
3.5.3. The oxidation process of the carbon nanotubes	108
3.5.1. Characterisation of carbon fibres and CNTs before and after oxidation	109
3.5.1. Dispersion of oxidised CNTs in aqueous solutions	110
3.5.1. Dip coating procedure and visualisation of the outcome	112
3.6 Results and discussion related to Hierarchical reinforcements produced via wet chemical protocols	113
3.6.1. Vibrational analysis of the oxidised CNTs and CFs	113
3.6.1.1. FT-IR spectroscopy	113
3.6.1.1. Raman spectroscopy	116
3.6.2. Chemical analysis of the CNTs	119

Study of the graphitic reinforcement of hierarchical epoxy matrix composites

3.6.3.	Thermal stability of CNTs via thermogravimetric analysis	122
3.6.4.	Production and characterisation of CNT INKs	123
3.6.4.1.	Monitoring of the dispersion process via EIS	123
3.6.4.2.	Long-term INK stability	127
3.6.5.	Visualisation of the outcome	128
3.6.5.1.	PHASE I: INK selection algorithm	128
3.6.5.2.	PHASE II: Selection of the optimal process conditions	130
3.6.5.3.	PHASE III: Validation	135
3.7	Conclusions related to Hierarchical reinforcements produced via wet chemical treatments	136
3.8	Overall conclusions and benchmarking of hierarchical reinforcements produced by CVD or wet chemical treatments	137
<i>Chapter 4 Physicochemical and Micromechanical characterisation of the hierarchical reinforcements</i>		139
4.1	Introduction	141
4.2	Experimental Section	143
4.2.1.	Materials	143
4.2.2.	Methods	143
4.2.2.1.	Raman spectroscopy for crystallinity and structural ordering evaluation	143
4.2.2.2.	Thermal stability measurements	144
4.2.2.3.	Single fibre tensile tests	144
4.2.2.4.	Measurements of the Raman strain sensitivity	145
4.3	Results and Discussion	146
4.3.1.	Structural Characterization	146
4.3.2.	Evaluation of the thermal stability of the hierarchical reinforcements	150

4.3.3.	Tensile properties of the hierarchical CF-CNTs	154
4.3.4.	Strain-induced Raman shifts	159
4.4	Conclusions	163
Chapter 5	<i>Evaluation of the hierarchical interphases</i>	165
5.1	Introduction	167
5.2	Materials and Methods	169
5.2.1.	Materials	169
5.2.2.	Static contact angle measurements	170
5.2.3.	Interfacial shear strength measurements	170
5.2.4.	SEM study of the fracture surfaces	172
5.2.5.	Residual stresses in model composites	173
5.2.5.1.	Strain / Stress Calibration of single CFs and CF-CNTs	173
5.2.5.2.	Preparation of model-composites	173
5.2.5.3.	Raman spectra acquisition and treatment	174
5.2.5.4.	Conversion of spectroscopic data to stress values	175
5.2.5.5.	Residual stress monitoring	175
5.3	Results and Discussion	175
5.3.1.	Wettability of hierarchical CFs	175
5.3.2.	Reinforcing ability by micromechanical tests and SEM fractography	176
5.3.3.	Calculation of the Raman stress sensitivity	185
5.3.4.	Residual stress profiles	186
5.4	Conclusions	189
Chapter 6	<i>Mechanical and electrical response of hierarchical composite laminates</i>	191
6.1	Introduction	193

Study of the graphitic reinforcement of hierarchical epoxy matrix composites

6.2	Materials and Methods	195
6.2.1.	Manufacturing of composite laminates	195
6.2.2.	Mechanical characterisation	195
6.2.3.	Evaluation of the fracture surfaces with SEM	196
6.2.4.	Measurement of the electrical properties of the hierarchical laminates	196
6.3	Results and Discussion	197
6.3.1.	Mechanical response of hierarchical composite laminates	197
6.3.2.	Evaluation of the electrical properties of the hierarchical composites	200
6.4	Conclusions	202
Chapter 7	<i>Conclusions and Suggestions for future research</i>	203
7.1	Conclusions	205
7.2	Suggestions for future research	209
	Literature	211
	Appendix	239

List of Abbreviations

AFM	Atomic Force Microscopy
CFRC	Carbon Fibre Reinforced Composite
CF	Carbon Fibre
CNFs	Carbon Nanofibres
CNT	Carbon Nanotube
CVD	Chemical Vapour Deposition
EIS	Electrochemical Impedance Spectroscopy
EPD	Electrophoretic Deposition
FE-SEM	Field Emission Scanning Electron Microscopy
FRC	Fibre Reinforced Composite
G_{Ic}	Mode-I fracture toughness
FTIR	Fourier Transform Infrared Spectroscopy
G_{IIc}	Mode-II fracture toughness
IFSS	Interfacial Shear Strength
ILSS	Interlaminar Shear Strength
MWCNT	Multi-walled Carbon Nanotube
NP	Nanoparticle
PAMAM	Polyamidoamine
PAN	Polyacrylonitrile
PEI	Polyethyleneimine
PI	Polyimide
POSS	Polyhedral oligomeric silsesquioxane
PVA	Polyvinyl Alcohol
RTM	Resin transfer moulding
SAED	Selected Area Electron Diffraction
SEM	Scanning Electron Microscopy
SAXD	Small Angle X-Ray Diffraction
SFFT	Single Fibre Tensile Test
SWCNT	Single-walled Carbon Nanotube
TEM	Transmission Electron Microscopy
TGA	Thermogravimetric Analysis
UD	Unidirectional
VARTM	Vacuum assisted resin transfer molding
WAXD	Wide Angle X-Ray Diffraction
XPS	X-Ray Photoelectron Spectroscopy

List of Figures

Figure 1. The plot presents the evolution of the activity in carbon fibre-CNT hierarchical composites from 1991.	43
Figure 2. Schematic representation of a typical CVD apparatus.....	45
Figure 3. TEM image of Ni NPs (black spheres) formed on a CF surface after the annealing process. Reprinted from [39], Copyright (2013), with permission from Elsevier.....	48
Figure 4. Continuous CVD set-up for synthesis of CF-CNTs, an overview photograph showing the fiber tow entry and exit from the reactor. Reprinted from [6] under a Creative Commons license. © 2018.....	51
Figure 5. FESEM images of bare CFs (a) after desizing by Soxhlet extraction and (b) hairy CF-CNTs grown by CVD. Reprinted with permission from [22]. Copyright 2017 American Chemical Society.....	52
Figure 6. SEM images of unsized CFs (a) before and (b) after the surface treatment, and CFs grafted by (c) entangled MWCNTs and (d–h) aligned MWCNTs with different length controlled by the growth time. Reprinted from [48], with permission from Elsevier.	53
Figure 7. (a) SEM image for the detachment of CNT, the left image is from prior to attaching AFM tip onto CNT, and the right image presents that the CNT was detached from CF surface. (b) SEM image for the fracture of CNT. (Reprinted from [65]., Copyright (2014), with permission from Elsevier.....	54
Figure 8. SEM images of fracture surfaces of a hierarchical composite with enhanced adhesion showing CNTs bridging between fibre and matrix. Reprinted from [4], Copyright (2015), with permission from Elsevier.....	58
Figure 9. Experimental scheme used to prepare the multiscale reinforcements. Reprinted from [88], Copyright (2007), with permission from Elsevier.....	61
Figure 10. Experimental scheme used to synthesize CF-CNTs through a series of processes such as desizing, oxidising, amine functionalising and CNTs grafting. Reprinted from [94], Copyright (2013), with permission from Elsevier.....	64
Figure 11. Schematic representation of the grafting procedure of carboxyl functionalised CNTs onto acid oxidized CFs by the use of PAMAM. Republished with permission of Journal of materials chemistry by Royal Society of Chemistry, from [98], Copyright (2012); permission conveyed through Copyright Clearance Center, Inc.	65

Figure 12. SEM micrographs of a) a CF–POSS–CNT hierarchical reinforcement, Reprinted from [105] Copyright 2011, with permission from Elsevier, and b) a sized hierarchical CF coated with PEI polyelectrolyte treated UV/O ₃ MWNTs. Reprinted from [107] Copyright 2012, with permission from Elsevier.	69
Figure 13. SEM micrographs of hierarchical CFs with increasing grafting densities of CNTs. Reprinted from [112] Copyright 2018, with permission from Elsevier.	70
Figure 14. Schematic representation of the EPD process. Reprinted from www.subtech.com.	72
Figure 15. SEM images showing carbon fibres a) before, b) after simple EPD process, c) after ultrasonically assisted EPD with acid functionalised MWCNTs and d) after ultrasonically assisted EPD with ozone-PEI treated MWCNTs. Reprinted from [117] and [120], with permission from Elsevier.....	73
Figure 16. Surface SEM images of a) as-received CF, b) hierarchical CF-CNT, c) hierarchical CF-CNT with radial alignment (low magnification), d) hierarchical CF-CNT with radial alignment (high magnification. Reprinted by permission from Springer Nature, Applied Physics A: Materials Science & Processing, [128], © Springer-Verlag Berlin Heidelberg 2016.....	76
Figure 17. Raman mapping of the interfacial and cross-sectional regions. (a) Optical microscopy image of the probed cross-sectional region; (b) Raman spectral scan of the image showing CNTs (pink and yellow color) located at the interface with thickness of 4 - 14 µm; (c) optical microscopy image of the probed interfacial region; (d) Raman spectral scan of the image showing CNTs (red color) at multiple locations along the interface. Reprinted from [134]. Copyright 2014, with permission from Elsevier.	79
Figure 18. Schematic representation of the electro spraying of CNTs onto carbon fibres. Reprinted from [139], Copyright (2016), with permission from Elsevier.	81
Figure 19. Evolution of the CNT during the first cycles of friction: (a) before friction, (b) after the first cycle of friction, (c) after 10 cycles of friction. Reprinted from [144], Copyright (2018), with permission from Elsevier.	84
Figure 20. Hybrid laminated composite with CNT inter-layer. (a) Fiber/CNTs for 52.50 mg; (b) Fiber/CNTs for 64.75 mg; (f) Fiber/CNTs for 185.25 mg. Reprinted from [147] under a Creative Commons license. © 2013	87
Figure 21. Schematic representation of the methods used by Awan et al. Reprinted from [151], Copyright (2018), with permission from Taylor & Francis Group.....	91

Figure 22. The horizontal tubular Carbolite furnace used for the CVD process.....	103
Figure 23. SEM micrographs depicting the morphology of a) a single CF, single CFs coated with CNTs produced by various CVD conditions, b) 750°C for 30 min, c) 750°C for 10 min, e) 850°C for 10 min, f) 900°C for 10 min and d) TEM image of the CNT coated CF produced by CVD at 900°C. Diameter measurements are shown in green colour.....	104
Figure 24. FE-SEM micrographs and the corresponding CNT diameter distribution plot revealing the morphology and structure of the produced CNTs. CF-CNT produced by CVD, CF-CNT@750/10 (a, b, c) CF-CNT@750/30 (d, e, f), CF-CNT@850/10 (g, h, i) and CF-CNT@850/30 (j, k, l).....	106
Figure 25. Schematic representation of the interdigital sensor used for electrical impedance measurements.....	111
Figure 26. Schematic representation of the experimental set up utilised for impedance monitoring of the dispersions.....	111
Figure 27. Photos of the experimental set up used for the coating procedure.....	112
Figure 28. FTIR spectra of the CNT samples before and after the various oxidative treatments. .	114
Figure 29. Relative changes of FTIR vibrational modes with respect to the as-received MWCNTs.	115
Figure 30. Raman spectra of the as received and oxidised CNT samples.....	116
Figure 31. The empirical formula describing the degree of functionalization of the CF surfaces with respect to their reaction time in nitric acid.	119
Figure 32. C1s core level X-ray photoemission spectra of as received CNT and oxidised samples: A, SA, ASL, AM, and AGK.....	120
Figure 33. O1s region of the XPS spectrum of the as-received CNTs.....	121
Figure 34. Thermal analysis curves (TGA%) of as received and oxidised CNTs.....	122
Figure 35. EIS plots of the dispersion process monitoring.	126
Figure 36. Photographs of the CNT dispersions 60 days after their production.	127
Figure 37. Flowchart of the optimisation process from the SEM studies.	130

Figure 38. SEM micrographs of unsized (a-d) and sized (e-f) CFs coated with INK_ASL_0.01 for 50 repetitions. As received CFs (a and e), oxidised in HNO ₃ for 30 min (b and f), 60 min (c and g) and 90 min (d and h). All scale-bars are equal to 5 μm.....	131
Figure 39. SEM micrographs of unsized CFs coated with INK_ASL_0.1 for 10 (a - d) and 30 (e - h) repetitions. As received CFs (a and e), oxidised in HNO ₃ for 30 min (b and f), 60 min (c and g) and 90 min (d and h). All scale-bars are equal to 5 μm.....	132
Figure 40. SEM micrographs of unsized (a, c, e and g) and sized (b, d, f and h) CFs coated with INK_ASL_0.1 for 50 repetitions. As received CFs (a and b), oxidised in HNO ₃ for 30 min (c and d), 60 min (e and f) and 90 min (g and h).	133
Figure 41. SEM micrographs of unsized CFs coated with INK_ASL_0.5 for 10 (a, c, e and g) and 30 (b, d, f and h) repetitions. As received CF (a, b), CF oxidised in HNO ₃ for 30 min (c, d), 60 min (e, f) and 90 min (g, h).	134
Figure 42. SEM micrographs of unsized CFs coated with INK_x_0.1 for 50 repetitions. a) 30 min oxidized CF/ INK_A_0.1, b) as received CF/ INK_SA_0.1, c) 90 min oxidized CF/ INK_AM_0.1 and d) 60 min oxidized CF/ INK_AGK_0.1.....	135
Figure 43. Raman spectra of CF and CF-CNT fibres from different CVD growth conditions. All spectra were normalised to the G band and shifted by 0.5 to facilitate presentation.	146
Figure 44. Raman spectra of CF and CF-CNT fibres from the wet chemical treatments. All spectra were normalised to the G band and shifted by 0.5 to facilitate presentation.....	147
Figure 45. Thermographs of the CF and the CF-CNTs from all CVD conditions. The solid lines represent the mass loss curves, and the dotted lines stand for the rate (first derivative - DTG) of the mass loss curves.	152
Figure 46. Thermographs of the CF and the CF-CNTs produced by wet chemical protocols. The solid lines represent the mass loss curves, and the dotted lines stand for the rate (first derivative - DTG) of the mass loss curves.	153
Figure 47. The differential calorimetric scan of the reference CF/S and the CF-CNT/S_30_50 and CF-CNT/S_30_50.	154
Figure 48. Strength to length relationships for the reference CF/UNS in comparison to the CF-CNT@850/30 (left), and the CF/S in comparison to the CF-CNT/S_30_50 and CF-CNT/S_60_50. (Strength measured in MPa and length in mm).....	155

Figure 49. Calculation of Young modulus for the reference CFs and the CF-CNTs via the system compliance as indicated by ASTM C 1557-14 [202].	157
Figure 50. Weibull plots for the hierarchical as well as the reference CF-CNTs.	159
Figure 51. Raman Shift vs strain Calibration curves, for the CF/UNS, the CF-CNT@750/30 and CF-CNT@850/30.	160
Figure 52. Raman Shift vs strain Calibration curves, for the CF/S, the CF-CNT/S_30_50 and CF-CNT/S_60_50.	161
Figure 53. Silicon rubber mould used for the fabrication of single fibre model composites.	170
Figure 54. The experimental set-up used for the SFFT measurements. The custom-made, horizontal tensile stage (right) placed under the Leica DM-4000M polarised optical microscope (left).	171
Figure 55. A characteristic Raman spectrum as acquired from the single-fibre model-composites (top), the spectrum of the epoxy resin (middle) and the emerging spectrum of the CF (bottom).	174
Figure 56. Histograms of the contact angle formed between the hierarchical or the reference CFs and the epoxy matrix. A characteristic droplet on CF was presented in each case, as well as the number of droplets for which the contact angle was measured.	176
Figure 57. Characteristic polarised optical birefringence patterns of fragmented model composites at 20x magnification. (a) CF, (b) CF-CNT@750/10, (c) CF-CNT@750/30, (d)CF-CNT@850/10 and (e) CF-CNT@850/30. The dashed-line arrows indicate the CF and CF-CNT crack locations.	178
Figure 58. Micrographs of the fracture surface of the CF/UNS model-composites with different magnifications.	179
Figure 59. Micrographs of the fracture surface of the CF/S model-composites with different magnifications.	180
Figure 60. Micrographs of the fracture surface of the CF-CNT@750/30 model-composites with different magnifications.	181
Figure 61. Micrographs of the fracture surface of the CF-CNT@850/30 model-composites with different magnifications.	182
Figure 62. Micrographs of the fracture surface of the CF-CNT/S_30_50 model-composites with different magnifications.	183

Figure 63. Micrographs of the fracture surface of the CF-CNT/S_60_50 model-composites with different magnifications.	184
Figure 64. Characteristic micrographs of the interfacial fracture mechanisms for the CF-CNT/S_60_50 tow composites.....	184
Figure 65. Micrographs of the imprints of the CF-CNT/S_60_50 on the epoxy host matrix after the pull-out process.	185
Figure 66. Residual axial stress profiles along the fibre length for the CF/S, CF-CNT@850/30 and the CF-CNT_60_50 embedded in the epoxy matrix.	187
Figure 67. Schematic representation of the hydrostatic field acting on a) a conventional CF and b) a hierarchical CF embedded in the epoxy matrix.....	188
Figure 68. Bar-chart summarising the short-beam strength values of the hierarchical and the reference composites.	197
Figure 69. Representative load-displacement curve as recorded for the hierarchical and the reference laminated composites.	198
Figure 70. SEM micrographs from fractured ILSS specimens. (a, b, c, d) Reference CF/epoxy specimens and (e, f, g, h) hierarchical CF-CNT/epoxy specimens.	199
Figure 71. High magnification SEM micrographs from the hierarchical CF-CNT/epoxy composites.	200
Figure 72. The electrical conductivity of the hierarchical CF-CNT/epoxy laminates and the reference CF/epoxy laminated composites in both the in-plane and the through-thickness directions.	201

List of Tables

Table 1. Description of the studied systems.....	109
Table 2. Experimental values of the as received and oxidised CNTs evaluated by Raman spectroscopy.....	117
Table 3. Experimental values of the as received and oxidised CFs evaluated by Raman spectroscopy.....	118
Table 4. Chemical analysis of the CNTs (All numbers represent percentages).....	121
Table 5. Combustion Temperatures and Residual Mass of the oxidised CNTs.....	123
Table 6. Ranking of oxidised CNTs.....	128
Table 7. Nomenclature of the studied hierarchical and reference CFs.....	143
Table 8. Fitting parameters of the Raman spectra of CF and for all CF-CNT.....	148
Table 9. Parameters of the strength to length relationships, average strength and strain values for CFs and CF-CNTs.....	156
Table 10. Mechanical properties of the hierarchical CF-CNTs and the reference CFs.....	157
Table 11. Weibull parameters of the reference CFs and the hierarchical CF-CNTs.....	158
Table 12. Linear fitting values and strain induced Raman sensitivities $\alpha\epsilon$	162
Table 13. Interfacial mechanical properties of the hierarchical and the reference model-composites.....	177

Chapter 1

Introduction to Carbon Fibres & their Composites

1.1 Carbon Fibres and Carbon Fibre Reinforced Composites

Carbon fibres (CFs) have been in the core of scientific interest since their discovery by Roger Bacon in 1958 and their first commercial manufacturing in 1959 [1]. The early development of CFs has been a fast process which led to their entry in the industry of “advanced composites” in less than five years, by 1963 [2]. Initial yarns of CFs were produced by rayon organic precursor fibres, until shortly after, when CFs from Polyacrylonitrile (PAN) were also produced and five years still later, pitch based CFs were invented. These thin filaments, 5-10 μm in diameter, exhibit high specific mechanical properties, strength and stiffness, which render them suitable for use in lightweight structural composites and thus entail great technological importance for many industrial applications. CFs also possess other interesting properties like very high thermal stability, a small coefficient of thermal expansion and high chemical resistance.

The combination of the CFs with traditional polymeric matrices, e.g. epoxy resins, leads to the manufacturing of Carbon Fiber Reinforced Composites (CFRCs). CFRCs are nowadays used in several structural and non-structural applications in various fields. The advantage of reduced weight simultaneously with enhanced mechanical properties, resistance to fracture and damage tolerance is beneficial for applications like aircraft and spacecraft, where less weight and better properties are coupled leading to improved fuel efficiency and reduced operational costs. CFRCs are also used in automotive, marine and civil engineering applications, transportation, wind turbines, microelectrodes, sports goods and musical instruments among others [3,4].

Over time, significant research efforts have been devoted to the understanding and engineering of the CF surfaces and the CF/ epoxy interphases/interfaces, in order to optimise the interconnection between them, for achieving improved mechanical properties [5]. The physicochemical as well as the mechanical response of CFRCs, and in general Fibre Reinforced Composites (FRCs), has also attracted tremendous scientific interest due to mainly the anisotropic properties of these materials. Specifically, although CFRPs exhibit excellent in-plane properties, their out-of-plane response including interlaminar shear strength and delamination resistance, their fracture toughness, and their flexural properties and damage tolerance need to be further improved for specific high-end

applications [6–9]. Composite engineers have addressed the inherent weakness of the interlaminar regions of FRCs on the macroscale by using 3D fibre architectures like weaving, stitching, braiding and Z-pinning [10] [11] [12] [13]. These methods introduce additional fibre yarns between adjacent fibre layers for improving structural properties under shear and compressive loads. However, these approaches also lead to the introduction of geometric defects due to fibre crimping, fracture and distortion as well as the potential for weak, resin-rich regions and therefore compromise the FRC in-plane strength significantly [14].

Today, the emergence of nanotechnology has led to the engineering of advanced materials, through processing techniques capable of arranging matter into specific configurations at several length scales, leading to the realisation of a bulk material with the desired properties. The incorporation of various nanomaterials in CFRCs has been realised by two distinct approaches, namely their dispersion into the matrix material (hybrid approach) or their attachment onto the primary reinforcement (the CFs). In this context, hierarchical fibre reinforced composites have been produced, by growing or depositing carbon nanotubes (CNTs) onto the surface of CFs [15]. The term *Hierarchical Composites* within the context of this dissertation refers to structural FRCs in which reinforcements of more than one length scale are used, and the geometry of the multiple scales is interconnected. Furthermore, the abbreviation CF-CNTs was used throughout this thesis when referring to these hierarchical reinforcements.

1.2 Motivation: Hierarchical Composites with Nano-engineered Architectures

The motive for this work was the ongoing evolution of composite materials into advanced, multifunctional architectures, which combine interconnected reinforcements of various length scales, from the macroscale and the micron scale down to the nanoscale, in order to extend materials' properties outside the limits of the previous conventional approaches. The use of nano-engineering has proved to be a promising way to overcome the inherent deficiencies of CFRCs as well as to transfuse new functionalities that will enable novel applications and better overall performance [16].

Practically, the integration of CNTs in CFRCs may be performed either by dispersion into the polymeric matrix or by attachment/growth onto the surface of the primary reinforcement (CF). Typical hybrid systems, where fibrous composites consist the primary reinforcement and nanophases are dispersed in the composite matrix, seldom manage to attain the expected properties that should stem from the unique properties of nano-sized graphitic entities such as CNTs. This is due to several manufacturing problems, i.e. agglomeration issues due to strong Van der Waals forces [17], or subsequent filtration issues due to high viscosities which hampered the full exploitation of their strengthening ability [18,19]. Alternatively, the attachment of CNTs onto CF surfaces and the subsequent incorporation of that “composite” CF-CNTs into the polymeric matrices leads to the realisation of multiscale hierarchical CFRCs [15].

Hierarchical CF-CNT architectures aim to improve fracture toughness, interfacial and interlaminar shear strength as well as other non-structural properties, like electrical and thermal conductivity and strain sensing ability of the advanced multifunctional CFRCs [20]. It should be noted that several designations can be met in literature for hierarchical reinforcements, i.e. “multi-scale” [21], “hairy” [22] or “fuzzy” [23] fibres.

1.3 Thesis Outline

In this thesis, hierarchical all graphitic reinforcements comprised of CFs covered by CNTs were evaluated. An overview and a presentation of the state-of-the-art of the hierarchical CFRCs is summarised in Chapter 2.

During this study, two different approaches were employed for the production of the hierarchical architectures, namely growing MWCNTs via catalytic chemical vapour deposition (CVD) and depositing CNTs from aqueous suspensions (inks) on the CF surface. The CVD process was assessed since it represents the most widely employed technique for the realisation of hierarchical reinforcements. On the other hand, a facile and scalable technique was developed which involved the wet chemical treatment of commercial CFs and CNTs and the subsequent interconnection of the two different scale reinforcements by a simple dip-coating process. An essential aspect for the successful preparation of hierarchical graphitic reinforcements by the latter method was the

optimisation of the CNT INKs. Both approaches are presented in detail in Chapter 3 along with a morphological characterisation of the produced hierarchical reinforcements.

Chapter 4 covers the hierarchical CF-CNT characterisation at the single fibre level. Specifically, the crystallinity and structural ordering of the produced hierarchical reinforcements were evaluated by Raman spectroscopy, and their thermal behaviour was assessed by Thermogravimetric analysis (TGA). Then, the effects of the CVD and wet chemical treatments on the mechanical properties at the single fibre level were quantified by Single Fibre Tensile Tests (SFFT). Moreover, the strain induced Raman sensitivity was evaluated as an additional inherent functionality of the produced hierarchical structures.

Subsequently, the hierarchical reinforcements were embedded into an epoxy matrix, and the interfacial properties were assessed in Chapter 5. In more detail, the interactions of the hierarchical reinforcements with the epoxy matrix were quantified by static contact angle measurements of the wetting effects. The interfacial shear strength (IFSS) was also evaluated by Single Fibre Fragmentation tests (SFFT) combined with polarised optical microscopy for the measurement of the number of fragments. The fractured surfaces of hierarchical model-composites were studied by Scanning Electron Microscopy (SEM) in order to identify the failure mechanisms acting at the hierarchical interfaces. Furthermore, the residual thermal stresses which generally accumulate on the CFs after the matrix polymerisation due to the difference in the thermal expansion coefficients were quantified by a Raman study.

The scale-up studies which included the manufacturing of quasi-isotropic hierarchical laminates and the evaluation of the interlaminar shear strength (ILSS) by the short-beam shear test, in comparison to the reference CF laminates, are presented in Chapter 6. After mechanical testing, a fractographic inspection of the fracture profiles was performed by SEM in order to identify possible differences in the energy dissipation mechanisms and the failure process. Furthermore, the electrical characteristics of the quasi-isotropic hierarchical laminates were also measured and compared with the reference CF laminates in Chapter 6.

Finally, the results of this thesis are summarised in Chapter 7 along with some suggestions for further research regarding several research directions that stemmed from this study. Finally, in the Appendix, additional details on the experimental procedures are presented.

In relation to the novelty of this thesis, the main breakthrough results that were produced during this study can be divided in three different research areas, namely i) the production of electrically conducting INKS, ii) the production of hierarchical CF-CNT reinforcements and their composites and iii) the advanced Raman studies on these hierarchical reinforcements and their composites.

In more detail, during this study a facile experimental method for the production of hierarchical graphitic reinforcements with controllable thickness of the deposited CNT coatings onto the carbon fibres was developed. These reinforcements exhibited increased thermal stability and significantly enhanced interfacial shear strengths when incorporated into the epoxy matrix.

Moreover, electrically percolated and stable with time oxidized CNT INKS in aqueous solvents without the use of binders and with the minimum possible degradation of the CNTs was achieved during this study. These INKS can be used in various production methods, e.g. printing, spray coating, slot die coating etc.

Furthermore, the advanced Raman studies on the hierarchical reinforcements and their composites, which were performed during this study, can be summarised to i) the evaluation of the strain induced Raman sensing ability of the hierarchical fibres in comparison to the reference single CFs in relation to the CVD and the wet chemical production methods and ii) the determination of the residual stresses of the hierarchical single fibre model epoxy composites in comparison to the reference single fibre model epoxy composites with Raman spectroscopy.

Chapter 2

Overview and State-of-the-art of Hierarchical Carbon Fibre Reinforced Composites

2.1 Introduction to Carbon Fibre-Carbon Nanotube reinforced Hierarchical Composites

Hierarchical composites reinforced with CF-CNTs have been systematically studied for almost twenty years by now. However, the most intense research effort by several research groups was presented during the current decade (Figure 1) and scaling up to industrial manufacturing has not as yet been achieved. The plot includes publications on hierarchical composites consisting of CNTs or a combination of CNTs and another nanostructure on CFs. The literature survey also was mostly focused on epoxy resin matrices except for some selected renowned publications on other matrices which were used as examples.

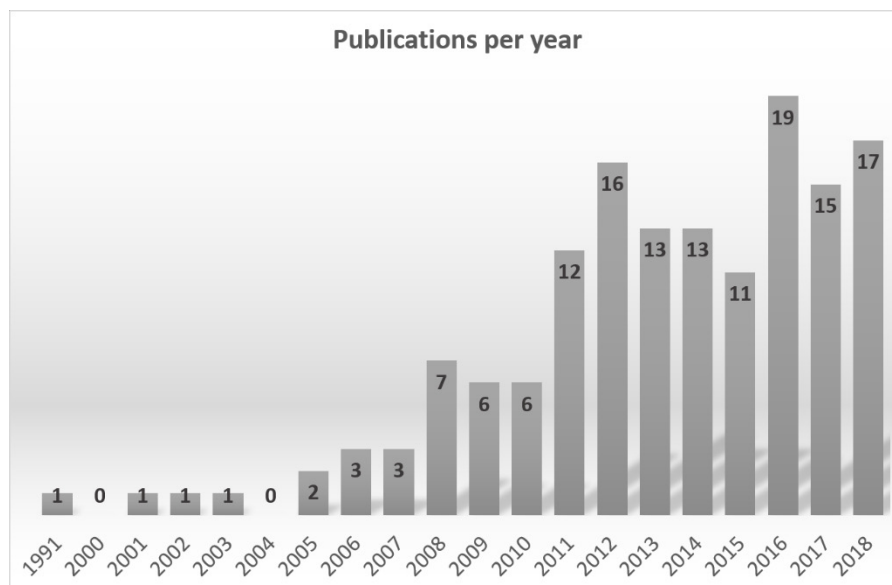


Figure 1. The plot presents the evolution of the activity in carbon fibre-CNT hierarchical composites from 1991.

Until today, several different methods have been reported in the literature for the production of hierarchical CF-CNT reinforcements and their composites. Among them, the CVD process attracted most of the research attention, while the grafting of CNTs onto CFs via chemical reactions, and the deposition of CNTs onto CFs by electrophoretic deposition (EPD) were also studied by many authors. Other techniques like i) the flame method, ii) the incorporation of CNTs into a polymeric sizing and the subsequent application of this nanomodified sizing onto CFs, iii) the spraying processes, iv) the electro-spraying

processes and v) the transferring of aligned CNT forests onto CF fabrics and preregs were more recently demonstrated.

The incorporation of these hierarchical reinforcements into polymeric matrices was also demonstrated in many publications for the manufacturing of hierarchical composites with improved in-plane and out-of-plane mechanical properties as well as additional non-structural functionalities. However, several obstacles still exist until the exploitation of the full potential of the nanostructures towards multiscale and multifunctional CFRCs with overall improved performance. The drawbacks related to each of the production processes are also presented in the following paragraphs.

An overview of the research efforts devoted to each production process along with a summary of the state of the art publications is presented in the following paragraphs. The development of each method is presented in a separate section, followed by a section which summarises some comparative studies of two or more production processes. Furthermore, the final section reports on the studies which focused solely on the demonstration of specific functionalities of the Hierarchical reinforcements and composites.

2.1.1. Hierarchical reinforcements produced by Chemical Vapour Deposition (CVD) and their composites

Chemical vapour deposition has been used for the growth of CNTs since 1890 [24]. During this deposition process which is schematically depicted in Figure 2, a hydrocarbon source usually in the gaseous phase is decomposed under elevated temperatures, an inert atmosphere and the presence of a metal catalyst into several carbon allotropes.

The first study on the chemical vapour deposition of carbon on CFs was presented by Pierson and Lieberman who performed a multi-parametric investigation in order to assess the pyrolytic carbon microstructures deposited onto the CFs with regards to the process conditions [25]. The authors considered temperature ranges of 1200-1450 °C, for pressures between 20 and 630 Torr, a C/H ratio in the methane hydrocarbon source ranging from 1/4 to 1/14, with total flow rates 2-16 l/min and carbon felt substrate densities 0.12-0.23 g/cm³. Within these conditions three distinct microstructures were produced, namely smooth

laminar (SL), rough laminar (RL) and isotropic (ISO). The results confirmed the predictions of a previously developed model for the deposition of carbon onto carbonaceous fibrous substrates as long as the model assumptions of gas phase equilibrium were retained. The authors concluded that SL, RL, and ISO microstructures were sequentially obtained with increasing temperature, decreasing C/H ratio, decreasing pressure, and increasing substrate CF density [25].

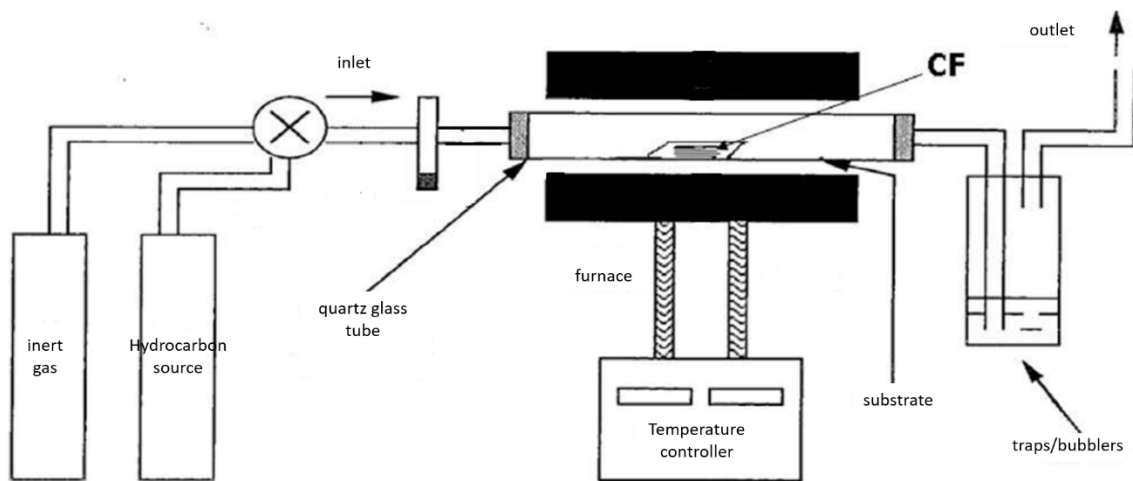


Figure 2. Schematic representation of a typical CVD apparatus.

The first hierarchical reinforcements were demonstrated by Downs and Baker, as early as 1991, who used CVD in order to grow Carbon Nanofibers (CNFs) onto the surface of PAN-based CFs, from an ethylene-hydrogen hydrocarbon and copper-nickel catalysts at 600°C [26]. With regards to CNTs, they were initially grown on a graphite foil by Li et al. [27] who sputtered a stainless steel catalyst film onto the substrate and performed CVD with acetylene source for 1 hour at 660°C. Li et al. demonstrated that the catalyst particle size was dependent on the initial catalyst film thickness and that the outer diameter of the grown CNTs also increased with catalyst particle size.

Shortly after, Thostenson et al. extended this work to a pitch based CF substrate [28]. The authors utilised the same experimental conditions but performed growth for 30 min. The IFSS of the CF-CNTs increased by 15% compared to the reference unsized CFs, while the CVD process without the growth of CNTs was found to degrade the IFSS of the reference CF by 37% [28].

While up to 2004, it was already evident that CFs presented a more challenging substrate for uniform CNT growth due to mainly their chemical inertness in comparison to other fibrous substrates [29]. On the other hand, studies on other fibres had already shown significant improvements upon CNT growth. For instance, Veedu et al. demonstrated that alumina fibres were suitable in fabric form for the growth of aligned CNTs [30]. The manufactured composites exhibited remarkably enhanced properties, i.e. mode I fracture toughness, G_{IC} by 348% and mode II fracture toughness G_{IIC} by 54%, increased flexural and damping properties, improved thermal expansion coefficient and thermal and electrical conductivities [30].

Early studies focused mainly on the production of hierarchical CF-CNT reinforcements at a small scale (single fibre or tow level) and their morphological and structural evaluation [31–34]. Since CVD was a commonly used method for the growth of CNTs onto various substrates [24,35,36], even in those initial studies, it was evident that the utilised growth conditions affected the resulting carbonaceous morphologies. Sharma and Lakkad examined the effects of different process parameters, i.e. growth temperature, duration and gas flow rates, on the morphology of the nano-species grown onto the CFs during the CVD process [37]. The size and morphology of the catalyst particles determined the diameter and the morphology of the grown nano-species, while a wide variety of nanostructures, i.e. nanofibers, nano-filaments, nano-onions, nano-cones, nano-spirals, nano-ladders and Y-junctions, accompanied the growth of CNTs. The overall yield of the nano-species increased with growth duration up to a point where catalyst poisoning phenomena hindered further growth. Moreover, the precise adjustment of the process parameters resulted predominantly in the desired carbon nanostructures such as nanotubes, nanofibers or filaments [37].

Along these lines, the catalyst type, size and catalyst deposition method before CVD growth was and remains a subject of interest for several authors [37–43], while the type and the flow rate of the precursor gas used for the CVD growth were also examined by others [37,44]. For instance, iron sputtering by pulse voltammetry led to uniform distributions of the catalyst nanoparticles and thence of MWCNTs onto CFs [38]. Deposition of the iron catalyst by spin coating onto woven CFs also led to a minimum amount of catalyst impurities [41].

The first study on the tensile properties of hierarchical CF-CNTs produced by CVD onto both PAN-based and pitch-based CFs reported that the tensile strength, the ductility and the Weibull modulus of the CF-CNTs were improved in comparison to the reference CFs [45]. However, several subsequent studies commented on the reduced tensile strength of CFs which followed CVD growth of CNTs onto their surfaces [46–51], while in some cases the degradation was significantly notable [52,53].

Therefore, some studies, like the work of Lee G. et al. investigated the mechanism which led to the degradation of CFs as a result of the catalytic growth of CNTs [42]. TEM, Raman, Wide Angle X-Ray Diffraction (WAXD) and Small Angle X-Ray Diffraction (SAXD) measurements assisted the authors in studying the microstructure and identifying the CF degradation mechanism. The authors concluded that when the energy of the catalytic nanoparticles was sufficient, they diffused into the CFs, thus generating microvoids near the surface which acted as stress-concentrators and decreased the strength of the CFs. This study also demonstrated that uniform CNTs could be grown on CFs by CVD at low-temperature (500 °C) when using a NiFe bimetallic catalyst without mechanical degradation of the CFs. The ability of that catalyst to lower the activation energy for CNT growth, enabled a lower CVD temperature to be used, thereby avoiding the inter-diffusion of the catalyst particles on the CF surface [42].

In another parametric study, Zhang et al. examined the effects of the CVD process conditions on the morphology of the produced CNTs and the tensile properties of two different CF substrates [54]. The authors demonstrated that the T650 unsized CFs maintained their tensile properties after CVD growth of CNTs at 750 °C whereas the same process significantly degraded the sized IM-7 CFs. However, by increasing the growth temperature to 800°C a 40% decrease in the mechanical properties of the T650 unsized CFs was also observed. [54].

Tanaka et al. studied the effects of the CVD growth temperature on the tensile strength of the substrate CF. The authors grew CNTs on CFs at temperatures from 550°C to 700°C using Ni as the catalyst and ethanol as the carbon source. SFTT were utilised for measuring the tensile strength of Ni-plated and CNT grafted CFs. CVD growth at 550°C and 600°C did not degrade the tensile strength of the Ni-plated nor the CNT grafted CFs, while at 650°C the tensile strength of both the Ni-plated and the CNT grafted CFs decreased by

21% and 10 %, respectively, and decreased even further by 48% and 45%, respectively, when growth was performed at 700°C. The authors attributed the degradation of the CF tensile strength during high-temperature CVD growth of CNTs on their surfaces to the accelerated diffusion of the Fe particles into the CFs [55].

Another experimental campaign, presented by Steiner et al., focused solely on understanding the main reason for the encountered loss in CF strength during CVD [56]. The authors studied two types of commercial PAN-based CFs and attributed the strength loss to thermally activated mechano-chemical changes in the CF microstructure. A fibre-specific critical threshold temperature was identified at 550 °C, and 500°C for the two studied CFs above which microstructural and chemical changes occurred, while the CVD processes performed below this critical temperature preserved the tensile strength and moduli of the CFs. Furthermore, when a certain amount of tension was applied on the CFs during CVD, which was performed above the critical temperature and up to 730°C, also preserved the CF mechanical response. The authors attributed the preservation of the CF mechanical properties to the fact that applied tension was used as a mechanical guide of the evolution of the chemical and microstructural changes, causing the alignment of the external CF layers which are known to be of higher strength than the CF core [56].

The effects of the catalyst thickness used for the fabrication of hierarchical CF-CNTs by CVD were also investigated by Kim et al. The average Ni nanoparticle (NP) diameter and the diameter and length of the produced CNTs increased with increasing thickness of the Ni catalyst film. The tensile strength of the CFs was reduced due to the catalyst treatment by 5.4 %, while after CVD growth of CNTs the CF strength increased by 14%. This was attributed to the deactivation of the catalyst particles after CNT growth, i.e. the CNTs used the Ni NPs, which were embedded into the outer layers of the CF surface (Figure 3), to grow via a tip growth

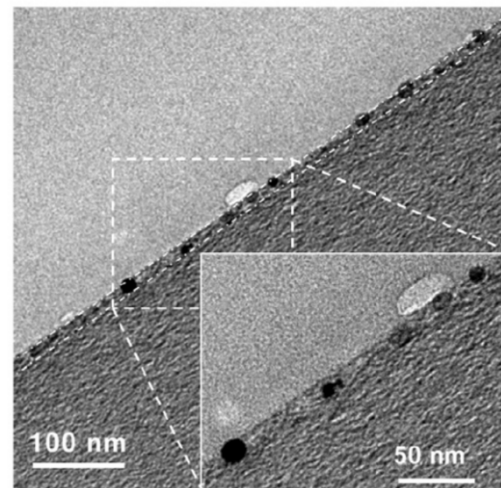


Figure 3. TEM image of Ni NPs (black spheres) formed on a CF surface after the annealing process. Reprinted from [39], Copyright (2013), with permission from Elsevier.

mechanism, pushing the NPs to their tip and filling the space left by them, thus restoring the CF substrate. The enhancement of the tensile strength after CVD growth was investigated by SEM, TEM and selected area electron diffraction (SAED). Overall the enhancement was attributed to i) the repairing of the damage incurred by Ni NPs, ii) the increased crystal size and iii) the cross-linking of the adjacent crystals due to the CVD process which led to longer paths for crack propagation in the hierarchical CFs [39].

Summarising, the loss in mechanical properties of the CFs due to CNT growth can be either attributed to diffusion mechanisms of the catalyst particles into the CF substrate due to the high temperatures of the CVD process or to thermally activated mechano-chemical changes in the CF structure. In any case although, the CNT growth itself was shown not to degrade the CF properties but rather to “heal” existing defects.

Healing of the defects of the CFs was further studied as a mechanism acting during catalytic growth of CNTs by Kim et al. [43]. The authors examined the variations in the tensile strength of the CFs undergoing the growth of CNTs. Only the coating process with the catalyst and the formation of the catalyst nanoparticles deteriorated the tensile strength of the CFs because it led to the formation of an amorphous region, easily penetrable from the NPs [43]. Conversely, the CVD process itself healed the damages present on the CFs, if proper process duration was implemented. Healing was achieved by carbon atoms from the hydrocarbon vapours dissociation which bridged the damaged edges of the graphite layers. The authors proposed a minimal catalyst thickness and prolonged growth duration within a cost-effective range as a possible optimisation method, capable of maintaining and even increasing the CF tensile strength during CVD growth of CNTs [43].

Healing of CFs during CVD growth of CNTs on their surfaces was also reported by Fan et al. who focused on improving the catalyst coating on CFs that were subsequently used for the production of hierarchical reinforcements by CVD growth. The proposed catalyst deposition technique achieved a uniform catalyst coating on continuously moving CFs. In this study, both the degradation of mechanical properties of the CFs and the decrease in the catalyst activity were inhibited by reducing the interaction time between the CFs and the catalytic NPs. The high catalyst activity was of interest since it has been proved effective for the healing and strengthening of CFs. The authors stated that a CVD process with Ni catalyst at 500°C resulted in CF-CNTs with 10% increased tensile strength in comparison

to the reference CFs. Lower growth temperatures led to low catalytic efficiencies, while higher growth temperatures resulted in serious catalyst-induced and mechano-chemical degradation of the CFs. Furthermore, a healing and crosslink model of adjacent carbon crystals by CNTs was developed in order to elaborate on the origins of the increase in tensile strength of CF-CNTs in comparison to the reference CFs [40].

The same authors in a similar study reported on the influence of the catalyst type on the morphology and the mechanical properties of CF-CNTs. The authors suggested that the addition of traces of Cu can remarkably enhance the catalytic activity of Fe catalyst, and can lead to hierarchical reinforcements with 12% enhanced tensile strength in comparison to the reference CFs [57].

In order to avoid the interactions of the catalyst particles with the substrate CF at the high temperatures used for the CVD growth, some authors used ceramic barrier coatings onto the CFs before the catalyst deposition. For instance, Gonzaga de Resende et al. suggested the use of an amorphous Si interface during the growth of MWCNT forests onto CFs as an effective barrier for avoiding the Fe catalyst particles diffusion into the CFs and thus preserving the CF tensile properties. Tensile tests indicated that 5 min of growth with the presence of a Si layer maintained the average fracture load in comparison to the reference CFs, while on the absence of the Si layer the fracture load of the CF-CNT severely decreased. The tensile strength although was not calculated and therefore the effects of the changes in the CF diameter due to CNT growth were not considered in this study [58].

In another study, Li et al. also produced hierarchical CF-CNTs by growing a high-yield of radially aligned CNTs onto unsized CF tows via CVD of acetylene over Fe catalyst. The CFs were functionalised with poly(styrene-alt-(dipotassium maleate)) (K-PSMA) in order to avoid catalyst dissolution into the CFs during the CVD process. The tensile strength and the IFSS of the hierarchical reinforcements with the epoxy matrix were preserved [59].

Some alternative CVD processes were also proposed for avoiding the degradation of the CFs mechanical properties due to the aggressive CVD process conditions and the interactions of the CF with the catalyst NPs. Felisberto et al. produced CF-CNTs by a modified thermal CVD method, whereby during growth, the CFs were placed in a region at 420°C - 460°C and the acetylene carbon source decomposed in a further region at 700°C.

The gas flow carried the carbon species from the high to the low-temperature region, due to the temperature gradient inside the CVD chamber, where CNTs grew on CFs. Catalytic nickel NPs were deposited on CFs before growth by a low energy double target DC sputtering system. The authors claimed no detrimental effect in the CF properties as indicated by TGA measurements [60].

Additionally, De Greef et al. demonstrated that the oxidative equimolar dehydrogenation reaction of acetylene and carbon dioxide could lead to the grafting of CNTs onto CFs without degrading the tensile strength of the CFs. This alternative route provided the possibility to grow CNTs at much lower temperatures, i.e. 500 °C and 600 °C, where damages to CFs were reduced. It also led to significantly reduced degradation at temperatures higher than 700°C, when compared with CF-CNTs prepared by catalytic thermal decomposition of ethylene [61]. The tensile properties of the CF-CNTs produced by this process were maintained equal to the reference CF tensile properties. Additional large defects were not created as indicated by the Weibull modulus during the equimolar reaction, and the process was found to heal already existing defects partially. This process was precisely controllable and thus suitable for up-scaling [62].

The most recent novel study, which addressed the same problem, was presented by Anthony et al. who applied a potential difference between the CFs and a graphite foil counter electrode (300 V, generating an electric field ca $0.3\text{--}0.7\text{ V }\mu\text{m}^{-1}$) during the CVD growth of CNTs onto CFs. The potential difference enhanced the uniformity of the CNT coating and limited the damage of the CFs, thus eliminating the requirement for protective barrier coatings and effectively inhibiting the degradation of the in-plane

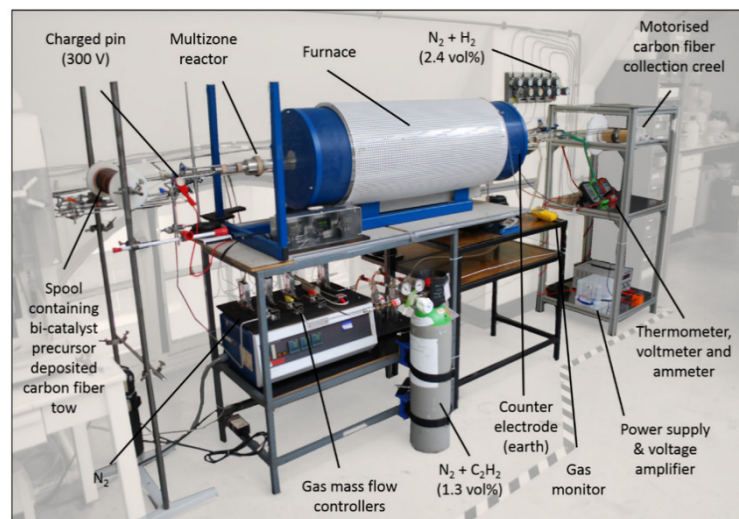


Figure 4. Continuous CVD set-up for synthesis of CF-CNTs, an overview photograph showing the fiber tow entry and exit from the reactor. Reprinted from [6] under a Creative Commons license. © 2018

mechanical properties of the CFs [63]. The same group extended this study by developing a continuous, open-ended thermal CVD reactor for producing CF-CNTs in a spool to spool process which in principle can be incorporated into traditional CF production processes (Figure 4). The process resulted in the production of CNTs with diameter ca. 10 nm and length ca. 125 nm, while it did not affect the underlying CF tensile strength [6].

In general, the thermal CVD process, which was used by most authors, led to thick and uniform coatings of CNTs onto the fibrous substrates, resembling the one presented in Figure 5, which altered the substrate CF diameter to some degree. The increased coating thickness was a result of the relatively high growth rates, i.e. 10

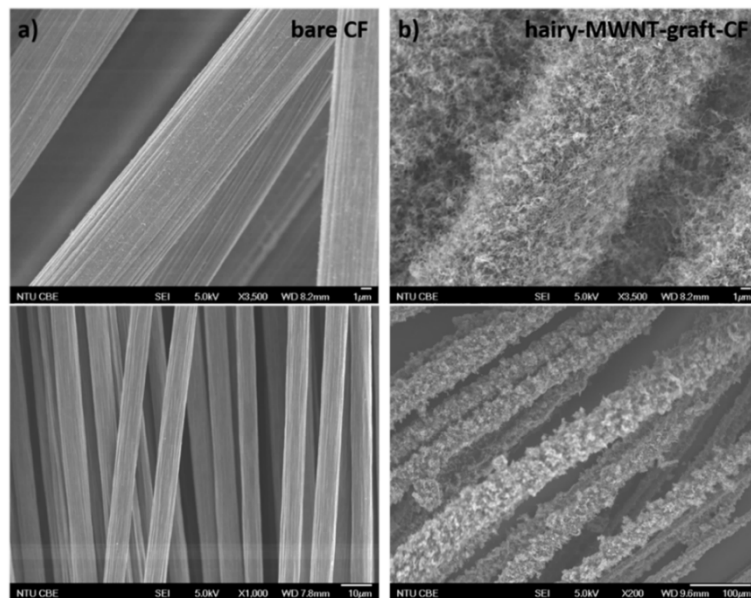


Figure 5. FESEM images of bare CFs (a) after desizing by Soxhlet extraction and (b) hairy CF-CNTs grown by CVD. Reprinted with permission from [22]. Copyright 2017 American Chemical Society.

$\mu\text{m}/\text{min}$ for the thermal CVD [64]. On the other hand, when the process conditions were not optimised the CFs were not covered entirely by CNTs [65]. While in many cases other nano-morphologies, as well as some amorphous carbon, were also present on the surface of the CFs, mainly depending on the presence of sizing on the substrate CF, the characteristics of the catalyst and the growth temperature [54]. Furthermore, most of the studies which utilised CVD for the production of hierarchical reinforcements have somehow examined and in many cases optimised the growth temperature and duration [37,43,48,66–69].

Different CVD processes were also used in order to improve the CNT deposition on CF substrates. Specifically, aerosol assisted CVD was demonstrated by An et al. to produce

MWCNTs onto the CF surface where ferrocene dissolved in acetone was fed into the CVD reactor in the form of an aerosol by a precision metering pump [46,49]. The floating catalyst method, where the metal catalyst was injected in gaseous form into the CVD system, and the CNT growth occurred as the catalyst particles were floating and falling to the substrate, was also demonstrated to be effective for the growth of MWCNTs onto CFs [24]. This method was also called injection CVD and was demonstrated by several authors as suitable to control CNT thickness and orientation [22,33,70,71]. This process was also proved feasible to grow vertically aligned CNT forests of controlled lengths (Figure 6) directly on CF surfaces [48].

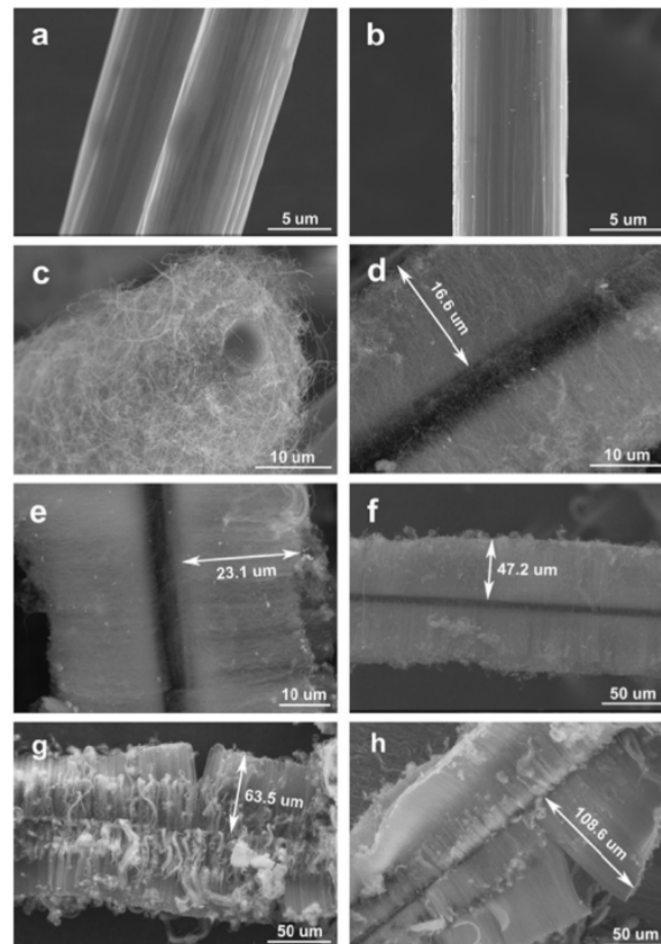


Figure 6. SEM images of unsized CFs (a) before and (b) after the surface treatment, and CFs grafted by (c) entangled MWCNTs and (d–h) aligned MWCNTs with different length controlled by the growth time. Reprinted from [48], with permission from Elsevier.

The hierarchical CF-CNTs were developed in all cases in order to be used as reinforcements in polymer matrix composites. Therefore, upon their incorporation in

polymeric matrices, the in-plane and the out-of-plane mechanical properties of the manufactured composites were studied either at the single fibre level, at the tow level or the laminated composite level. For the assessment of the interfacial properties at the single fibre and the tow level, composites were prepared by impregnating a single CF or a CF tow into a polymeric resin and these composites were referred to as “model” composites in order to be distinguished from the laminated composites which were manufactured by using CF fabrics or woven textiles.

Riccardis et al. qualitatively demonstrated the strong anchorage of the CNTs grown onto the CF substrates by CVD by subjecting the hierarchical reinforcement to several stressing environments (immersion, magnetic stirring, centrifugation and ultrasonic bath sonication) [72]. A similar approach was adopted by An et al. who demonstrated the strong adhesion between CFs and CNTs via ultrasonication of the CF-CNTs. The ultrasonication, in this case, caused a decrease in the “composite” fibre diameter (from 19.1 μm to 10.5 μm), which was attributed to the removal of non-graphitized carbon and some catalyst particles resulting in higher ordering of the sonicated CNTs, as proved by Raman measurements. In this study, the CF-CNTs were produced by an aerosol-assisted CVD method, where H_2 was added into the carrier gas during the CVD growth for narrowing of the diameters of the produced CNTs (22 μm after 40 min of growth). The size of the catalyst particles was shown to regulate the CNT diameters which grew via a tip growth mechanism. These hierarchical reinforcements presented a 10% degradation of the tensile strength of the CF [46].

The grafting force between the CNTs and the CFs in the hierarchical CF-CNT reinforcements produced by CVD were quantified by Wang et al. who used a SEM with a nano-manipulator AFM tip to measure the grafting

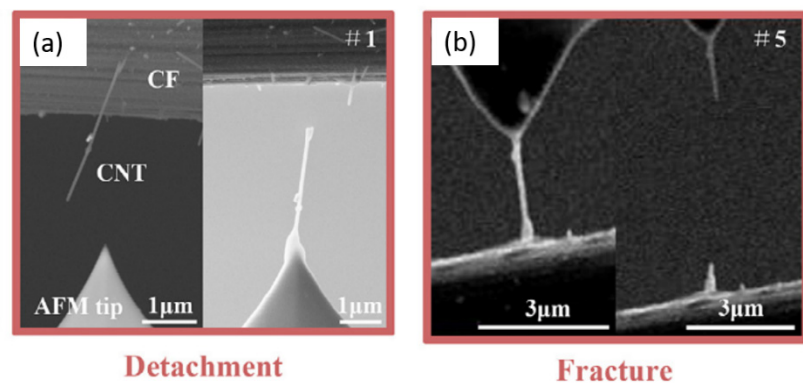


Figure 7. (a) SEM image for the detachment of CNT, the left image is from prior to attaching AFM tip onto CNT, and the right image presents that the CNT was detached from CF surface. (b) SEM image for the fracture of CNT. (Reprinted from [65]., Copyright (2014), with permission from Elsevier.

forces between a single CF and individual CNTs (Figure 7). These forces were strong enough in order to sustain the fracture of the CNTs while their other end was still attached on the CF surface. Force values up to 8.5 μN were measured, while the average failure strength was equal to 40 GPa. However, the wettability of the CF-CNTs decreased due to the deposition of the catalyst. These competing processes with regards to the interfacial properties led to only a 30% increase in the IFSS (microdroplet test) of the CF-CNT model composites in comparison to the reference model composites. The experimental results were also accompanied by an analytical model which was developed in order to predict the effects of CNT/CF grafting force on the interfacial improvement and showed good agreement with the measured values [65].

The IFSS of the hierarchical model composites was evaluated by several authors, and a wide range of values can be found in the literature. Specifically, relative improvements in the IFSS of the hierarchical model composites in comparison to the IFSS of the reference model composites ranging from 10% and up to 108% were reported [47,49,50,52,66,73–76]. Notably, some studies reported even higher improvements in the IFSS, i.e. 134% [69], 175% for model composites with aligned grown CNT arrays onto the CFs [48] and an extraordinary enhancement of 470% by [39]. Conversely, the IFSS of the hierarchical model composites produced by Kim et al. who grew radially aligned CNTs onto CFs were preserved in the same values as the reference CF model composites [59], similarly to the IFSS of the hierarchical model composites prepared by Anthony et al. via the continuous CVD reactor which was discussed in detail above [6].

It is also interesting to note that, according to Sager et al. the IFSS of model hierarchical composites with CNTs randomly oriented onto the CFs exhibited a higher improvement (71%) compared to the IFSS of model hierarchical composites with aligned CNTs onto the CFs (11%) with regards to the reference model composites [53]. Conversely, Lv et al. noticed a much higher enhancement in the IFSS for the model hierarchical composites with aligned CNTs onto CFs (175%) compared to the IFSS for the model hierarchical composites with entangled CNTs onto CFs (28.2%) with regards to the reference model composites [48].

The enhancements in the IFSS of the hierarchical composites in comparison to the reference model composites were mainly attributed to increased surface area, enhanced

wettability and mechanical interlocking and the emergence of additional fracture mechanisms due to the presence of the CNTs in the interfacial region.

Unfortunately, the assessment of the mechanical properties of hierarchical CF-CNT laminated epoxy composites, where the CF-CNT reinforcement was produced by CVD, was only reported by a few authors. The lack of much experimental evidence might be attributed to the difficulty of this processing method to be applied in large CF substrates since most of the CVD reactors used in laboratory scale have restricted volume. For this reason, some studies which used other matrices than epoxies will also be reported in this section.

With regards to the in-plane properties of hierarchical laminated composites, Sharma and Lakkad evaluated the tensile strength of UD laminates manufactured with CF-CNTs produced by CVD. The tensile strength of the multiscale composites increased by 69% as compared to the reference composites which had undergone similar heat treatment as the CF-CNTs. [77]. In another study, Mathur et al. used CVD to grow CNTs onto UD CF tows, 2D CF cloth and 3D CF felt [78]. The hierarchical reinforcements were used for the manufacturing of phenolic composites with increased tensile strength (up to 75% and 66%) and modulus (up to 54% and 46%) over the CF cloth and felt, respectively [78].

With regards to the out-of-plane mechanical properties of hierarchical laminated composites, Kepple et al. evaluated the mode I fracture toughness, G_{IC} , of woven CF laminates with grown CNTs, which remained flexible after the growth process. An improvement of 50% was obtained in comparison to the reference CF laminates [79].

In another study, Fan et al. focused on improving the catalyst coating on CFs that were subsequently used for the production of hierarchical reinforcements by CVD growth. The ILSS of CF-CNTs increased by 28.8% compared with the untreated CFs [40].

Samsur et al. also produced CF-CNTs by CVD and manufactured CF-CNT composite laminates by VARTM. The flexural strength and the flexural modulus increased by 34% and 126%, respectively along with a significant reduction in electrical resistivity (from 25 Ω m to 0.2 Ω m) [41].

Khan et al. also assessed the effects of CNTs grafting on the average mechanical properties and mode-II fracture toughness of CFRCs. Two growth strategies were used in a CVD

process, namely type-1 where only the top surface of the fabrics was coated with CNTs, and type-2 where both sides of the CF fabrics were uniformly coated with CNTs. ILSS was improved by 32% and 102% for type-1 and type-2 composites, respectively. Type-2 composites also exhibited increased bending stiffness by 20%, apparent shear strength in 3 point bending by 16% and mode II fracture toughness, G_{IIc} , by 53% over the reference CF laminates. However, due to their radial orientation, the CNTs did not support any load in the CF direction. Therefore no changes were observed in the tensile properties of the hierarchical composites. Fractography revealed a smooth and clean fracture morphology for the reference unsized composites in comparison to a rougher surface with resin remnants attached to the CFs for the type-2 CF-CNT/epoxy composites. The fractographic study indicated that the weakest point was the CNT/epoxy interface while a stronger interconnection existed between the CNTs and the CF [7].

In a series of different publications, Lomov et al. studied the compressibility and the permeability of CF yarns and weaves coated with CNTs and carbon nanofibers (CNFs) by CVD, with regards to the RTM and the VARTM composite manufacturing techniques [80] [81]. The authors demonstrated that high contents of CNT/CNF (39 wt%) on the CF fabric significantly decreased both its compressibility and its permeability, while when the CNT/CNF grafting density was kept low (5 wt%), the permeability was not affected while the compressibility was still severely hampered. Therefore, the authors advised that the change of compaction behaviour of a CF-CNT preform should be taken into account during manufacturing of nano-engineered FRCs since the fibre volume fraction, achievable by compaction under pressure of 0.1 MPa (1 bar), was decreased by 10-15% due to CNT growth. Furthermore, CF-CNT yarns extracted from the CVD grown woven fabrics were studied under successive compression cycles. The addition of the catalyst by simple wet impregnation and the subsequent heat treatment rendered the unsized CFs softer and reduced their waviness as well as their thickness by 16.4%, while at the same time sized tows became more rigid with a thickness reduction of only 1.9%. More pronounced effects on the compressibility of the tows were the result of the CNT growth on both the unsized and the sized CFs. For unsized tows, the thickness under 1 bar pressure increased by 39.7% in comparison to the virgin and the corresponding increase for the sized CFs was 68%. No hysteresis in the compression behaviour of the tows was observed due to CNT grafting. A

previously developed model [82] was also used by the authors for the validation of their results, which led to the conclusion that the change of compressibility due to the CNT growth is an intra-yarn, inter-fibre phenomenon [83].

Regarding the mechanical properties of hierarchical laminated composites with aligned CNTs onto CFs produced by CVD, Kim et al. produced hierarchical CF-CNT epoxy matrix composites and evaluated the mode I fracture toughness. Vertically aligned CNT forests were grown for 30 min by CVD on plain weave CF fabrics, with acetylene as the hydrocarbon source. A Ti adhesion layer (5nm) was firstly placed on the CFs, then an alumina thermal barrier layer (10 nm) was sputtered on top of the Ti layer, and a Fe catalyst film (1nm) was placed by e-beam evaporation onto the alumina barrier layer. These layers induced chemical bonding between the CNT forests and the CFs, while Scotch tape tests confirmed the enhanced adhesion. The mode I fracture toughness of the CF-CNT composites increased by 51% in comparison to the reference CF composites. Both the matrix and interface were toughened due to the addition of the CNT forests, while after fracture CNTs were still attached to the CFs as indicated by fractography (Figure 8) [4].

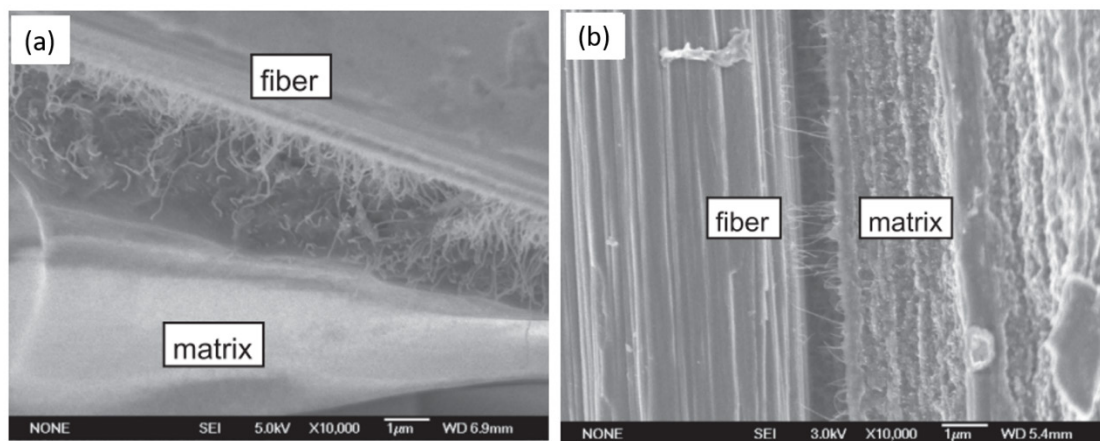


Figure 8. SEM images of fracture surfaces of a hierarchical composite with enhanced adhesion showing CNTs bridging between fibre and matrix. Reprinted from [4], Copyright (2015), with permission from Elsevier.

In another study, Li R. demonstrated that non-covalent functionalization of CFs enabled the catalyst adhesion onto woven carbon fabrics and a low-temperature CVD process for the growth of radially aligned CNTs. The produced reinforcements were used to manufacture hierarchical CFRCs by vacuum assisted epoxy resin infusion. Laminates with 50% microfiber and lower than 1% CNT volume fraction were fabricated and tested by the short-beam shear (SBS) method. The SBS strength was higher for the baseline laminates

on average, with the CNT- reinforced laminates having a lower initial failure that sets the SBS strength. However, all fuzzy CFRP cases exhibited significantly enhanced toughness. These conflicting results were attributed principally to inhomogeneities of the CNT coverage in the produced laminates [84].

Guzmán de Villoria et al. manufactured aerospace-grade UD CF laminates reinforced with high densities of aligned CNTs (A-CNTs) which acted as nano-scale stitches. This kind of reinforcement of the ply interfaces increased the interlaminar fracture toughness in [85] and in this work the laminate in-plane strengths were also increased. The authors observed the suppression of the delamination damage modes associated with pre-ultimate failure in the in-plane loaded laminates. The absence of delamination led to remarkably increased load-carrying capability. Specifically, the tension-bearing (bolt pull out) critical strength increased by 30%, the open-hole compression ultimate strength increased by 14%, and the L-section bending energy and deflection increased by more than 25%. Notably, there was no increase in interlaminar or laminate thickness due to the CNTs addition in comparison to the results presented by Lomov et al. [80,81]. Conversely, in this work, the ~10 nm diameter CNTs interlaced between CFs in adjacent laminae indicating that the observed reinforcement does not stem from the formation of a thicker interlayer but rather from the CNT bridging [86].

Overall, when incorporated in epoxy composites the CVD produced hierarchical CF-CNT reinforcements resulted in a 69% improvement of the tensile strength of UD CF-CNT composites [77]. With regards to the out-of-plane mechanical properties the mode I fracture toughness, G_{IC} , increased by up to 50% [79], while the ILSS was shown to improve by up to 102% [7]. Furthermore, the flexural strength and the flexural modulus increased by 34% and 126%, respectively along with a significant reduction in electrical resistivity (from 25 Ω m to 0.2 Ω m) [41]. Additionally, the bending stiffness improved by 20%, the apparent shear strength in three-point bending by 16% and the mode II fracture toughness, G_{IIc} , by 53% [7]. With regards to aligned CNT-CF/epoxy composites the mode I fracture toughness increased by 51% [4], while more specialized experiments related to the real application of the hierarchical composites showed that the tension-bearing (bolt pull out) critical strength increased by 30%, the open-hole compression ultimate strength

increased by 14%, and the L-section bending energy and deflection increased by more than 25% [86].

Some results regarding CF-CNTs in other than epoxy matrix composites are further reviewed. CF-CNTs were produced by the floating catalyst CVD process by Rahmanian et al. and then used for the fabrication of short fibre–polypropylene composites. Randomly oriented CNTs provided effective micromechanical coupling and improved the efficiency of stress transfer between the fibre and matrix, as indicated by fractography. The hierarchical reinforcements exhibited increased tensile modulus (57%), flexural modulus (51%), flexural strength (35%) and Izod impact energy (34%) compared to the reference short fibre-composites [71].

Hu et al. deposited pyrolytic carbon (PyC) and CNTs onto CFs in order to optimise the interfacial bonding between the CNTs and the SiC matrix. The PyC protective layer weakened the CNT/SiC matrix interfacial strength and led to long pull-out of CNTs compared to the brittle fracture of the uncoated CNTs. A CF-PyC/SiC-(CNT + PyC)-(CNT + SiC) structure was formed using this process, which exhibited enhancement of 39.5% in bending strength, 19.4% in Young modulus, 25.5% in fracture toughness, 17.6% in IFSS, 29.1% in tensile strength and a 75.4 % decrease in nano-hardness [74].

Su et al. produced hierarchical CF-CNT fabrics by CVD which were then used for the fabrication of polyimide-based hierarchical composites which exhibited improved mechanical properties with increasing amounts of CNTs. Notably, the CF-CNT/PI composites, where the CVD growth lasted for 40 min, showed improvements of 33% in flexural strength, 42% in flexural modulus, 17°C in the temperature at 5 wt% of weight loss, 27 °C in glass transition temperature and five orders of magnitude in through-thickness electrical conductivity as compared to the reference PI composites. The authors attributed the overall enhancement to the synergy of different scale mechanisms, nanoscale to macroscale. The CNTs restricted the segmental motion of PI molecules and reinforced the PI matrix at the molecular level. At the single CF level, strong anchoring interactions were established between the CF-CNTs and PI resin, which improved stress transfer. At the bundle and interlaminar level, the CNTs penetrated the matrix-rich regions among individual CFs and between the layers of laminated composites and therefore created electrically or thermally conductive pathways [67].

Bedi et al. also investigated the relationship between the wetting characteristics of hierarchical CF-CNTs produced by CVD and the average mechanical properties when of the CF-CNT/polymer composites compared to the reference unsized CFs and CF/polymer composites, respectively. More effective wetting (smaller contact angle) was achieved in CF-CNT/epoxy composites, while the wetting decreased (bigger contact angle) in the CF-CNT/polyester composites compared to the reference CF/epoxy and CF/polyester composites, respectively. The IFSS was improved by 41% (single fibre pull-out tests) and the ILSS by 80% for the CF-CNT/epoxy composites in comparison to the reference CF composites, while only minor changes were exhibited by CF-CNT/polyester composites [75].

2.1.2. Hierarchical reinforcements produced by wet chemical treatments and their composites

The production of hierarchical CF-CNT reinforcements by wet chemical treatments was firstly reported in 2007 by He et al. who chemically grafted CNTs onto CFs [87]. The chemical process which is schematically depicted in Figure 9 involved hexamethylene diamine functionalised MWCNTs and desized, and acid treated CFs for the covalent grafting of CNTs onto CFs via nucleophilic substitution reaction between amine groups and acyl chloride groups [87]. The IFSS of CF-CNT reinforcements produced by this

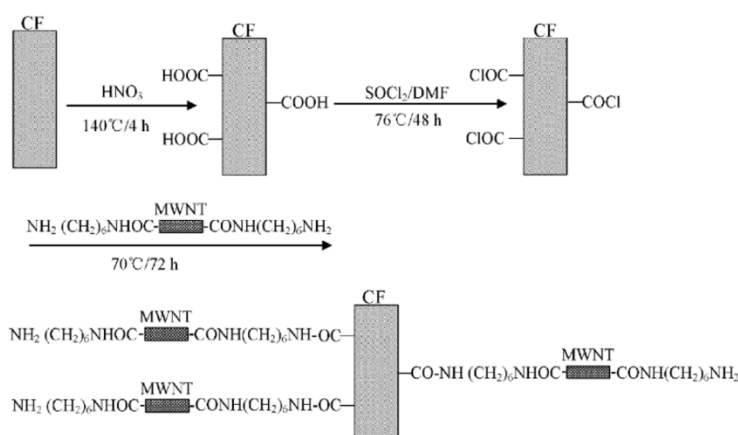


Figure 9. Experimental scheme used to prepare the multiscale reinforcements. Reprinted from [88], Copyright (2007), with permission from Elsevier.

method was 150% higher than the IFSS of the reference CFs, while the main reinforcing mechanisms according to the authors were the chemical bonding, the Van der Waals binding, the mechanical interlocking and the surface wetting [88].

In a more straightforward process by Laachachi et al., the CNTs were acid treated and then dispersed in different solvents (acetone, DMF or toluene) and deposited drop by drop onto the thermally treated in nitrogen and then oxidised in air CFs [89]. CNTs dispersed in acetone solvent were successfully grafted onto CFs by esterification, anhydration or amidization reactions [89]. In this case, although the reactions were not confirmed by any means.

Various authors demonstrated the oxidation of CF as a solution in order to increase the reactivity of the CFs by adding oxygen moieties to their surfaces. However, in many cases oxidation also led to severe degradation of the CF tensile properties. For instance, Vivet et al. grafted commercial MWCNTs on CFs by following a process which included desizing of the CFs at 450°C under a nitrogen atmosphere for 15 min and subsequent oxidation of the CFs at 450°C in the air for 30 min. CNTs were also oxidised in a mixture of sulfuric and nitric acids and then anchored on the CFs by esterification reaction using the Sterling method. In this method, both a coupling agent (dicyclohexylcarbodiimide – DCC) and a catalyst (3-dimethylamino-pyridine - DMAP) were used for preparing a dispersion of the oxidised MWCNTs in dichloromethane with the help of DCC. The catalyst was also used for the preparation of a second solution in the same solvent. Both solutions were then drop cast onto CF tows for the esterification reaction to occur. This method resulted in a 53% degradation of the CF tensile strength due to the oxidation, the strength was partially restored after CNT grafting but never reached the reference CF strength [90].

Li M. et al. deposited carboxylic acid-functionalized and hydroxyl-functionalized CNTs onto two different CF substrates by an aqueous suspension immersion method, without removing the commercial sizing of the CFs. The addition of a non-ionic surfactant, polyoxyethylene octyl phenyl ether (Triton X-100), into the aqueous suspension of the CNTs in order to increase the CNT content in the suspension was also investigated. The authors achieved a thin uniform distribution of randomly oriented CNTs which led to increased surface roughness compared to the reference CF. The deposition of CNTs was affected by the properties of the CNTs, the surface morphology of the reference CF as well as the presence of the CF sizing. The IFSS of the CF-CNT/epoxy model composites increased by 43% for the T700SC with COOH-CNTs, which had more functional groups than OH- CNTs. Interfacial friction, chemical bonding and resin toughening near the

interphase were mainly responsible for IFSS enhancement. The tensile modulus of CF-CNT/epoxy composites remained unaffected while the tensile strength increased from 1459 ± 56 MPa to 1622 ± 65 MPa and the ILSS increased by 13 % [91].

Oxidized CFs and oxidised CNTs were also grafted together by ester linkages via a mild thermal treatment by Tsirka et al. by a simple dip coating procedure. The effects of the oxidation duration, the concentration of CNTs into the acids during the oxidation process and the mechanical aiding of the dispersion on the morphology of the produced hierarchical structures were evaluated. An algorithmic process was followed whereby the studied parameters were evaluated and ranked based on the experimental evidence provided by TGA, XPS, FT-IR and Raman characterisations. Combined experimental findings suggested that two competing mechanisms were simultaneously present during CNT oxidation, i.e. (i) the introduction of oxygen-based functional moieties and (ii) the purification of the CNTs. Optimisation of the aqueous dispersions of CNTs was also performed by measuring the dielectric properties of the dispersion via Electrochemical Impedance spectroscopy (EIS). Then, CNTs were successfully grafted on both oxidised and reference CFs confirming that when a stable electrically percolated dispersion of CNTs is used there is no need for further oxidation of the CFs for the CNT grafting to be achieved. A thin homogeneous veil of CNTs was deposited by this method onto the CFs, and furthermore, the grafting density could be controlled by the dip-coating process [92].

In a similar process, Lavagna et al. dispersed oxidised CNTs in acetone and then deposited them onto the CFs by drop casting. The CNT/CF ratio was evaluated in a parametric study which revealed that a high concentration of CNTs in acetone was needed to cover the CFs fully. The authors also observed spherical nanostructures which formed at intermediate CNT/CF ratios and identified them as carbon nano-onions, comprising a novel multiscale CNT/CNO/CF structure, whereby CNTs acted as ropes interconnecting the CNOs onto the CFs [93].

Other authors grafted oxidised CNTs with amino functionalised CFs towards the production of hierarchical reinforcements. For instance, Li Y. et al. used propodiamine for the functionalization of desized and oxidised CF as schematically depicted in Figure 10. The CNT coating was sparse and very thin with rather short CNTs, while the concentration of the 1,3-propodiamine affected the grafting density. The surface energy increased due to

the CNT grafting on the CFs, as well as the IFSS by 92.2% (37.2 to 71.2 MPa) for a grafting density of 35 per m^2 . This IFSS improvement was attributed to the strong chemical bonding (confirmed by IR and XPS) and the pull out of CNTs from the matrix which was observed by a fractographic SEM study [94].

In a similar approach, Zhao M. et al. grafted oxidised CNTs onto amino functionalised CFs by a layer by layer grafting process.

This method resulted in successive thin layers of CNTs, treated by melamine in order to

increase the amine groups. XPS confirmed the bonds between CFs and CNTs. Single fibre tensile tests showed slightly increased fibre strength. IFSS increased due to the CNT grafting especially for double layer CNT/CF structures (117%). Impact strength also increased by 49.8% for triple layer CNT/CFs in comparison to the reference CFs. SEM confirmed the morphology (increasing CNT homogeneity and thickness with the increasing number of CNT layers), and the failure mechanisms which were acting during the fracture process. Significantly more cracks were observed in the CNT/CF composites, and resin remnants were bound on CFs after single fibre pull-out in comparison to the reference CF-epoxy composites [95].

Several coupling agents were also examined by different research groups in an attempt to increase the bonding between CFs and CNTs and therefore the CNT coating density onto the CFs. Polyamidoamine (PAMAM) dendrimers, Poly (acryloyl chloride) (PACl), 3-aminopropyltriethoxysilane (APS), Polyvinyl Alcohol (PVA), polyhedral oligomeric silsesquioxane (POSS) were all demonstrated as active coupling agents for the efficient grafting of CNTs onto CFs, towards hierarchical reinforcements and composites with improved mechanical properties.

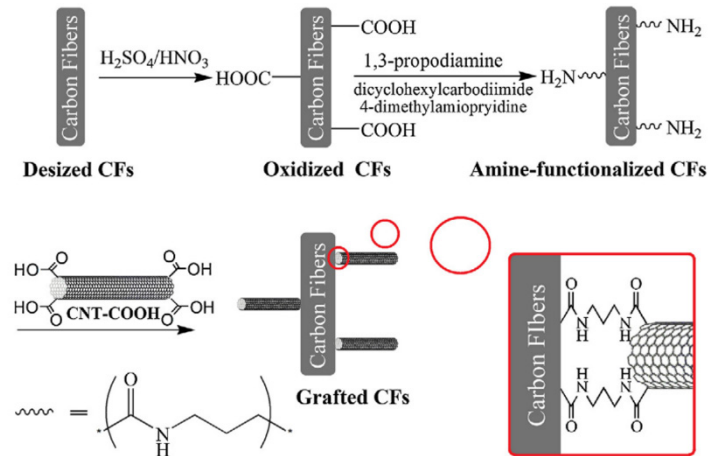


Figure 10. Experimental scheme used to synthesize CF-CNTs through a series of processes such as desizing, oxidising, amine functionalising and CNTs grafting. Reprinted from [94], Copyright (2013), with permission from Elsevier.

In more detail, PAMAM dendrimer as the coupling agent was efficiently used by Mei et al. in a grafting procedure which resulted in a scarce grafting of really short CNTs on CFs surfaces. The authors evaluated only the functional groups (XPS, IR) and the morphology of the CNTs (SEM) [96]. In a later publication, Mei et al. measured a 176% improvement in the IFSS of a model epoxy composite in comparison to the unsized T300 CF model composite [97]. The authors also performed molecular simulations which indicated that the interaction energy of the CF-CNT hierarchical composite was 2.7 times higher than the reference, due to both the chemical adhesion of the matrix to the fibre and the mechanical interlocking due to the presence of the nanotubes [97].

PAMAM dendrimer in the presence of a coupling agent (HATU) was also used by Peng et al. in order to demonstrate a uniform grafting of short oxidised CNTs onto the surface of desized and then oxidised CFs (Figure 11) [98]. The IFSS decreased by 8.5% upon oxidation of the CFs, while both the sequential deposition of PAMAM and CNTs onto the oxidised CFs increased IFSS by 56% and 36%, respectively. The authors attributed these enhancements to chemical bonding and the increased mechanical interlocking [98].

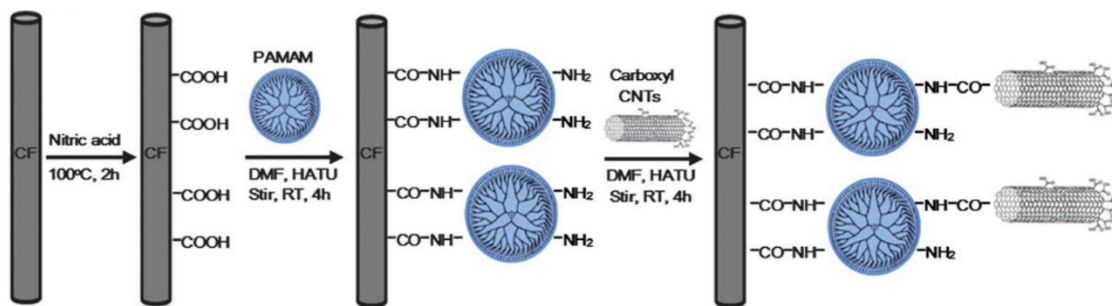


Figure 11. Schematic representation of the grafting procedure of carboxyl functionalised CNTs onto acid oxidized CFs by the use of PAMAM. Republished with permission of *Journal of materials chemistry* by Royal Society of Chemistry, from [98], Copyright (2012); permission conveyed through Copyright Clearance Center, Inc.

Chen et al. focused on improving the tribological properties of CF/epoxy composites by grafting CNTs onto the CFs with the use of PAMAM as the bridging agent. This process resulted in a thin and sparse deposition of CNTs onto the CF surfaces, whereby PAMAM macromolecules with multiple amino groups were firstly chemically and physically adsorbed onto the surface of oxidised CFs, and then, functionalized CNTs were successfully grafted onto the CFs by reacting with the PAMAM. The friction and wear properties of the hierarchical composites were improved due to increased mechanical

interlocking and chemical bonding interactions between the CF-CNT and the epoxy matrix, which protected CFs from being pulled out under shear stresses during the wear process. CNTs were also undertaking some of the applied load on the CF surface and thus protected the CFs from being broken due to stress concentration [99].

Poly (acryloyl chloride) (PACl) was also demonstrated as a coupling agent by Wu et al. for uniformly grafting a high density of CNTs onto CFs. Further, grafting with undecylenic alcohol produced chemical bonds between the CF-CNTs and the unsaturated polyester matrix. The surface energy and mechanical interlocking were improved, and this led to a 44.5% increment in ILSS and a similar enhancement in impact toughness of the composites [100]. This approach was reproduced later by Lv and Peng, leading in almost identical results [101].

Wu et al. proposed 3-aminopropyltriethoxysilane (APS) as the bridging agent for uniformly grafting CNTs on CFs. The authors used the hierarchical reinforcements for manufacturing methylphenylsilicone resin composites and evaluated their interfacial properties and heat resistance. The formation of chemical bonds between the CNTs and the CFs was confirmed by FTIR and XPS measurements. The surface energy and the wettability of the CF-CNTs increased significantly, leading to the ILSS and the impact toughness enhancement by 53.10% and 33.17%, respectively in comparison to the reference CFs. CF pull-out and interfacial de-bonding were not observed during fractography for the composites with hierarchical reinforcements in comparison to the reference composites. Also, the hierarchical composites outperformed the reference composites both in thermal stability (TGA studies) and the heat oxidation resistance (thermal oxidative ageing experiments) [102].

In a similar approach, Rong et al. grafted MWCNTs dispersed in Polyvinyl Alcohol (PVA) onto the surface of CFs and then subjected the grafted CFs to a thermal treatment (30min at 800°C under N₂ atmosphere), leading to the formation of chemical bonds between the CNTs and CFs [103]. The authors observed 21% enhancement in the tensile strength of CFs due to CNT grafting and attributed this improvement to the remediation of the surface defects and the reduction of the stress concentrations due to the excellent dispersion of CNTs on the surface of the CFs and the strong interfacial bonds. The formation of chemical bonds, although was not supported by any evidence [103].

Zhao and Huang focused on the chemical grafting of CNTs onto CFs by the use of polyhedral oligomeric silsesquioxane (POSS). The authors used CF oxidation in nitric acid and a series of steps including reactions in EDA, THF, EDC and DMAP for several hours (39 hours) for achieving the final CF-POSS-CNTs. Short CNTs homogeneously covered the CF surface, and the chemical grafting resulted in no apparent degradation of the tensile strength and an improvement of 105% of IFSS measured via single fibre pull out experiments [104]. In another publication, the same authors reported that the CF-POSS-CNT reinforcements exhibited maintained CF tensile strength and the produced hierarchical epoxy composites showed considerably increased ILSS (by 36%) and impact resistance compared with the untreated CFRCs [105].

Some years later Zhang et al. also co-grafted CNTs and POSS on CFs in order to improve the interfacial properties of CF/epoxy matrix composites. A very thin layer of CNTs was grafted onto CFs as confirmed by FT-IR, TGA, XPS and SEM measurements. The wettability and the dynamic contact angle measurements indicated an increase in the surface energy and the number of functional groups present on the CFs after CNT deposition. Also, the ILSS of the CF-CNTs-POSS composites was improved by 31.6% compared to the reference CF composites due to the mechanical interlocking caused by the CNTs [106].

Furthermore, both cationic and anionic polyelectrolytes, i.e. poly(diallyl dimethyl ammonium) chloride (PDAC), Polyethyleneimine (PEI) and Poly (4-styrene sulfonic acid) sodium salt (SPS), were successfully employed by Kamae and Drzal for producing a stable dispersion of UV oxidised CNTs [107]. Subsequently, these dispersions of CNTs were used for the coating of CFs by a simple dip-coating process. The authors practically demonstrated that by making use of the attractive forces between the cationic electrolyte treated CNTs and the negatively charged CFs, uniform CNT coatings onto the CF surfaces could be obtained. The basic requirement for the prevention of aggregation during the condensation (drying) process was a substantially strong positive charge which was achieved both for the PDAC, and the PEI treated MWNTs. The IFSS values for sized CFs were notably high, and comparable to the PDAC and PEI treated CNT-CFs mainly due to limited debonding, while the most pronounced IFSS was exhibited by the PEI treated CNT-CFs [107].

Additionally, a two-step diazonium coupling procedure from in situ generated diazonium salts was proposed by Liu et al. to covalently attached CNTs onto CFs. In this process, β -cyclodextrin was encapsulated for controlling the density and regularity of the CNT layers. The process was performed in an aqueous solution which permits scalability and lasted for only some minutes but resulted in a thin coverage of the CFs with CNTs. The CF-CNTs exhibited increased tensile strength (9.55%), rougher surfaces and enhanced interfacial adhesion (114% in IFSS) with the epoxy matrix in comparison to the pristine and amino-functionalized CFs [108].

In a similar approach, Wang et al. grafted CNTs onto CFs by a two-step aryl diazonium reaction, whereby aminated CFs were grafted with CNTs using isoamyl nitrite. The chemical grafting was confirmed by Raman, FT-IR, and XPS measurements. The surface roughness and the surface energy of the CFs increased remarkably after grafting of CNTs, which also led to a 104% increment in the IFSS of the CF-CNT reinforcements in comparison to the reference CF. The tensile strength of the CF-CNTs also increased by 8.69% compared to the reference CFs [109].

Moreover, Chen X. et al. proposed a novel and efficient in-situ template polymerisation method for assembling poly(cyclotriphosphazene-co-4,4'-sulfonyldiphenol) (PZS) functionalized CNTs onto CFs. The IFSS of the PZS-CNT-CF/epoxy composites improved by 26.4% due to better wettability and increased mechanical interlocking in comparison to the CF/epoxy composites. The tensile strength of the PZS-CNT-CF also improved by 6.6-16.3% compared to the reference CF, due to the healing of the surface flaws and defects of the CFs by the PZS-CNT deposition [110].

Another interesting study was presented by Dong et al. who studied the effects of physical drying with chemical modification of CNTs, on the through-thickness properties of CF/epoxy composites. The authors immersed CFs into a dispersion of CNTs and polyvinyl pyrrolidone in water prepared either by sonication or magnetic stirring. Then, the CFs were dried by either heat drying or freeze drying to investigate the resulting CNT organisation in CF-CNT preforms and composites. Extended aggregation was observed when the heat-drying method was used accompanied by randomly scattered CNTs, while when freeze drying was employed, continuous CNT networks were always assembled. The authors named this formation mechanism of the CNT networks as “freeze drying within confined

space". Furthermore, both non-functionalized CNTs (NOCNTs) or hydroxyl-modified CNTs (OHCNTs) were studied. The OHCNTs formed networks exhibited significantly higher electrical conductivity (78%) than composites with CNT aggregates and scattered CNTs. The ILSS increased by 11.3% (freeze-drying) in composites with NOCNT networks and by 8.1% (heat drying) in composites with scattered OHCNTs, whereas composites with OHCNT networks (both heat and freeze-dried) showed slightly enhanced flexural strength and modulus [111].

Overall, the wet chemical route for the production of hierarchical CF-CNT reinforcements and their polymeric composites was demonstrated as an easy and industrially relevant process. However, until recently the CNT grafting density for wet chemical processes was low (Figure 12a) for most studies except for the study presented in [107] (Figure 12b), while only recent studies achieved higher and controllable grafting densities resembling the ones presented in Figure 13. The mechanical properties of the substrate CF were either not affected [104] or even increased up to 21% [103,108–110], except in the study by Vivet et al. where severe degradation of the strength of the CFs was observed [90].

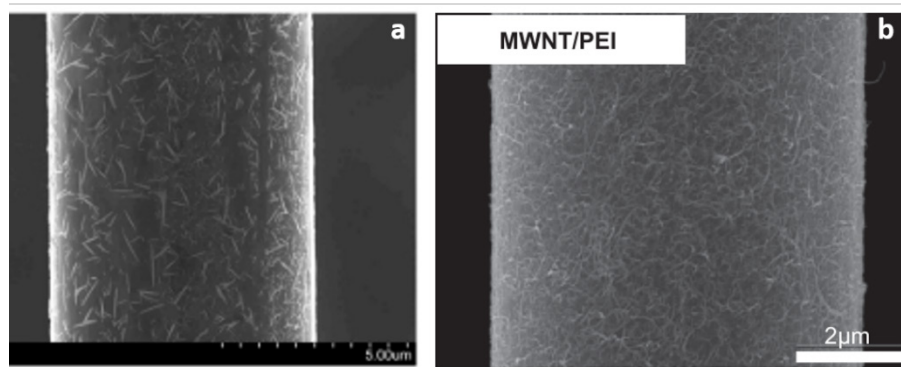


Figure 12. SEM micrographs of a) a CF-POSS-CNT hierarchical reinforcement, Reprinted from [105] Copyright 2011, with permission from Elsevier, and b) a sized hierarchical CF coated with PEI polyelectrolyte treated UV/O₃ MWNTs. Reprinted from [107] Copyright 2012, with permission from Elsevier.

Regarding the interfacial mechanical properties, the hierarchical reinforcements produced by several wet chemical treatments are at least comparable and in most cases outperformed the CF-CNT reinforcements produced by CVD. To put that conclusion into numbers, the observed improvements in IFSS ranged from 92.2% [94] to 176% [97], with several studies reporting IFSS values in between this range [88,95,104,109], while only three publications reported IFSS enhancements lower than 50% [91,98,110]. At this point an

interesting study should be noted, in which Deng et al. designed and performed a novel twin-fibre single-lap joint test for the determination of the IFSS of CF/epoxy and CNT-CF/epoxy composites with a standard micro-mechanical testing machine [112].

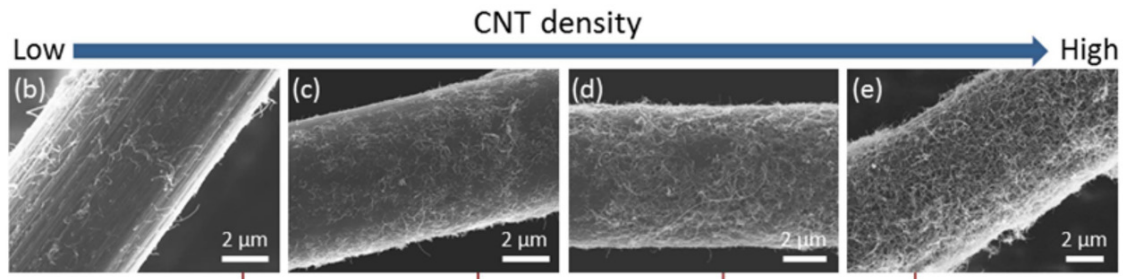


Figure 13. SEM micrographs of hierarchical CFs with increasing grafting densities of CNTs. Reprinted from [112] Copyright 2018, with permission from Elsevier.

In this study, the CF-CNTs were prepared by esterification reactions between CNT-COOH and CF-OH. A 153% improvement in IFSS was measured for CF-CNT/epoxy composites over the reference CF/epoxy composites [112]. It was also shown that by increasing the grafting density of CNTs (10.9, 25.8, 35.1, and 58.8 CNTs per μm^2) the IFSS also further improved by 51%, 101%, 155% and 273% compared to the reference CF/epoxy. Furthermore, a multi-scale theoretical model was demonstrated for predicting the IFSS of CF-CNT/epoxy composites. This model correlated the micro-scale IFSS to the nano-scale CNT grafting strength as obtained by in situ SEM pull-out tests. There existed a good correlation between the measured and the predicted IFSS values for specimens with different grafting densities [112].

Islam et al. [113] presented an interesting comparison of the aforementioned CNT grafting strengths between a single CNT and a CF in hierarchical CF-CNT composites produced by wet chemical treatments and ester linkages, as measured by the SEM pull-out tests by to other existing similar measurements. Islam et al., measured grafting strengths of 25-30 GPa in comparison to the 5-90 MPa measured by He et al. for hierarchical reinforcements produced by the wet chemical treatments with a PAMAM coupling agent [114]. Furthermore, Wang et al. measured an average grafting strength value of 40 GPa for CNTs in hierarchical CF-CNT composites produced by the CVD process. These values demonstrate that the chemical grafting process by the use of ester linkages provides

stronger bonding than the chemical grafting process by the use of dendrimers, but weaker bonding in comparison to the CVD approach.

To summarise the out-of-plane mechanical properties of laminated CF-CNT/polymer composites where the CF-CNT reinforcements were produced by wet chemical treatments were also improved in comparison to the reference CF/polymer composites. Specifically, the deposition of CNT-COOH on sized CFs by an aqueous suspension immersion method resulted in 13% improvements in the ILSS of CF-CNT/epoxy composites [91]. The use of POSS in hierarchical CF-POSS-CNT reinforcements led to a 32-36% enhancement in the ILSS as well as to a 33% improvement of the impact toughness of the hierarchical laminates [104] [106]. A more notable enhancement was observed in the ILSS of CF-CNT/polyester composites (44.5%) and CF-CNT/methyl phenyl silicone composites (53.1%), where PACl and APS, respectively, were used as the coupling agents for the preparation of the CF-CNT reinforcements [100,102]. The same composites also exhibited a 44.0% and a 33.2% enhancement in the impact toughness, respectively [100,102]. A 50% increase in the impact strength was also observed in CF-CNT/epoxy composites where the reinforcements were produced by the layer by layer grafting of oxidised CNTs onto amino-functionalized CFs [95].

2.1.3. Hierarchical reinforcements produced by Electrophoretic deposition (EPD) and their composites

EPD is a two-step deposition process, where charged particles dispersed in a suitable solvent are migrating towards the surface of an electrode under an applied electric field (first step - electrophoresis). These particles are deposited on the electrode via coagulation and their accumulation results in the formation of a homogeneous and rigid deposit (second step-deposition). A schematic representation of the process is depicted in Figure 14. In EPD suspensions with relatively low solid contents can be used, providing processing and handling advantages, while the method can be applied to dispersed solid particles with small sizes (<30 μm). Deposition occurs only on conducting surfaces, and therefore CFs can be used as electrodes and coated with NPs during EPD [115].

In 2007, Bekyarova et al. demonstrated for the first time that EPD was successful in producing randomly oriented coatings of both MWCNTs and SWCNTs onto CFs [116]. The manufactured composites exhibited a 27% increment in the interlaminar shear strength (ILSS) and significant enhancement in the electrical conductivity in comparison to the reference composites [116].

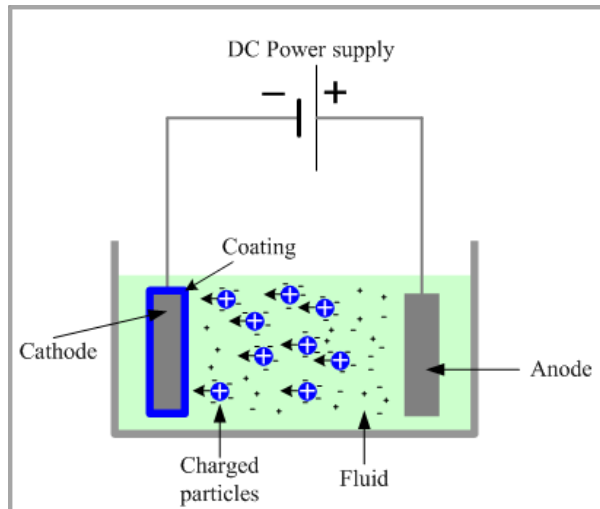


Figure 14. Schematic representation of the EPD process. Reprinted from www.subtech.com.

The deposition of carboxylic-

functionalized CNTs onto CF tows using EPD with ethanol as the solvent was demonstrated by Guo et al., as a scalable and continuous method for the production of hierarchical composites [117]. These hierarchical reinforcements exhibited improved tensile strength by 16% and Weibull modulus by 41% in comparison to the reference CFs [118]. Furthermore, a decreased surface energy and enhanced wettability by the epoxy resin led to 68.8% increments of IFSS [118].

In a later work, Guo et al. focused on the problem of water electrolysis which caused non-uniform deposition of CNTs onto CFs during the EPD process [119]. The authors demonstrated that ultrasonication assisted EPD could overcome this problem and lead to a uniform deposition of acid oxidised CNT networks onto the CFs. Moreover, the CF-CNT reinforcements exhibited increased tensile strength, by 16%, and Weibull modulus, by 40.7%, in comparison to the reference CFs. With a dense deposition of CNTs, the IFSS was improved by 65 % (from 68.8 MPa to 113.6 MPa), due to increased surface roughness (AFM measurements) and mechanical interlocking [119].

During the same year, An et al. from the same research group produced CF-CNTs by chemically grafting the ozone-treated CNTs with a polyethyleneimine (PEI) dendrimer via EPD. The IFSS and the fracture energy of the CF-CNTs were significantly increased by 70% and 80%, respectively, due to the increased amounts of CNTs that occupied the resin-rich interlaminar regions [120]. Representative images of the CF-CNTs without and with

the application of ultrasonication, as well as after the treatment with PEI dendrimer are presented in Figure 15.

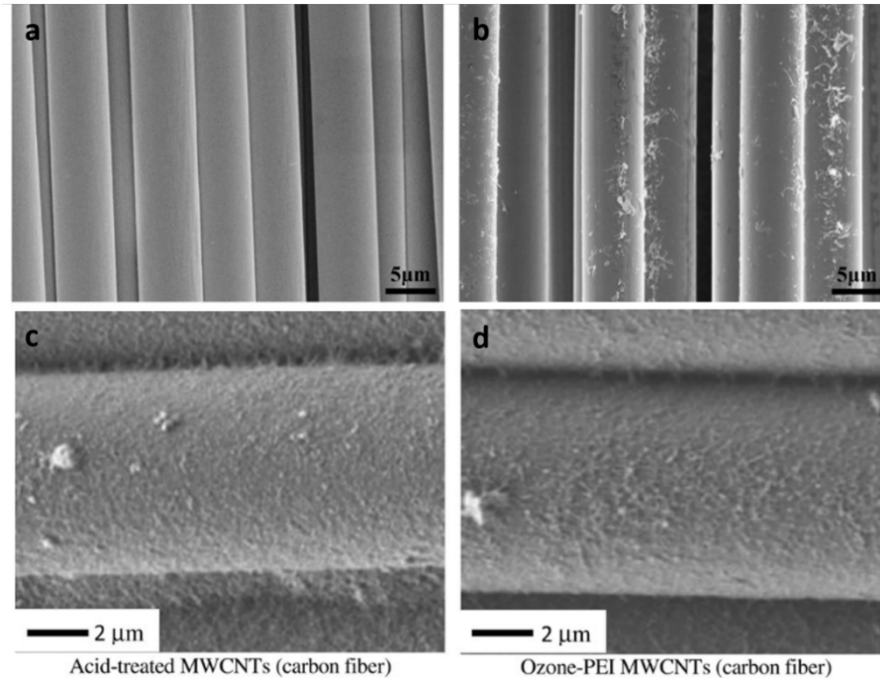


Figure 15. SEM images showing carbon fibres a) before, b) after simple EPD process, c) after ultrasonically assisted EPD with acid functionalised MWCNTs and d) after ultrasonically assisted EPD with ozone-PEI treated MWCNTs. Reprinted from [117] and [120], with permission from Elsevier.

Jiang et al. also produced CF-CNTs by ultrasonically assisted EPD. The CF-CNTs exhibited increased surface roughness and a higher amount of polar groups (C=O and C-O) in comparison to the reference CFs, while the CNTs formed a uniform coating on the CFs [121].

Zhang et al., in 2013, proposed an easy and effective way to prepare hierarchical CF-CNTs by combining EPD with a sizing step into a continuous process which is suitable for industrial applications. Acid-treated MWCNTs suspended in dimethylformamide (DMF) was used during EPD with an annular electrode, and phthalazinone ether ketone (PPEK) was used for the sizing process. This method produced a sparse coating of short CNTs tightly attached to the CF surface after the PPEK sizing application. Enhanced wetting and IFSS by 35.6% compared to re-sized CF reinforced PPEK model composite were measured [122].

All the subsequent studies also examined the mechanical properties of laminated composites. For instance, Moaseri et al. produced hierarchical CF-CNTs by EPD of acid-functionalized MWCNTs on CFs followed by immersion in a 10% solution of petroleum pitch in toluene and then pyrolysis under N_2 . A uniform deposition was achieved which resulted in up to 120% enhancement of the tensile strength and a 100% increase in the elastic modulus of the CF-CNT/epoxy composites compared to composites reinforced by the reference CFs. Fractography indicated a robust interlocking between the epoxy matrix and the CF-CNTs [123].

The same authors in a later study proposed the application of alternating and direct electric fields in combination, in order to deposit amino-functionalized MWCNTs radially on CFs by EPD. A uniform thick and porous layer of CNTs was achieved by this process which also preserved the mechanical properties of the CFs. Enhanced interfacial adhesion resulted in a remarkable increment in the tensile strength of CF-CNT/ epoxy composites (126%) in comparison to the reference CF composites. Notable improvements were also observed in the fatigue life of CF-CNT composites especially in the low-stress, and the high-cycle regimes. Debonding was identified as the primary failure mechanism during the fracture of both the CF-CNT/epoxy and the reference CF/epoxy composites by fractography [124].

Battisti et al. produced hierarchical CF-CNTs by EPD on oxidised CFs and then measured the ILSS of the composites with double-notch compression specimens. The amount of the deposited CNT coating essentially depended on the applied current with a maximum around 1 A. Up to a 40% improvement was measured, but the enhancement did not correlate with the amount of deposited CNTs. Thus, other factors besides CNT deposition affecting the interfacial properties were investigated by SEM. Interface roughening was observed for both CF-CNTs and oxidised-only CFs, but only little interaction between CNTs and CFs was evident. The IFSS was quantified by quasi-static single fibre push-out measurements and was found unaffected by the deposition of CNTs. Similarly, the interfacial toughness as assessed by cyclic loading–unloading during the CF push-out test was found unaffected. However, the interfacial friction after fibre debonding changed significantly with CF-CNTs possessing higher frictional energy dissipation than the reference CFs. This suggested increased plasticity of the CF-CNT, possibly due to the high

loading of CNTs in the interphase, which was also confirmed by finite element simulations which accounted for friction when reproducing the load-displacement plots from CF push-out [125].

Mei et al. also produced hierarchical CF-CNTs via EPD on oxidised CFs. CNTs were uniformly grafted to the carboxyl functional groups on the CF surfaces with strong interactions which overcame the aggregation tendency of the CNTs. The increased roughness of the CFs after CNT deposition resulted in improved adhesion between the matrix and the hierarchical reinforcements. The tensile strength, the failure strain and Young's modulus of the hierarchical composites increased by 35.7%, 21.7%, and 70.0%, respectively, in comparison to the reference composites. Additional reinforcing mechanisms due to the presence of the CNTs depended on their bridging ability, while two pulling-out modes were identified. Specifically, for a strong bond between the CNTs and the matrix or the CFs, CNTs fractured partially or completely, while for a weak bonding, CNTs were separated from the matrix or the CF surfaces [126].

The same authors in another study used commercial carboxyl modified CNT solutions during the EPD process, while after the CNT deposition, the CF-CNTs were impregnated with a bisphenol A dicyanate ester (BADCy) resin. The EPD process duration (2, 6 and 10 min) was examined as a parameter during this study. Hierarchical composites were manufactured with increased tensile strength by 45.2% (for an EPD duration of 2 min) in comparison to the reference composites. The presence of CNTs enhanced the CF-epoxy interface while CNT pull-out from the matrix was identified as the main toughening mechanism. Conversely, the flexural strength of the hierarchical composites decreased gradually with EPD duration due to the stress concentration built between CNT-free and CNT-rich matrix regions, which weakened the adhesion between CF fabrics and therefore promoted delamination failure. According to the authors, CNTs enhanced the micro interface but weakened the macro interface of the composites [127].

In an alternative approach, Moaseri et al. studied the effect of electrostatic repulsion on the mechanical properties of MWCNT-CF/epoxy composites [128]. The authors deposited CNTs on CFs by the EPD process and then applied a high-voltage direct electric field in order to radially relocate the deposited CNTs onto the CF filaments (Figure 16). The tensile strength and the elastic modulus of the hierarchical composites improved by 157 %

and 70 %, respectively, in comparison to the reference CF composites. The mechanical properties of the hierarchical composites were dependent upon the applied voltage and the process duration. Furthermore, fibre pull-out was significantly decreased, and transverse cracks at the interfacial region were eliminated in the failure process of the hierarchical composites in comparison to the reference composites. The authors attributed these changes during failure to increased mechanical interlocking between the hierarchical CF-CNTs and the epoxy matrix [128].

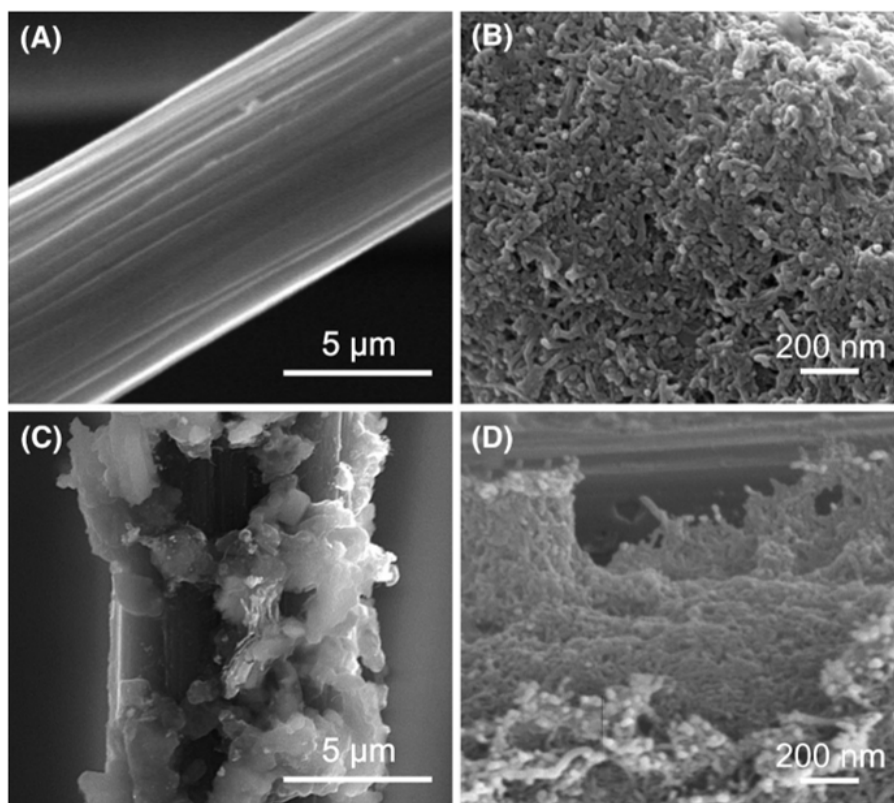


Figure 16. Surface SEM images of a) as-received CF, b) hierarchical CF-CNT, c) hierarchical CF-CNT with radial alignment (low magnification), d) hierarchical CF-CNT with radial alignment (high magnification). Reprinted by permission from Springer Nature, *Applied Physics A: Materials Science & Processing*, [128], © Springer-Verlag Berlin Heidelberg 2016.

The same authors also deposited aminated CNTs onto CFs via EPD and then radially aligned the CNTs onto the CFs by applying a high electric field making use of the strong repulsion forces between the tubes. The CNTs were also introduced in the epoxy matrix separately to reinforce the rest of the matrix. Upon application of a high electric field, the mechanical properties of the composites were remarkably enhanced, i.e. by 193% in tensile

strength and 86% in elastic modulus. This enhancement was attributed to the radial alignment of the CNTs on the CFs, which however was not confirmed by SEM images. Fractography confirmed the enhanced interfacial adhesion between the CF-CNT hierarchical reinforcement and the epoxy matrix [129].

Sui et al. used a continuous EPD process for introducing a transition layer of oxidised CNTs onto CFs in order to synergistically improve the interfacial and fatigue-resistant performance of CF/epoxy composites. This transition layer exhibited intermediate modulus as indicated by SEM/EDS and force modulation AFM measurements and was the critical factor for the synergetic improvement of interfacial and fatigue performance of CF/epoxy composites, according to the authors. The IFSS, ILSS, flexural strength and modulus of the hierarchical composites were improved by 33.3%, 10.5%, 9.4% and 15.4%, respectively. Moreover, under certain experimental conditions (5 min EPD), enhanced damage resistance was observed for the hierarchical composites in comparison to the reference composites indicated by a 4.5% increase in the residual bending strength retention. The CNT-toughened transition layer was detected by energy dispersive X-ray spectroscopy and AFM in force mode and was thought responsible for the enhanced interface by reducing stress concentration and diverging destructive cracks along multiple paths, therefore, enhancing the damage resistance [130].

Xue et al. reported the production of hierarchical CF-SWCNTs by EPD, the authors also incorporated a hexahapto-metal complex, $\text{Cr}(\text{CO})_6$, leading to the production of a novel hierarchical structure, CF- $\text{Cr}(\text{CO})_6$ -SWNTs, in order to improve the IFSS of the hierarchical reinforcements with the epoxy matrix. The orientation of the deposited CNTs was dependent on the applied voltage during the EPD process. Low voltages (30V) led to a few randomly oriented SWCNTs onto the CFs, medium voltages (50V) led to SWCNT forests radially aligned on the CFs, while high voltages (70V) produced dense randomly oriented SWCNT networks on the CFs. The authors identified possible coordination between SWNTs and CF due to the presence of Cr by the intensity changes in RBM and the wavenumber shift of G- band in the Raman spectra. The coordination resulted in the reconstruction of the electronic structure due to the replacement of the Van der Waals forces by a chemical complexation bonding between the tubes and the CFs. These chemical alterations resulted in 193% improvement in the tensile strength of the CF-

Cr(CO)₆-SWNTs epoxy composite in comparison to the referenced desized CF/epoxy composite and 19% compared to CF-SWCNTs/epoxy composite. The heat resistance of the CF-Cr(CO)₆-SWNTs/epoxy composite was also improved due to the introduction of the Cr element as indicated by TGA measurements [131].

Lee et al. developed a CNT/Cu hybrid structure by applying a cathodic EPD process whereby ionised copper and CNTs were simultaneously deposited onto CFs. Since copper particles grew dominantly at the CNT crossing sites and linked the separated tubes, therefore a mechanically strong and highly conductive formicary-like hybrid network was established. CFRCs were fabricated using VARTM by these CNT/Cu-CFs, resulting in a 50% enhancement of the in-plane electrical conductivity and an improvement of 15% in ILSS [132].

In a similar study, Yan et al. produced CNT-Cu-CF composites by effectively depositing CNTs and copper on the surface of CFs by a simple and low-cost EPD process, with an aim to improve the thermal conductivity and interfacial characteristics of CFRPs. Cu particles and CNTs generated networks and bridges with each other, thus producing continuous heat conduction pathways and significantly enhancing both the specific surface area and the roughness of the CF surface. As a result, the thermal conductivity and ILSS of the CNT-Cu-CF/epoxy composites increased by 292% and 39.5%, respectively, compared with CF/epoxy composites [133].

Overall, the EPD process was demonstrated as another effective technique for the deposition of CNTs onto CFs towards the production of hierarchical reinforcements. This process was shown not to degrade the tensile properties of the substrate CFs, therefore, leading to increments of the tensile strength and modulus of the CF-CNT/epoxy composites up to 193% and 100%, respectively [129] [123]. The incorporation of the hierarchical reinforcements produced by this method into epoxy matrix model composites enhanced the IFSS by up to 70% [120], while the ILLS of laminated CF-CNT/epoxy composites also increased by up to 40% [125].

2.1.4. Recent and advanced techniques for the production of hierarchical reinforcements

2.1.4.1. Spraying and electro spraying processes

The spraying process was also demonstrated by several authors as an industrially scalable technique for the efficient production of hierarchical reinforcements and their composites. According to this method, CNTs are dispersed in a solvent or polymer and then sprayed onto CF fabrics. Furthermore, all the studies which utilised the spraying method have reported on the mechanical properties of laminated hierarchical composites, since this production process permits working on large CF substrates.

Almmuhammadi et al. were the first authors who performed spraying of functionalized MWCNTs on CF preregs and manufactured composites in order to increase the mode I interlaminar fracture toughness. Double Cantilever Beam (DCB) specimens were employed for fracture testing. The CF-CNT/epoxy composites exhibited a 17% enhancement in the propagation fracture toughness, mainly due to the ability of the nano-reinforcement to spread the damage through CNTs pull-out, peeling and bridging. Hence, the modifications in the fracture mechanisms were mostly observed at the micro-scale, while only slight modifications were induced in the macroscopic mechanisms of failure and this limited further enhancement in the fracture toughness.

Additionally, SEM imaging and Raman mapping (Figure 17) were employed to

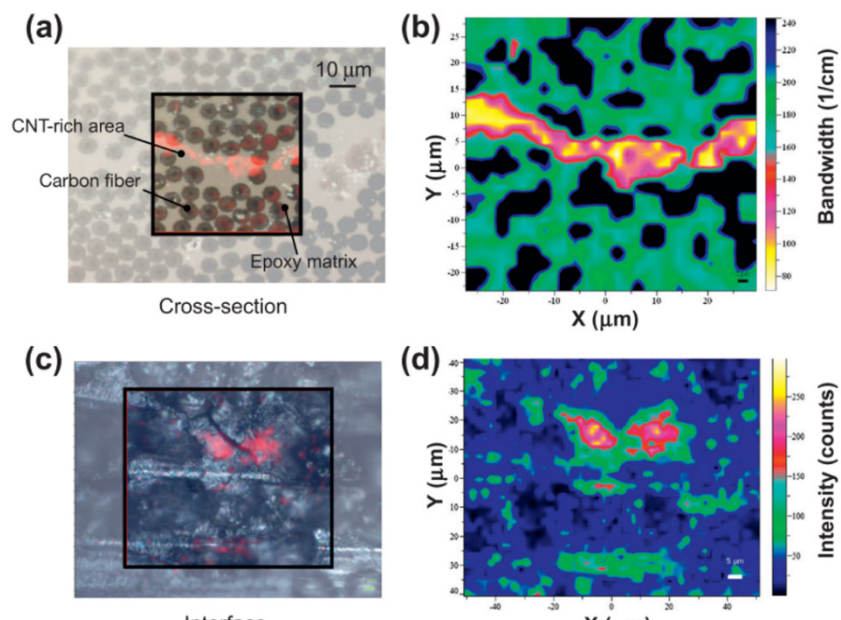


Figure 17. Raman mapping of the interfacial and cross-sectional regions. (a) Optical microscopy image of the probed cross-sectional region; (b) Raman spectral scan of the image showing CNTs (pink and yellow color) located at the interface with thickness of 4 - 14 μm; (c) optical microscopy image of the probed interfacial region; (d) Raman spectral scan of the image showing CNTs (red color) at multiple locations along the interface. Reprinted from [134]. Copyright 2014, with permission from Elsevier.

evaluate the failure process along the cross-sectional fracture surfaces which permitted quantification of the actual penetration of the CNTs within the adjacent prepreg layers. A 10 μm thick CNT-rich layer was observed, while the propagating cracks were often diverted from the nano-reinforced to the plain epoxy matrix [134].

The spraying method was also reported by Zhang et al. who used an airbrush system to deposit a CNT in ethanol solution onto CF prepreg with the potential of localised deposition to damage prone zones. Deposition of CNTs within the inter-ply regions led to an enhancement of 22% and up to 47% in the Mode I interlaminar fracture toughness of CF-CNT/epoxy composites with CNT concentrations of 0.02 wt.% and 0.047 wt.%, respectively. Moreover, the manufactured composites were evaluated regarding the damage-sensing functionality for the structural health monitoring of their integrity. Stable electrical resistance sensing signals were recorded during Mode I tests which revealed a good correlation between the crack propagation and the electrical resistivity [135].

Lee et al. also produced hierarchical reinforcements by spraying a CNT/Polyacrylonitrile (PAN) solution in DMF on CF woven fabrics, followed by a stabilisation process of PAN at 300 °C for 3 h. CF-CNT composites were manufactured by VARTM with an epoxy resin matrix. The CF-CNT composites exhibited a 22% enhancement in tensile strength in comparison to the reference CF composites. The CNTs hindered the propagation of micro-cracks and micro-delamination around the CFs and the CF yarn boundaries as indicated by fractography [136].

MWCNTs were also sprayed on CF fabrics by Chaudhry et al. They studied the effects of the amount of the deposited CNTs on the Mode I Interlaminar fracture toughness of woven CFRCs by double cantilever beam tests. Several CNT loadings, ranging from 0 g/m^2 to 4.0 g/m^2 by an increment of 0.5 g/m^2 , were sprayed on the surface of woven CF prepreg. CFRCs were then manufactured with an out-of-autoclave process. Fractography revealed a uniform distribution of CNTs in the interlaminar surface. It was observed that small CNT loadings improved the interlaminar fracture toughness due to the additional energy required for the breakage of the CNTs by the propagating crack. Specifically, 1.0 g/m^2 of CNTs enhanced the fracture toughness by 32% in comparison to the reference CFRC. Conversely, when the CNT loading increased beyond 1.0 g/m^2 , a consistent decrease in the

fracture toughness was observed, which was attributed to the slippage among CNTs causing the initiation of micro-fracture in the matrix [137].

In a recent publications Yao et al. grafted multi-walled CNTs and vapour-grown carbon nanofibers (VGCNFs) with poly(styrene-co-maleic anhydride) (SMA) and poly(glycidyl methacrylate) (PGMA) by free radical polymerisation. The polymer grafted fillers were used as the secondary reinforcements in multiscale CFRCs, by simply suspending them in ethanol and spraying them onto the surface of CF fabrics. Interestingly, the polymer-grafted VGCNFs with much larger diameters and lower grafting ratios were more effective reinforcements than the polymer-grafted CNTs; and the SMA-grafted VGCNFs were more effective than the PGMA-grafted VGCNFs. The addition of only 0.4 wt% of SMA-grafted VGCNFs notably increased the ILSS by $\sim 73\%$ and the flexural strength by $\sim 21\%$. This enhancement was attributed to the straightness and large aspect ratio of SMA-grafted VGCNFs which led to a strong interaction with the epoxy matrix [138].

The spraying method was recently modified in a novel study by Li Q. et al. who extended the method in an electro spraying process (Figure 18) [139]. The equipment consisted of a stainless-steel needle which was connected to a precision high voltage power supply and a steel platform as the ground electrode. A maximum applied voltage of 50 kV could be delivered to the needle with a resolution of 0.1 kV. The inlet of the needle was connected

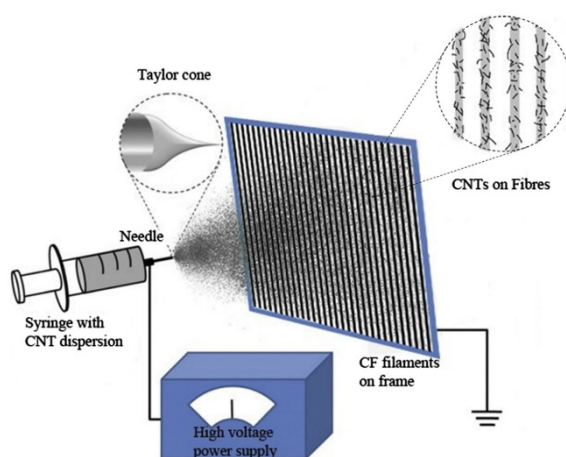


Figure 18. Schematic representation of the electro spraying of CNTs onto carbon fibres. Reprinted from [139], Copyright (2016), with permission from Elsevier.

via silicone tubing to a hypodermic needle fitted to a 6 mL syringe which was placed firmly in a precision syringe pump delivering a constant 2 mL/h flow rate. The electro spray atomization of CNT dispersions with a binder was adequate for the controllable deposition of CNTs onto CFs. The applied voltage was identified by high-speed camera observations as the factor which determined the mode of electro spray. Electric field simulations by the finite

element method suggested that the electric field was concentrated around the CF collectors. Both the applied voltage and the spraying distance affected the CNT orientation by mediating the anchoring strength and the force of the electric field. Additionally, the temperature of the substrate affected the droplet size and the solvent evaporation rate and also led to different orientations of CNTs. It was demonstrated that a binder with appropriate wetness gave freedom to the CNTs, and allowed them to orientate radially on the CFs. Moreover, the coating efficiency (the amount of CNTs coated onto CFs for a specific spraying duration) onto single CFs was much higher than onto CF bundles. Linear density (LD) measurements and thermogravimetric analysis revealed that a 10 min coating increased the LD of a single CF filament by up to 31.7% while a 1 h treatment increased fibre bundle mass by 1% [139].

The same authors subsequently investigated the effects of the electro-spraying process temperature and duration, the applied potential difference and the target distance, on the morphology and the mechanical properties of the produced reinforcements and the interfacial mechanical properties of the manufactured hierarchical composites [140]. The electrospray process did not affect the tensile strength of the CFs nor did it introduce more new weak points to the CF, as indicated by the Weibull modulus. Moreover, the IFSS of the CF-CNTs, especially for those prepared using potential differences to target distance ratios of 10 kV/5 cm at 100°C and 20 kV/10 cm at room temperature and 100°C, were improved by up to 124% as indicated by the SFFT. The interfacial reinforcing mechanism was identified using several surface measurements. Particularly, good wettability, significant increases in roughness, friction and BET surface area, especially for the sample prepared by 20 kV/10 cm at 100°C, and increased dispersive surface energy were observed for the hierarchical CF-CNTs in comparison to the reference CFs. Moreover, the fibre pull-out length and the size of the delamination zones between the CF and the matrix were notably decreased due to the CNTs as indicated by fractography. Adhesive failure was the mainly observed mode which always occurred at the interface near the CFs in these hierarchical structures, with the CNTs being bonded with the resin after failure. Therefore, this was the weakest point in the composite structure, and further improvements in the IFSS could likely be obtained by selecting a suitable binder to strengthen the connection between the CNTs and the CFs [140].

Overall, the spraying technique was demonstrated as an efficient and scalable process for the preparation of hierarchical reinforcements and composites with moderately enhanced mechanical properties, in comparison to the hierarchical reinforcements produced by wet chemical processes or CVD.

2.1.4.2. The flame method

The flame method is another recent technique used for the production of hierarchical reinforcements, where the CNTs are directly grown on CFs with a Ni catalyst in an ethanol flame. This process was developed by Du et al. in 2012, who immersed CFs into a NiCl₂ catalyst solution for 60 s, dried the CFs at 90 °C and then inserted the CFs into an ethanol flame for 300 s [141]. The temperature of the flame was measured at 700 °C with a K-type thermocouple, where CNTs were formed onto the CFs by the ethanol flame. The reducing atmosphere in the flame preserved the CFs from decomposing. Furthermore, the thickness and density of the CNT coating were affected by the concentration of the catalyst while the process also exhibited a catalyst selectivity, i.e. Ni²⁺ was effective for the CNT growth while Fe³⁺ was not effective. Furthermore, the authors measured the grafting force of a single CNT onto the CF, into a SEM with an AFM nano-manipulator, to be as high as 307 nN [141].

These grafting force values were comparable to the grafting forces measured by He et al. for CF-CNTs produced by wet chemical treatments with a PAMAM coupling agent (from 57 and up to 950 nN) [114], but were lower than both the grafting forces measured by Islam et al. for hierarchical CF-CNT reinforcements produced by wet chemical treatments and ester linkages (from 588 and up to 2141 nN) [113], and the grafting forces measured by Wang et al. for CF-CNTs produced by the CVD process (from 4255 and up to 8504 nN) [65].

The flame method (acetylene flame and ferrocene as the catalyst) was used by Guignier in a series of publications in order to produce hierarchical CF-CNT reinforcements. The authors studied the frictional properties of the CF-CNTs with a linear reciprocating tribometer and identified the wear mechanism which indicated a plastic behaviour for the CNTs. The presence of CNTs increased the coefficient of friction (higher friction

resistance) for the first 30 cycles in comparison to the plain CFs. The wear mechanism in detail included a transfer film formation from the CNTs after the first five cycles, which acted as a lubricant and diminished the friction resistance. This film was cracked after 25 cycles and then removed from the CF surface after around 50 cycles of friction, indicating a good adhesion between the CNTs and the CF [142].

Guignier et al. in a more extensive study focused on the behaviour of CF-CNTs under friction and adhesion stress with regards to catalysts with different particle size used during CNT growth by the flame method. The use of thicker catalyst particles, which led to CNTs with bigger diameters, exhibited increased friction resistance in comparison to the thinner catalyst particles, which led to CNTs with smaller diameters. Upon application of a normal

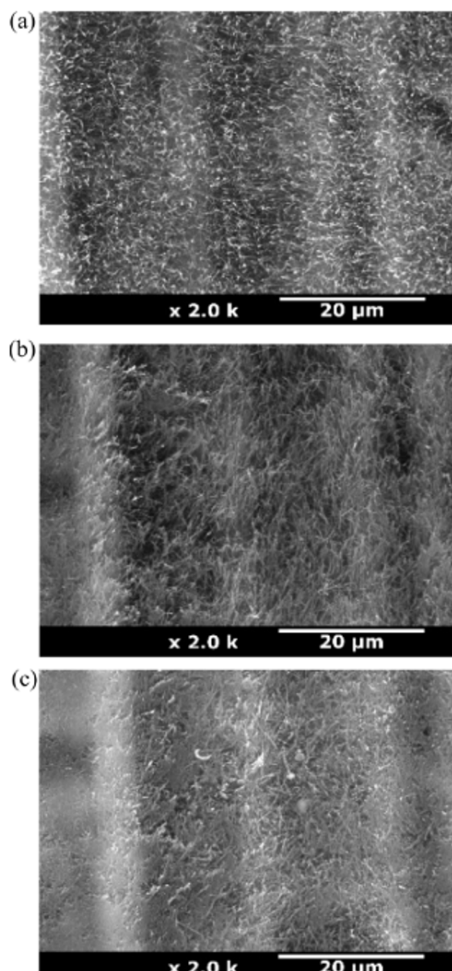


Figure 19. Evolution of the CNT during the first cycles of friction: (a) before friction, (b) after the first cycle of friction, (c) after 10 cycles of friction. Reprinted from [144], Copyright (2018), with permission from Elsevier.

load higher than 1 N during the friction test, the thin CNTs were removed after 2000 cycles of friction, while the thick CNTs were still present on the CFs. Furthermore, the adhesion test was performed with a spherical indenter which was covered with an adhesive tape. The indenter subjected the CF fabrics to loading-unloading cycles and recorded the load required for the removal of the CNTs from the CF fabrics. In general, CNTs were quite resistant to removal. Conversely to the frictional behaviour, a greater adhesion between the CNTs and the CFs was observed for the thinner catalyst particle size (CNTs with smaller diameters) and was attributed to the presence of fewer defects in the CNT structure which resulted in higher tensile properties [143].

Furthermore, in a more recent study, Guignier et al. examined the effects of the stresses, such as friction and pull-out, which are typically developed by winding and unwinding processes, during the industrial-scale use of the CF-CNT reinforcements produced by the flame method, when the method is

applied as an assembly-line process. In an attempt to determine the behaviour of the CNTs under these kinds of stresses and to study their consequences in composite processing, the authors performed adhesion and friction tests as well as wettability measurements on CF-CNT wraps. The authors found that the frictional forces increased significantly (47%) for CNTs with bigger diameters. The surface of the CF-CNTs before and after the friction tests are depicted in Figure 19. Moreover, adhesion forces of CNTs to the CFs surface also increased by 111% when a few defects were present on the CNTs. A transfer film was formed during friction which although did not alter the chemical composition nor the wettability of the CF surface [144].

2.1.4.3. Introduction of the CNTs into a polymeric sizing

An alternative approach for introducing CNTs onto CFs is the dispersion of CNTs into a sizing/coating polymer and the subsequent application of this sizing onto the CFs. This approach does not lead to purely hierarchical structures but is more relevant to the matrix modification in the locus of the interface. Some examples are presented for comparison purposes.

Yu et al. dispersed 0.05 wt% CNTs into silane coating and deposited this nano-modified coating onto CFs, to observe a 26.3% increase in the IFSS in comparison to CFs with a plain silane coating. For comparison, an 18.1% increase in IFSS was observed by dispersing 0.1 wt% CNTs into the epoxy matrix. Crack-bridging and interface-interlocking acted simultaneously in the CNT-modified composites, while the chemical bonding due to the silane coupling agent had the most pronounced effect in augmenting the IFSS for CF-CNT composites [145].

Along the same lines, Yao et al. proposed a process, whereby several sizing treatments were applied on CFs for producing hierarchical CF-CNTs by a continuous and straightforward method which can also be applied in industrial scale. The authors identified a gradient transition interphase by SEM/EDS and force modulation AFM studies of the hierarchical composite interfaces. The content and distribution of CNTs in the interphase affected the interfacial properties of the hierarchical composites. The thickness of the gradient interphasial region and the resulting mechanical properties of the

composites increased when the thickness of the uniformly distributed CNTs on the CF surface increased by more repetitions of the sizing treatment. A 13.45% improvement in ILSS along with a 20.31% enhancement in the flexural strength was obtained for the hierarchical composites with five repetitions of the sizing treatment in comparison to the virgin CF composites. However, further sizing treatment led to the deterioration of the mechanical properties due to the CNT agglomeration [146].

Zhou et al. studied the effect of the distribution and content of the CNT reinforcement on the strength and fracture behaviour of CFRCs both experimentally and numerically. The authors added CNTs into the matrix or the polymeric sizing of the CFs and then manufactured and tested Short Beam Shear specimens. SEM was used to evaluate the damage evolution in the composites. The reference CFRCs exhibited delamination cracks soon after getting into the nonlinear stage in the load-deflection curves as the primary damage mechanism. These cracks propagated along the CF axes direction at the composite interfaces until breakage and final failure. The addition of the CNTs into the CF sizing improved the fibre/matrix interface bonding. When CNTs were added only in the CF sizing, the delamination damage began in the interface between the CF sizing and matrix and was strongly dependent upon the distribution of the CNTs in the sizing. On the other hand, integration of the CNTs in the matrix improved the bonding of the CF sizing and matrix, and hence the toughness and the resistance to the propagation of the delamination cracks. This was exhibited as a long nonlinear stage in the load-deflection curves, leading to an increase of ILSS by 77% in comparison to the reference composite. The addition of CNT in the fibre sizing enhanced the toughness by 36%-53% in comparison to the reference composite, while the addition of CNTs in both the CF sizing and in the matrix increased the ILSS by 42%-88%. These results were in agreement with the results of computational simulations. The authors concluded that the strongest reinforcement was achieved when small concentrations of CNTs in the polymer matrix were accompanied by high contents of CNTs in the CF sizing [3].

2.1.4.4. Other advanced techniques

An advanced technique for the fabrication of multiscale hierarchical composites consists of the pre-growth of high quality aligned CNT forests by CVD onto a planar substrate and their subsequent transfer onto CF preregs. This technique was demonstrated as early as 2008 by Garcia et al., who placed the CNT forests onto the middle layer of a 24-ply composite laminate manufactured by unidirectional (UD) prepreg carbon tapes, in order to assess the effects of the aligned CNT forests (average height of 60 μm) on the mechanical properties of the composites [85]. The four-point bending technique was used on end notched flexure specimens which exhibited a 1.5-2.5 x enhancement in the Mode I fracture toughness and a 3 x improvement in Mode II fracture toughness compared to the reference composite laminates [85].

In an alternative approach, Carley et al. grew CNTs onto glass fibres which were then introduced as interlayers in CF/epoxy laminated composites. This approach led to an increment of 85% of the peak tensile stress. After the failure, the CNTs were distributed between and around the CFs and also exhibited crack bridging (Figure 20). Cracks between CFs (adhesive failure) were observed in composites with light interlayers (52.50 and 64.75 mg of CNTs), while the cracks were found on the CFs (cohesive failure) for heavier CNT interlayers (136.50 mg and 185.50 mg). CF breaking was the primary failure mode for even higher CNT loadings (206.30 mg), and a strong bond between fibre/CNTs was observed by SEM [147].

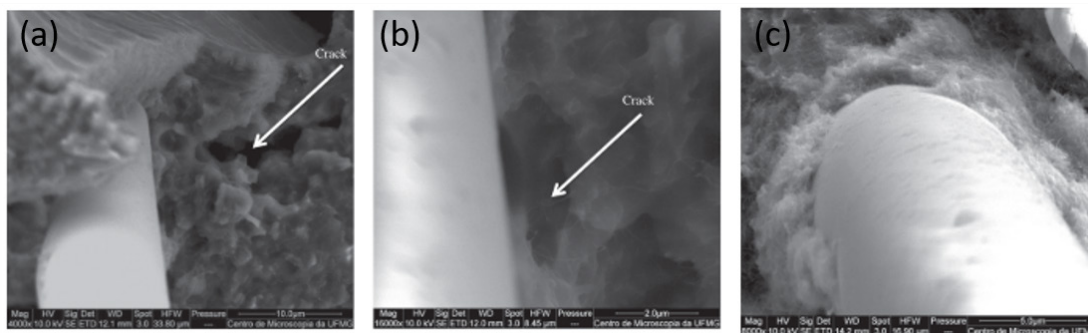


Figure 20. Hybrid laminated composite with CNT inter-layer. (a) Fiber/CNTs for 52.50 mg; (b) Fiber/CNTs for 64.75 mg; (f) Fiber/CNTs for 185.25 mg. Reprinted from [147] under a Creative Commons license. © 2013

Some advanced techniques based on alterations of the CVD process were also presented by some authors. For instance, Tehrani et al. proposed a new method, namely graphitic structures by design (GSD) where a low temperature (550 °C), a Ni catalyst and ethylene hydrocarbon were used for the growth of CNTs on CFs under atmospheric pressure. A SiO₂ thermal barrier film was also applied to CFs before CNT growth. The CF-CNTs produced by GSD were compared to CF-CNTs produced by thermal CVD and outperformed them regarding stiffness and tensile strength. Only a 3.5% reduction in the tensile strength of the CF-CNTs produced by GSD was observed in comparison to the reference CFs [148].

Very recently, Kalfon-Cohen et al. in a pioneering study reported the first experimental investigation of two promising composite laminate technologies, namely the use of aligned CNT interlaminar reinforcement of thin-ply UD prepreg-based CF laminates, in a hierarchical architecture termed ‘nano-stitching’. The authors manufactured and tested four laminate configurations, to compare thin and standard thickness plies, as well as nano-stitching of both in order to get insight into the damage progression and how it is affected by each technology separately, and together. A 50% increase in the thickness of the interlaminar region was measured after transferring the aligned CNTs via a transfer printing technique. ILSS was improved by 10% in the thin and a further 5% in the thin nano-stitched laminates compared to the thick reference laminates. A suppression of large matrix-dominated cracks and notably the complete suppression of delamination in the nano-stitched region were observed in nano-stitched thin-ply laminates, by synchrotron-based computed tomography of postmortem specimens. Finite element predictions of damage progression confirmed the ~15% improvement in Modes I and II interlaminar fracture toughness due to the aligned CNTs at the thin-ply interfaces [8].

2.1.5. Comparative studies on the production of hierarchical reinforcements and their composites

Several studies have also been reported in the literature which attempted to benchmark the hierarchical approach with regards to the hybrid approach. Some indicative comparative studies are reviewed in the following paragraphs, which proposed the hierarchical

approach as the most effective nano-modification method for advanced composites with enhanced mechanical properties.

In more detail, Gorbatiikh et al. compared the reinforcing ability of CNTs when they are added in the polymeric matrix, integrated into the polymeric sizing or grown onto the CFs. The authors demonstrated that an 80% enhancement was achieved in the interlaminar fracture toughness of UD CFRCs in comparison to the other modification approaches which resulted in an only small increment of the CFRC toughness [149].

In another study, Zhao Z. et al. produced hierarchical CF-CNT UD composites by EPD as well as hybrid CNT-epoxy UD composites by dispersing CNTs into the matrix in order to benchmark the two most common nano-reinforcing methods of CFRCs, namely matrix modification and interface modification. The hybrid CF/CNT-epoxy composites exhibited improvements in the tensile strength, the flexural strength and modulus by 10.41%, 10.22% and 15.14%, respectively, while the corresponding enhancements for the hierarchical CF-CNT/epoxy composites were 24.42%, 18.43% and 27.01%, respectively in comparison to the reference CF/epoxy composites. Furthermore, the ILSS and the IFSS of the CF-CNT/epoxy increased by 15.47% and 45.2%, respectively in comparison to the CF/epoxy composites, while the matrix modification with CNTs led to only 4.77% and 10.14% improvements in the ILSS and the IFSS, respectively in comparison to the reference CF/epoxy composites. A gradient interface layer between CFs and matrix was observed by EDS, f-AFM and TEM measurements in the CF-CNT/epoxy composites which was absent from the CF/CNT-epoxy composites. This layer was responsible for the superior mechanical properties of the CF-CNT/epoxy composites since it could decrease stress concentration, enhance stress transfer from the matrix to the reinforcements and improve the ultimate performance of the composites according to the authors. Based on these results, the authors proposed the approach of interface modification as more effective towards composites with excellent in-plane and interfacial mechanical properties. On the other hand, the matrix modification approach is more straightforward and compatible with standard industrial techniques, but it leads to a robust interfacial bonding between the functionalized CNTs and the matrix instead of a strong interface between the CF and the matrix [150].

In a similar study, Wang et al. demonstrated that there exists a synergistic effect when combining two CNT networks, namely epoxy matrix nano-modification with SWCNTs dispersed with the aid of a copolymer and "hairy" CFs, deposited with MWCNTs grown by CVD. ILSS enhancement with respect to the reference CF/epoxy system was found for both reinforcing routes when they were applied separately, i.e. by 34.8% for the hairy CF/epoxy and by 10.2% for the 0.2% SWCNTs/epoxy in comparison to the reference CF/epoxy. A more notable improvement was observed for the combination of hairy CF/0.2% SWCNTs/epoxy by 56.3% and hairy CF/0.5% SWCNTs/epoxy by 105% in comparison to the reference CF/epoxy composites [22].

Other studies attempted to compare the effectiveness of different methods towards the production of hierarchical reinforcements and composites. Some of these studies are reviewed in the following paragraphs.

Awan et al. studied the interfacial mechanical properties of hierarchical CF-CNT reinforcements produced via four different methods. CNTs were deposited onto CF fabrics by dip-coating, hand lay-up with a brush, spray coating and EPD. Uniform CNT depositions were achieved in all cases except hand lay-up, but the authors focused on the EPD process since it resulted in a single very thin layer of CNTs onto the CFs in comparison to the dip-coating and spraying which resulted in thick CNT coatings with some CNT aggregates present on the CFs. Therefore, the CF-CNTs produced by EPD were impregnated with epoxy resin for the manufacturing of hierarchical CFRCs. Three-point bending and short beam shear tests were performed in order to assess the flexural and interlaminar shear properties of the composites. The dispersion and deposition of MWCNTs on carbon fibres were retained after the impregnation with epoxy and the flexural and interlaminar shear strengths increased by 15% and 18%, respectively in comparison to the reference CF/epoxy composites. Moreover, fractography indicated that CNT pull-out and CNT bridging were the main reinforcing mechanisms [151].

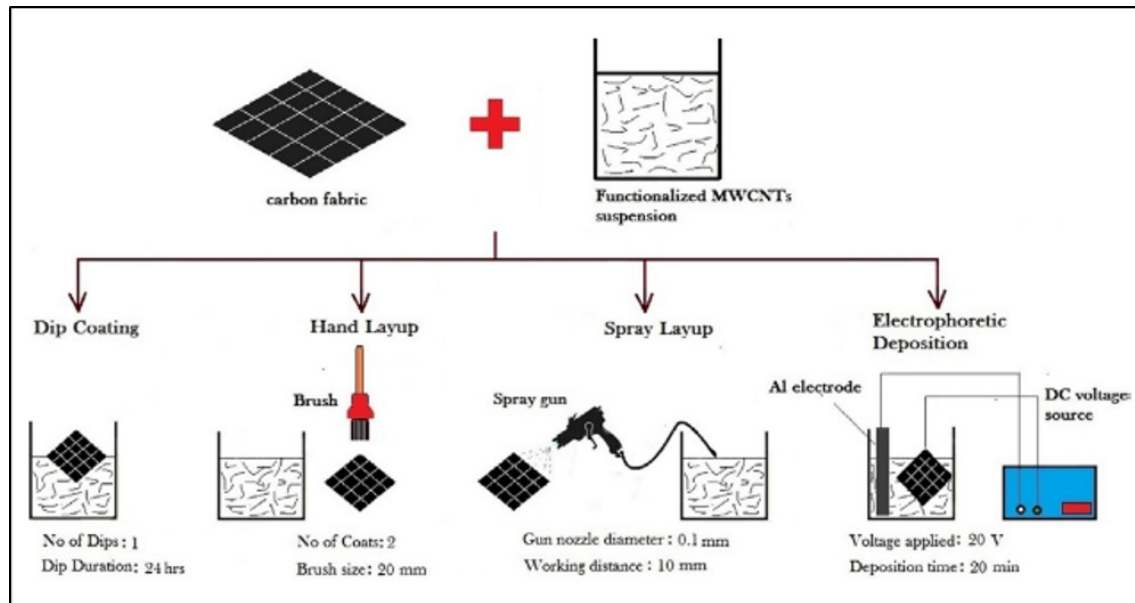


Figure 21. Schematic representation of the methods used by Awan et al. Reprinted from [151], Copyright (2018), with permission from Taylor & Francis Group.

Naito studied several common CF modifications in relation to their effects on the tensile properties of the modified CFs. Naito demonstrated that the following treatments, i) coating with CNTs by CVD, ii) polyimide (PI) dip-coating, iii) PI coating by high T Vapour deposition polymerization, iv) a combination of I and II, and v) a combination of II and III, did not alter the PAN and pitch based CF Young modulus. However, both the tensile strength and the Weibull modulus were enhanced by all the modifications and especially the hybrid ones (iv and v). These improvements were due to the healing of the surface defects while in some cases also the inner defects were remedied [152].

Lutz et al. incorporated CNTs in CF/epoxy composites by growing CNTs onto ex-PAN CFs and by using CNTs in the form of CNT-fibers and investigated the synergy between CNTs and CFs. IFSS was improved by 87% and 104% upon CNT growth depending on the neat CF (unsized and oxidized, respectively). In contrast, CNT fibres specimens did not exhibit any fibre break during SFFT. Since failure modes are strongly affected by the fibre/matrix adhesion the morphological damages were also assessed by acoustic emission and optical microscopy. Only a few matrix cracks and extensive debonding were observed for oxidised CF/epoxy and unsized CFs/epoxy composites, with the existence of weak interfaces being confirmed by the low amount of AE signals. On the other hand, in sized-

CF/epoxy composites and CF-CNT/epoxy composites, many matrix cracks and limited debonding were observed and accompanied by increased AE activity which indicated a strong chemical bonding between the CF and the matrix. Conversely, since CNT-fibers strongly interacted with the epoxy matrix, no acoustic signature could be produced. The interactions between the CNT network and the macromolecular chains of the polymeric matrix, at the molecular level, were probed by Raman measurements. The CNT-fiber/epoxy composites exhibited an improvement of the stress transfer efficiency by eight times in comparison to the bare CNT-fibers [153].

2.1.6. Functionalities of hierarchical composites

The hierarchical approach towards the production of advanced multiscale CFRCs was also reported to enhance other non-structural properties of the final composites. Several studies exist in the literature which mainly focused on the improvement of these additional functionalities of the hierarchical CF-CNTs, i.e. sensing ability, electromagnetic interference shielding, current collectors and electrochemical microelectrodes and fibrous supercapacitors. Some of these studies are presented in the following paragraphs.

Initial evidence of the multi-functionality, in particular as novel microelectrodes for the electrochemical oxidation of methanol in fuel cells was provided by Qu et al. [154]. These novel microelectrodes were prepared by transferring long aligned CNTs onto CFs, coating the produced CF-CNT fibres with polypyrrole conducting polymer by electrodeposition and then depositing Pt nanoparticles onto the polypyrrole-CF-CNTs using the substrate enhanced electroless deposition process [154]. The potential of the hierarchical CF-CNTs with aligned CNTs for biosensing was also demonstrated by the authors by attaching glucose oxidase molecules onto the CF-CNTs and using these electrodes to detect glucose addition into a phosphate buffer solution. Both applications indicated a high sensitivity and reliability for the CF-CNT electrodes [154].

Patton et al. focused on the electromechanical characterisation of CNTs grown on SiO₂ coated CFs in order to assess their stress and strain sensor capability [155]. The authors measured the force, strain, stiffness and electrical resistance simultaneously during localised compression tests at low loads and small displacements. Hysteretic energy loss

associated with internal friction between the entangled CNTs was observed along with increased resistance during decompression [155].

Further studies by Kar et al. demonstrated enhanced magnetic properties of CVD grown CNTs onto CF fabric with potential applications in electromagnetic shielding; these CF-CNTs also exhibited remarkably enhanced IFSS and storage modulus [156].

Li et al. in a short communication demonstrated that the oxidation resistance of C/C composites was enhanced due to the addition of hierarchical CF-CNTs [157]. Both randomly oriented and radially grown CNTs effectively inhibited the formation of rapid oxidation channels and thence increased the oxidation resistance of the composites [157]. The randomly oriented CF-CNTs not only acted as an interfacial reinforcement but also inhibited the annular matrix cracking in a long range by causing a change in the oxidation mode of the composites [157].

Chen et al. examined the effects of the structure of current collectors in the EPD process on the electrochemical response of MWCNT films by using a CF as the current collector [158]. The cationic cetyltrimethylammonium bromide (CTAB) was used for the chemical charging and the dispersion of MWCNTs in water which resulted in the formation of a porous MWCNT film on the CF cathode. The produced CF-CNTs exhibited a high specific capacitance (102 F g^{-1}), rapid charge/discharge response and stable cycling characteristics. The authors proposed the combination of 0.1 mg ml^{-1} MWCNTs, 3 mM CTAB, 10 V cm^{-1} potential for one hour as the optimum conditions for obtaining high-performance CF-CNT electrodes for EDLC applications [158].

Lu et al. in a series of experiments studied the synergistic effect of CFs and carboxylic acid-functionalized CNTs on the shape memory polymer (SMP) nanocomposites, where the actuation was achieved by electrically resistive Joule heating. Bonding of the CNTs with the CFs assisted in the transfer of the resistive Joule heating between the CF-CNTs and the SMP. The electrically induced recovery was evaluated for an electric voltage of 10 V , and the temperature distribution of the SMP nanocomposite with 0.2 g of CNTs was simultaneously monitored during the recovery process. The authors demonstrated a simple method for producing electro-activated SMP nanocomposites by using CF-CNTs instead of

CFs which enabled Joule heating of the nanocomposites at low electrical voltage values [159].

Pozegic et al. reported a low-temperature photo-thermal CVD which employed a substrate water-cooling system for the growth of CNTs on CFs and was compatible with large-area production. CF-CNT composites were also manufactured by VARTM and exhibited improvements of 510% in the out-of-plane and 330% in the in-plane electrical conductivities in comparison to the reference CF composites. The electron transport mechanism was a charge – hopping in the reference CF composite, while it transformed into an Ohmic diffusive mechanism for the CF-CNT composite [51].

In another study, Pozegic et al. also demonstrated that high-quality CNTs could replace the commonly used polymeric sizing on the surface of the CFs and simultaneously provide electrical and thermal functionalities. The authors used CVD to grow a high density of CNTs onto CFs and applied an aluminium interlayer before CNT growth in order to mitigate the diffusion of the iron catalyst particles into the CFs. The produced hierarchical composites exhibited 300%, 450% and 230% enhancement in the electrical conductivity on the ‘surface’, ‘through-thickness’ and ‘volume’ directions, respectively. Furthermore, the thermal conductivity in the through-thickness direction increased by 107%, suggesting the potential application for lightning strike protection and efficient de-icing systems for aerospace applications[160].

Fogel et al. in an attempt to improve and homogenise the through-thickness electrical conductivity of CFRCs dispersed CNTs into the polymeric matrix by a calendaring process and then sprayed this mixture with an airbrush onto dry CF plies. CFRCs were manufactured using these modified plies which exhibited a small improvement in the transverse (2.1 over 0.8 S m^{-1}), and longitudinal (13.8 over 9.3 S m^{-1}) electrical conductivity was achieved which was homogenised throughout the laminate [161].

A very recent and novel study was presented by Zou et al. who produced monolithic CF-CNT fibres by directly growing a 3D highly porous CNT sponge layer with macroscopic-thickness (up to several mm) on single CFs. In these monolithic structures, the CF lies in the middle of a highly porous CNT layer and is connected with it by a thin amorphous carbon transition layer which leads to strong interfacial adhesion. This transition layer was

shown to completely inhibit CF slippage from the matrix upon fracture in monolithic CF-CNT/epoxy composites. The authors also demonstrated that these monolithic structures could be effectively used as 3D porous substrates for the fabrication of CF-CNT-polyaniline (organic) and CF-CNT-MnO₂ (inorganic) fibre electrodes, high-performance fibre-shaped solid-state supercapacitors and fibre-type lithium-ion batteries with high performances. The authors also claimed that the produced monolithic CF-CNT fibres, comprised of a thick CNT layer could overcome delamination problems and slippage of CF when used for the production of hierarchical CFRCs. Furthermore, they stated that the application of the proposed method on woven CF fabrics could result in the production of integrated CF-CNT hybrid fibre electrodes and flexible energy storage textiles [162].

Chapter 3

From Carbon Fibres towards
Hierarchical Graphitic Reinforcements:
Production routes

Part of the results included in this Chapter which are related to the CVD process have been published at the Composites Science & Technology peer-reviewed scientific journal as part of the study “Optimal Synergy between micro and nano scale: Hierarchical all carbon composite fibres for enhanced stiffness interfacial shear strength and Raman strain sensing” and can be found under <https://doi.org/10.1016/j.compscitech.2018.07.003>. Additionally, part of the results which are related to the wet chemical modification of the unsized CFs and the CNTs, the optimization of the CNT solutions (INKs) and the production of carbon-based hierarchical reinforcements from these INKs have been published at the peer-reviewed scientific Journal of Colloids and Interface Science under the title “Production of hierarchical all graphitic structures: A systematic study” and can be found under <https://doi.org/10.1016/j.jcis.2016.10.075>.

3.1 Introduction

The deposition of CNTs on CFs towards the production of hierarchical CF-CNT reinforcements was reported in the literature by various methods, as described in Chapter 2 of the current thesis. Among them, the most widely used process is the CVD, which has been shown to result in uniformly coated CF-CNT structures when the utilised experimental conditions were optimised. However, this process most of the times resulted in the deposition of additional nanostructures along with CNTs onto the CF surfaces and most importantly it was accompanied by a reduction in the tensile properties of the underlying CFs [46–53]. Moreover, the restricted volume of most of the CVD reactors used in laboratory scale poses additional limitations regarding the deposition of CNTs on large CF woven fabrics towards the preparation of hierarchical CF-CNT/epoxy laminated composites with improved mechanical properties.

As an alternative to CVD, the use of wet chemical methodologies has already been demonstrated in order to deposit CNTs on the fibre surface. Wet chemical processes include treatment of the surface of CFs [163,164] and/or of CNTs with acids [89,90], polymers [96,98,107], electrophoretic deposition [116,117,120] and application of binders [103] or polymer sizing [146,165] containing the dispersed nano-phase onto the CF surface. Wet methods also offer the possibility of easier upscaling for mass production, when compared to CVD, with reduced cost since they (i) are low-temperature processes,

(ii) do not require special environment (inert/ carrier gases) and (iii) may be easily applied in-line, e.g. in a typical roll to roll process.

The wet chemical processes usually focused on enhancing the affinity between the two inert surfaces of the graphitic reinforcements [166]. A standard methodology for achieving increased interconnection between CFs and CNTs is the use of an acidic treatment with a mixture of sulfuric (H_2SO_4) and nitric acid (HNO_3) for the cleaning and subsequent oxidation of the surface of carbonaceous materials [89,90,167–169]. However, the different experimental protocols that have been reported in the literature present a high variability in both the CNT to acid solution ratios and exposure times and the use of mechanical means for the assistance of the reaction. Fundamentals to the efficiency of the wet chemical process are the determination of the precise concentration of CNTs or CFs in the acid solution, the reaction time, as well as the mechanical aiding for the oxidation process usually performed either by ultrasonication or magnetic stirring protocols [89,90,167–174].

For the above reasons, CVD was used in the current thesis as the most common technique for the deposition of CNTs onto CF single fibres and tows, while a more facile wet chemical route was developed for the preparation of hierarchical laminated composites. The current chapter describes the experiments and the results related to the optimisation of the production of the hierarchical reinforcements and their morphological characterisation. The experimental details and results related to each method are presented sequentially in the following paragraphs and are followed by concluding remarks.

In more detail, CNT growth by CVD was initially studied on single CF filaments for a preliminary investigation of the effects of the growth temperature and duration on the resulting CF coatings. For this reason, an extensive SEM study was conducted, which indicated the most suitable process conditions for producing hierarchical reinforcements homogeneously covered with MWCNTs. Subsequently, these conditions were applied to 12K tows of CFs, and the resulting morphologies were evaluated with SEM.

Furthermore, the grafting of commercial MWCNTs on the CF surfaces using wet chemical protocols was studied in parallel. In this process, an optimisation of the dispersion of the MWCNTs in an aqueous medium was conducted which was subsequently used for coating

individual CFs. In this case, both the CFs and the CNTs were treated with acids in order to enhance the affinity between them by, i) removing the commercial sizing from the surface of the CFs, ii) imparting additional oxygen-containing functional groups on the surface of both the CFs and the CNTs which then further promoted the creation of chemical bonds between them and, iii) overcoming the dispersion issues related to the CNTs which are a result of the strong Van der Waals forces inherently present in these nanomaterials.

This work was organised as a parametric study considering the effects of the concentration of the CNTs into the acidic mixture and the mixing methods used during the oxidation process of the CNTs while targeting for the optimisation of the wet chemical processes for the coating of individual CFs. A primary quality index for the studied processes was the minimum change of the CF diameter after the coating process, i.e. for the CNTs to create a thin homogeneous veil around the CF surface. At the same time, the study intended to produce the best surface coating possible while inducing the least possible degradation in the structure and properties of the constituent materials. A detailed morphological characterization of the structural details of the surface and the physicochemical properties of the oxidized CFs and CNTs via the use of Scanning Electron Microscopy (SEM), Thermogravimetric analysis (TGA), X-Ray photoelectron (XPS), Fourier Transform Infra-Red (FT-IR) and Raman spectroscopies provided the required evidence concerning the effects of the chemical processes on the produced reinforcements.

After their functionalization with oxygen moieties, the CNTs were dispersed in distilled water. At this stage, an online monitoring protocol of the electrical characteristics of the produced CNT dispersions (henceforward referred to as INKs) via Electrochemical Impedance Spectroscopy (EIS) was performed. The EIS evaluation confirmed the existence of the electrical percolation, i.e. the formation of a conductive path in the INKs, [175], which in this work was regarded as a measure of the dispersion quality.

Finally, an in-house designed controlled dip coating methodology was employed for the coating of the CFs with CNTs. Scanning Electron Microscopy (SEM) was employed to evaluate the quality of the coating on the surface of CFs with regards to the various studied parameters such as oxidation degree, INK dispersion quality and stability, and different coating protocols.

3.2 Materials and Methods related to the CVD process

3.2.1. Materials

The M40 unsized high modulus PAN fibres (Torayca) with a tensile strength of 2.74 GPa, modulus of 392 GPa and failure strain 0.7%, as stated by the manufacturer, were used in this study. The fibre diameter was 6.6 μm as determined by density measurements. Argon and acetylene were used as the carrier gas and the hydrocarbon source for the CVD process.

3.2.2. Methods

3.2.2.1. The growth of CNTs on the CF surface via CVD

The growth procedure followed during this study was based on a previous study by Boura et al. [73]. Initially, a preliminary study on single CFs was conducted, and then the optimal conditions were applied to 12k CF tows in order to produce a sufficient number of coated filaments.

Metal nitrates were used for the preparation of aqueous solutions, which were subsequently deposited on CFs by the use of wet impregnation in order to form the FeCo bimetallic catalyst required as active sites for the CNT growth during CVD. In more detail, two aqueous solutions were prepared by diluting under vigorous stirring $\text{Fe}(\text{NO}_3)_3 \cdot 9\text{H}_2\text{O}$ or $\text{Co}(\text{NO}_3)_2 \cdot 6\text{H}_2\text{O}$ in distilled water. The two solutions were then mixed and further stirred for 30 min. For each deposition process, several single CFs, or a CF tow, were placed along a stainless steel frame, dipped in the solution of the bimetallic catalysts for 4 h and then dried at room temperature.

For the synthesis of the CNTs on the fibre substrate, the frame with the aligned fibres was placed in an alumina crucible within a quartz tube, located in the horizontal tubular furnace (Carbolite – Figure 22). The sample was heated up to the desired temperature (750°C, 850°C or 900°C) under an argon atmosphere with a rate of 5 °C/sec. The hydrocarbon source (acetylene) was admixed with the carrier gas (argon), upon reaching the desired temperature, at flow rates of 10 $\text{cm}^3 \text{min}^{-1}$ and 90 $\text{cm}^3 \text{min}^{-1}$, respectively. These flow rates were recommended by Policicchio et al. who used acetylene as the hydrocarbon source for

the growth of CNTs over, MgO supported, Fe–Co bimetallic catalysts [176]. CNTs were grown at each selected temperature for a certain amount of time, ranging from 10 min to 30 min. Then acetylene flow was stopped, and the furnace was allowed to cool down to room temperature under argon atmosphere, before exposing the hierarchical fibres to the air. The CNT modified CFs were used without any further purification for further characterisation.



Figure 22. The horizontal tubular Carbolite furnace used for the CVD process.

3.2.2.2. Microstructural characterisation of the hierarchical reinforcements

The morphology of the hierarchical reinforcements, which were produced via CVD using single CF filaments, was evaluated using the JEOL JSM 6510 LV SEM/Oxford Instruments Scanning Electron Microscope. The hierarchical CFs were stabilised on a double-sided carbon adhesive tape. The accelerating voltage was kept at 10 kV, and images were acquired from several CFs for each experimental condition. Additionally, the morphological characterisation of the hierarchical reinforcements, which were produced via CVD using 12 k CF tows, was performed with an ESEM Quanta 250 FEG (FEI, The Netherlands) Field-emission scanning electron microscope (FE-SEM) operating at an accelerating voltage of 3.0 – 5.0 kV. The fibres were placed on a double-sided copper adhesive tape to be stabilised and coated with a thin layer of platinum (5 nm) before the SEM analysis to avoid charging effects. In this case, the diameter distribution of the grown

CNTs was measured from the acquired FE-SEM images of a population of 60 CNTs for each growth condition.

Furthermore, Transmission electron microscopy (TEM) with an HR-TEM 2100, Jeol Co was performed in order to measure the CNT diameters in specific samples. For the preparation of the samples for TEM investigations, a quantity of CNT coated CFs were sonicated in acetone and then drop cast onto carbon-coated copper grids (CF300-CV-UL). An accelerating voltage of 200kV was used for the microscope operation.

3.3 Results and discussion related to Hierarchical reinforcements produced via CVD

3.3.1. Screening study at the single fibre level

A preliminary investigation of the growth process of CNTs on CFs was conducted on single CF filaments, in order to optimise the CNT homogeneity and coverage onto the CF surface. The CF surface (Figure 23a) had a typical high modulus CF morphology with the outer graphene sheets aligned parallel to its axis, forming an irregular external surface with longitudinal fissures [177].

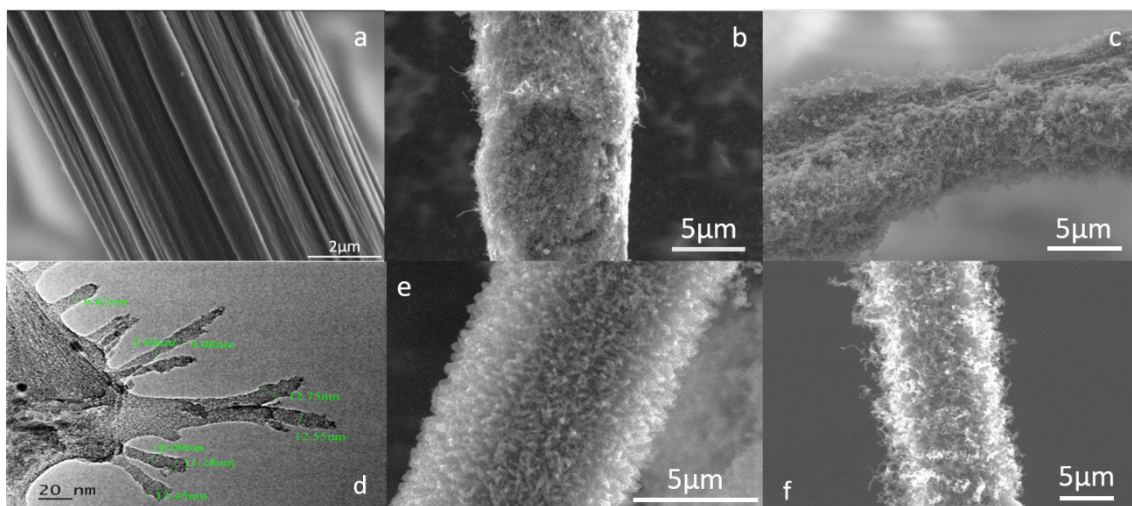


Figure 23. SEM micrographs depicting the morphology of a) a single CF, single CFs coated with CNTs produced by various CVD conditions, b) 750°C for 30 min, c) 750°C for 10 min, e) 850°C for 10 min, f) 900°C for 10 min and d) TEM image of the CNT coated CF produced by CVD at 900°C. Diameter measurements are shown in green colour.

The growth process on single CFs was initially evaluated for 30 min at 750°C [73] based on the study of Boura et al. [73]. These conditions resulted in excessive coverage of CNTs on the CF surface (Figure 23b). By reducing growth time at 750 °C to 10 min, the CNT coating on the fibre surface was less thick but inhomogeneous (Figure 23c). By increasing the growth temperature to 850°C (Figure 23e) and 900 °C (Figure 23f), more uniform coatings were produced, with distinctly reduced CNT diameters. The diameters of the grown CNTs on the fibre surface at 900°C were measured by TEM measurements to be 10.15 ± 2.95 nm (Figure 23d).

Subsequently, the growth process was implemented on 12k CF tows in order to produce a sufficient number of coated filaments. CNT growth on CF tows was conducted at 750°C and 850°C for 10 min and 30 min, to avoid very high CVD growth temperatures which could lead to severe degradation on the CF tensile strength [62]. The selection of these growth temperatures could ensure both the radial (850 °C) and random (750 °C) orientation of CNTs on CFs, while simultaneously accounting for enough time (10 or 30 min) for sufficient coverage of the tows.

3.3.1. Morphological study of CF-CNT tows

Figure 24 shows the FE-SEM images of CF-CNT structures. For all the CF-CNT samples, curly and entangled CNTs were observed covering the fibre surfaces with more homogeneous CNT coatings for the longer deposition times (30 min) at both temperatures. Compared to the reference CF (Figure 23a), all the CF-CNT (Figure 24) had increased diameters due to the CNT forest length.

For CF-CNT@750/10 (Figure 24a, Figure 24b and Figure 24c) short CNTs, up to 1 µm length, with a coiled morphology and average diameters of $46.2 \text{ nm} \pm 19.2 \text{ nm}$ were produced. Prolonged growth time at the same temperature (Figure 24d, Figure 24e and Figure 24f) resulted in longer, less twisted CNTs with an average diameter of $50.3 \text{ nm} \pm 20.0 \text{ nm}$ and lengths in the range of 5 to 10 µm, which is an anticipated value for MWCNTs [178]. Precise determination of the CNT lengths was not feasible as the CNTs were neither straight nor separated from each other. Figure 24g, Figure 24h and Figure 24i depict the morphology and the diameter size distribution plot of the CNTs for the CF-

CNT@850/10 with an average diameter of $74.4 \text{ nm} \pm 24.0 \text{ nm}$. Similarly, Figures 2j, 2k and 2l correspond to the CF-CNT@850/30. Long ($5 - 10 \text{ }\mu\text{m}$) and thin (average diameter of $38.0 \text{ nm} \pm 13.7 \text{ nm}$) CNTs were also produced at this reaction temperature.

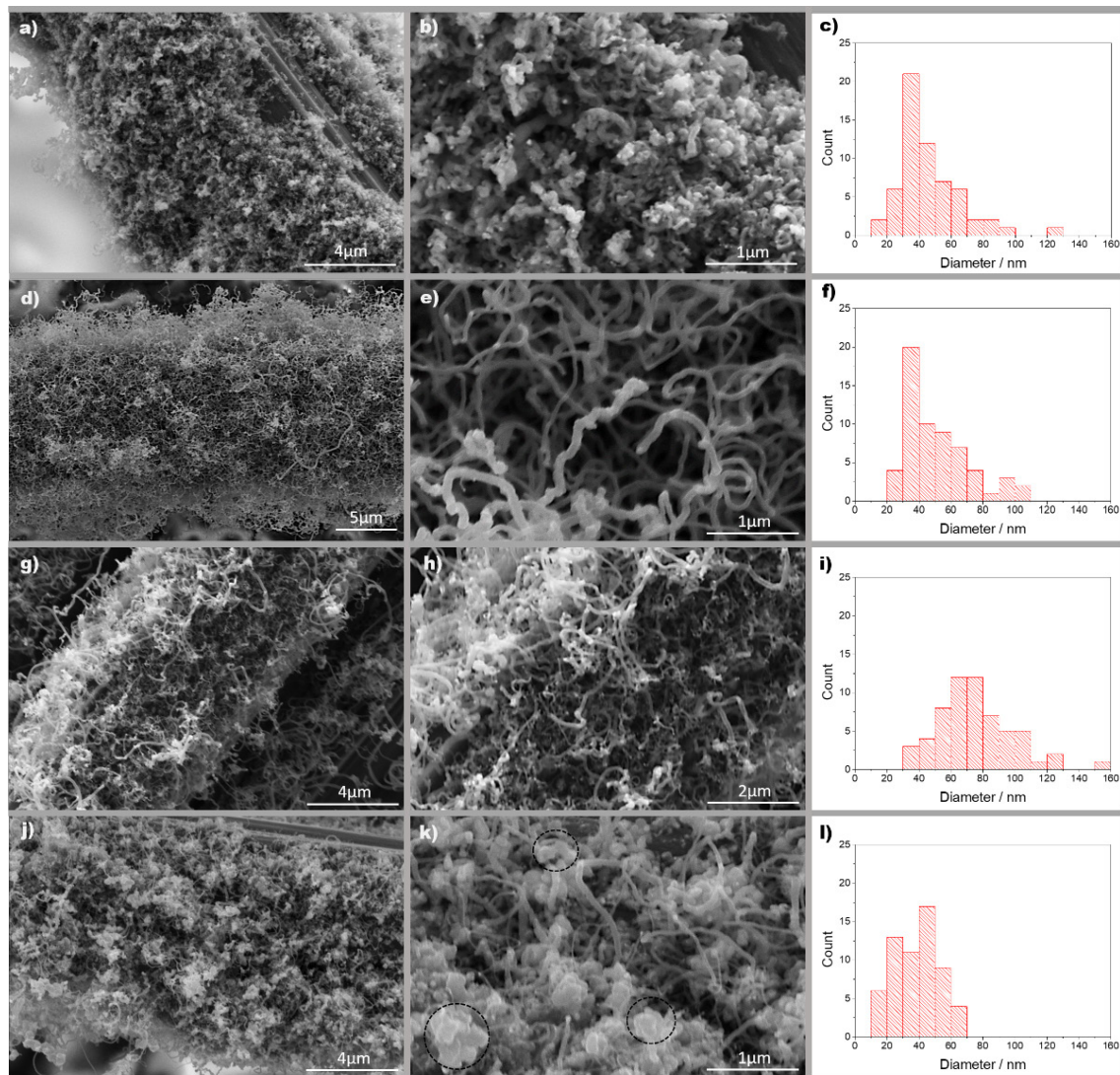


Figure 24. FE-SEM micrographs and the corresponding CNT diameter distribution plot revealing the morphology and structure of the produced CNTs. CF-CNT produced by CVD, CF-CNT@750/10 (a, b, c) CF-CNT@750/30 (d, e, f), CF-CNT@850/10 (g, h, i) and CF-CNT@850/30 (j, k, l).

Additionally, for the CF-CNT@850/30 the presence of platelet-like graphite nanoparticles was observed, indicated by black dashed-line circles in Figure 24h. These particles were intercalated into the CNT forest grown onto the CF surface constituting a binary carbon-based CVD-grown coating. Similar structures were recently reported by Lavagna et al. for

hierarchical reinforcements produced by chemical treatment and deposition of commercial CNTs onto the surface of CFs [179]. The authors identified these nano-spheres as Carbon Nano-Onions (CNOs) and attributed their formation to the aggressive acidic treatment used in their study, which was assumed to separate graphitic clusters with a different orientation from the CF surface. These clusters were then rearranged in CNOs. In the present study, the use of FeCo catalyst particles during the CVD process led to the formation of both CNTs and onion-like structures. The latter could be mainly attributed to catalyst particles rich in Co content since the composition of the catalyst particles at a CNT tip were shown to determine the morphology of the CNTs, with Co-rich particles tending to produce onion-like structures [180].

3.4 Conclusions related to Hierarchical reinforcements produced by CVD

Overall, the growth process on CF tows was successfully implemented, producing various morphologies which were subsequently evaluated regarding physicochemical and mechanical properties (see next chapters). In general, the CVD process resulted in a dense coverage of the CF surface with a porous layer of MWCNTs. Other nanostructures were also observed under certain growth conditions which were further discussed in the following chapters. Unfortunately, the radial arrangement of the CNTs onto the surfaces of the CFs, which was observed when growth was conducted at 850°C for 10 min on single carbon filaments, was not achieved when growth was conducted on fibre tows. Furthermore, the optimisation of the growth process on fibre tows was out of the scope of the current study since it would require the use of sputtering [38] or spin coating [41] which would render the process much more complicated, difficult to scaling-up and cost inefficient. Consequently, the produced hierarchical reinforcement were used for the benchmarking study of the structural and mechanical properties at the single fibre (Chapter 4) or model composite level (Chapter 5), while the thesis focused mainly on the production of CF-CNTs by attaching commercial CNTs onto the surface of CFs by wet chemical modifications and grafting for the characterization of the mechanical properties of hierarchical laminated CF-CNT/epoxy composites (Chapter 6).

3.5 Materials and Methods related to the wet chemical process

3.5.1. Materials

The ONEX MW 1000C1 CNT provided by Glonatech SA were used in this study. The CNTs had diameters ranging from 20 nm to 45 nm and lengths $\geq 10 \mu\text{m}$, purity $\geq 94\%$, metallic inclusions $\leq 5.9\%$, amorphous carbon $< 0.1\%$ and bulk density $\leq 80 - 120 \text{ kg/m}^3$, as reported by the manufacturer. Sulfuric acid (H_2SO_4 - 95-97 % v/v) and nitric acid (HNO_3 – 65 % v/v) ACS reagents by Sigma Aldrich were used as received for the oxidation process. Distilled water (pH: 7) was used as the solvent for the dispersion.

The CFs employed were the unsized M40 CFs (Torayca), while selected experimental conditions were also applied on the sized M40 CFs in order to evaluate the effects of the polymeric sizing on the resulting CNT coatings and to ensure that scale-up to laminated composites will be feasible regardless on the presence of sizing. These CFs have a tensile strength of 2.7MPa and tensile modulus of 392 GPa as stated by the manufacturer.

3.5.2. The oxidation process of the carbon fibres

The CFs were oxidised using HNO_3 (65 % v/v). During this process, 100mg was carefully removed from a bundle of CFs and placed in a flask along with 100ml of HNO_3 . The mixture was bath sonicated for time durations of 30, 60, or 90 minutes. CFs were then washed several times with distilled water and dried at 80°C overnight.

3.5.3. The oxidation process of the carbon nanotubes

A mixture of concentrated sulfuric and nitric acids (ratio 3:1 v/v) was used for the chemical modification of CNTs. A quantity of the as-received CNTs was suspended into the acids solution and sonicated or stirred for distinct amounts of time. Table 1 lists the studied cases and adopted coding. All the dispersions will be hitherto referred to as INKs along with their code.

Table 1. Description of the studied systems.

Code	CNTs quantity (g)	Acids quantity (ml)	Mixing during oxidation	Oxidation duration(hours)
A	1	100	Ultrasonication	3
SA	1	100	Magnetic stirring	3
ASL	1	100	Magnetic stirring	6
AM	1	200	Ultrasonication	3
AGK	1	400	Ultrasonication	3

The ultrasonication was performed in a Branson 3510 bath sonicator working at 100W and 42kHz. After sonication or stirring the solutions were left to cool down to ambient temperature, subsequently filtered through a polycarbonate membrane (pore size 40 μ m) and then repetitively washed with deionised water until their pH reached neutral values. Finally, the acid functionalized CNTs were dried at 80°C under vacuum overnight.

3.5.1. Characterisation of carbon fibres and CNTs before and after oxidation

The presence of functional groups onto the surface of CNTs was evaluated with a Jasco FTIR-6200 Fourier Transform Infrared Spectrometer. The KBr pellet method was used, for the acquisition of 64 scan spectra at frequencies ranging from 400 cm^{-1} to 4000 cm^{-1} . FT-IR was also employed for the evaluation of CFs after the oxidative treatments, but the acquired spectra could not efficiently reflect the formation of additional functional groups, possibly because CFs are blacker than CNTs [89]. These results can be found in Section A2 of the Appendix.

A Labram HR - Horiba scientific Raman system was used in order to measure the relative changes in the Id/Ig intensity ratios of the oxidised CFs and CNTs. The 514.5 nm line of an argon ion laser operating at 1.5mW at the focal plane was employed for the Raman excitation. An optical microscope served as the collector of the Raman scattering equipped with a 50x long working distance objective. Raman spectra in the range of 100-3500 cm^{-1} were collected with acquisition times of 20 sec.

X-ray photoelectron spectroscopy (XPS) measurements were performed under ultrahigh vacuum conditions with a base pressure of 5×10^{-10} mbar in a SPECS GmbH instrument equipped with a monochromatic MgK α source ($h\nu = 1253.6$ eV) and a Phoibos-100 hemispherical analyser. The energy resolution was set to 0.3 eV, and the photoelectron take-off angle was 45° with respect to the surface normal. Recorded spectra were the average of 3 scans with energy step set to 0.05 eV and dwell time of 1 sec. All binding energies were referenced to the C1s core level at 284.6 eV. The spectral analysis included a Shirley background subtraction and peak deconvolution employing mixed Gaussian–Lorentzian functions, in a least-squares curve-fitting program (WinSpec) developed at the Laboratoire Interdisciplinaire de Spectroscopie Electronique, University of Namur, Belgium.

Thermo-gravimetric analysis (TG) was performed in a Perkin Elmer Pyris Diamond TG instrument. Samples of approximately 3-3.5 mg were heated in still air from 15 °C to 700 °C, with a 5 °C min⁻¹ heating rate.

3.5.1. Dispersion of oxidised CNTs in aqueous solutions

Aqueous suspensions of oxidised CNTs were prepared after 90 min sonication time using the Hieschler UP100H sonicator at 0.2% of the full amplitude capacity of the sonicator, quoted at 100 W by the manufacturer. The total sonication energy was 0.036 KWh. During sonication, each suspension was simultaneously monitored by Electrochemical Impedance Spectroscopy (EIS) in order to determine the combination of time and concentration values at which percolation was achieved. Three different concentrations of the nanomaterial in distilled water were prepared and monitored by EIS, namely 0.01%, 0.1% and 0.5% w/w.

EIS measurements during the dispersion process were performed using the Advanced Dielectric Thermal Analysis System (DETA-SCOPE) supplied by ADVISE, Greece. Purposely made interdigital sensors manufactured by Gel Instrumente AG, Switzerland Figure 25 were employed, and a sinusoidal voltage of 10V was applied to the sensor.

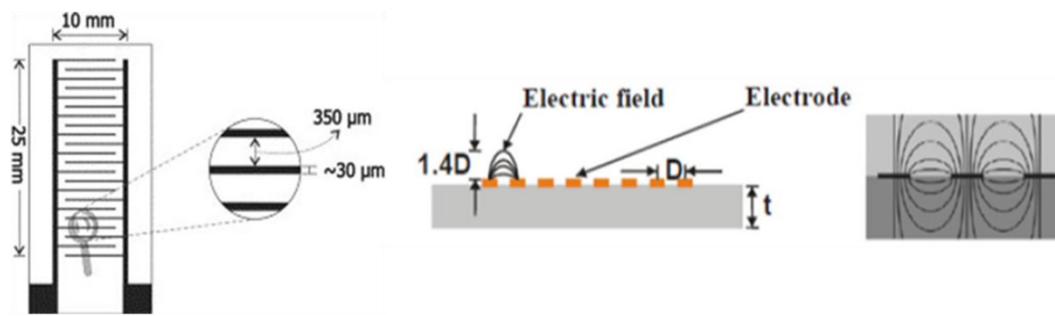


Figure 25. Schematic representation of the interdigital sensor used for electrical impedance measurements.

Scans were performed between two frequency values (0.1 Hz and 100 kHz) at 24 different frequencies with the duration of each scan to be approximately 108 seconds. The utilised dielectric sensor consisted of an assembly of interdigital gold electrodes, printed with a spacing of 250 μm on a thin polymeric film which operated as a flat condenser with an electric field penetration depth of 350 μm (Figure 25). The dielectric sensor was placed inside the monitored suspension along with a thermocouple which concurrently provided temperature readings during the sonication process. A schematic representation of the experimental set up is presented in Figure 26.

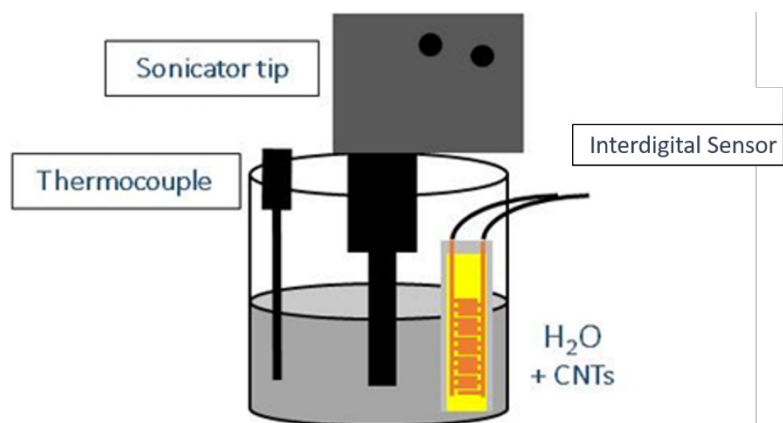


Figure 26. Schematic representation of the experimental set up utilised for impedance monitoring of the dispersions.

After the dispersion and before the coating process mild centrifugation was applied to all INKs in order to force large non-dispersed aggregates to settle at the bottom of the containers. This particular step was adopted since the initial trials for the production of the

hierarchical reinforcements revealed the presence of some residual aggregates on the surface of the CFs.

The stability of the manufactured suspensions was evaluated 60 days after their production when all produced inks were visually checked for sedimentation. Photographs of the CNT dispersions at 60 days were acquired.

3.5.1. Dip coating procedure and visualisation of the outcome

The experimental setup utilised for the coating procedure is depicted in Figure 27. The CFs were aligned carefully on the four sides of the purposely made frame. The frame was then fixed on a motor which submitted it to a rotational movement inside the container with steady rpm (27 rpm), thereby repetitively dipping the CFs in the CNT dispersion in a controlled and reproducible manner.

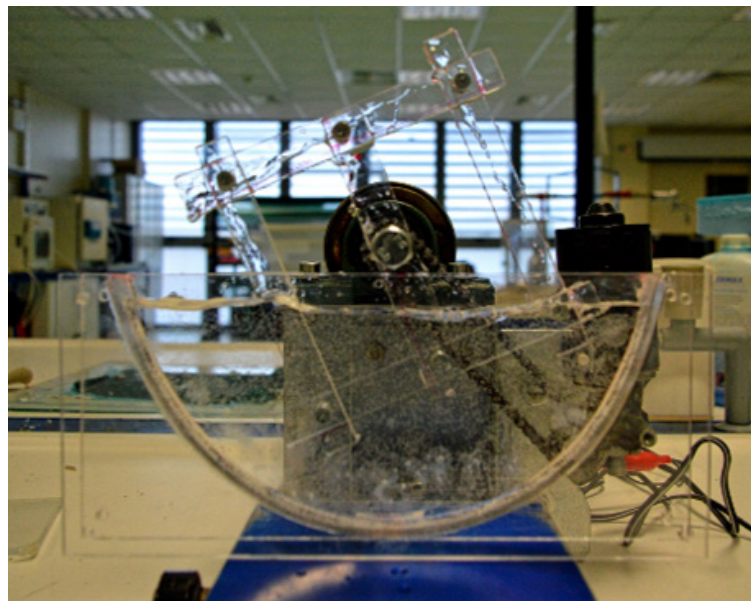


Figure 27. Photos of the experimental set up used for the coating procedure.

Finally, an extensive SEM study using the JEOL JSM 6510 LV SEM/Oxford Instruments established the effectiveness of each combination of processes and the resulting CNT coating on the oxidised CFs.

3.6 Results and discussion related to Hierarchical reinforcements produced via wet chemical protocols

The oxidation process of CNTs in an acidic environment is a typical, widely employed and easily applied wet chemical treatment. It offers the possibility of a variety of subsequent functionalizations tailor-made for each specific application. However, oxidation for a prolonged time may result in substantial degradation of the inherent characteristics of the CNTs [181]. Hence, this study aimed at the production of hierarchical all graphitic reinforcement by using the milder possible process conditions both for the CNTs and CF surfaces, minimising the detrimental effects on their structural and functional integrity.

The oxidation reaction of the CNTs was mechanically aided by stirring or sonication. Among the studied parameters were (i) the duration of the oxidation process for the CNTs oxidised by stirring (3 and 6 hours) and (ii) the concentration of CNTs in the acidic mixture when the CNTs were oxidized by sonication (100, 200 and 400 ml of acidic mixture per 1g of CNTs). The oxidation of the CFs was carried out in a milder oxidant (HNO_3) than the mixture used for CNTs oxidation [174]. As mechanical stirring would inevitably lead to the CF breakage, only bath sonication was utilised for their oxidation. The effect of sonication time of the CFs in the acidic environment was studied, for 30, 60 and 90 min of oxidation. The effect of the chemical functionalization processes on the surface of the CNTs was examined by FTIR, Raman and XPS spectroscopies and the changes in the thermal stability were evaluated via TGA measurements. CFs were also characterised by Raman spectroscopy before and after the oxidation procedures.

The results of this extended characterisation campaign served as indicators for the subsequent selection of those oxidised CNTs which used during the preliminary dip-coating experiments for the production of hierarchical reinforcements.

3.6.1. Vibrational analysis of the oxidised CNTs and CFs

3.6.1.1. FT-IR spectroscopy

Figure 28 compares the FTIR spectra of the as received as well as the acid-treated CNTs. As can be seen, the spectrum of the as-received CNTs was easily distinguished from the

spectra of all the oxidised samples. The major activity found in the as-received MWCNTs resulted from stretching vibrations of the O-H groups ($3400\text{-}3550\text{cm}^{-1}$), which were assigned to the corresponding groups of adsorbed water or covalently bonded functional groups. The other two main vibrational modes appearing in the spectrum of the as-received CNTs were the 1620 and 625 cm^{-1} , allocated to the C=C deformation [121] and the C-OH stretching [173] vibrations, respectively. A comparison of the presented spectra revealed the formation of three new peaks in all the functionalized spectra as well as an additional fourth peak in the samples that were oxidised either in a more acidic environment (AM, AGK) or for prolonged oxidation times (ASL). The three vibrations that appeared in the $1735\text{-}1741\text{cm}^{-1}$, $1363\text{-}1372\text{cm}^{-1}$ and $1214\text{-}1220\text{cm}^{-1}$ regions, were attributed to the stretching of the C=O bond of the carboxyl and carbonyl moieties [182], the C-C stretching vibrations [121] and the stretching of the C-O bond of ether moieties and carboxylic groups [100], respectively. Common to the more “aggressively” oxidised samples (AM, AGK and ASL) was the band located at $1437\text{-}1440\text{cm}^{-1}$, which was due to the combination

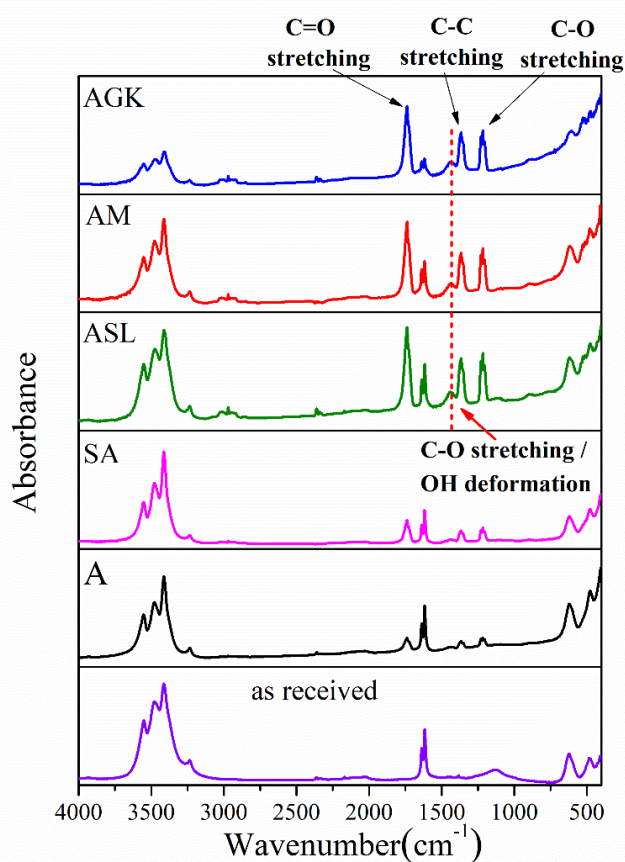


Figure 28. FTIR spectra of the CNT samples before and after the various oxidative treatments.

of the C-O stretching and O-H deformation vibrations in carboxyl moieties [183] (see Figure 28).

Furthermore, the degree of functionalization was quantified via a Gaussian shape line fitting analysis of the normalised IR spectra. A characteristic spectrum along with details on the fitting procedure can be found in Section A1 of the Appendix, while the relative

intensities of the fitted vibrational modes concerning the as-received CNTs are shown in Figure 29.

In the cases of prolonged stirring time (ASL) and higher acids / CNT ratio (AM and AGK), the increased amount of carboxyl functional groups was confirmed through the appearance of their combined stretching and deformation vibrational mode at 1437-1440 cm^{-1} (Figure 28), which was more prominent for the ASL (Figure 29). This low-intensity complex vibrational mode is thought to emerge due to the more aggressive oxidation conditions. On the other hand, samples A and SA underwent a milder oxidation process, which resulted in the formation of carboxyl moieties appearing as new peaks (Figure 28) in their FT-IR spectra, albeit with much lower intensities in comparison to AM, AGK and especially ASL (Figure 29).

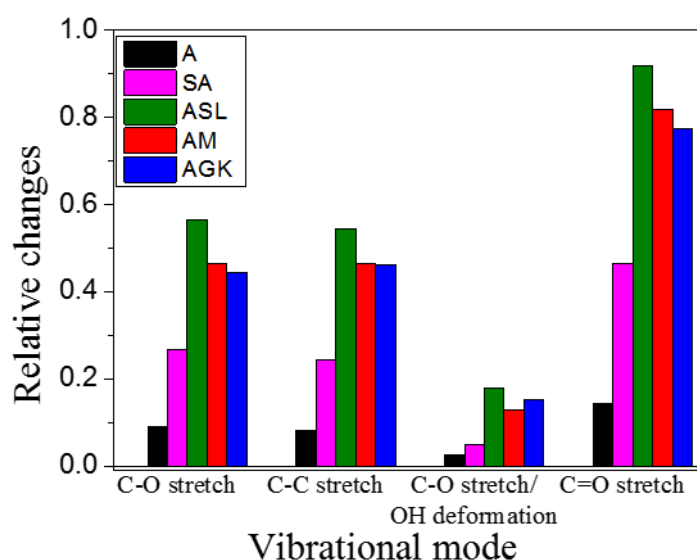


Figure 29. Relative changes of FTIR vibrational modes with respect to the as-received MWCNTs.

Overall, FT-IR measurements not only confirmed the successful functionalization procedure of all the CNT samples but also revealed differences regarding the extent of oxidation.

3.6.1.1. Raman spectroscopy

Evaluation of CNTs

Characteristic Raman spectra of the as received as well as the oxidised CNTs are presented in Figure 30. An analysis of the origins of the most common in graphitic materials vibrational modes, along with details on the spectral treatment, can be found in Section A3 of the Appendix, while for the ease of presentation these specific vibrational modes were annotated in Figure 30.

The Raman spectra of the oxidised CNTs (Figure 30) indicated that the chemical treatment did not introduce any new peaks. The observed differences were related to the ratio of the intensities of the D to that of the G band, I_D/I_G . This ratio is typically used in literature in order to quantify the relative changes induced to the samples due to the incorporation of functional groups [167,172,182]. Additionally, the position and full width at half maximum (FWHM) of the D and G bands were evaluated since they reflect the purity and size distribution of the studied nanostructures, respectively [184].

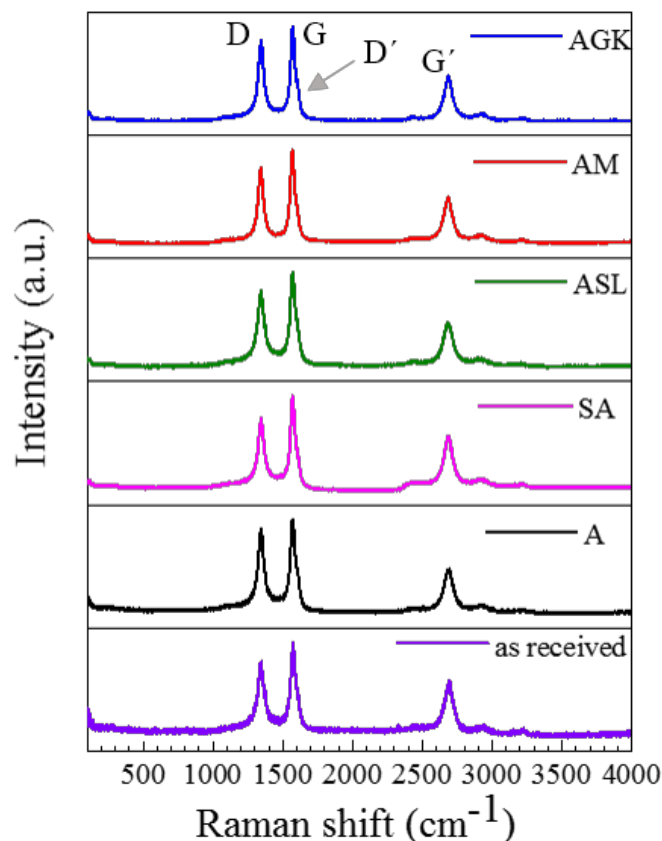


Figure 30. Raman spectra of the as received and oxidised CNT samples.

The relative changes in the position and FWHM of the D and G vibrational modes, as well as the ID/IG ratio, are summarised in Table 2. In general, all the oxidative treatments caused an increase in this ratio in comparison with the as-received CNTs, clearly indicating that the oxidation process induced structural defects in the form of functional moieties in between the carbon lattice of the CNTs, manifested by the relative increase of the D line. Specifically, oxidation by stirring (SA, ASL) resulted in lower degradation in comparison to oxidation by sonication (A, AM, AGK).

The effect of processing time was studied only for the process involving stirring during oxidation, whereas in the case of sonication, which is by definition a more aggressive process than stirring, this study was evaded because even higher processing duration could lead in extended degradation of the CNTs. The higher I_D/I_G values suggested an increase in the functionalization degree with processing time for stirring during oxidation (A and ASL). On the contrary, increasing the acid to CNT ratio used in the oxidation process by sonication (A, AM, AGK) did not lead to substantial changes in the CNT I_D/I_G ratio, indicating that this parameter is not of primary importance to the degradation of the CNT structure.

Table 2. Experimental values of the as received and oxidised CNTs evaluated by Raman spectroscopy.

	D BAND		G BAND		I_D/I_G
	Position (cm^{-1})	FWHM (cm^{-1})	Position (cm^{-1})	FWHM (cm^{-1})	
AS RECEIVED	1343 \pm 1.7	53.6 \pm 7.2	1570 \pm 2.6	42.0 \pm 4.3	0.63 \pm 0.07
A	1347 \pm 2.6	46.9 \pm 2.5	1575 \pm 3.5	38.0 \pm 1.8	0.77 \pm 0.03
SA	1348 \pm 3.3	53.4 \pm 4.4	1576 \pm 4.2	42.1 \pm 2.8	0.72 \pm 0.04
ASL	1349 \pm 0.7	49.6 \pm 2.5	1578 \pm 2.2	39.0 \pm 1.8	0.74 \pm 0.04
AM	1347 \pm 2.6	47.9 \pm 2.5	1575 \pm 3.3	38.8 \pm 1.9	0.77 \pm 0.03
AGK	1348 \pm 0.8	50.0 \pm 2.1	1577 \pm 1.0	40.0 \pm 1.4	0.77 \pm 0.02

As is also noteworthy, the frequencies of the Raman active vibrational modes (referred to as “Position” in Table 2) of the CNTs changed after the acidic treatment, exhibiting a redshift in comparison to the peak frequencies of the as-received CNTs. This shift suggested a deviation from crystallinity [184] induced by the acceptor-type dopants used in this study. These produced a charge transfer from the CNTs to the acceptor molecule [185] resulting in the

displacement of the bands to higher wavenumbers. This behaviour was also observed in a study involving the acidic treatment of CNTs [186]. A direct comparison of the position of the G vibrational mode of the CNTs showed that slightly higher charge transfer was induced for prolonged oxidation by stirring (ASL) than by sonication (A, AM and AGK). The frequency of the D vibrational mode presented similar behaviour.

Regarding the FWHM of all the studied peaks (Table 2), they presented a stiffening in comparison to the as-received CNTs except SA (mildest treatment conditions). This narrowing of the bands can be attributed to improved structural ordering since the impurities are being eliminated during the oxidation process [182]. This finding is in close agreement with the TGA results presented below.

Summing up the results from the Raman measurements on CNTs, the successful functionalization of all the samples was confirmed. Moreover, the results indicated that acid oxidation might have enhanced the structural ordering of the CNT powders by eliminating the impurities from the samples volume. Additionally, the stirring process (SA, ASL) was found to impose lower degradation to the CNTs in comparison to the sonication assisted process (A, AM, AGK). Amongst the studied samples, ASL was the one which presented the most moderate behaviour based on the I_D/I_G ratio values.

Evaluation of CFs

The ID/IG ratio was also evaluated for the CFs before and after the oxidation process. The results indicated that the average value of the ID/IG ratio increased marginally (Table 3) but linearly (Figure 31) with treatment duration.

Table 3. Experimental values of the as received and oxidised CFs evaluated by Raman spectroscopy.

	I_D/I_G
As received	0.66 ± 0.06
30 min oxidation	0.68 ± 0.08
60 min oxidation	0.69 ± 0.07
90 min oxidation	0.72 ± 0.07

This slight increment in the I_D/I_G ratio indicated a minimal degradation and a mild functionalization of the CF surfaces with 30, 60 or 90 min of bath sonication in HNO_3 , as was also demonstrated by the IR study presented in Section A2 of Appendix A.

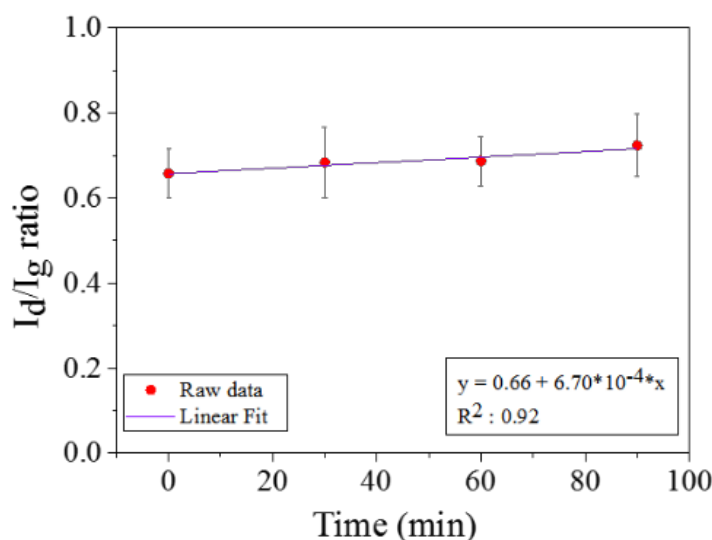


Figure 31. The empirical formula describing the degree of functionalization of the CF surfaces with respect to their reaction time in nitric acid.

3.6.2. Chemical analysis of the CNTs

XPS spectra in the C1s energy window of as received CNTs and oxidised samples are shown in Figure 32. The reference CNT spectrum was typical of commercial CNTs [187]. Upon deconvolution with combined Gaussian–Lorentzian functions and interpretation, the C1s spectrum of as received CNTs was found to consist of four main contributions. The lowest binding energy component at 284.6 eV which contributed 75.3% to the total C1s integrated intensity was assigned to C-C bonds from the CNTs. Three more peaks with descending contribution to the integrated intensity followed at higher binding energies. The peak at 285.8 eV (15.6%) was attributed to C-O bonds of the hydroxyl moieties, while the next one at 286.7 eV (6.6%) was correlated with C-O-C groups from epoxides/ethers. Finally, the 287.9 eV band (2.5%) was ascribed to C=O groups [188] from ketones. The fact that oxygen-containing groups appeared in the C1s spectrum, with oxygen also detected in the O1s region (Figure 33) implied that the as-purchased CNTs were not pure and, as expected, had defects [187], a conclusion also supported by Raman spectroscopy.

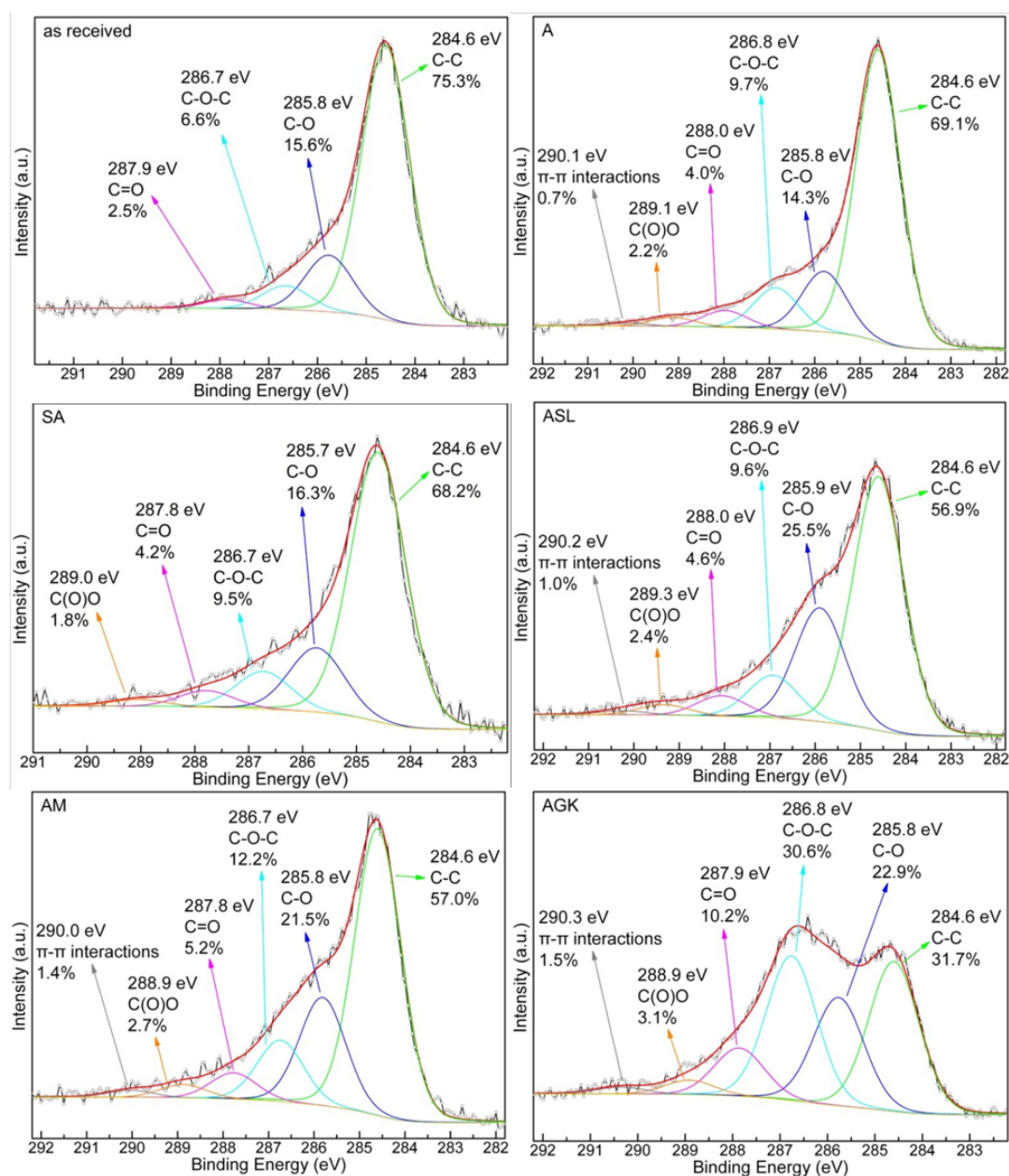


Figure 32. C1s core level X-ray photoemission spectra of as received CNT and oxidised samples: A, SA, ASL, AM, and AGK.

The C1s spectra of the oxidised samples exhibited lower C-C contribution compared to that of as received CNTs with the contribution varying from 31.7% up to 69.1%. Moreover, the contribution of more oxidised species was enhanced, and an additional component at ~289.0 eV emerged which was linked to highly oxidised carbon atoms from carboxylic groups, C(O)O. In most cases, i.e. except for sample SA, a minor band was also

observed above 290.0 eV which was associated with π - π interactions [188]. The elemental analysis values were summarised in Table 4 for the ease of comparisons.

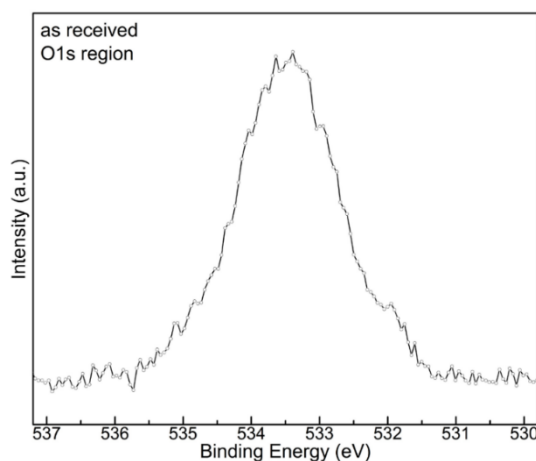


Figure 33. O1s region of the XPS spectrum of the as-received CNTs.

The overall C1s spectrum profiles and the specific contributions of oxygen-containing groups (shown inside the plots) revealed that the A and SA samples were the less oxidised ones suggesting a mild treatment and subsequent functionalization. Materials AM and ASL exhibited moderate oxidation, while the AGK sample was by far the most oxidised material implying harsh treatment. Nevertheless, XPS spectroscopy exposed the successful oxidation of CNTs in all cases and was in reasonable agreement with FTIR. Moreover, XPS analysis revealed an increase in the number of oxygen moieties with increasing CNT to acid ratio.

Table 4. Chemical analysis of the CNTs (All numbers represent percentages).

	C-C	C-O	C-O-C	C=O	C(O)O	π - π interactions
As received	75.3	15.6	6.6	2.5	-	-
A	69.1	14.3	9.7	4.0	2.2	0.7
SA	68.2	16.3	9.5	4.2	1.8	-
ASL	56.9	25.5	9.6	4.6	2.4	1.0
AM	57.0	21.5	12.2	5.2	2.7	1.4
AGK	31.7	22.9	30.6	10.2	3.1	1.5

3.6.3. Thermal stability of CNTs via thermogravimetric analysis

Additional conclusions for the effect of the applied oxidising treatments can be drawn by the thermal analysis curves (TGA%) of the CNTs (Figure 34). The most significant finding was that the as-received CNTs exhibited very high thermal stability up to ~ 500 °C with a weight loss of less than 5% while at the same time, the oxidised materials lost ~ 10 -15% of their weight in the same temperature region. This difference was directly linked with the presence of oxygen functionalities which are known to decompose gradually at lower temperatures compared to the combustion of the neat CNTs [187]. Furthermore, the increase of the combustion temperature of the CNTs with acidic treatment was observed.

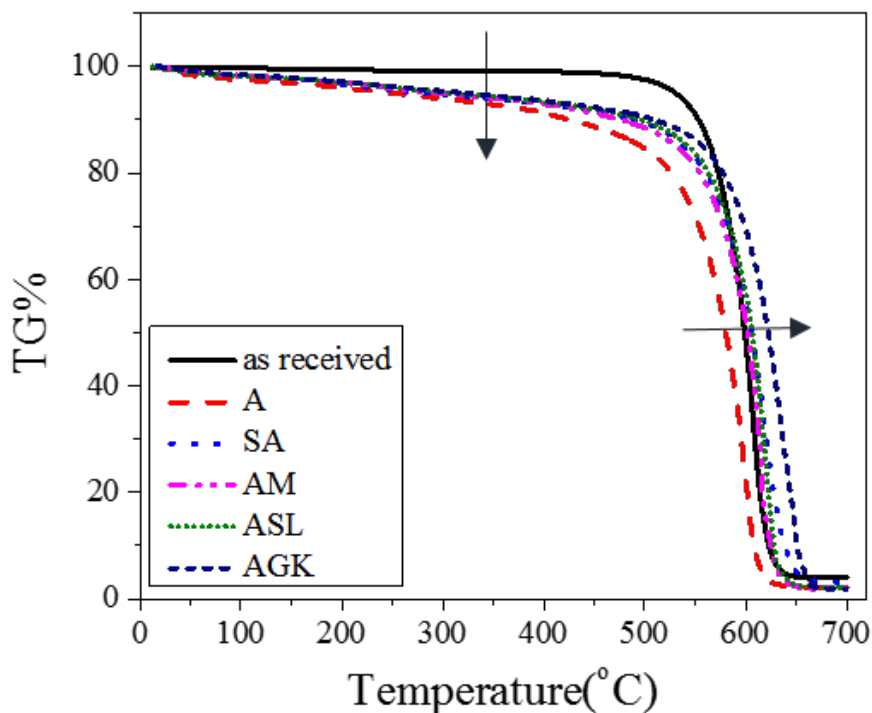


Figure 34. Thermal analysis curves (TGA%) of as received and oxidised CNTs

The values of the combustion temperatures along with the residual weight fraction after combustion are presented in Table 5. The as-received CNTs were burnt at 603.1°C , whereas all the oxidised samples exhibited higher combustion temperatures culminating at 644.1°C for the most intensely oxidised one (AGK). As suggested by the XPS measurements, the carbon content in the oxidised materials decreased in favour of the added oxygen. A possible explanation for the highest thermal stability was the elimination of the disordered carbon during the oxidation process. Thus, the remaining carbon content

in the oxidised samples exhibited a higher degree of crystallinity compared to the as-received CNTs. This postulation was supported both by the residual values presented in Table 5 as well as by the reduction of the FWHM of the bands in the CNTs Raman spectra, as discussed above.

Table 5. Combustion Temperatures and Residual Mass of the oxidised CNTs.

CNTs	Combustion Temperature (°C)	Residual Mass (%)
AS RECEIVED	603.1	4.0
A	594.4	2.1
SA	612.7	3.2
AM	609	2.0
ASL	617.3	2.3
AGK	644.1	1.9

Overall, a direct comparison of the IR, Raman, XPS and TGA results indicated that two competing mechanisms were acting simultaneously during the oxidation of the CNTs. The first mechanism concerned the introduction of functional moieties into the crystal lattice of the CNTs while the second led to the purification of the graphitic structure through the elimination of metal impurities and amorphous carbon.

3.6.4. Production and characterisation of CNT INKs

Subsequently, INKs with three different concentrations (0.01%, 0.1% and 0.5% w/v) were prepared using tip sonication with simultaneous EIS monitoring. The produced INKs will henceforth be referred to as INK_ [sample name] _ [concentration].

3.6.4.1. Monitoring of the dispersion process via EIS

The addition of a conductive phase in a dielectric media is capable of increasing the conductivity of the solution. The dynamic changes in the dielectric behaviour of the solution can be monitored online using EIS [189], as has successfully been performed for internal

damage evaluation and quantification in nanomodified composites [190]. Typically, during the dispersion process, the magnitude of the impedance at the DC regime (i.e. the ohmic resistance) is expected to decrease, and the transition from frequency independent to frequency dependent behaviour is expected to shift to higher frequencies.

The magnitude of the impedance or $|Z|$ as a function of frequency is presented in Figure 35. In this figure, every row represents a different INK, and every column stands for an increasing duration of sonication. The impedance study was an in-line process, whereby measurements were taken at specific intervals while the sonication was interrupted. As should be noted, $|Z|$ values above ca. $10^{10} \Omega$ were at the detection limits of the employed setup, and thus all INKs that remained highly dielectric exhibited higher $|Z|$ fluctuations, independent of dispersion time, or INK type and concentration. At the same time, inductive phenomena due to the employment of the dielectric sensors may also affect the accuracy of the measurements at low frequencies.

INK_A (Figure 35a) exhibited minor differences in the $|Z|$ values among the examined concentrations at the first 5 min of the dispersion process. $|Z|$ remained at approximately $10^9 \Omega$. For 60 min of CNT dispersion time (Figure 35b), INK_A_0.5 demonstrated a drop of one order of magnitude in $|Z|$, which may be regarded as an indication of percolation. Respectively, INK_A_0.1 demonstrated a drop of almost one order of magnitude in $|Z|$ at 90 min sonication time (Figure 35c). In contrast, at 90 min, INK_A_0.01 exhibited an increase of almost two orders of magnitude in its $|Z|$ values at low frequencies (Figure 35c). This increase in $|Z|$ may be readily attributed to the induced structural degradation which is well known to take place during the sonication of CNTs [191,192]. This structural degradation which was primarily manifested as a reduction in the length of the CNTs led to the partial destruction of the percolation network [192]. In contrast, both INK_A_0.1 and INK_A_0.5 presented a decrease by less than two orders of magnitude in their $|Z|$ values when compared to the first 5 min of the sonication process, indicating that the dispersion process favoured breakage to de-agglomeration of the CNTs.

INK_SA at 5 min of sonication exhibited initial $|Z|$ values of almost $10^{10} \Omega$ (Figure 35d) suggesting inhomogeneous dispersion. As aforementioned, the high values in combination with low frequency led to noisy EIS spectra for INK_SA (Figure 35d). With the continuation of sonication up to 60 min, $|Z|$ decreased linearly and the noise was eliminated due to the

gradual dispersion of CNTs (Figure 35e) and $|Z|$ was almost the same for all INK concentrations starting from ca. $10^9 \Omega$, (Figure 35e). At 90 min (Figure 35f) the only difference observed was a decrease in the initial $|Z|$ value by approximately one order of magnitude for INK_SA_0.01. Overall, INK_SA exhibited indications of percolation between 5 and 60 min with minor differences regarding concentration.

In the case of INK_ASF, the $|Z|$ frequency spectrum for INK_ASF_0.01 remained almost the same for all sonication times (Figure 35g, h, i), indicating that there were no percolation effects. For 5 min sonication time, INK_ASF_0.1 and INK_ASF_0.5 exhibited distinctly lower $|Z|$ than INK_ASF_0.01 (Figure 35g). The higher concentrations of INK_ASF_0.1 and INK_ASF_0.5 presented a substantial decrease in $|Z|$ from 5min (Figure 35g) to 60 min (Figure 35h) and a subsequent stabilisation from 60 min (Figure 35h) to 90 min (Figure 35i). In this case, the transition from Ohmic to non-Ohmic behaviour shift to higher frequencies with respect to the increase in the concentration of the nanophase was more pronounced. This upshift in the transition frequencies indicated that the solution became less dielectric. The three orders of magnitude difference in $|Z|$ among the studied concentrations was a clear indication of the formation of a percolated network of CNTs for INK_ASF_0.1 and INK_ASF_0.5 occurring between 5 and 60 min of sonication time.

For 5 min sonication time, the dielectric behaviour of INK_AM was similar for all concentrations of the nanophase with initial $|Z|$ ranging at ca. $10^{10} \Omega$ (Figure 35j). Both INK_AM_0.01 and INK_AM_0.5 remain highly dielectric at 60 min of sonication time, whereas INK_AM_0.1 exhibits indications of percolation phenomena (Figure 35k). INK_AM_0.01 and INK_AM_0.5 show reduced initial $|Z|$ values for 90 min, whereas INK_AM_0.1 exhibits further reduction in its $|Z|$ values (Figure 35l). Unexpectedly, INK_AM_0.5 presented higher $|Z|$ values for both 60 min (Figure 35k) and 90 min (Figure 35l) by an order of magnitude in comparison to INK_AM_0.1 and INK_AM_0.01. At both 60 and 90 min sonication time, INK_AM_0.1 exhibits lower $|Z|$ values than both INK_AM_0.01 and INK_AM_0.5, that is, a non-monotonic behaviour with respect to concentration.

A similar effect albeit less pronounced was observed for INK_SA at 90 min sonication time (Figure 35f). Although this phenomenon cannot be readily interpreted, it may be attributed to the fact that higher CNT concentrations demand higher total energy input to de-agglomerate

the CNT aggregates and thus percolation is observed earlier for lower concentrations and the same amount of total energy input [193].

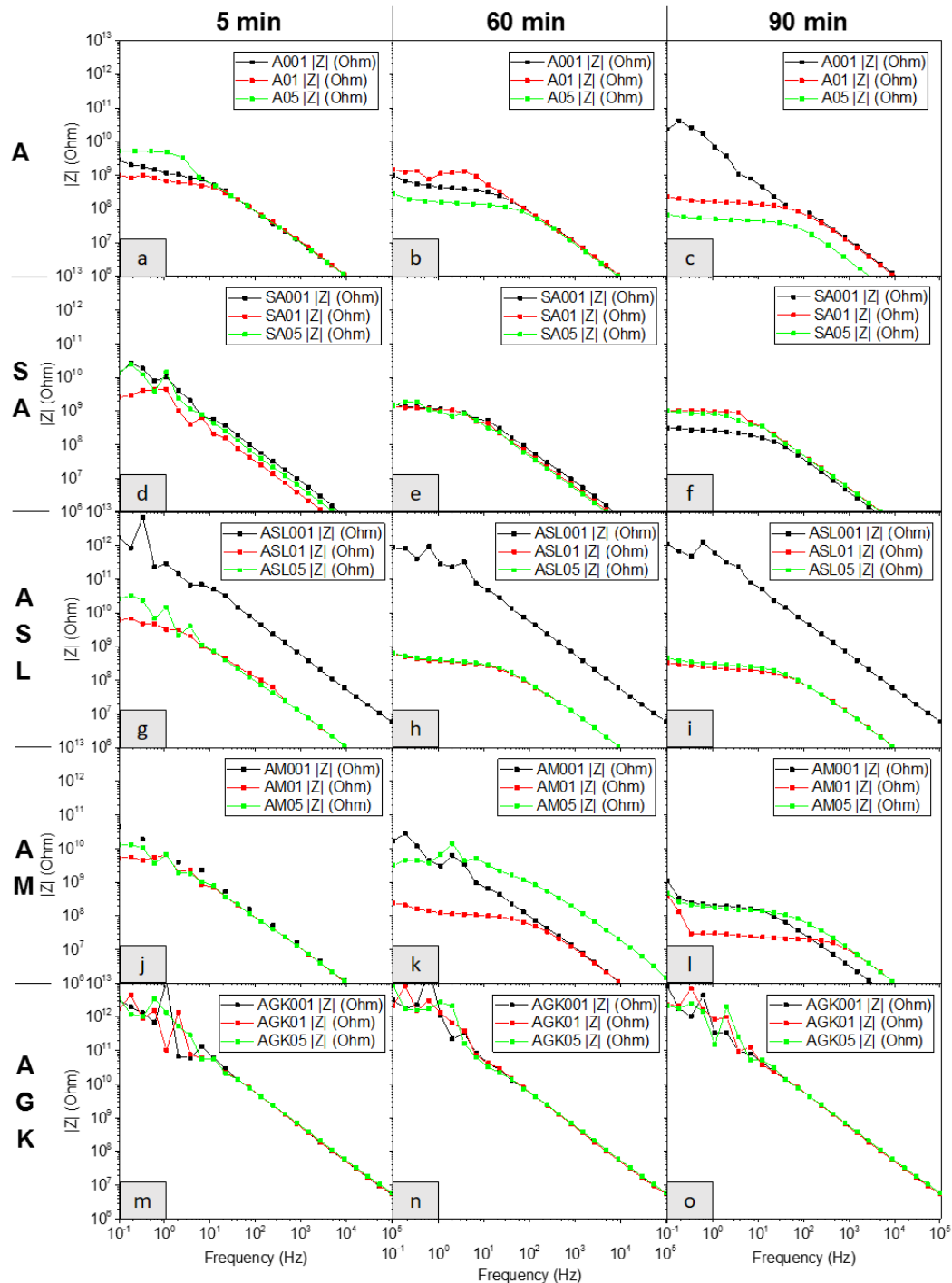


Figure 35. EIS plots of the dispersion process monitoring.

INK_AGK presented an overall different electrical behaviour from the rest of the INKs with respect to both the increase in concentration as well as sonication time. The initial $|Z|$ values ranged at ca. $10^{12} \Omega$ and the DC to AC (Ohmic to non-Ohmic) transition took place at lower frequencies than 0.1 Hz, i.e. both parameters lied outside the range of the employed setup. In all cases, INK_AGK exhibited inferior electric properties, which probably related to extensive degradation caused by the harsh oxidation conditions which led to low CNT aspect ratio and consequent inability to form a percolation network [194].

In conclusion, EIS monitoring of the dispersion process indicated that the realisation of a percolation threshold of CNTs was observed for all studied INKs except for INK_AGK, presumably due to the extensive degradation of the CNTs. INK_A exhibited signs of degradation of the CNTs due to the sonication process. Both INK_SA and INK_AM exhibited non-monotonic behaviour with respect to concentration. Finally, INK_ASL exhibited consistent behaviour with regards to concentration for all sonication times.

3.6.4.2. Long-term INK stability

An amount of each of the produced INKs was stored in sealed glass containers at 23 °C for 60 days in order to evaluate their stability concerning time. Photographs of the INKs after 60 days are presented in Figure 36. Among the produced INKs only INK_A_0.5 exhibited sedimentation after the period mentioned above.

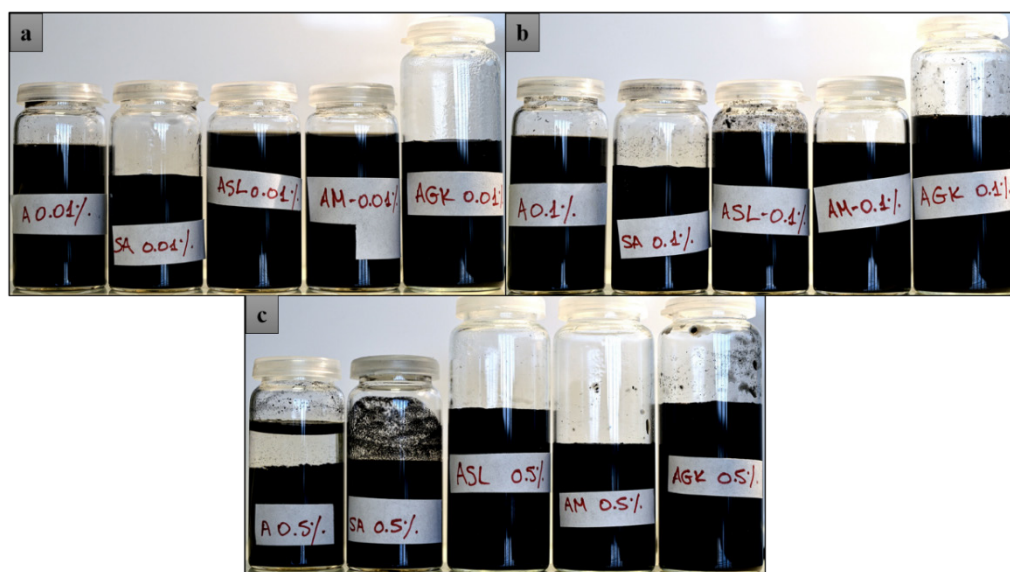


Figure 36. Photographs of the CNT dispersions 60 days after their production.

3.6.5. Visualisation of the outcome

3.6.5.1. PHASE I: INK selection algorithm

Before the employment of the CNT INKs for CF coating, the application of an INK selection algorithm was mandatory due to the large number of combinations among the studied parameters. The algorithm should lead to the choice of the most suitable INK to be used for a screening study in order to define the best combination of parameters for the production of hierarchical all graphitic structures. The realisation of the algorithm was achieved by ranking the results from each utilised characterisation technique. Specifically, numbers ranging from 1 to 5 were given to every CNT sample for each characterisation method. The ranking procedure is summarised in Table 6.

Table 6. Ranking of oxidised CNTs.

METHOD\CNTS	A	SA	ASL	AM	AGK
¹ IR	1	2	5	3	4
² RAMAN (I_D/I_G)	3-1	5	4	3-1	3-1
³ XPS	1	2	3-4	3-4	5
⁴ TGA (COMBUSTION T)	1	3	4	2	5
⁵ EIS	2	3-4	5	3-4	1
TOTAL SCORE	6-8	15-16	21-22	12-16	16-18

¹ Lower RANK represents less functionalization

² Lower RANK represents higher I_D/I_G ratio, i.e. higher degradation

³ Lower RANK represents less functionalization

⁴ Lower RANK represents lower Combustion T

⁵ Lower RANK represents less percolation tendency

As can be seen, INK_A and INK_SA exhibited the lowest degree of functionalization (IR, XPS, TGA). Moreover, INK_A was the only suspension that exhibited sedimentation in the long-term stability study. Among the rest of them, INK_AGK was the most aggressively oxidized sample exhibiting the second highest values in the intensity of its IR bands related to carboxyl vibrations, the highest oxygen content according to its XPS values, the highest combustion temperature indicated by the TGA results, as well as the highest deviations from the sp^2 hybridization according to Raman measurements. INK_AM presented medium to high values of functionalization (IR, XPS) but also lower combustion temperature (TGA) than INK_AGK and INK_ASL along with a higher I_d/I_g ratio than INK_ASL. The best combination of properties was exhibited by INK_ASL, gathering the higher total score during the ranking process, as it presented the highest functionalization values in IR and the second highest in XPS, the second highest combustion temperature (TGA) along with moderate values of distortion of its sp^2 nature.

As indicated by EIS results, percolation could not be achieved with INK_AGK, most probably due to the extensive degradation of the CNTs resulting from the aggressive oxidation. INK_A showed signs of degradation due to sonication whereas INK_SA and INK_AM exhibited non-monotonic behaviour. INK_ASL was the only one exhibiting a consistent percolation behaviour concerning concentration. Therefore, based on this comparative evaluation, INK_ASL was selected as the most suitable one for the preliminary SEM study.

A flow chart depicting the algorithm which was followed for the realisation of the preliminary and final SEM studies is presented in Figure 37.

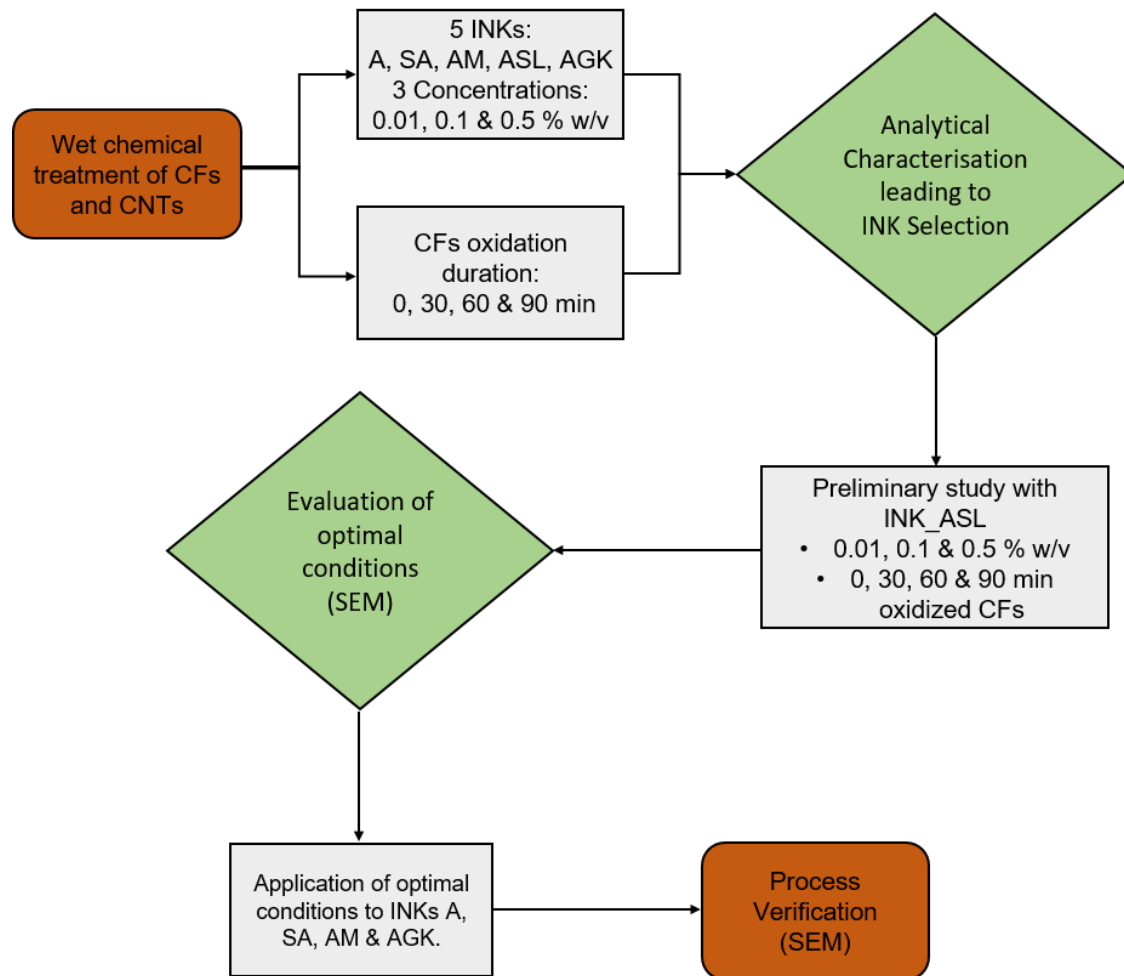


Figure 37. Flowchart of the optimisation process from the SEM studies.

3.6.5.2. PHASE II: Selection of the optimal process conditions

As aforementioned, INK_ASL was selected to be used in the screening experiments. During this preliminary study, the concentrations of the INKs previously monitored by EIS (INK_ASL_0.01, INK_ASL_0.1 and INK_ASL_0.5) were used to coat the surface of as received and oxidised for 30, 60 and 90 min CFs. The CFs were immersed into each INK using the purposely made device presented in Figure 27. This study was conducted with both unsized and sized CFs.

During PHASE II, the number of immersions of the CFs into the CNT INKs were also investigated together with the INK concentration. 10, 30 and 50 immersions were carried out for INK_ASL_0.01 and INK_ASL_0.1. In the case of INK_ASL_0.5, only 10 and 30

immersions were attempted since excessive coverage was already observed for 30 immersions.

In the micrographs presented in Figure 38, the coating process was repeated for 50 times using INK_AS_L_0.01. The micrographs in the first row (Figure 38 a - Figure 38 d) correspond to unsized CFs, while the sized CFs are depicted in the micrographs of the second row (Figure 38 e - Figure 38 h). It has to be noted that, similar micrographs were also acquired for the 10 and 30 immersions, but the coverage of the CF surfaces with CNTs was even more scarce. Therefore, only the 50 immersions in the INK_AS_L_0.01 are presented (Figure 38).

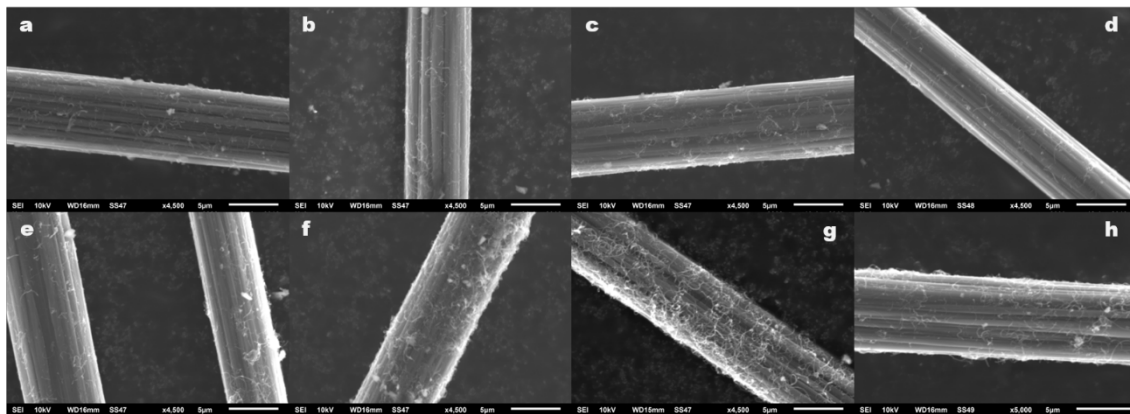


Figure 38. SEM micrographs of unsized (a-d) and sized (e-f) CFs coated with INK_AS_L_0.01 for 50 repetitions. As received CFs (a and e), oxidised in HNO₃ for 30 min (b and f), 60 min (c and g) and 90 min (d and h). All scale-bars are equal to 5 μm.

A direct comparison of the unsized and sized CFs indicated that the presence of the polymeric sizing enhanced the affinity between the CFs and CNTs. Furthermore, a closer observation of the micrographs showed that, CNTs coverage on the CF surface increased with increasing the duration of oxidation for both the unsized and the sized CFs, from 0 min (Figure 38 a and e) to 30 min (Figure 38 b and f) and increased further for 60 min (Figure 38 c and g). However, for 90 min CF oxidation time (Figure 38 d and h), the CNTs did not efficiently cover the CF surface. This observation implies that increased oxidation of the CF surface reduced its affinity to the CNTs. Although this effect was consistently observed, it may not readily be explained and should be further investigated. Possibly, initially, oxidation causes point defects at the CF surface increasing the affinity with the nanophase, whereas at later stages it may lead to peeling of the outer graphene layers

rendering the surface inert again. In all cases, this protocol resulted in a discontinuous coating with several spots whereby the underlying CF was visible.

Moving to the higher concentration (INK_ASL_0.1), although an increased loading of CNTs was observed for this INK concentration in comparison to INL_ASL_0.1, the 30 or 50 immersions were still insufficient for a homogenous coverage of the unsized CF surfaces with CNTs (Figure 39). It was also interesting that the as-received CFs presented increased affinity to the CNTs in comparison to the oxidised CFs. Similar behaviour was observed for these conditions for the sized CFs (not presented here).

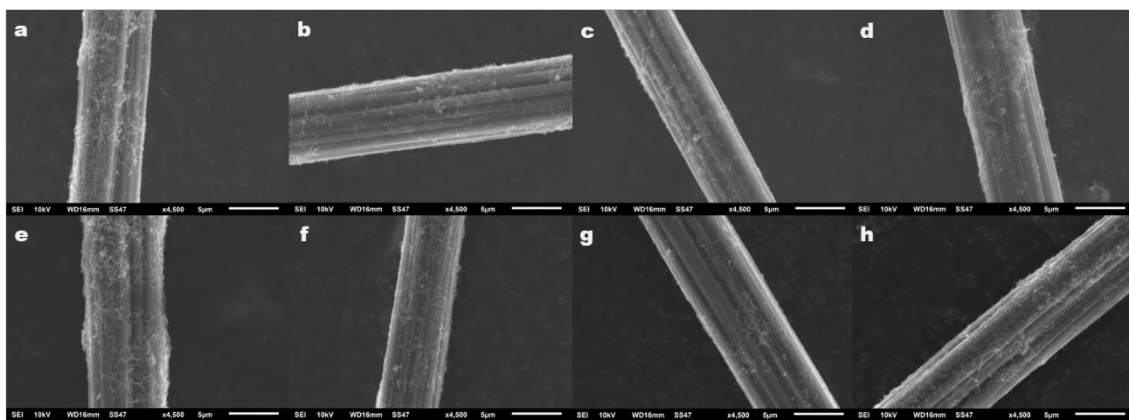


Figure 39. SEM micrographs of unsized CFs coated with INK_ASL_0.1 for 10 (a - d) and 30 (e - h) repetitions. As received CFs (a and e), oxidised in HNO_3 for 30 min (b and f), 60 min (c and g) and 90 min (d and h). All scale-bars are equal to 5 μm .

On the contrary, in all cases including the as received unsized and sized CFs, uniform coatings with a homogeneous layer of CNTs, free of aggregates and most importantly thin enough to not significantly change the fibre diameter were observed for 50 immersions in INK_ASL_0.1 (Figure 40). Conversely, 90 min of oxidation was shown to deteriorate the CNT coating for the sized CFs, as also observed for INK_ASL_0.01.

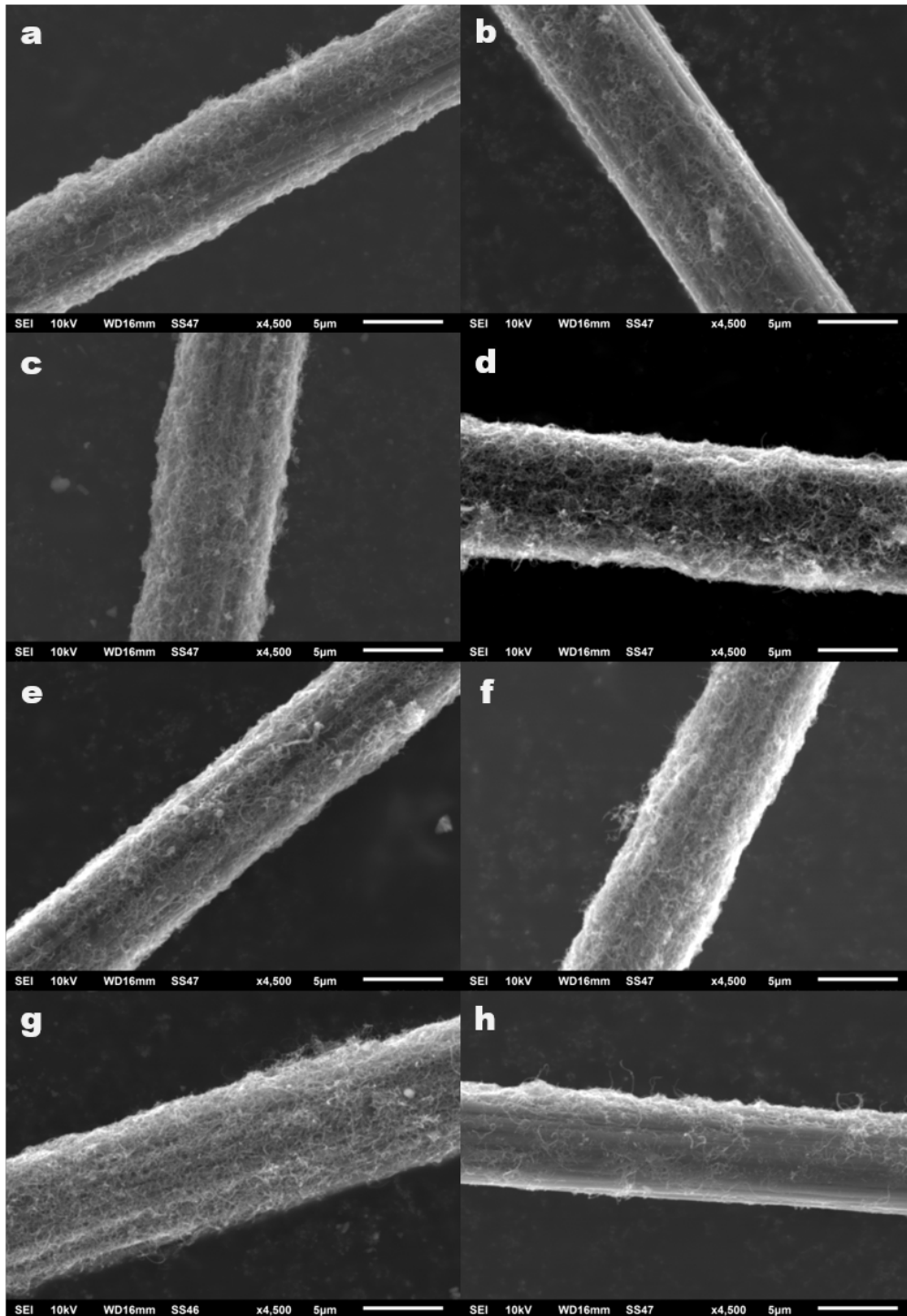


Figure 40. SEM micrographs of unsized (a, c, e and g) and sized (b, d, f and h) CFs coated with INK_AS_L_0.1 for 50 repetitions. As received CFs (a and b), oxidised in HNO_3 for 30 min (c and d), 60 min (e and f) and 90 min (g and h).

In the case of INK_AS_L_0.5 (Figure 41), only 10 immersions were sufficient to produce a homogeneous coverage of the unsized CF surface (Figure 41 a, c, e, g). Increasing the

number of immersions to 30 (Figure 41 b, d, f, h) resulted in excessive coverage and formation of aggregates on the surface for all cases. As far as the CF oxidation time is concerned, CNT coverage was found to marginally improve from 0 (Figure 41 a) to 30 min (Figure 41 c) CF oxidation time. As in the case of INK_AS_L_0.01, a slight deterioration in the uniformity of the CNT coating for 60 min (Figure 41 e) and 90 min (Figure 41 g) was observed. Overall, the best results were produced for 10 immersions and both for 0 and 30 min of CF oxidation time, with the 30 min exhibiting marginally better behaviour. The sized CFs (not presented here) exhibited similar behaviour.

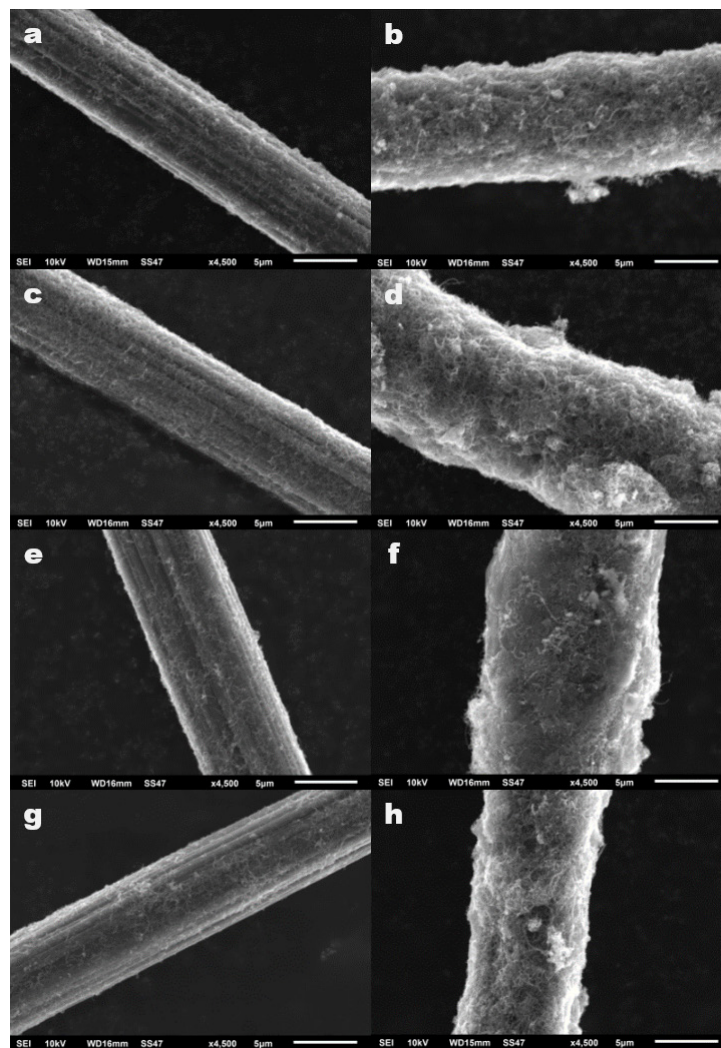


Figure 41. SEM micrographs of unsized CFs coated with INK_AS_L_0.5 for 10 (a, c, e and g) and 30 (b, d, f and h) repetitions. As received CF (a, b), CF oxidised in HNO_3 for 30 min (c, d), 60 min (e, f) and 90 min (g, h).

Summarising, the screening study of INK_ASL showed that both INK_ASL_0.1 and INK_ASL_0.5 produced satisfactory hierarchical structures depending on the number of immersions. In the laboratory conditions, INK_ASL_0.1 may be chosen because it produced coatings of CNTs with more controllable thickness due to its lower concentration when compared to INK_ASL_0.5. Thus, every immersion resulted in a smaller increment in the CNT thickness and therefore offered the possibility of reproducible and uniform coatings.

3.6.5.3. PHASE III: Validation

The protocol which led to the realisation of the most uniform hierarchical graphitic reinforcements (INK_ASL_0.1/ 50 repetitions), described in detail above, was applied for the rest of the INKS both on the unsized and the sized CFs. Figure 42 shows representative micrographs revealing the existence of extensive surface coverage. INK_AM_0.1 (Figure 42 c) and INK_AGK_0.1 (Figure 42 d) exhibited a high amount of CNT agglomerates, rendering the coating inhomogeneous. INK_A_0.1 (Figure 42 a) and INK_SA_0.1 (Figure 42 b) exhibited aggregates too, albeit smaller and fewer in comparison to INK_AM_0.1 and INK_AGK_0.1. This finding suggested that the agglomeration degree increased as the oxidation conditions of CNTs became harsher.

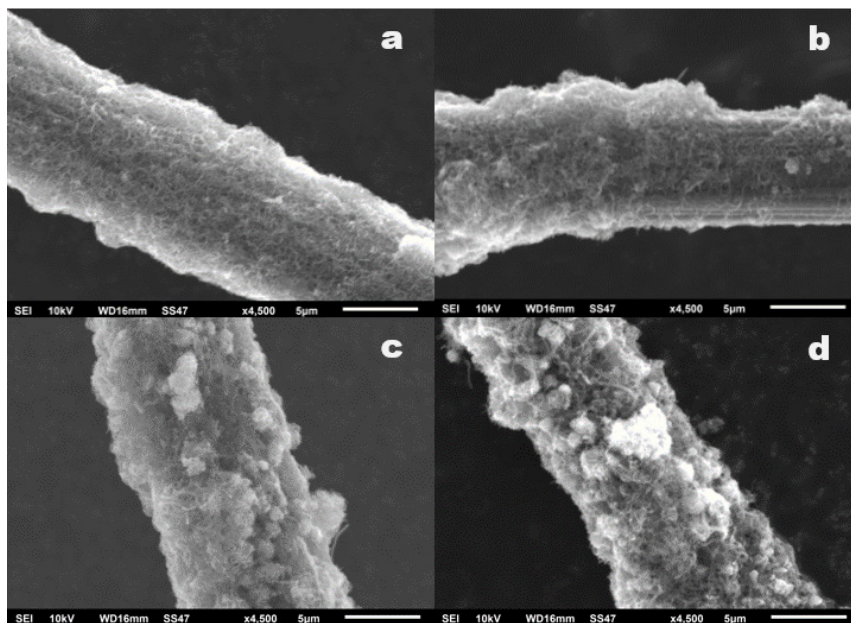


Figure 42. SEM micrographs of unsized CFs coated with INK_x_0.1 for 50 repetitions. a) 30 min oxidized CF/ INK_A_0.1, b) as received CF/ INK_{SA}_0.1, c) 90 min oxidized CF/ INK_{AM}_0.1 and d) 60 min oxidized CF/ INK_{AGK}_0.1.

Overall, SEM micrographs shown in Figure 42 confirmed the efficiency of the utilised algorithm since INK_AS_L still proved to be the most suitable one for the CF coating with CNTs.

3.7 Conclusions related to Hierarchical reinforcements produced via wet chemical treatments

Overall, the current work established a precise roadmap for the production of hierarchical all graphitic structures by wet chemical treatments and dip coating processes. The systematic approach followed during this study included the use of an algorithmic process whereby the studied parameters (oxidation duration, concentration of CNTs in acids and mechanical aiding of the dispersion) were evaluated and ranked based on the experimental evidence provided by various analytical techniques. Among these techniques, EIS was for the first time to our knowledge used as an indicator of the success of the dispersion process of CNTs in aqueous media. Finally, the optimised INK was used as a coating on oxidised carbon fibres. SEM micrographs revealed that the formation of a thin homogeneous veil of CNTs onto the CF surface was feasible. The viability and validity of the process were verified by confirming the INK choice in relation to the rest of the produced INKs.

Furthermore, valuable conclusions on the mechanisms acting during oxidation of the nanostructures were drawn, and the factors affecting the homogeneity and thickness of the CNTs veil onto the CF surface were identified. Combined experimental findings suggested that two competing mechanisms were simultaneously present during oxidation, i.e. (i) the introduction of oxygen-based functional moieties and (ii) the purification of the CNTs.

Summarizing, the governing conditions for the production of the all graphitic hierarchical structures were (i) the moderate oxidation of CNTs by stirring which facilitated (ii) the production of a homogeneous, electrically percolated INK by sufficient sonication and a final (iii) systematically controlled dip coating process of the CFs in the produced INK.

3.8 Overall conclusions and benchmarking of hierarchical reinforcements produced by CVD or wet chemical treatments

Overall, the CVD process resulted in a denser coverage of the CF surface with a porous layer of MWCNTs, which significantly altered the substrate CF diameter, in comparison to the wet chemical process. On the other hand, the wet chemical dip-coating procedure, which was developed and optimised during this study, was more efficient in controlling the thickness of the deposited CNTs onto the CFs.

A comparison of the two production processes indicated that the wet chemical treatment route is more viable for upscaling towards the manufacturing of hierarchical CFRCs. Consequently, the hierarchical reinforcements produced by the two different techniques were used for the benchmarking study of the structural and mechanical properties at the single fibre (Chapter 4) or model composite level (Chapter 5). Conversely, only the wet chemical modification and the dip-coating process were used for the production of reinforcements which were utilised in the manufacturing of hierarchical laminated CF-CNT/epoxy composites for the characterisation of the out-of-plane mechanical properties (Chapter 6).

Additionally, the developed and optimised CNT inks are suitable for several applications as printing materials for implementation in various processes other than dip-coating, i.e. spraying, roll-to-roll printing via screen printing technologies.

Chapter 4

Physicochemical and Micromechanical characterisation of the hierarchical reinforcements

Part of the results included in this Chapter which are related to the CVD process have been published at the Composites Science & Technology peer-reviewed scientific journal as part of the study “Optimal Synergy between micro and nano scale: Hierarchical all carbon composite fibres for enhanced stiffness interfacial shear strength and Raman strain sensing” and can be found under <https://doi.org/10.1016/j.compscitech.2018.07.003>. Additionally, some of the results of this Chapter which are related to the evaluation of the strain induced Raman sensitivity have been published at the peer-reviewed scientific Journal of Materials Engineering and performance as part of the study “Strain sensing ability and residual stress profiles of hierarchical carbon fibres produced via different methods” and can be found under <https://www.springerprofessional.de/en/raman-strain-sensing-and-interfacial-stress-transfer-of-hierarch/15979264>.

4.1 Introduction

Although the knowledge and the research efforts on advanced multiscale CFRCs have ever been increasing during the last decade as shown in Chapter 2, there is ample space for further enhancement in their mechanical properties, as the composite properties do not yet adequately reflect the potential of the reinforcing phases. The hierarchical approach provides a facile method for the improvement of the inherently poor out-of-plane mechanical properties of the CFRCs by targeting to reinforce the interfacial region. However, most of the production processes reported so far lead to some degradation of the in-plane mechanical properties of the CF substrate [54,59].

Therefore, a detailed study of the physicochemical and the mechanical properties of the hierarchical reinforcements before their incorporation into a polymer matrix is indispensable in order to design and fabricate hierarchical CFRCs with improved overall performance. Practically, the structural characteristics of the grown or deposited CNTs, the thickness and the orientation of the CNT coating onto the CFs can affect the mechanical properties of the hierarchical reinforcements.

At the same time, a corollary of the hierarchical nature of such reinforcements is often demonstrated by various added functionalities. Gao et al. reported on the strain, humidity and temperature sensing ability of hierarchical glass fibres, coated with commercial oxidised CNTs by electrical measurements [195]. Tzounis et al. presented the

thermoelectric response of single glass fibres coated with CNTs [196]. Furthermore, Raman spectroscopy has extensively been employed for stress or strain sensing of crystalline carbon micro and nano-scaled reinforcements, whereby the inclusions act as sensing elements with a sub-micron spatial resolution [197,198]. The basic principle underlying the employment of Raman spectroscopy for strain monitoring is the change in the frequency of distinct vibrational modes when an external load is applied, due to the anharmonicity of the molecular bonds [198]. Thus, a molecular displacement is translated to an actual strain or equally stress profile that in the case of a composite material, can describe its stress and strain state. This method can potentially be applied as a non-destructive evaluation technique for in field applications using modern portable spectrometers [199], or fibre optic based systems [200].

Raman sensing from commercial CNTs deposited onto glass or carbon fibre surfaces has been reported by Liu et al. who studied strain induced Raman shifts of hierarchical glass fibres coated with a silane coating containing dispersed single-walled CNTs. The strain induced Raman shift exhibited a dependence on the coating thickness, with thicker coatings resulting in increased values, namely $16.6 \text{ cm}^{-1} / \% \text{ strain}$ [201]. In a similar study, Jin et al. reported on the strain induced Raman sensing ability of high ($5.8 \text{ cm}^{-1} / \text{GPa}$) and low modulus ($4.8 \text{ cm}^{-1} / \text{GPa}$) CFs coated with a silane containing single-walled CNTs [165]. Both studies referred to the 2D graphitic vibrational mode, and to the author's knowledge are the only studies referring to hierarchical fibres. However, the strain induced Raman sensing ability of hierarchical reinforcements where the nano reinforcement (CNTs) is grown or deposited on the fibre surface has not as yet been reported. This is the approach adopted in the current study, where hierarchical reinforcements produced by CVD are benchmarked against CF-CNTs produced by wet chemical treatments.

More analytically, in this chapter, the crystalline structure and the thermal stability of hierarchical CF-CNTs produced either by CVD or wet chemical treatments were evaluated by Raman and TGA measurements, respectively. Then, the effects of the production processes on the tensile properties of the hierarchical reinforcements were assessed by Single Fibre tensile tests accompanied by a detailed Weibull statistical analysis. Finally, the hierarchical reinforcements were evaluated as strain sensors by measuring their strain induced Raman sensing ability.

4.2 Experimental Section

4.2.1. Materials

The unsized hierarchical CFs produced by CVD as well as the unsized and sized hierarchical CFs produced by wet chemical treatments and deposition of CNT INKs were studied in this chapter. Additionally, both the unsized and the sized M40 high modulus PAN fibres (Torayca) with a tensile strength of 2.74 GPa, modulus of 392 GPa and failure strain 0.7%, as stated by the manufacturer, were used as the reference. The reference CF diameter was 6.6 μm as determined by density measurements. The code names for each of the studied reinforcements were summarised in Table 7.

Table 7. Nomenclature of the studied hierarchical and reference CFs.

Code Name	Carbon Fibers	Production Process details
CF/UNS	unsized	No treatment used as received
CF/S	sized	No treatment used as received
CF-CNT@X/Y	unsized	CVD at “X” temperature in [$^{\circ}\text{C}$] for “Y” duration in [min]
CF-CNT/UNS_X_Y	unsized	Wet treated for “X” min of oxidation and “Y” repetitions of coating
CF-CNT/S_X_Y	sized	Wet treatment with “X” min of oxidation and “Y” repetitions of coating

4.2.2. Methods

4.2.2.1. Raman spectroscopy for crystallinity and structural ordering evaluation

Raman spectra of the hierarchical reinforcements were recorded with a Labram HR – Horiba scientific system. The 514.5 nm line of an argon ion laser operating at 1.5mW at the focal plane was employed for the Raman excitation. An optical microscope served as the collector of the Raman scattering equipped with a 100 \times objective. Raman spectra in the range of 100–3500 cm^{-1} were collected for the characterisation of the degree of order of the

hierarchical CFs. Acquisition times were 30 s. The spectral analysis included baseline subtraction and fitting procedures with Lorentzian and Gaussian distributions. More details on the spectral treatment can be found in section A3.1 of the Appendix.

4.2.2.2. Thermal stability measurements

The thermal behaviour of CF and CF-CNT hierarchical structures after CVD-growth were investigated by thermogravimetric analysis (TGA) using a Leco TGA701 instrument (for the CVD grown CF-CNTs and the reference CF/UNS) or a Netzsch STA 449C instrument (for the CF-CNTs produced by wet chemical protocols). Thermal scans were performed under oxygen flow from 30 °C to 1000 °C with a heating rate of 10 °C/min. Differential scanning calorimetry was also recorded with the Netzsch STA 449C instrument for the CF-CNTs produced by wet chemical protocols and the reference CF/S in order to further study the contributions of the CFs and the CNTs.

4.2.2.3. Single fibre tensile tests

CFs and CF-CNTs were tested at three gauge lengths, i.e. 10 mm, 25 mm and 40 mm, following the ASTM C1557-14 [202]. The strength of the CFs was assessed experimentally before (CF/UNS and CF/S) and after the CVD growth of CNTs onto their surfaces utilizing the “harshes”, in terms of temperature and duration, growth conditions (CF-CNT@850/30), as well as after coating of the CFs with CNTs following wet chemical protocols and dip-coating (CF-CNT/UNS_X_Y and CF-CNT/S_X_Y). The number of filaments tested from each category was about 60 for each length, but cases which exhibited slippage or nonlinearity were excluded, and thus around 20 CFs in each studied length are presented. Furthermore, the Weibull shape, m , and scale parameters were calculated for all the tested CFs and CF-CNTs by considering the following statistical analysis [203].

If a CF filament is regarded as a single chain of units with length L_0 , which fail at stresses equal to σ_i , then the cumulative probability of failure for the entire chain is given by the Weibull distribution from equation (1).

$$P = 1 - \exp \left[-L \left(\frac{\sigma}{\sigma_0} \right)^m \right] \quad (1)$$

where σ is the applied stress, σ_0 is a scale parameter, and m is the dimensionless Weibull modulus.

Equation (1) can also be written in linear form as

$$\ln(-\ln(1-P)) - \ln(L) = m \ln(\sigma) - m \ln(\sigma_0). \quad (2)$$

Thus, if the $\ln(-\ln(1-P))$ is plotted against $\ln(\sigma)$, then the Weibull modulus can be calculated from the slope of the curve while the scale parameter can be estimated from the value of the intercept through equation (3)

$$\sigma_0 = \exp \frac{\text{Intercept}}{m} \quad (3)$$

plots of the hierarchical CF-CNTs and the reference CFs were plotted using the equation (4)

$$\ln \ln \left(\frac{1}{1-P} \right) = m \ln \sigma - m \ln \sigma_0. \quad (4)$$

The probability of failure was calculated in this study by the maximum likelihood estimator which is given by the equation (5)

$$P = \frac{\sigma^{-0.5}}{n} \quad (5)$$

where σ is the failure stress of each CF and n is the number of tested CFs.

4.2.2.4. Measurements of the Raman strain sensitivity

For the strain sensing measurements, the response of the 2D peak, ($\sim 2700 \text{ cm}^{-1}$), of CNTs and CFs to externally applied strain was monitored with an acquisition time of 20 sec. Individual CFs and CF-CNTs, with gauge lengths of 15 mm, were bonded to the jaws of a custom designed straining rig ($\pm 1 \text{ }\mu\text{m}$ precision), with their longitudinal axes aligned parallel to the stretching direction to $\pm 5^\circ$. The CFs were tensioned at distinct levels of strain, and the response of the 2D graphitic vibrational mode was monitored. Five Raman spectra were acquired at each straining level using the 514.5 nm line of an argon ion laser operating at 1.5mW at the focal plane. The HR – Horiba scientific system equipped with a

100× objective was used. Additional details on the treatment of the spectra for the quantification of the Raman strain sensitivity parameter can be found in Appendix A.

4.3 Results and Discussion

4.3.1. Structural Characterization

Characteristic Raman spectra of the CF and all the CF-CNT reinforcements produced both by CVD (Figure 43), and wet chemical protocols were acquired (Figure 44). In all cases, the most prominent bands were the four commonly known bands in graphitic materials, i.e. D, G, D' and 2D. More details on the origins of these bands can be found in section A.3.3 of the Appendix.

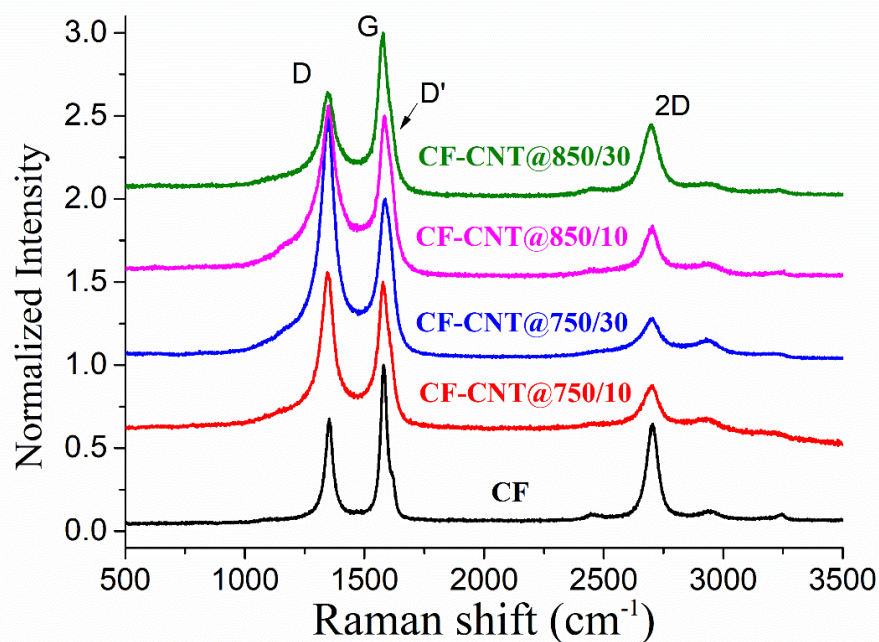


Figure 43. Raman spectra of CF and CF-CNT fibres from different CVD growth conditions. All spectra were normalised to the G band and shifted by 0.5 to facilitate presentation.

Additionally, several other bands existed in the spectra of the hierarchical CF-CNTs. Not all of these features were easily noticed in the normalised data of Figure 43 until the spectra were fitted by Lorentzian bands, as presented in Section A.3.3 of the Appendix. It

has to be noted at this point that, all measurements presented below from CF-CNTs come solely from the CNTs and not the underlying fibre. This statement is supported by the fact that the penetration depth of Raman measurements in graphite as reported by Tuinstra and Koenig, as early as in 1970, is only 50 nm due to the graphite high extinction coefficient [204].

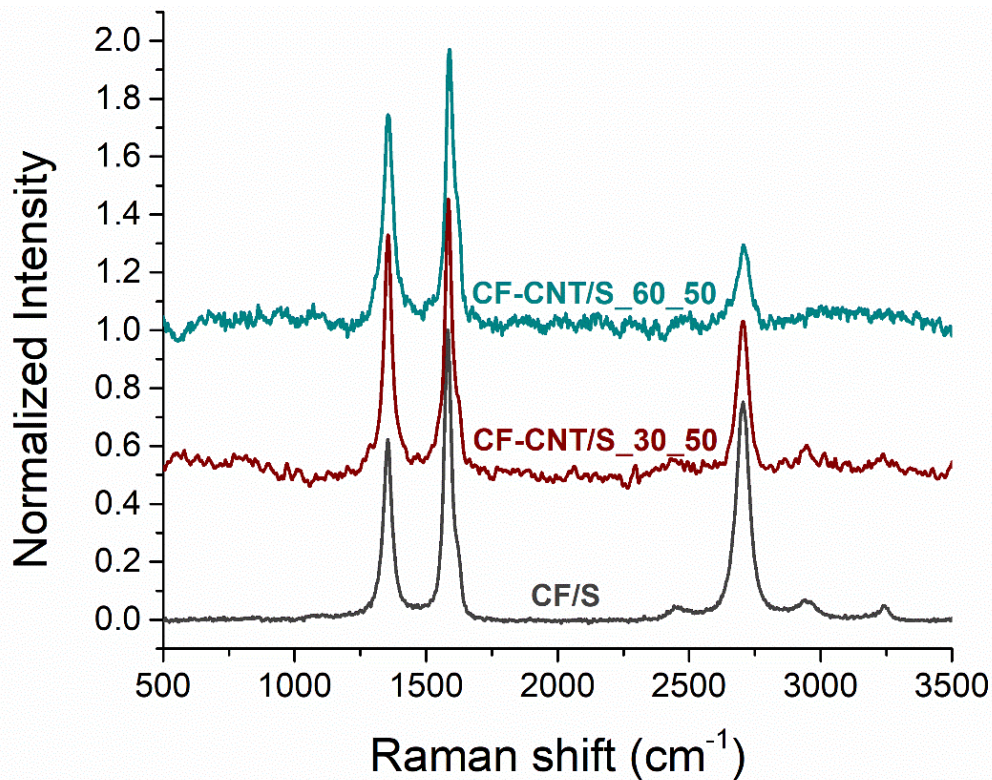


Figure 44. Raman spectra of CF and CF-CNT fibres from the wet chemical treatments. All spectra were normalised to the G band and shifted by 0.5 to facilitate presentation.

Several ratios of the fitted parameters were used in the literature in order to quantify the amount of disorder as well as the graphitisation degree of CNTs [205]. The most extensively utilised one was the intensity ratio of the D peak to the G peak (I_D/I_G), which depicted the degree of disorder present in the samples as normalised by the amount of purely graphitic sites, or in other words the short-range graphitic order. Then, the intensity ratio of the 2D peak to the G peak (I_{2D}/I_G) was correlated to the long-range order of CNTs, as the 2D peak coming from a two-phonon process required some long-range order capable of producing the coupling effect. Consequently, the intensity ratio of the 2D peak to the D peak (I_{2D}/I_D) was a very sensitive index of the overall crystalline quality of the graphitic

structures, increasing with enhanced long-range ordering and increased inter-defect distance. The values of the aforementioned ratios were summarised in Table 8.

These values indicated that the graphitisation degree was dependent both on the growth temperature and duration of the CVD process. More specifically, the degree of order was found to increase with respect to growth duration at 850°C, while a decreasing trend was observed for growth at 750°C. This alteration in the degree of order of the produced structures with respect to growth duration might be attributed to different growth mechanisms occurring at 750°C and 850°C.

With regards to the hierarchical reinforcements produced by the wet chemical treatments and dip-coating process, the degree of order was found to only slightly decrease with the increasing duration of oxidation. Furthermore, it is interesting to note that the average I_D/I_G values are within experimental error slightly decreased in comparison to the respective values of the CNTs after the oxidation and before the deposition process onto the CFs (Table 3). This could indicate that some of the oxygen-containing functional groups on the CNT sidewalls have been eliminated by grafting to the CFs.

Table 8. Fitting parameters of the Raman spectra of CF and for all CF-CNT.

	I_D/I_G	I_{2D}/I_G	I_{2D}/I_D	L_a [nm]
CF/UNS	0.69 ± 0.15	0.54 ± 0.10	0.82 ± 0.28	4.92 ± 1.28
CF-CNT@750/10	1.18 ± 0.44	0.30 ± 0.04	0.28 ± 0.10	3.05 ± 1.07
CF-CNT@750/30	1.62 ± 0.17	0.30 ± 0.07	0.19 ± 0.06	1.97 ± 0.41
CF-CNT@850/10	1.28 ± 0.34	0.23 ± 0.12	0.18 ± 0.12	2.17 ± 0.48
CF-CNT@850/30	0.70 ± 0.19	0.53 ± 0.07	0.79 ± 0.27	4.38 ± 0.82
CF/S	0.58 ± 0.05	0.74 ± 0.04	1.28 ± 0.15	6.02 ± 0.61
CF-CNT/S_30_50	0.66 ± 0.15	0.46 ± 0.09	0.71 ± 0.17	5.40 ± 0.93
CF-CNT/S_60_50	0.71 ± 0.17	0.52 ± 0.33	0.72 ± 0.33	4.88 ± 1.28

In more detail, among the produced hierarchical CF-CNTs by the CVD process, the CF-CNT@850/30 presented the highest degree of order exhibiting the smallest amount of

crystal defects (lowest I_D/I_G) alongside with enhanced long-range ordering (highest I_{2D}/I_G) and increased inter-defect distance (highest I_{2D}/I_D). The values of all the aforementioned ratios for the CF-CNT@850/30 were comparable to the crystalline ordering of the reference CF/UNS, indicating an extended crystalline ordering of the CNTs analogous to the crystalline CF/UNS. These values also corroborate the morphological SEM analysis (Figure 24), whereby long and thin CNTs together with graphitic platelet-like particles were found for this growth condition, indicating that those nanoparticles were crystalline and not amorphous. The rest of the samples showed a lower degree of order than the CF-CNT@850/30. The sample with the highest number of defects and the lowest degree of order was the CF-CNT@750/30 as the Raman peak ratio values indicated. Morphologically, this sample consisted of long and individual CNTs arranged in bundles without any present graphitic nanoparticles. The absence of these particles and the lower CNT degree of order were possibly the reasons for the lowest values of I_{2D}/I_G . Intermediate ordering and crystallinity were found for the two samples, which were exposed to 10 min CNT growth at 750°C and 850°C.

On the other hand, the hierarchical CF-CNTs produced by the wet chemical and dip-coating process exhibited much smaller amounts of crystal defects (lower I_D/I_G) in comparison to the hierarchical reinforcements produced by the CVD process. Moreover, the CF-CNT/S_30_50 and the CF-CNT/S_60_50 exhibited similar long-range ordering (I_{2D}/I_G) and inter-defect distance (I_{2D}/I_D) which were slightly reduced in comparison to the reference CF/S and were comparable to the values exhibited by the reference CF/UNS and the CF-CNT@850/30.

Table 8 also summarises the in-plane correlation length, L_a , as calculated from the peak fitting parameters using the Knight formula (equation (6)),

$$L_a = C \left(\frac{I_d}{I_g} \right)^{-1} \quad (6)$$

where C equals 4.4 nm for a laser wavelength of 514.5 nm [206]. This parameter defined the graphitic cluster diameter or, in other words, the amount of undisturbed interacting π states in the studied system [207]. With regards to the hierarchical reinforcement produced by CVD, the most graphitised CF-CNT@850/30 showed the most prominent L_a (4.38 nm) comparable to that of the reference CF/UNS (4.92 nm). All the other CF-CNT presented

lower values of L_a stemming from the higher number of defects (i.e. pentagons, heptagons and vacancies) present in their crystalline structure.

Furthermore, the reference CF/S exhibited higher L_a in comparison to the reference CF/UNS, leading to hierarchical reinforcements with more pronounced L_a (CF-CNT/S_30_50 and CF-CNT/S_60_50) in comparison to the hierarchical reinforcements produced by the CVD process.

4.3.2. Evaluation of the thermal stability of the hierarchical reinforcements

Subsequently, the thermal stability and graphitisation degree of the CF and the CF-CNT samples were evaluated via TGA. Figure 45 and Figure 46 revealed pronounced changes in the thermal behaviour of all the CF-CNT reinforcements when compared to the reference CFs. It has to be noted that unfortunately due to technical issues different TGA instruments were used for the thermogravimetric measurements of the CF-CNTs produced via CVD and wet chemical protocols, nevertheless in each case the reference CF was also evaluated for comparison purposes. It should also be noted that the absolute values of the DTG data were plotted in Figure 45 and Figure 46 for the ease of presentation.

With regards to the hierarchical reinforcements produced by CVD (Figure 45), all the CF-CNTs exhibited a weight loss of 19-23% up to 500°C, while at the same time the reference CF/UNS lost 13% of its initial weight. The combustion temperature of the CF-CNT samples was also lower in comparison to CF/UNS. Nevertheless, all the CF-CNT samples remained stable up to ~500 °C, revealing a comparable but less ordered crystalline structure in comparison to the commercial CNTs used for the wet chemical treatments, i.e. the combustion temperature of the commercial as received CNTs was 603°C (Table 5).

In more detail, the thermographs (Figure 45) can be divided into two distinct temperature regions. According to literature, for the first region 25°C – 400°C, combustion of the oxygen-containing groups, physically or chemically adsorbed on the CF and CF-CNTs, occurred [40]. CF and CF-CNTs produced during this study presented a sudden weight loss during the first 100 °C associated with the evaporation of water adsorbed on their surface. Moreover, the aforementioned combustion was manifested as a small peak centred around 340 °C for the CF/UNS and the CF-CNTs. The second region (400 °C – 1000 °C) was the

temperature window where the final combustion of the CF/UNS and CF-CNT occurred. The CF/UNS combustion, represented by a broad peak in the DTG curve, was found at 846 °C and decreased for all the CF-CNT samples to 770 °C, except from CF-CNT@750/30 for which 809 °C was the respective temperature.

Furthermore, the CF-CNT thermal profiles were different from the CF/UNS at this temperature region, presenting an additional peak before the final combustion peak, indicated by the cyan circle in Figure 45. That peak was found at 590 °C for the CF-CNT@750/10, 630 °C for the CF-CNT@850/10 and 635 °C for the CF-CNT@750/30 and CF-CNT@850/30 and was attributed to the combustion of the mixture of carbon allotropes, composed mainly of CNTs, grown on the CF surfaces. These values are in agreement with other literature studies on the thermal stability of carbon allotropes such as CNFs and CNTs produced via CVD for which combustion took place between 500 °C and 600 °C [41,42].

The mass content of the CF and CNTs was evaluated by the TGA curves. The reference CF/UNS was composed of 87.3% carbon, while the rest 12.7% was attributed to absorbed water and some oxygen-containing functionalities. Water and oxygen groups, as well as residual amounts of metal catalyst particles, were also present for the CF-CNTs. For the hierarchical CF-CNTs produced by CVD, higher growth temperature resulted in lower CNT mass content, and this effect was more pronounced for the extended growth duration. The weight content of CFs and CNTs in the hierarchical samples were 26.0 % CNTs and 53.2 % CFs, 16.6 % CNTs and 64.7 % CFs, 20.9 % CNTs and 57.7 % CFs, and 9.6 % CNTs and 67.6 % CFs, for the CF-CNT@750/10, the CF-CNT@750/30, CF-CNT@850/10 and the CF-CNT@850/30, respectively. In any case, these CNT contents are far higher than previously reported CNT contents in hierarchical composites [208].

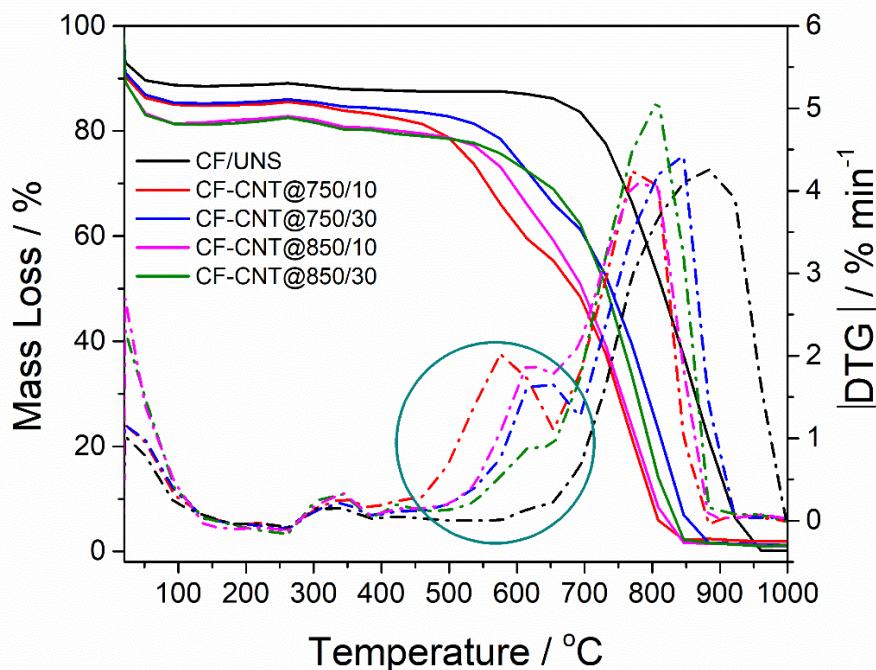


Figure 45. Thermographs of the CF and the CF-CNTs from all CVD conditions. The solid lines represent the mass loss curves, and the dotted lines stand for the rate (first derivative - DTG) of the mass loss curves.

Conversely, the thermographs of the CF-CNTs produced by the wet chemical protocols as well as the reference CF/S exhibited a different trend, being stable (almost negligible mass loss) up to 500°C. In detail, a minor activity was only observed for the reference CF/S from 250 °C and up to 360°C, while the masses of the CF-CNT/S_30_50 and the CF-CNT/S_60_50 decreased only marginally during this temperature window. Furthermore, only one asymmetric peak was found for all cases in the second temperature region (400 °C – 1000 °C), with increased asymmetry for both CF-CNTs in comparison to the reference CF. This finding suggested the presence of another material on the surface of the substrate CFs but did not permit for the quantification of the amount of the CNTs. The most interesting evidence was the increase of the combustion temperature (thermal stability) of the hierarchical reinforcements in comparison to the reference CF/S (817 °C) by 12 °C and 25 °C, for the CF-CNT_30_50 (829 °C) and the CF-CNT_60_50 (842 °C), respectively.

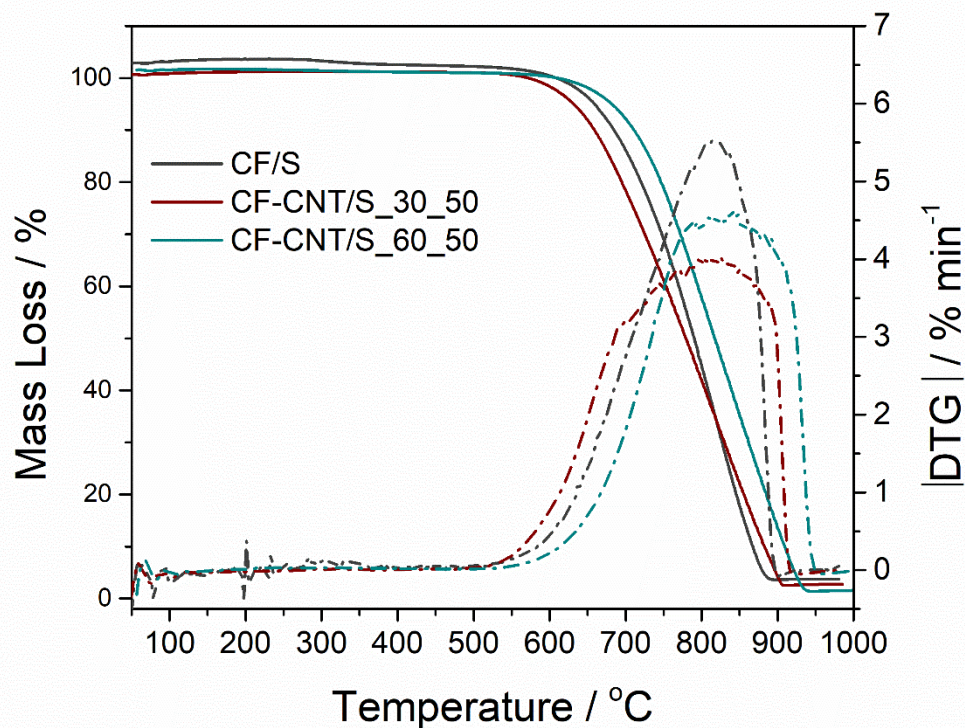


Figure 46. Thermographs of the CF and the CF-CNTs produced by wet chemical protocols. The solid lines represent the mass loss curves, and the dotted lines stand for the rate (first derivative - DTG) of the mass loss curves.

In order to distinguish the contributions of the two graphitic phases, a DSC scan was also recorded (Figure 47). A single exothermic reaction with a peak temperature of 809 °C was recorded for the reference CF/S, while two overlapping reactions were observed for the hierarchical CF-CNTs produced by the wet chemical method. The culminating temperature of the first reaction was observed at 772 °C and 781 °C for the CF-CNT/S_30_50 and CF-CNT/S_30_50, respectively. The peak temperature of the second reaction was notably high for both CNT/S_30_50 (898 °C) and CF-CNT/S_60_50 (902 °C).

If we attribute the former combustion temperature observed in the DSC scans to the CNTs, since their combustion temperature in powder form before being grafted onto the CFs was measured to 617.3 °C (Table 5), then the second combustion temperature can be attributed to the CF/S with a combustion temperature 809 °C before being coated with CNTs. In any case, these two overlapping reactions enhanced both the combustion temperature of the CFs and that of the CNTs in the CF-CNT/S reinforcements. This enhancement might be attributed to the presence of the CNT coating onto the surface of the CFs, which acted as a

thermal barrier, absorbing heat and protecting the CFs from burning, until the very same CNTs started to burn and then the CFs were exposed to the air for their combustion to take place.

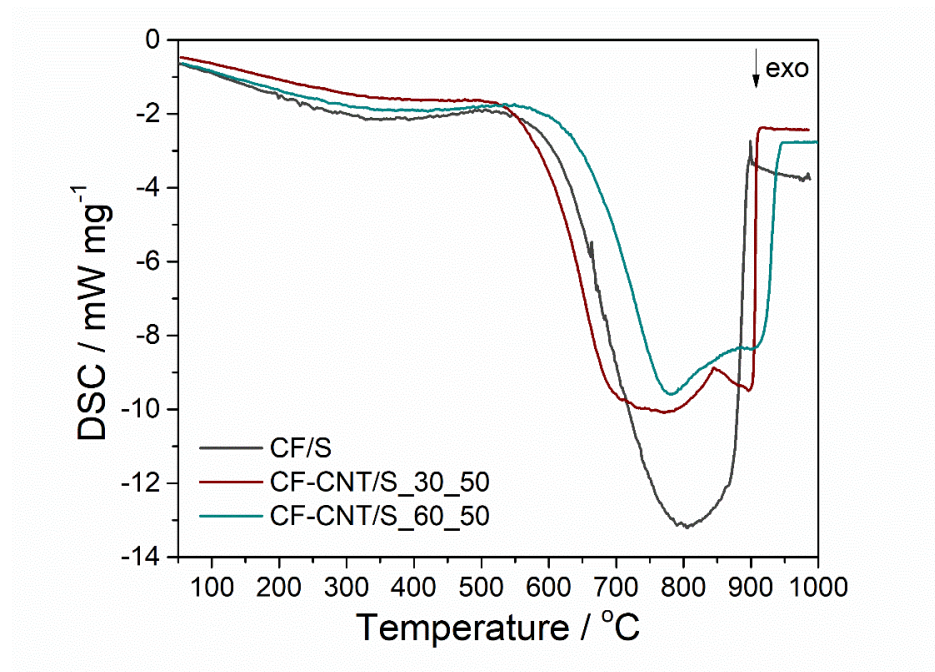


Figure 47. The differential calorimetric scan of the reference CF/S and the CF-CNT/S_30_50 and CF-CNT/S_60_50.

Overall, the TGA results confirmed the presence of the CNTs onto the CF surface, while the CF-CNTs produced by the wet chemical treatments outperformed the CF-CNTs produced by CVD in terms of thermal stability

4.3.3. Tensile properties of the hierarchical CF-CNTs

The strength to length relationships for the reference CFs and all the CF-CNTs were established via tensile tests of single fibres at different lengths (10, 25 and 40mm) (Figure 48). The parameters which describe the dependence of the fibre strength with respect to variations in its length were summarised in Table 9. The average strength, as well as the average strain values, were also summarised in this Table. These values were calculated by considering the average values of all the three measured lengths in each case.

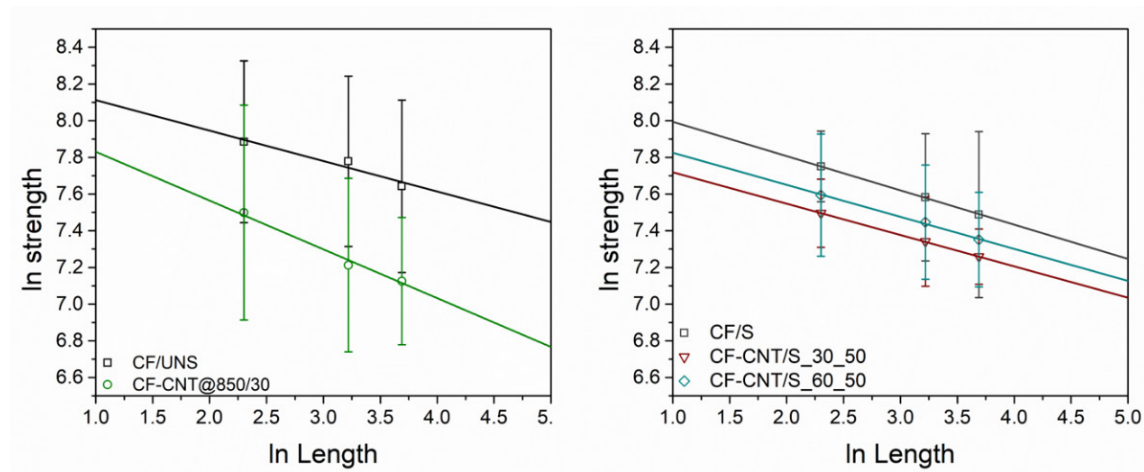


Figure 48. Strength to length relationships for the reference CF/UNS in comparison to the CF-CNT@850/30 (left), and the CF/S in comparison to the CF-CNT/S_30_50 and CF-CNT/S_60_50. (Strength measured in MPa and length in mm).

The estimated equations reflected the effects of the CNT growth or grafting on the CF strength and permitted an extrapolation to the submillimetre lengths recorded during the SFFT (Chapter 5). Both the CVD growth process and the wet chemical protocols resulted in some degradation of the CF tensile properties, as expected. Specifically, the CF strength decreased due to the growth process by 37.1%. Similar strength values were mentioned in literature for the growth processes of CNTs onto CFs at similar growth temperatures [54,62]. On the other hand, the wet chemical protocols resulted in 24.6 % (30 min of oxidation) and 14.5 % (60 min of oxidation) strength loss. It would typically be expected that increased oxidation duration would lead to higher degradation of the CF tensile properties. However, it has to be noted that the CF-CNT/S_30_50 exhibited bigger diameters than the CF-CNT/S_60_50 and this led to lower strength average values in comparison to CF-CNT/S_60_50. This behaviour was also observed by [209] who reported that the diameter of PAN-based CFs gradually decreased with increasing oxidation duration in nitric acid, while the fracture load for CFs remained unaltered for oxidation durations higher than 20 min and up to 120 min. Therefore, the observed behaviour can be attributed to the effects of the oxidation duration of the CFs and not the CNT coating onto the CF surface.

Table 9. Parameters of the strength to length relationships, average strength and strain values for CFs and CF-CNTs.

Code	Intercept	Slope	R ²	Strength [MPa]	ε [%]
CF/UNS	8.278	-0.166	0.939	2604.7 ± 278.6	0.55 ± 0.17
CF-CNT@850/30	8.097	-0.266	0.983	1637.8 ± 387.5	0.39 ± 0.15
CF/S	8.179	-0.186	0.999	2144.1 ± 195.1	0.61 ± 0.17
CF-CNT/S_30_50	7.888	-0.171	0.999	1617.4 ± 199.0	0.53 ± 0.24
CF-CNT/S_60_50	7.999	-0.174	0.996	1832.1 ± 244.7	0.42 ± 0.19

Moreover, the Young moduli (E) of the CFs and the CF-CNTs were calculated using the system compliance plot, as described by ASTM C1557-14 [202]. The reciprocal of the slope of the linear regression lines in the plot (Figure 49) equals to Young's modulus of the tested CFs. The estimated E values were summarised in Table 10. These values indicated that all the hierarchical CF-CNTs were stiffer than the reference CFs, or in other words required an increased amount of load in order to deform. While among the hierarchical CF-CNTs produced by the CVD and the wet chemical treatment process, the latter were observed to be stiffer possibly due to the thinner CNT coating onto the CFs as well as the increased crystalline order of the commercial CNTs used during the wet treatments in comparison to the grown CNTs, as previously indicated by the Raman measurements. It has to be noted that the extremely increased values of stiffness should be furthered examined and benchmarked since normally such changes require changes in the CF material volume and cannot be fully explained through the CNT coating deposition. Particularity in the case of CF-CNT/S_30_50 where the coefficient of determination presented values as low as 0.74 indicating a questionable correlation between the studied parameters.

Table 10. Mechanical properties of the hierarchical CF-CNTs and the reference CFs.

Code	Intercept	Slope	R ²	E (GPa)
CF/UNS	-0.045	2.563 10 ⁻⁶	0.984	390.1
CF-CNT@850/30	0.453	1.667 10 ⁻⁶	0.996	599.9
CF/S	0.191	2.377 10 ⁻⁶	0.943	430.3
CF-CNT/S_30_50	0.829	1.099 10 ⁻⁶	0.742	809.9
CF-CNT/S_60_50	0.653	1.027 10 ⁻⁶	0.905	761.8

Furthermore, a comparison between the hierarchical reinforcements produced by CVD and by wet chemical treatments indicated that the later were much stiffer. This might be explained by the better organisation of the crystalline structure of the commercial CNTs in comparison to the CVD produced ones, as indicated by the Raman measurements, which resulted in improved mechanical properties of the CF-CNT reinforcements.

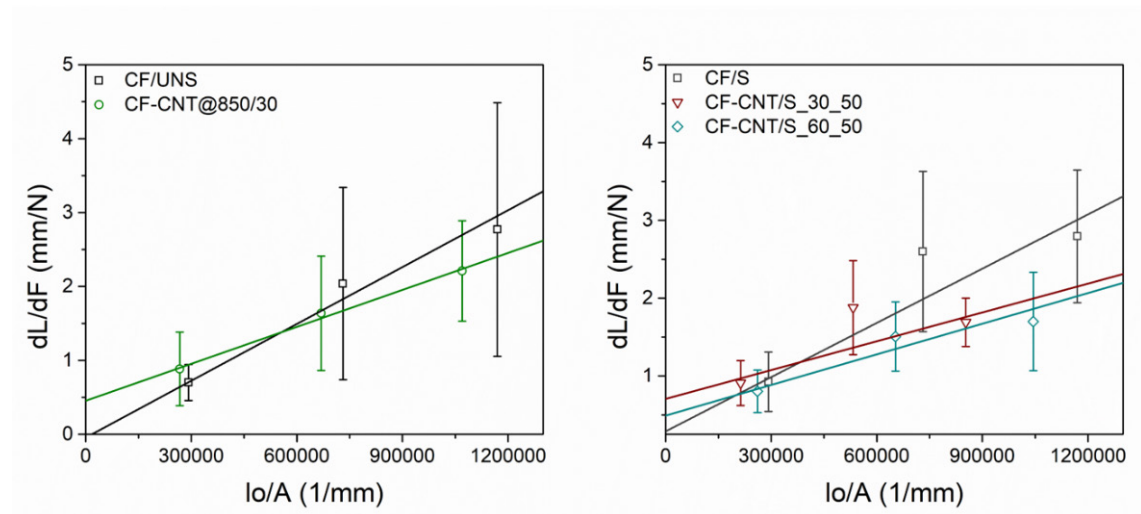


Figure 49. Calculation of Young modulus for the reference CFs and the CF-CNTs via the system compliance as indicated by ASTM C 1557-14 [202].

Additionally, the Weibull shape, m , and scale, σ_0 , parameters were evaluated for all the tested CFs and the CF-CNTs from the plots presented in Figure 50. The results were also summarised in Table 11. In general, a high Weibull modulus, m , value indicates limited scattering in the fracture stress data and the absence of weak CF filaments [203]. As can be seen from Table 11 the CF/UNS and the CF-CNTs produced by the CVD process exhibited

m values in the range of 2 to 3 indicating that some weak filaments were also present in the tested population, where more defects were present on the CF surface. On the other hand, the hierarchical reinforcements produced by the wet chemical process as well as the reference CF/UNS presented a different behaviour and exhibited more scattered m values for the three different tested lengths, ranging from 2.3 and up to 7.8. The improved m values indicate that the presence of fewer defects in those CFs.

Table 11. Weibull parameters of the reference CFs and the hierarchical CF-CNTs.

	Weibull Shape m	Weibull Scale σ_0 (MPa)	R ²
CF/UNS_10 mm	2.77	3260.30	0.96
CF/UNS_25 mm	2.67	2958.29	0.97
CF/UNS_40 mm	2.56	2602.88	0.92
CF-CNT@850/30_10 mm	2.11	2358.35	0.99
CF-CNT@850/30_25 mm	2.46	1701.44	0.89
CF-CNT@850/30_40 mm	2.98	1501.38	0.69
CF/S_10 mm	6.10	2546.22	0.89
CF/S_25 mm	3.39	2319.06	0.89
CF/S_40 mm	2.32	2274.16	0.72
CF-CNT/S_30_50_10 mm	6.49	1962.74	0.95
CF-CNT/S_30_50_25 mm	4.39	1749.91	0.76
CF-CNT/S_30_50_40 mm	7.80	1524.30	0.93
CF-CNT/S_60_50_10 mm	3.45	2336.87	0.86
CF-CNT/S_60_50_25 mm	3.85	1983.12	0.94
CF-CNT/S_60_50_40 mm	4.48	1764.90	0.88

It should be noted that in some cases the two-parameter Weibull distribution did not adequately describe the recorded strength data as can be seen from the R^2 values in Table 11. A deviation from linearity was mainly observed in the low-stress regime and was in agreement with the observations of [210] who commented that such behaviour is commonly observed in sample populations smaller than 80 specimens. However, due to the time-consuming nature of these experiments, such a high number of specimens was practically impossible to perform.

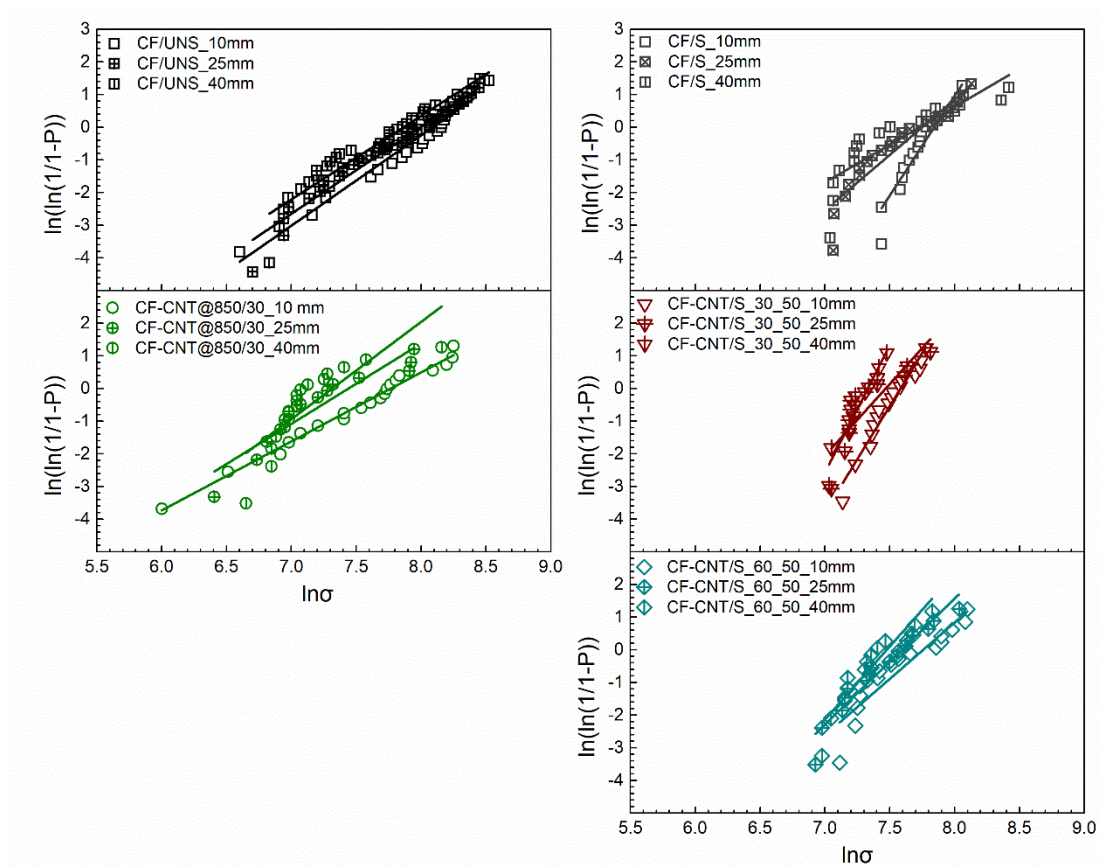


Figure 50. Weibull plots for the hierarchical as well as the reference CF-CNTs.

4.3.4. Strain-induced Raman shifts

Highly ordered crystalline materials like CFs and CNTs exhibit a strain induced shift in the characteristic vibrational modes of their Raman spectra when loaded to tension (or compression). The strain induced Raman sensitivity is only observed when macroscopic deformation affects the material at the molecular level, while the principles and theoretical

background which explains the reasons for this strain dependence of the Raman bands have been recently reviewed by [198].

In this thesis, the Raman strain sensitivity of the CF-CNTs produced by the CVD method (CF-CNT@750/30 and CF-CNT@850/30) and by the wet chemical protocols (CF-CNT/S_30_50 and CF-CNT/S_60_50), as well as the reference CF/UNS and CF/S were evaluated, and the results were presented in Figure 51 and Figure 52. The strain induced Raman sensitivity, a_{ϵ} , for each case is represented by the slope of the linearly fitted line in the experimental plots of Raman wavenumber shift versus externally applied strain. The second order, 2D vibrational mode was monitored for four fibres of each of the aforementioned categories. Raman strain sensitivities a_{ϵ} were summarised in Table 12.

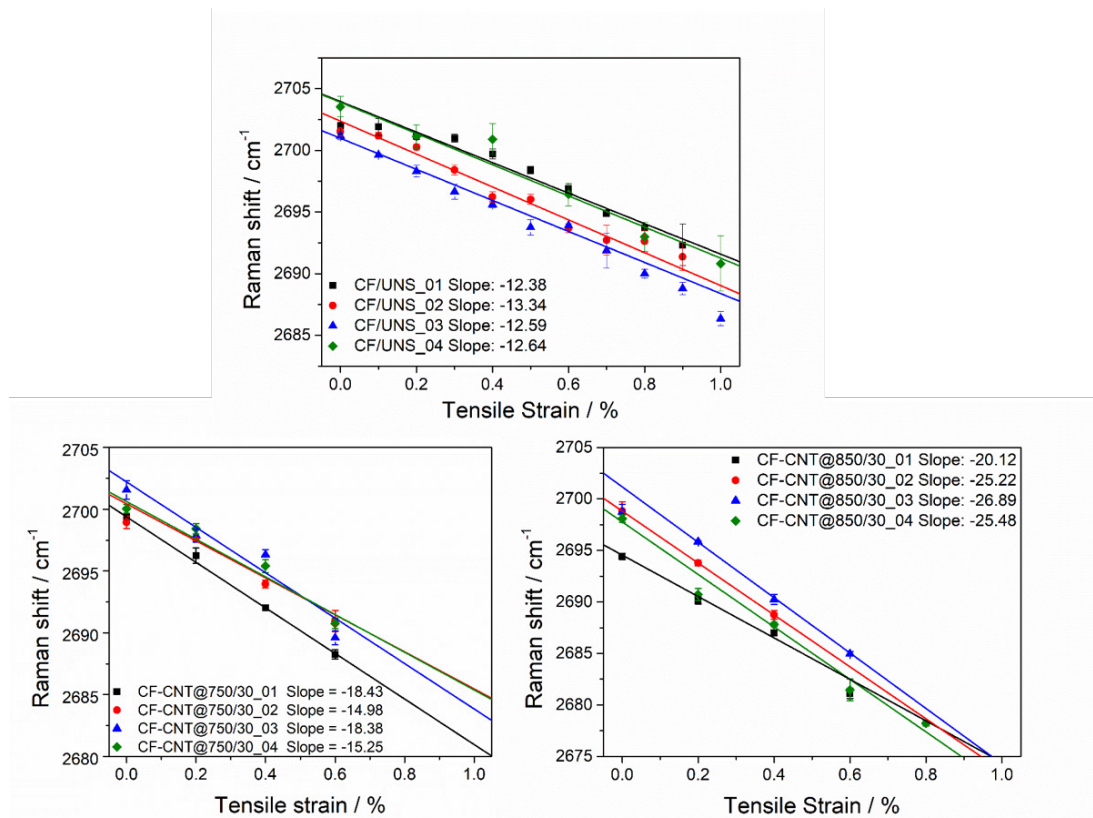


Figure 51. Raman Shift vs strain Calibration curves, for the CF/UNS, the CF-CNT@750/30 and CF-CNT@850/30.

In comparison to the CF/UNS, both CF-CNT “sensors” produced by the CVD method presented enhanced sensitivity. Notably, the measured strain sensitivity values increased from 12.8 cm⁻¹/‰ ϵ for the reference CF to 16.8 cm⁻¹/‰ ϵ and 24.4 cm⁻¹/‰ ϵ for the CF-

CNT@750/30 and the CF-CNT@850/30, respectively. Both the 31.6 % and 91.8 % increments in the strain sensitivity of the CF-CNT@750/30 and the CF-CNT@850/30, respectively, were attributed to the CNT coating of the CFs since the acquired Raman signals stem solely from the CNTs and not the underlying CFs, as previously explained. The higher increment in strain sensitivity found for the CF-CNT@850/30 stemmed possibly from its increased graphitisation in comparison to the CF-CNT@750/30 as presented in section 3.2.

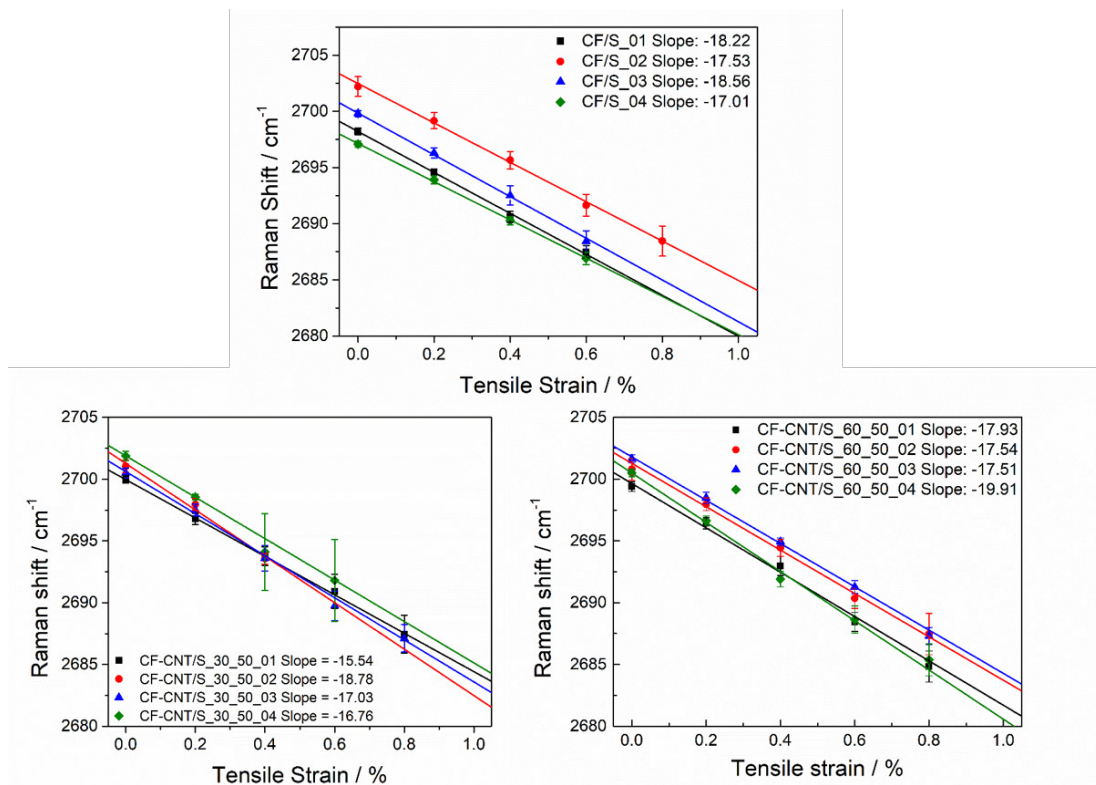


Figure 52. Raman Shift vs strain Calibration curves, for the CF/S, the CF-CNT/S_30_50 and CF-CNT/S_60_50.

On the contrary, both CF-CNT “sensors” produced by wet chemical protocols exhibited similar sensing functionality to the reference CF/S. In particular, the relative changes in the measured strain sensitivity values for both the CF-CNT/S_30_50 and the CF-CNT/S_60_50 were lower than 5 % in comparison to the CF/S and not statistically significant within the calculated experimental error.

Table 12. Linear fitting values and strain induced Raman sensitivities *ae*.

	a_e [cm ⁻¹ /% strain]	Standard deviation
CF/UNS	-12.74	0.42
CF-CNT/750_30	-16.76	1.90
CF-CNT/850_30	-24.43	2.96
CF/S	-17.83	0.69
CF-CNT_30_50	-17.03	1.34
CF-CNT_60_50	-18.22	1.14

The fact that only the CF-CNTs produced by CVD exhibited enhancement of the Raman strain sensing functionality might be attributed to the morphology and orientation of the CNTs onto the CF surface. The CNTs produced by CVD (Figure 24) formed a thicker coating onto the CFs in comparison to the CNTs produced by the wet chemical protocols (Figure 40). Moreover, although in both cases the CNTs were randomly distributed on the surface of the CFs, in the former case (Figure 24) a mixture of vertically, randomly and in parallel oriented CNTs to the axis of the substrate CF were observed, while all CNTs in the latter case (Figure 40) were “lying” in parallel to the CF axis. Therefore, upon the application of an external load to the hierarchical CFs, the CNTs produced by CVD underwent greater deformation in comparison to the CNTs produced by wet chemical treatments which were translated in increased bond deformation and enhanced Raman sensitivity. To further elaborate on this statement, the mixture of CNTs produced by CVD on the CF substrate would undergo a complex deformation, since the amount of CNTs which were oriented vertically or at some angle to the CF axis were trying to align to the direction of loading (parallel to the CF axis) while they were simultaneously subjected to space confinement due to the CNTs which were oriented in a parallel direction to the loading axis.

Moreover, the Raman strain sensitivity was shown to scale with the Young modulus values both by the author [69] as well as by other researchers, who measured the Raman strain sensitivity for CNTs, graphene and polymer composites reinforced with such nanostructures [201,211–213]. A detailed presentation of the relationship between the

Young modulus and the strain induced Raman sensitivity can be found in [69], where the hierarchical CF-CNT reinforcements were shown for the first time to attain an equivalent stiffness for the CNT reinforcement close to theoretically obtained values.

4.4 Conclusions

Summarising the results of this Chapter, the hierarchical CF-CNT reinforcements produced by the wet chemical treatments and dip coating procedure outperformed in most of the evaluated properties the CF-CNTs prepared by the CVD process. Specifically, the CF-CNTs produced by the wet chemical method exhibited increased crystalline order and in-plane correlation length as well as improved thermal stability in comparison to the CVD grown CF-CNTs.

With regards to the tensile properties, all the CF-CNTs exhibited decreased strength, as anticipated, along with substantially improved stiffness. The CF-CNTs produced by the wet chemical method showed lower tensile strength degradation and more notable enhancement in the elastic modulus values when compared to the CF-CNTs produced by CVD. Moreover, the Weibull modulus indicated a smaller flaw distribution for the CF/S, the CF-CNT/S_30_50 and the CF-CNT/S_60_50 in comparison to the CF/UNS and the CF-CNT@850/30.

Conversely, the strain induced Raman sensitivity was higher for the CF-CNT@850/30 in comparison to the CF-CNT/S_30_50 and the CF-CNT/S_60_50, indicating that the CVD process should be used for the production of hierarchical reinforcements when more sensitive strain sensors are required.

Chapter 5

Evaluation of the hierarchical interphases

The results of this Chapter which are related to the evaluation of the residual stresses in model-composites have been published at the peer-reviewed scientific Journal of Materials Engineering and performance as part of the study “Strain sensing ability and residual stress profiles of hierarchical carbon fibres produced via different methods” and can be found under <https://www.springerprofessional.de/en/raman-strain-sensing-and-interfacial-stress-transfer-of-hierarch/15979264>.

5.1 Introduction

The properties of structural CFRCs are governed by the properties of the interface or in other words the regions where the constituent materials come into contact. Hence, the fibre/matrix interfacial properties of CFRCs have been in the core of scientific interest for more than half a century [214]. The integration of the CNTs in the interfacial region of the hierarchical composites by growing or grafting CNTs onto the CF surfaces ensures the interconnection and synergy of the various length scales when the CF-CNTs are used as reinforcements in advanced multiscale hierarchical composites.

The hierarchical approach was proposed by several authors as a biomimetic approach towards multiscale reinforcements with improved wettability [102,106,118], increased adhesion [4,46,97,124,126,143], more robust mechanical interlocking [88,97–100,106,119,128] and enhanced interfacial stress transfer [47,49,120,50,52,66,69,73–76] due to the emergence of additional energy dissipation mechanisms related to the CNTs.

The integration of the CNTs onto the CFs significantly alters the interfacial region in the hierarchical composites leading to a gradient interphase which was shown to have a considerable thickness [130,146,150,215]. In a more recent study, Bedi et al. quantified the thickness of the interphase in hierarchical CF-CNT/epoxy composites [68]. The authors used nanoindentation in order to identify the thickness of the interphase by assessing the changes in the elastic modulus of the interfacial region. The measured values indicated a 2 μm thick interphase for CF/epoxy composites, which increased to 5 μm and 8 μm for CF-CNT/epoxy composites where the CNTs were grown by CVD for 15 and 30 min, respectively [68].

Therefore, it is more realistic to talk about interphase instead of an interface which essentially refers to a gradient instead of an abrupt transition from one material to another.

This interphase is a region where complex physicochemical interactions take place and is also responsible for the overall performance of the hierarchical composites.

In order to evaluate the interactions of the hierarchical CF-CNTs with the epoxy matrix usually the wettability of the reinforcement by the resin is assessed by contact angle measurements [102,106,110,118,140,144]. Practically, the smallest the contact angle the better the wetting of the CF-CNTs by the epoxy matrix and the more effective the interfacial stress transfer.

Several micromechanical methods and modelling approaches exist for the determination of the interfacial stress transfer characteristics of composite materials, i.e. single fibre fragmentation tests, single fibre pull-out tests, microbundle pull-out tests, microbond or microdroplet tests, and microindentation tests [216]. Furthermore, Raman spectroscopy is a well-established tool used to evaluate the level of interfacial adhesion in polymer-based composites, as it can provide non-destructively in situ axial strain/stress measurements with a resolution of one micrometre [197,198].

The utilisation of Raman spectroscopy as a non-destructive characterisation technique for the determination of stresses in CFRPs is based on the frequency sensitivity of the graphitic vibrational modes to externally applied strain. In more detail, when a CF is strained, Raman bands shift to lower wavenumbers due to tension and to higher wavenumbers due to compression. This shift is caused by changes in the interatomic distance and is due to the anharmonicity of the bond potential [198]. The necessary condition for the macroscopic strain to result in frequency shift is that the applied macroscopic field translates to actual bond deformation. This is the case for highly ordered structures, as CFs. The stress-induced changes in the Raman spectrum of different types of CFs have been thoroughly studied both for the first and the second order Raman vibrational modes [211,217,218]. Furthermore, similar studies on hierarchical reinforcements have been reported by Jin et al. who deposited a silane coating consisting of carboxylated single-walled CNTs on low and high modulus CFs and measured the interfacial stress profiles via Raman spectroscopy [165,219].

In this Chapter, a thorough characterisation of the interfacial properties of the hierarchical CF-CNTs produced by CVD or wet chemical treatments and dip-coating was presented.

Initially, the wettability of the hierarchical reinforcements by the host epoxy matrix was assessed by static contact angle measurements. Then, the IFSS of the hierarchical CF-CNTs/epoxy model composites was evaluated in comparison to CF/epoxy model composites, by SFFT combined with polarised optical microscopy observations of the number of CF-CNT or CF fragments. An extensive fractographic study accompanied the IFSS measurements in order to gain a more profound understanding of the failure process and the fracture mechanisms acting at the hierarchical interphases in comparison to the reference CF/epoxy interphases.

Finally, the effects of the grown or grafted CNTs onto CF surfaces were evaluated by Raman spectroscopy. To this end, the thermal stresses developed in model hierarchical composites were studied in comparison with the residual thermal stresses in CF/epoxy model composites by monitoring the distribution of the frequency shifts of the 2D Raman vibrational mode for the CNTs or the CFs. As is well known, during the high-temperature curing process of the epoxy matrix residual stresses are formed on the reinforcing fibres due to the mismatch in the thermal expansion coefficients of the components ($65\text{-}70 \cdot 10^{-6} / ^\circ\text{C}$ for the epoxy and $-0.36 \cdot 10^{-6} / ^\circ\text{C}$ for the CFs [220]). These residual stresses built up due to the shrinkage of the epoxy when cooling from elevated temperatures to temperatures below its glass transition, T_g [221]. Therefore, this study aimed to lighten the understanding on the interaction of the primary reinforcement (CF) and the secondary reinforcement (CNTs) via the evaluation of the residual stresses in hierarchical reinforcements, produced either by CVD or wet chemical treatments.

5.2 Materials and Methods

5.2.1. Materials

The hierarchical CFs produced via CVD (CF-CNT@750/30 and CF-CNT@850/30), and wet chemical protocols (CF-CNT/S_30_50 and CF-CNT/S_60_50) were evaluated in this chapter. The reference CF/UNS and CF/S were also evaluated for comparison.

The matrix employed for the fabrication of the single fibre model-composites was the two-component MY-750 / HY-951 epoxy system (Huntsman, MY-750: unmodified liquid

epoxy resin, and HY-951: triethylenetetramine curing agent). This matrix exhibits a tensile strength of 75-90 MPa along with an elongation at break of 3-4% and a modulus of 3.5-4.0 GPa. Before mixing with the hardener, the epoxy resin was heated under vacuum at 40°C for 30 min in order to minimise the volume of trapped air in the viscous liquid. After mixing with the curing agent at a ratio 4:1, only 5 min of degassing under full vacuum were applied, in order to avoid a possible exothermic reaction due to the limited pot life of the mixture.

5.2.2. Static contact angle measurements

The adhesion of the hierarchical CF-CNTs and the reference CFs was evaluated by static contact angle measurements. Droplets of epoxy resin were placed on the surface of the fibres, and optical micrographs were acquired with Leica DM-4000M optical microscope. The contact angle was measured from at least 20 micrographs of different droplets using the Image J open source image analysis software [222].

5.2.3. Interfacial shear strength measurements

Preparation of the single fibre model-composites

The Single Fiber Fragmentation Test (SFFT) was used for the quantification of IFSS of the hierarchical CF-CNTs with the epoxy matrix. Model-composite specimens with dog-bone shape were fabricated by aligning

a single fibre axially on the pins of a silicone rubber mould (Figure 53) with the aid of a superglue. Then, the mould was filled with the two-part epoxy

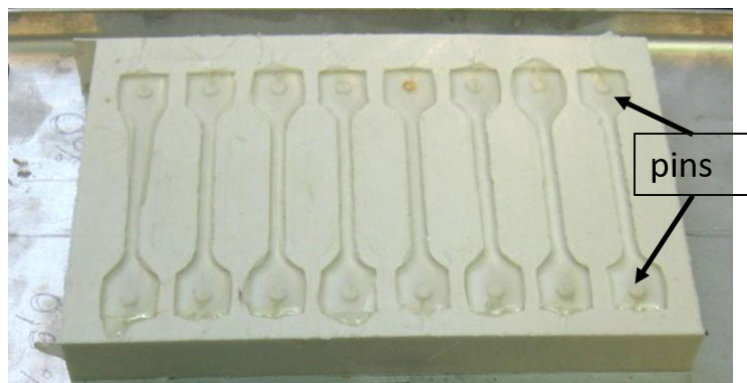


Figure 53. Silicon rubber mould used for the fabrication of single fibre model composites.

resin system, and the specimens were cured for 2 h at 60 °C.

Upon completion of the curing cycle, the specimens were left to cool down to room temperature before removing them from the mould. Subsequently, a post-curing cycle was performed at 120°C for 1.5 h. The specimens were again left to cool down to ambient

conditions prior to removing from the oven. Subsequently, their surface was appropriately prepared by sanding with 800, 1000, 1200, 2400 and 4000 grit sandpapers in sequence and then polished with a cloth and 3 μm diamond paste. The specimens were ready for microscopic characterisation when the fibre was at approximately 0.2 mm from their surface.

Description of the SFFT

During the fragmentation test, these specimens were loaded to tension, with a strain rate of $0.25 \cdot 10^{-2} \text{ min}^{-1}$, up to approximately 6 % strain with a custom-made horizontal tensile stage which was placed under the optical microscope (Figure 54). All the coupons were loaded at incremental strain levels until saturation. Each experiment was paused every 0.2% of applied strain, and the fragments of the CFs and the hierarchical CF-CNTs were measured from the birefringence patterns via polarised optical microscopy. Five samples were tested for each category, and each fibre diameter was evaluated before testing by averaging at least 10 optical measurements along its active length.

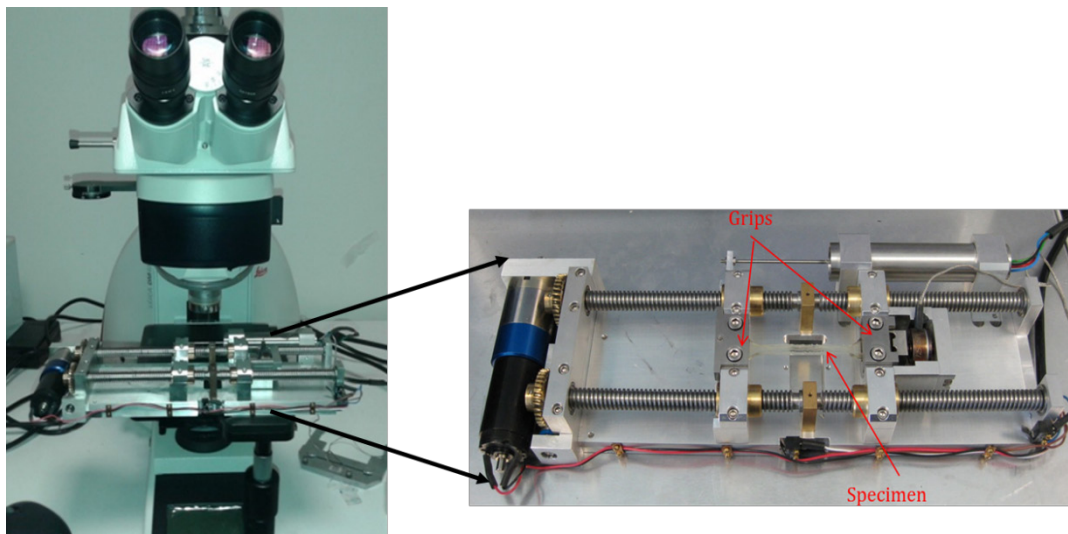


Figure 54. The experimental set-up used for the SFFT measurements. The custom-made, horizontal tensile stage (right) placed under the Leica DM-4000M polarised optical microscope (left).

Theoretical considerations related to the SFFT

Upon loading of the model-composite coupons, the stress is transferred by the resin to the CF through the interfacial region. As the externally applied load increases, the CF breaks into increasingly smaller fragments at locations where the CF axial stress reaches its tensile

strength. This fragmentation process is continued by further stressing of the specimens until all the CF fragments are too small to reach their tensile strength for further fragmentations to occur. This stage is described as the saturation stage and the shortest fragment length observed during saturation is named the critical length, l_c . Another characteristic length is the mean fragment length which represents an average fragment length achieved during the saturation stage [223].

The IFSS was calculated by using the Kelly and Tyson model [224],

$$\tau = \frac{\sigma_f}{2} \left(\frac{d}{l_c} \right) \quad (7)$$

where σ_f is the tensile strength of the fibre at the critical length l_c and d is the diameter of the fibre. The critical length was calculated by equation (8)

$$l_c = \frac{4}{3} l_f \quad (8)$$

whereby, l_f is the average fragment length which is equal to the length of the CF being monitored during the SFFT divided by the number of fragments at the saturation stage.

5.2.4. SEM study of the fracture surfaces

A fractographic study was performed in order to assess the main damage mechanisms involved in the failure process of the interface in the SFFT model-composite coupons. For this study, model-composites comprised of a tow of CFs from each category in epoxy resin were manufactured and then loaded to tension up to failure. The study of the fracture surfaces of the hierarchical reinforcements produced by the CVD method, as well as the reference CF/UNS was conducted with the ESEM Quanta 250 FEG (FEI, The Netherlands) Field-emission scanning electron microscope, operating at an accelerating voltage of 3.0 – 5.0 kV. The specimens were placed on a double-sided copper adhesive tape to be stabilised and coated with a thin layer of Pt (5 nm) before the SEM analysis to avoid charging effects. A JEOL JSM 6510 LV SEM/Oxford Instruments Scanning Electron Microscope was used, operating at an accelerated voltage of 10 kV, for the evaluations of the fracture process of the reinforcements produced by wet chemical protocols as well as the reference CF/S. In this case, the specimens were placed on a

double-sided carbon adhesive tape to be stabilised and coated with a thin layer of Au/Pd (5 nm) prior to the SEM analysis to avoid charging effects.

5.2.5. Residual stresses in model composites

5.2.5.1. Strain / Stress Calibration of single CFs and CF-CNTs

The calibration of the stress/strain response of single CFs is conducted via the measurement of their Raman strain sensitivity following the procedure described in section 3.2.2.5. The strain induced Raman sensitivity (Table 12), α_ε , is a strain proportionality constant (Figure 52) between the Raman shift, ν (cm^{-1}), and the applied strain, ε %, and is described by the simple linear equation (9)

$$\Delta(\nu) = \nu(0) + \alpha_\varepsilon \varepsilon \quad (9)$$

whereby the CF is considered as a long chain composed of identical fibrils arranged in series. The stress induced Raman sensitivity is also described by a similar linear equation,

$$\Delta(\nu) = \nu(0) + \alpha_\sigma \sigma \quad (10)$$

Therefore, and since $\sigma = E \varepsilon$, α_ε can be converted to the stress proportionality constant, α_σ , when divided by the Young modulus of the CF [225].

5.2.5.2. Preparation of model-composites

A similar procedure to the one described in section 4.2.3 was used for the preparation of the single fibre model-composites for the stress transfer studies. The only difference was the length of the CFs and hierarchical CF-CNTs which in this case was 1-3 mm. The sanding procedure described above was also performed for the preparation of the surfaces of the model-composites until the embedded fibre was 50 - 100 μm away from the surface. This small distance was required in order to be able to record the Raman activity of the CFs which were embedded into the epoxy resin.

5.2.5.3. Raman spectra acquisition and treatment

The model-composite samples were placed under the Raman microscope, without any applied tension in order to assess the residual stresses. The 2D Raman vibrational mode was monitored during this study. The epoxy resin does exhibit a considerable amount of Raman activity throughout the spectrum, whilst luckily at the region of interest only two vibrational modes with low intensities were observed (Figure 55, middle plot). These bands can be attributed to the stretching of the N-CH₃ bonds present in the hardener [226,227]. In order to remove the contribution of the epoxy resin, a spectral deconvolution technique was utilised. It should be noted at this stage that the epoxy matrix Raman Spectrum does not exhibit wavenumber dependence, because it is not crystalline for the far field deformations to affect it at the molecular level [228].

The maximum possible resolution from the Raman spectrum of the embedded fibre was achieved by eliminating the resin contribution. This was achieved by i) normalising the spectra of the resin (Figure 55 middle) and the composite (Figure 55 top) to the first intensity value, ii) scaling both spectra by the maximum observed intensity (2866 cm⁻¹ vibration) and iii) subtracting the resin spectrum from the composite spectrum. Thereby, the Raman activity of the CF emerged (Figure 55 bottom).

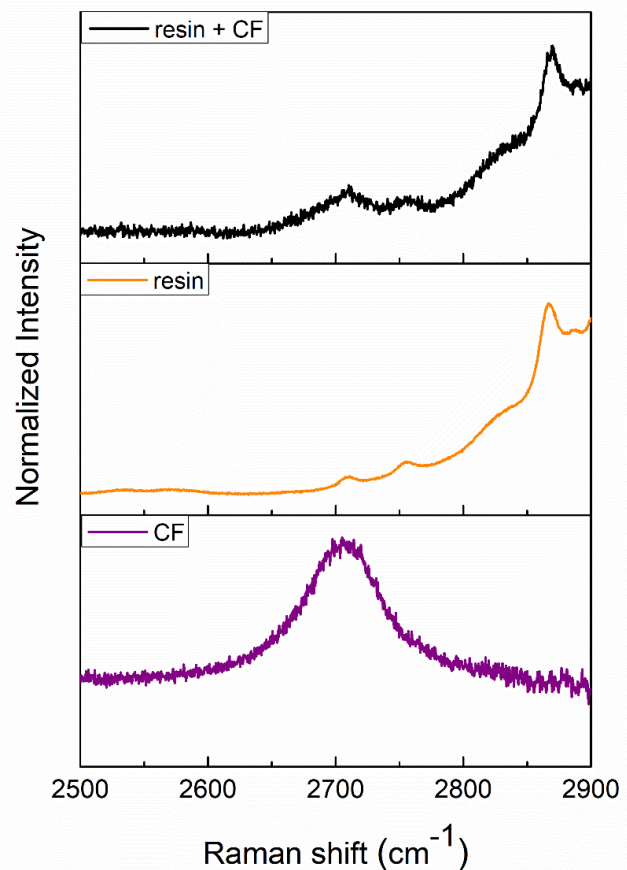


Figure 55. A characteristic Raman spectrum as acquired from the single-fibre model-composites (top), the spectrum of the epoxy resin (middle) and the emerging spectrum of the CF (bottom).

5.2.5.4. Conversion of spectroscopic data to stress values

Frequent calibration values of unstressed fibres in air, ν_{ref} , were obtained for the 2D vibrational mode and used as a reference for zero stress. Subsequently, these values, ν_{ref} , were subtracted from the measured Raman shift values, ν , in order to calculate the relative shift of the 2D band, $\nu - \nu_{ref}$, at each strain level. Finally, the axial stress values σ_z were obtained through the use of the calibration curves obtained for the CF/S, CF-CNT@850/30 and CF-CNT/S_60_50 (Figure 52) via the equation (11)

$$\sigma_z = \frac{\nu - \nu_{ref}}{\alpha_\sigma} \quad (11)$$

5.2.5.5. Residual stress monitoring

Raman spectra of the 2D vibrational mode were acquired from both ends of each fibre, up to a distance of about 300 μm along the fibre axis and away from either end. Sampling was carried out at steps of 2 μm at the vicinity of the fibre ends (from 0 to 50 μm), then at steps of 5 μm (from 50 to 150 μm) and, finally, at steps of 10 μm (from 150 to 300 μm) 300 μm .

5.3 Results and Discussion

5.3.1. Wettability of hierarchical CFs

Static contact angle measurements evaluated the adhesion of the hierarchical CF-CNTs produced by CVD (CF-CNT@750/30 and CF-CNT@850/30) and wet chemical protocols (CF-CNT/S_30_50 and CF-CNT/S_60_50) as well as the reference CF/UNS and CF/S with the host epoxy matrix. All the hierarchical CF-CNTs exhibited enhanced wetting behaviour from the epoxy matrix in comparison to the reference CFs (Figure 56). In more detail, the CF-CNT@750/30 ($36.0^\circ \pm 5.6^\circ$) and the CF-CNT/S_60_50 ($35.0^\circ \pm 3.8^\circ$) exhibited similar average wetting properties with 13.0 % and 12.6 % decrease in the contact angle values in comparison to the reference CF/UNS ($41.4^\circ \pm 3.0^\circ$) and CF/S ($40.0^\circ \pm 3.0^\circ$), respectively. The contact angle was also decreased by 8.0 % for the CF-CNT@850/30 ($38.1^\circ \pm 2.8^\circ$) and by 9.7% for the CF-CNT/S_30_50 ($36.2^\circ \pm 3.9^\circ$) in comparison to the reference CF/UNS and CF/S, respectively.

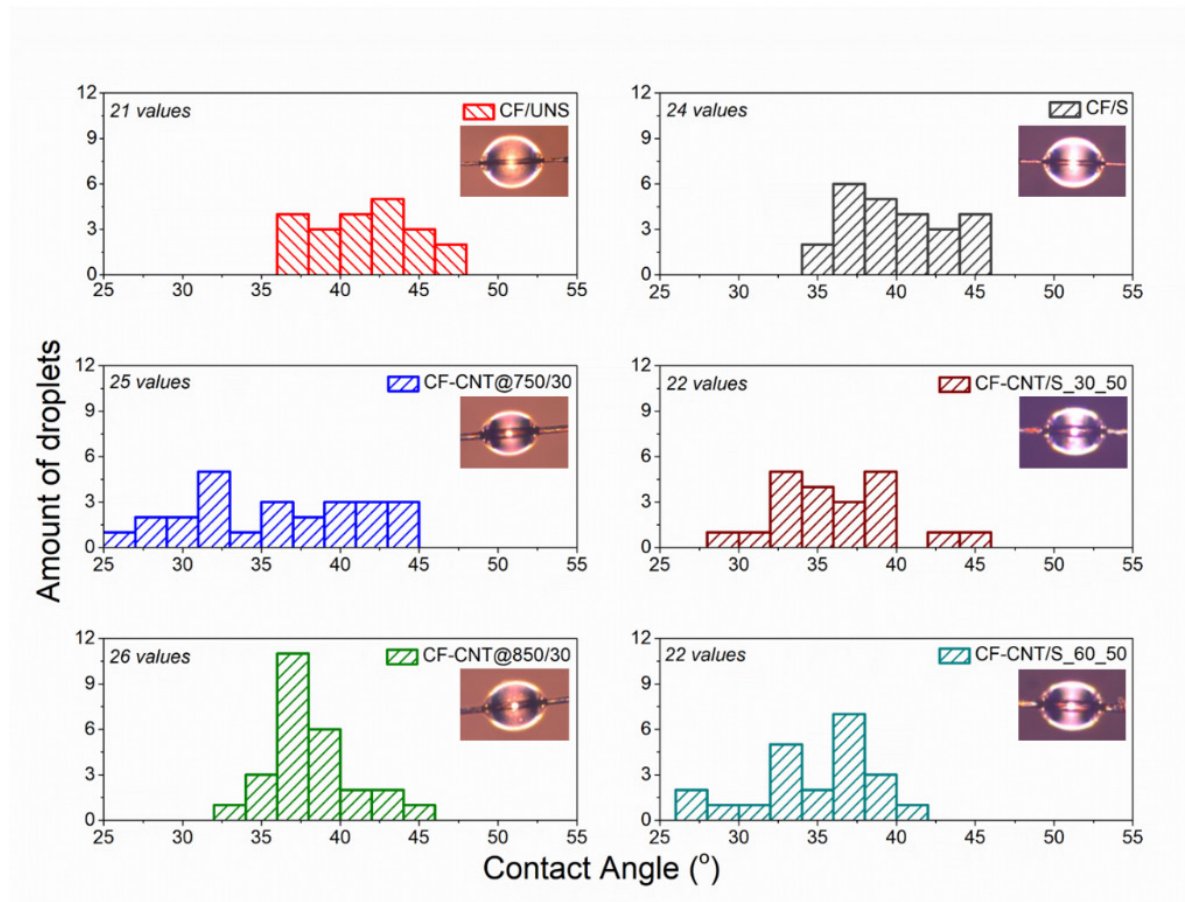


Figure 56. Histograms of the contact angle formed between the hierarchical or the reference CFs and the epoxy matrix. A characteristic droplet on CF was presented in each case, as well as the number of droplets for which the contact angle was measured.

Practically, the improved wetting properties of the hierarchical CF-CNTs in comparison to the reference CFs are expected to increase the chemical interactions and the mechanical interlocking between the hierarchical “composite” fibres and the epoxy matrix leading to enhanced interfacial mechanical properties [101,122].

5.3.2. Reinforcing ability by micromechanical tests and SEM fractography

The IFSS of the hierarchical and the reference CFs was evaluated by Single Fibre Fragmentation testing. The enhanced IFSS values measured for all the model CF-CNT composites are summarised in Table 13. These values counterbalanced the decreased CF strengths (Table 10) and the alterations in the diameters of the CFs due to the CVD growth

process or the wet chemical treatments. These values were also a first indication of the achieved synergy between the different scale reinforcements constituting the hierarchical CF-CNTs.

Table 13. Interfacial mechanical properties of the hierarchical and the reference model-composites.

	τ [MPa]	% Change	l_f [μm]	l_c [μm]
CF/UNS	23.89 ± 1.81	0	417 ± 62	557 ± 82
CF-CNT@750/10	55.9 ± 5.29	+134.0	253 ± 27	338 ± 36
CF-CNT@750/30	52.13 ± 7.57	+118.2	257 ± 20	342 ± 27
CF-CNT@850/10	40.99 ± 1.63	+71.6	272 ± 17	364 ± 22
CF-CNT@850/30	42.30 ± 12.69	+77.1	269 ± 13	358 ± 17
CF/S	22.31 ± 2.02	0	439 ± 32	585 ± 43
CF-CNT/S_30_50	30.45 ± 3.24	+36.5	334 ± 16	445 ± 21
CF-CNT/S_60_50	37.72 ± 3.03	+69.1	284 ± 23	378 ± 31

All the hierarchical reinforcements produced by the CVD process exhibited improved IFSS, while the more pronounced IFSS value was measured for, the lower growth temperature of 750°C for 10 min growth time. More analytically, the ranking of the CF-CNTs in increasing IFSS magnitude was CF-CNT@850/10 < CF-CNT@850/30 < CF-CNT@750/30 < CF-CNT@750/10 with the respective enhancement ranging from 71.6 % up to 134 % in comparison to CF/UNS, respectively.

Notable IFSS enhancement was also exhibited by the hierarchical CF-CNTs produced via wet chemical protocols. In this case, longer oxidation led to more prominent interfacial properties for the CF-CNT/S_60_50 with a 69% IFSS enhancement, while the short duration of oxidation (CF-CNT/S_30_50) resulted in a moderate 36.5% increase in the IFSS, in comparison to the reference CF/S.

The hierarchical CF-CNTs produced CVD for most of the growth conditions demonstrated significantly higher IFSS values than the CF-CNTs produced by wet chemical treatments. It has to be noted although that, part of this compelling increase in the IFSS is attributed to the

substantially increased CF diameter due to the CNT growth which was accounted for in the calculation of the IFSS along with the changes in CF strength.

The significantly increased IFSS values denoted enhanced stress transfer between the different scale reinforcements at the studied hierarchical interfaces. More specifically, improvements were due to increased interfacial adhesion and thus interactions both at the CF (micron) / CNTs (nano) interface and the CF-CNT (micron) / host epoxy matrix (macro) interface. The first indication of this improved interfacial adhesion was the increased number of fragments for all the CF-CNT/epoxy model composites in comparison to the CF/epoxy model composites for the same fibre length. Some characteristic optical birefringence patterns observed during SFFT for the CF-CNTs produced by CVD can be seen in Figure 57. Similar patterns were also observed for the CF-CNTs produced by wet chemical treatments.

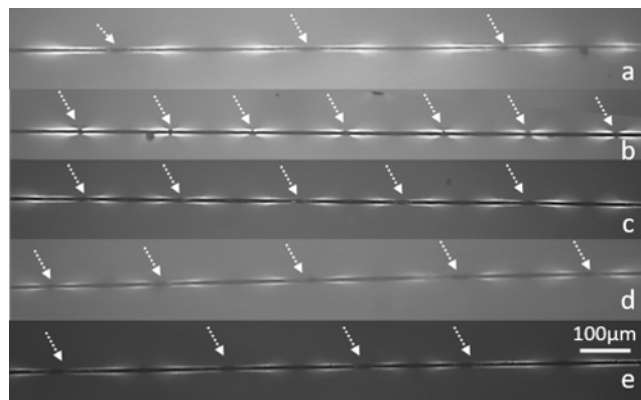


Figure 57. Characteristic polarised optical birefringence patterns of fragmented model composites at 20x magnification. (a) CF, (b) CF-CNT@750/10, (c) CF-CNT@750/30, (d) CF-CNT@850/10 and (e) CF-CNT@850/30. The dashed-line arrows indicate the CF and CF-CNT crack locations.

Additionally, the amount of energy released during the fragmentation, which was responsible for these optical birefringence phenomena, seemed to corroborate the values of IFSS as the most intense / brighter patterns were encountered for CF-CNT@750/10 (Figure 57). The corresponding values of average fragment length and average critical fragment length (Table 13) confirmed this observation. The average l_f of CF/UNS was 417 μm and decreased down to 253 - 272 μm for all the CF-CNT. The l_f decreased, likewise, from 439 μm for the reference CF/S to 334 μm and 284 μm for the CF-CNT/S_30_50 and the CF-CNT/S_60_50, respectively. These findings corroborated the wettability enhancements mentioned above for all the hierarchical reinforcements in comparison to the reference CFs.

Furthermore, fractography was performed in order to strengthen the understanding of the failure mechanisms acting at the hierarchical interfaces. The fracture surfaces of the specimens with extended growth duration (CF-CNT@750/30 and CF-CNT@850/30) produced by the CVD method and the hierarchical model-composites produced by wet chemical treatments (CF-CNT/S_30_50 and CF-CNT/S_60_50) were examined by SEM. The reference CF/UNS and CF/S model-composites were also studied for comparison.

The fracture process for both the reference CF/UNS (Figure 58) and CF/S (Figure 59) coupons was similar. Extended debonding of the CFs from the epoxy matrix (Figure 58b Figure 58d and Figure 59a) at the interfacial failure zones was observed for both cases. The excessive debonding explained the low interfacial shear strength values summarised in Table 13. Sufficient bonding was also observed, occasionally, for some CF/UNS (Figure 58c) while all CF/S exhibited debonding regions, confirming the lower IFSS values of the CF/S in comparison to the CF/UNS (Table 13).

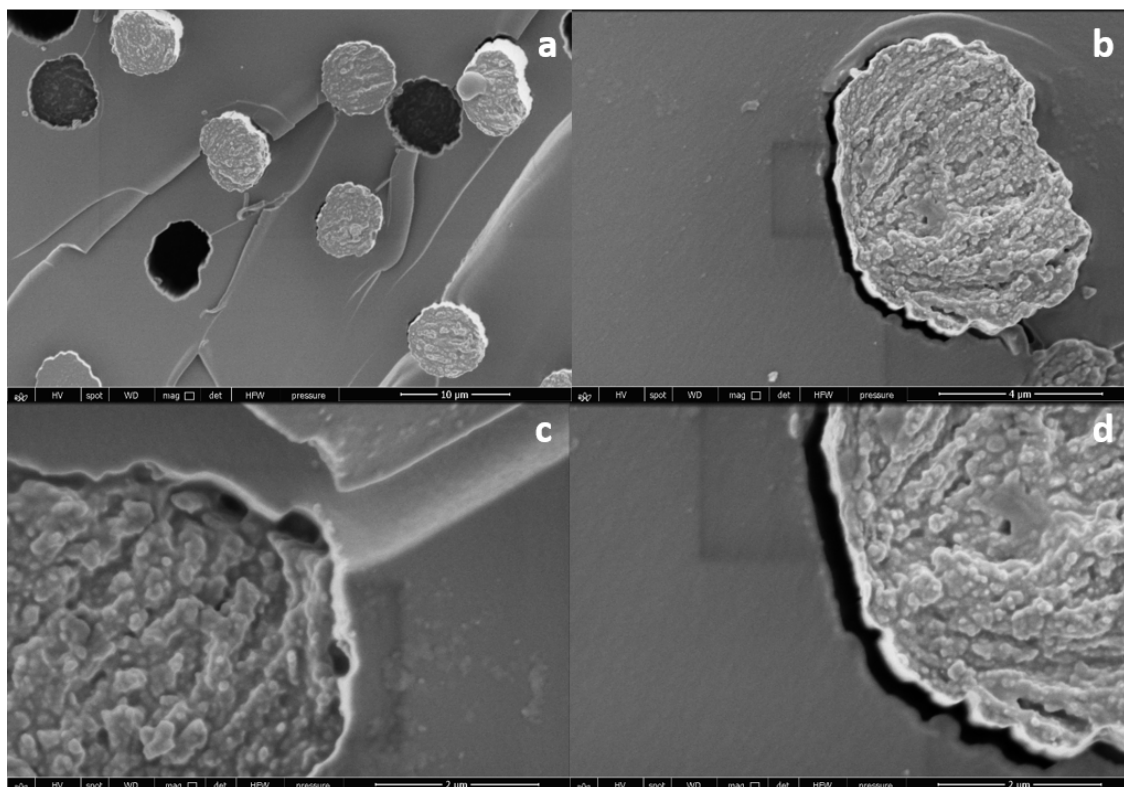


Figure 58. Micrographs of the fracture surface of the CF/UNS model-composites with different magnifications.

Moreover, fibre pull-out due to the fracture process was observed for both the reference CF/epoxy model-composites. The existence of mechanical interlocking as the main adhesion mechanism between the reference CFs and the host epoxy matrix was evident too (Figure 58d and Figure 59c); where the epoxy resin behaves like a matrix that envelops the CFs and follows the relief of their surface. The stress transfer for these model-composites included only stresses that were transferred from the matrix to the uncoated CFs until the adhesive failure of the specimens.

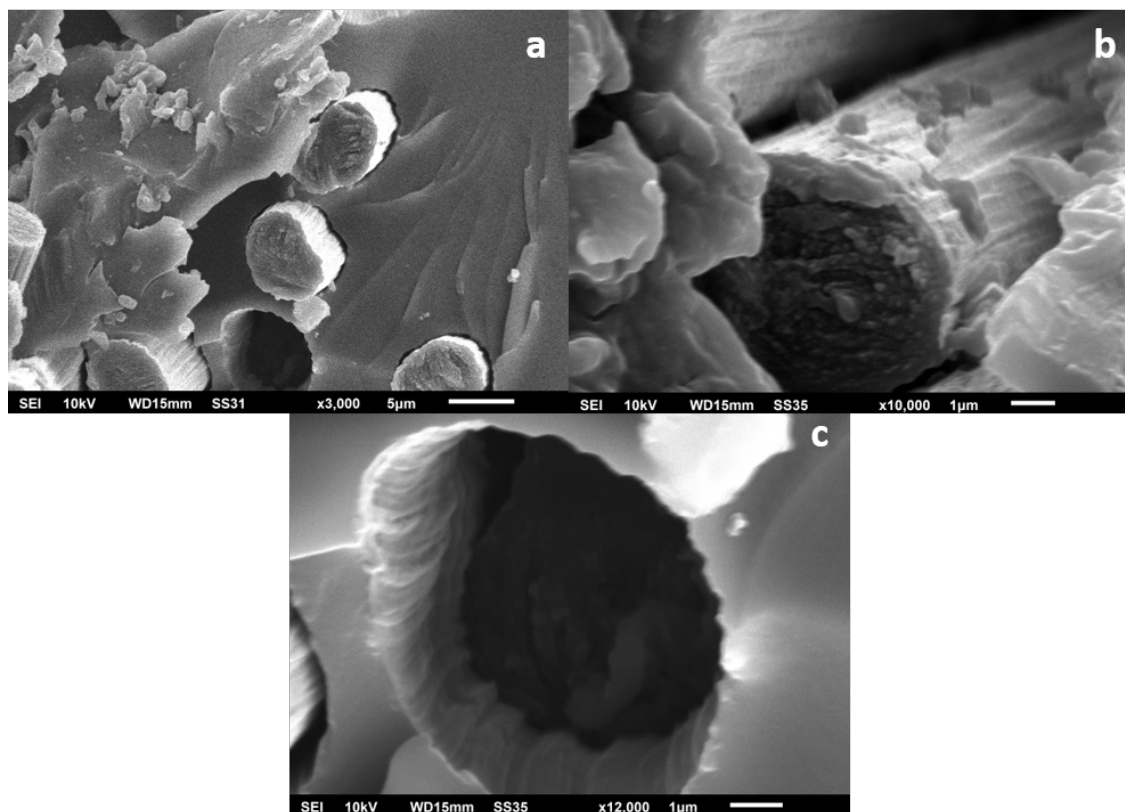


Figure 59. Micrographs of the fracture surface of the CF/S model-composites with different magnifications.

The fracture process was altered upon incorporation of the CNTs on the CF surfaces into the hierarchical model-composite interfaces. Specifically, debonding due to fracture was limited in a smaller scale for the CF-CNT@750/30 (Figure 60) and was further limited for the CF-CNT@ 850/30 (Figure 61), leading to more cohesive interfaces, which yielded higher stress transfer (Table 13). Fibre pull-out was also substantially decreased for both hierarchical reinforcements produced by CVD (Figure 60 and Figure 61) in comparison to the reference CF/UNS (Figure 58). Moreover, two failure mechanisms related to the CNTs were identified, confirming that the shear stresses included not only stresses transferred

from the matrix to the CF-CNT but also stresses transferred from the matrix to the CNTs and from the CNTs to the CF.

The failure process of the CF-CNT@750/30 model-composite was accompanied by the fracture mechanisms of the breakage of the CNTs (indicated by the green arrow in Figure 60c) and the presence of “bridging effects” between the CF and the epoxy matrix as demonstrated by the CNTs (indicated by the red arrow in Figure 60c). Both these mechanisms were previously reported in the literature for hierarchical CF-CNT composites [124,126,151] and confirmed that the enhanced IFSS values (Table 13) were achieved due to the effective stress transfer between the epoxy matrix and the CFs via the CNTs.

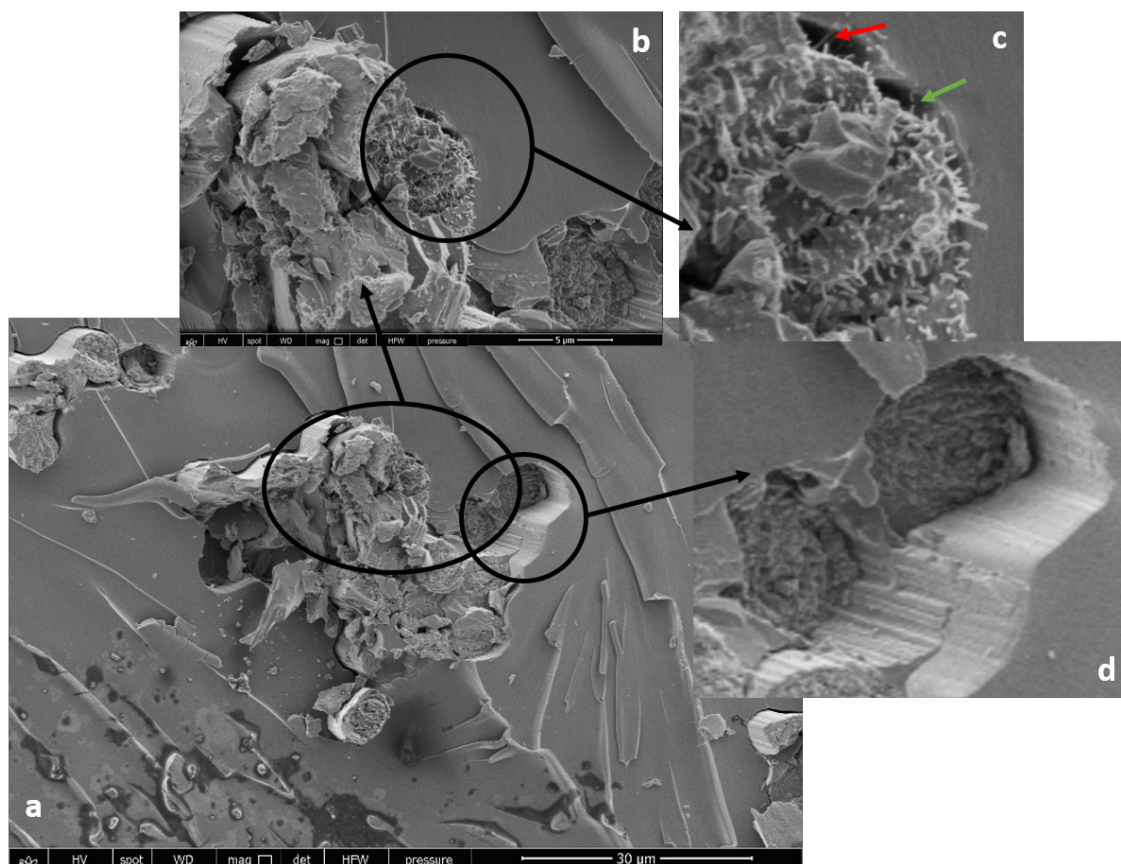


Figure 60. Micrographs of the fracture surface of the CF-CNT@750/30 model-composites with different magnifications.

Bridging effects were also observed on the CF-CNT@850/30 model-composite fracture surface (indicated by the red arrow in Figure 61c), while CNT breakage was not evident in this case and this can explain the lower IFSS values in comparison to the CF-CNT@750/30 model-composite (Table 13). Furthermore, several CNTs were found to be detached from the

CF surface (Figure 61) or drifted by the host matrix (Figure 61b). This finding indicated that the CNTs grown at higher temperatures (850°C for 30 min) had a better affinity with the matrix than with the CF, maybe due to their higher graphitisation degree as observed in the Raman study (I_d/I_g ratio Table 8).

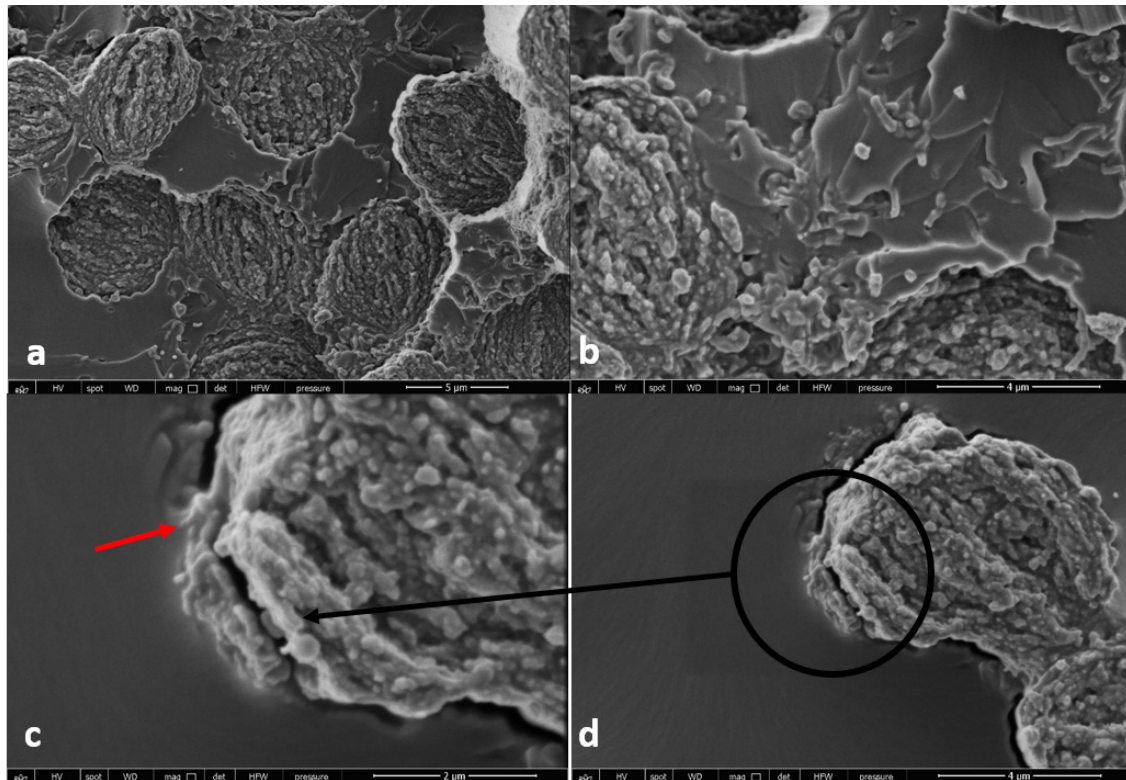


Figure 61. Micrographs of the fracture surface of the CF-CNT@850/30 model-composites with different magnifications.

The fracture behaviour of the CF-CNT/S_30_50 (Figure 62b and Figure 62c) resembled that of the reference CF/S (Figure 59) for many of the studied hierarchical CFs since significant debonding was present. Some differences were identified although, which were responsible for the moderate enhancement of the IFSS values (Table 13) in comparison to the reference CF/S. Epoxy resin was attached on the surface of many CFs in the CF-CNT/S_30_50 specimens after the fibre pull-out process (Figure 62 a). It can be assumed that the increased adhesion was due to the presence of the CNTs onto the CFs which were also shown to enhance the surface wettability by the resin (Figure 56). Unfortunately, the CNTs were not apparent in the examined CF-CNT/S_30_50 model-composites since all the studied fibres were vertically oriented to the fracture surface. Furthermore, detached interfacial regions were also observed for the CF-CNT/S_30_50 (Figure 62d) rendering the failure mode from

adhesive for the reference CF/S to cohesive for the hierarchical model composites. A similar alteration to the failure mode from adhesive to cohesive was observed by Qian et al. during the pull-out experiments of CVD grown CNTs onto unsized CFs [52]. Therefore, CNTs are believed to be present in the outer surface of these regions like in the CF-CNT@850/30 model composites (Figure 61 c and Figure 61d).

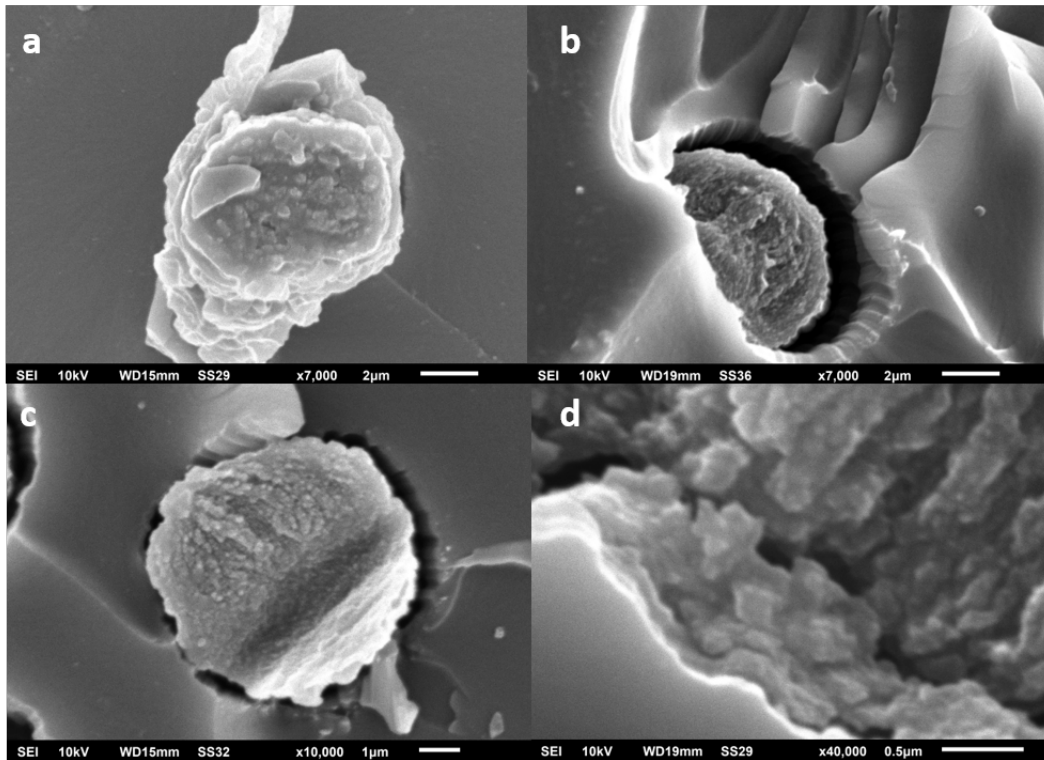


Figure 62. Micrographs of the fracture surface of the CF-CNT/S_30_50 model-composites with different magnifications.

Finally, debonding due to fracture was substantially limited for the CF-CNT/S_60_50 (Figure 63a) in comparison to the reference CF/S (Figure 59). In this case, a thin CNT veil was evident on the surface of the CF-CNT/S_60_50 reinforcements (Figure 63 and Figure 64). Moreover, both CNT fracture (indicated by the green arrow in Figure 64c) and “bridging effects” by the CNTs (indicated by red arrows in Figure 63b and Figure 64b, Figure 64c and Figure 64d) were consistently observed corroborating the 70 % increase in IFSS values (Table 13) in comparison to the reference CF/S. It is also interesting to note that, the CNTs were impregnated with the epoxy matrix in most of the regions where CNT-induced bridging effects were observed (Figure 63 and Figure 64), further confirming that

Evaluation of the hierarchical interphases

the affinity of the CNTs with both the CF/S and the epoxy resin was significantly improved for CF-CNT/A_60_50 model-composites.

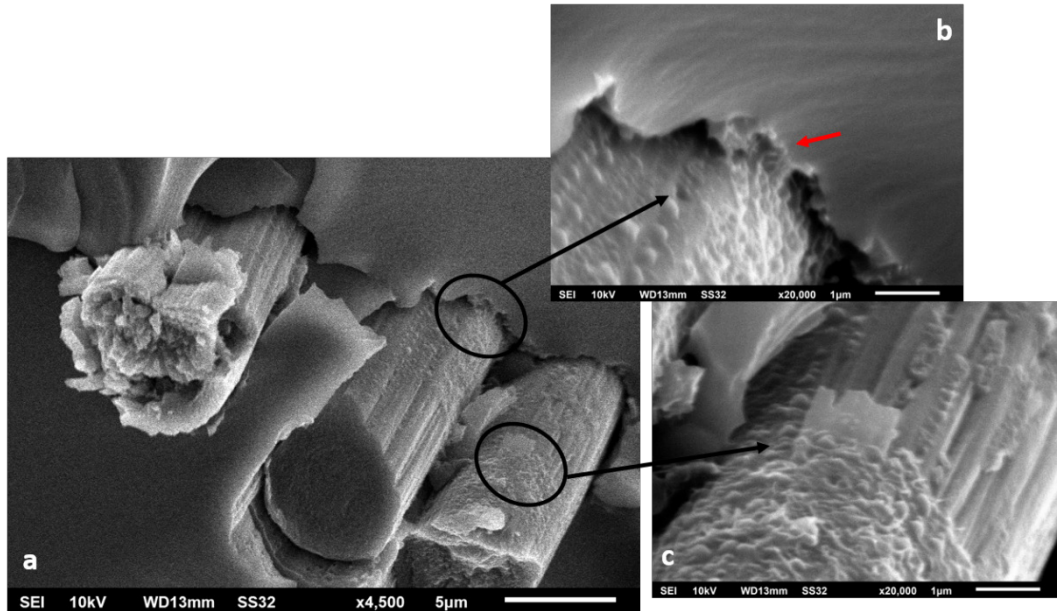


Figure 63. Micrographs of the fracture surface of the CF-CNT/S_60_50 model-composites with different magnifications.

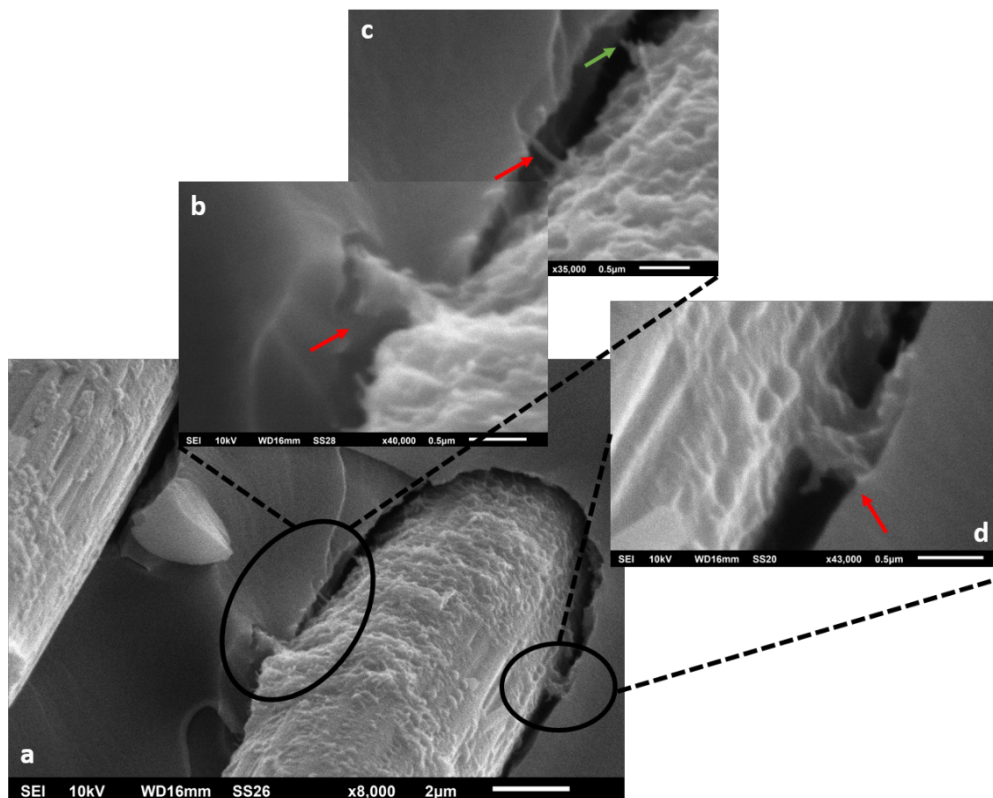


Figure 64. Characteristic micrographs of the interfacial fracture mechanisms for the CF-CNT/S_60_50 tow composites.

Another interesting observation was that the imprints of the CF-CNT/S_60_50 (Figure 65) on the epoxy host matrix after the pull-out process were rougher than the respective imprints of the reference CF/S (Figure 59c) and the CF-CNT@750/30 (Figure 60d). This finding implied that increased interactions and mechanical interlocking existed between the CF-CNT/S_60_50 and the epoxy matrix and thus more energy was dissipated during the pull-out process in comparison to the reference CF/S and the CF-CNT@750/30.

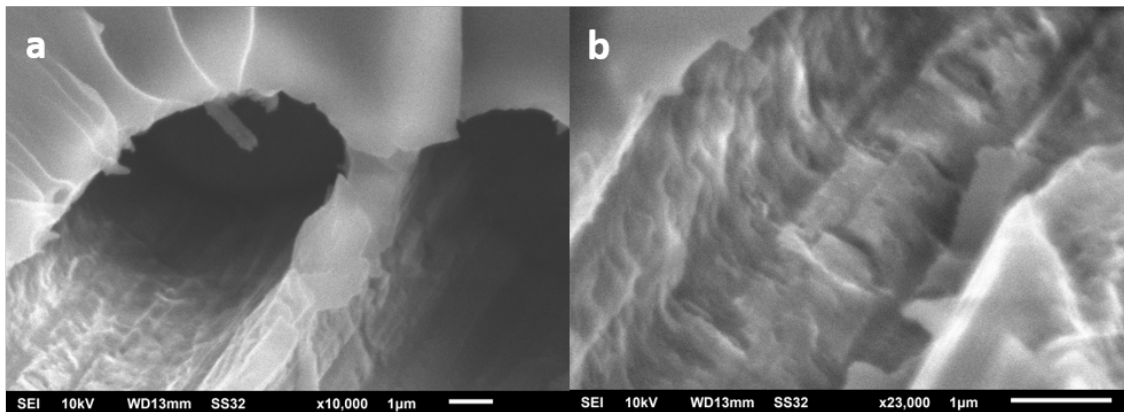


Figure 65. Micrographs of the imprints of the CF-CNT/S_60_50 on the epoxy host matrix after the pull-out process.

5.3.3. Calculation of the Raman stress sensitivity

The strain-induced Raman sensitivities, α_ϵ , were summarised in Table 12. These values are a measure of the sensitivity of the Raman 2D vibrational mode when the material is subjected to externally applied tensile loading. The CF-CNT@850/30 and the CF-CNT/S_60_50 were selected for the evaluation of the residual thermal stresses in model-composites, while the sole criterion for this selection was the magnitude of the α_ϵ value. The reference CF/UNS and CF/S were also evaluated for comparison but since they exhibited similar behaviours only the CF/S results were presented.

The corresponding stress-induced Raman sensitivity values, α_σ , for the CF/UNS and the CF/S were $-3.27 \text{ cm}^{-1} \text{ GPa}^{-1}$ and $-4.57 \text{ cm}^{-1} \text{ GPa}^{-1}$, respectively, for a modulus of 390 GPa as quoted by the manufacturer. In the case of CF-CNTs although, the young moduli values of the commercial and the CVD grown CNTs were unknown and thus were assumed to be 1TPa as reported in the literature [229,230]. The corresponding α_σ values were -2.44 cm^{-1}

GPa⁻¹ and $-1.82 \text{ cm}^{-1} \text{ GPa}^{-1}$ for the CF-CNT@850/30 and the CF-CNT/S_60_50, respectively.

Although CNTs typically exhibit higher order than CFs, the apparent stress sensitivity is lower, which stems directly from the fact that the CNTs (i) were not aligned in the loading direction and (ii) did not necessarily follow the macroscopic deformation of the CF with 100% efficiency, as this depended much on the bonding of the CNTs on the fibre surface. However, it was directly proven that for both CF-CNT@850/30 and CF-CNT/S_60_50 there was established interaction between the primary reinforcement (CF) and the secondary reinforcement (CNTs) which was a prerequisite in order to exploit the synergy between the micron and nano-sized phases.

5.3.4. Residual stress profiles

The residual stress profiles of the CF/S, the CF-CNT@850/30 and the CF-CNT/S_60_50 are presented in Figure 66. Although the coupons are not under any macroscopic stress field, the measured stresses on the fibre stem from the differential thermal expansion coefficient between the fibre and the matrix. The symmetry of the stress tensor requires that the fibre end is at zero stress as was observed. However, compressive stresses were found to build up from the fibre ends towards the middle of the embedded fibre, as compression was transferred via the fibre matrix interface. Therefore, the CF/S exhibited overall a compressive residual stress profile (top plot in Figure 66), building down from the fibre ends [216]. The profile of the CF/UNS, not presented here, was similar to that of the CF/S. More analytically, the ends of the CF were free of stresses, while moving from the ends towards the middle of the fibre compressive residual stresses developed uniformly from 0 to 1.15 GPa average values at about 120 μm from the fibre end. The maximum compression was in the order of -1.50 GPa. As aforementioned, this behaviour was attributed to the difference in the thermal expansion coefficients of the epoxy matrix ($65\text{--}70 \cdot 10^{-6} / ^\circ\text{C}$ as stated by the manufacturer) and of the CFs ($-0.36 \cdot 10^{-6} / ^\circ\text{C}$ [220]) leading to the formation of a hydrostatic field on the fibre which affects the stress transfer.

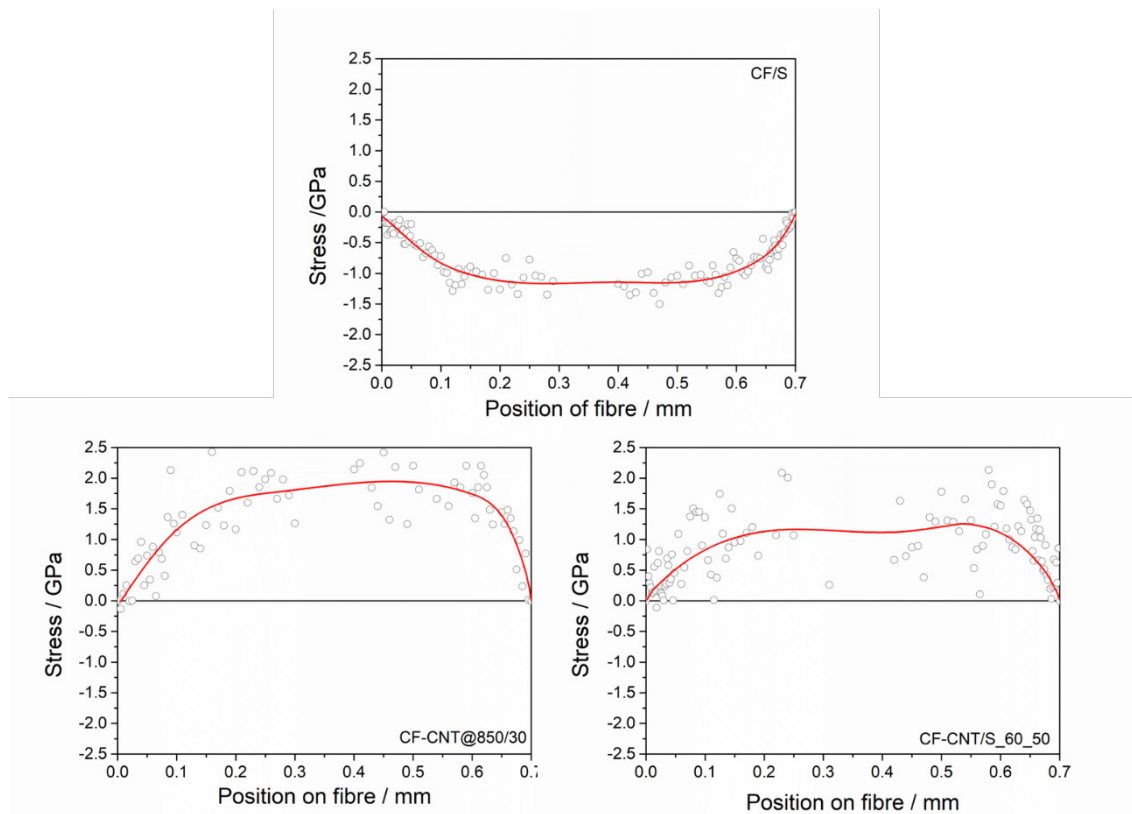


Figure 66. Residual axial stress profiles along the fibre length for the CF/S, CF-CNT@850/30 and the CF-CNT_60_50 embedded in the epoxy matrix.

On the other hand, both the CNT coated fibres exhibited tensile residual stress profiles. In this case, as well, the ends of both the CNT coated fibres were free of stresses. However, while moving towards the middle of the fibre, tensile residual stresses gradually built up along the fibres until they reached a steady value at some distance away from the fibre ends. The CF-CNT/S_60_50 exhibited average tensile residual stress values of 1.22 GPa reaching maximum values in the order of 2.09 GPa. The CF-CNT@850/30 exhibited even higher tensile residual stresses with average values in the order of 1.76 GPa and maximum values in the order of 2.42 GPa.

The tensile residual stress state of the CNTs in comparison to the expected compressive residual stress state of the CFs could be any or a combination of the following factors; i) synergy among the different length scales existed in the hierarchical fibres which is a prerequisite for residual stresses to be formed; ii) bonding of the CNTs with the CF substrates and the epoxy matrix also existed, as the CNTs remain intact on the fibre surface but also

follow the stress state of the matrix due to increased bonding between them; iii) other factors than the above or the mismatch in thermal expansion coefficients of the CNT and the epoxy matrix.

It would be expected that usually, the CNTs should also be in compression similar to the underlying fibre, as both the fibre and the CNTs independently are within a compressive hydrostatic field caused by the thermal mismatch coefficient of the surrounding matrix and the reinforcing phases. As the results indicated, the CNTs were in tension after the post-curing process following the local stress field of the resin which counterbalanced the compressive field on the CF. A possible explanation for this behaviour is related to the differences in the macroscopic alignment of the CF and the CNTs. On the one hand, the CF did not possess any curvature and, as it was macroscopically aligned, it was directly compressed along its axis by the surrounding matrix. On the other hand, the CNTs exhibited a considerable curvature along their axis and were far from being macroscopically aligned. Therefore, the hydrostatic compressive field was not directly translated to axial compression on the CNTs as schematically depicted in Figure 67.

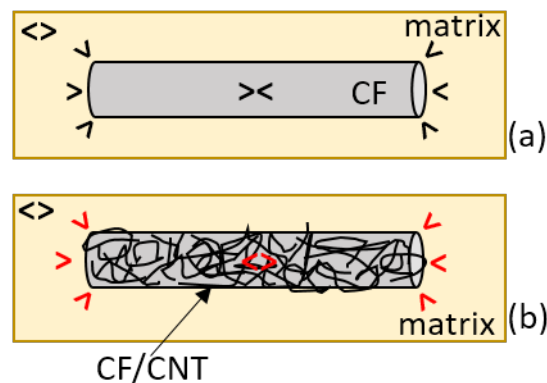


Figure 67. Schematic representation of the hydrostatic field acting on a) a conventional CF and b) a hierarchical CF embedded in the epoxy matrix.

In an alternative approach, it was established that CNTs were partially connected on the CF surface. The bonded end of the CNTs on the CF surface was displaced following the axial local displacement of the fibre whereas the rest of the CNTs resisted this displacement due to its interfacial bonding with the surrounding matrix. As the parent structure (CF) is ca. two orders of magnitude larger than the secondary structure (CNTs),

the relative displacement for the same compressive strain was considerably larger for the CF. If the two reinforcements were not attached, both would exhibit the same compression. However, the partial attachment of the CNTs on the CF resulted in a net tensile field on the CNT, as the local displacement due to the hydrostatic compression for the CF was considerably larger. In its turn, this resulted in a red shift in the Raman spectrum, which directly translated to the tensile field on the CNT coating.

The direct corollaries of this rationale are that, i) the matrix has efficiently penetrated the CNT coating (as already shown by the SEM fractography) and ii) in contrast with the CF, no compressive strain was detected on the CNT coating of the hierarchical structures, something that would be feasible if the CNTs did not exhibit any curvature. In all cases, it was apparent that the CNTs exhibited adequate bonding both with the parent structure, i.e. the CF and with the epoxy matrix, which led to the formation of the tensile residual stresses on them. Moreover, the presence of the CNTs radically changes the stress field at the vicinity of the interface for hierarchical reinforcements via an anchoring mechanism between the CF surface and the surrounding matrix.

5.4 Conclusions

In this chapter, the hierarchical CF-CNT reinforcements produced by CVD or wet chemical treatments and dip-coating were incorporated into an epoxy matrix, and the interactions of the CNTs with the substrate CF and the epoxy in the interfacial region were evaluated. All the hierarchical reinforcements exhibited improved wettability by the epoxy resin which also affected the IFSS of the hierarchical CF-CNT/epoxy model composites, leading to notably improved adhesion and distinctly shorter fragment lengths during the SFFT. Specifically, the hierarchical reinforcements produced by CVD growth at 750°C exhibited the most pronounced IFSS enhancement, by up to 134 % in comparison to the reference CF/UNS. On the other hand, when CVD growth was performed at 850°C, the hierarchical CF-CNTs demonstrated IFSS values comparable to the hierarchical CF-CNTs produced by the wet chemical method (CF-CNT/S_60_50), exhibiting a 69-77% improvement when compared to the reference CF/UNS and CF/S, respectively.

Furthermore, the failure process of the hierarchical CF-CNT/epoxy model composites was evaluated by SEM fractography. The fracture surfaces of the hierarchical model composites were significantly altered when compared to the fracture surfaces of the reference model composites. In more detail, smaller debonding of the hierarchical CF-CNTs from the epoxy matrix was observed alongside with restricted CF pull-out and rougher imprints after the CF-CNT pull-out process. Additional fracture phenomena related to the CNT nano-reinforcement were also observed, like CNT bridging effects and CNT rupture, which further justified the improvements in the IFSS values for the hierarchical model composites. Moreover, the fracture process was altered for some of the hierarchical reinforcements produced by the wet chemical protocol, from adhesive where the epoxy matrix at the interfacial regions failed during fracture of the specimens, to cohesive where the CF reinforcement failed during the fracture of the specimens.

Finally, during this Chapter, the residual thermal stresses accumulated onto the CF/epoxy and the CF-CNT/epoxy model composites during the polymerisation process due to the differences in the thermal expansion coefficients of the CFs, the CNTs and the epoxy matrix were assessed by Raman spectroscopy. The presence of the CNTs was found to radically alter the stress field at the vicinity of the interface for the hierarchical reinforcements via an anchoring mechanism between the CF-CNT surface and the surrounding matrix. The incorporation of the CNTs onto the CFs changed the residual stress profiles from compressive for the CF/epoxy model composites, to tensile for the CF-CNT/epoxy model composites.

Chapter 6

Mechanical and electrical response of
hierarchical composite laminates

6.1 Introduction

The primary objective of the hierarchical approach is to enhance the inherently insufficient out-of-plane mechanical properties of advanced CRFCs with the least possible degradation in their in-plane mechanical response. The out-of-plane mechanical response of CFRCs is typically determined by various experimental tests depending on the final application of the composites.

Specifically, through the hierarchical approach the fracture toughness, the interlaminar shear-strength, the flexural properties and the resistance to impact of the final composites are anticipated to be improved since this method of nano-reinforcement focuses mainly on the enhancement of the stress transfer at the interfacial region. Along these lines, many authors evaluated the flexural and interlaminar properties as well as the resistance to fracture for hierarchical reinforcements.

In more detail, the hierarchical CF-CNT/epoxy reinforcements produced by the deposition of CNT-COOH on sized CFs by an aqueous suspension immersion method resulted in 13% improvements in the ILSS of CF-CNT/epoxy composites [91]. The use of POSS in hierarchical CF-POSS-CNT reinforcements led to a 32-36% enhancement in the ILSS as well as to a 33% improvement of the impact toughness of the hierarchical laminates [104] [106]. A more notable enhancement was observed in the ILSS of CF-CNT/polyester composites (44.5%) and CF-CNT/methyl phenyl silicone composites (53.1%), where PACl and APS, respectively, were used as the coupling agents for the preparation of the CF-CNT reinforcements [100,102]. The same composites also exhibited a 44.0% and a 33.2% enhancement in the impact toughness, respectively [100,102]. A 50% increase in the impact strength was also observed in CF-CNT/epoxy composites where the reinforcements were produced by the layer by layer grafting of oxidised CNTs onto amino-functionalized CFs [95].

Additionally, the hierarchical approach can endow several functionalities in the advanced multiscale CFRCs. Numerous studies exist in the literature which mainly focused on the improvement of these additional functionalities of the hierarchical CF-CNTs, i.e. sensing ability, electromagnetic interference shielding, current collectors and electrochemical microelectrodes and fibrous supercapacitors.

Among these functionalities, the enhancement of the electrical performance of the hierarchical composites has been the main objective of several research efforts. For instance, Dong et al. who studied the effects of physical drying with chemical modification of CNTs, on the through-thickness properties of CF/epoxy composites, reported that the use of hydroxyl-modified CNT networks resulted in hierarchical composites with significantly enhanced electrical conductivity, by 78% compared to the reference CFRCs [111].

A 30% enhancement in both the in-plane and the out-of-plane electrical conductivities in comparison to the reference composites was also reported by Bekyarova et al. for hierarchical composites produced by EPD [116]. An even higher enhancement of 50% in the in-plane electrical conductivity was reported by Lee et al. for the hybrid CNT/Cu-CF/epoxy composites, where the reinforcements were produced by a cathodic EPD process [132].

The CVD process for the production of CF-CNTs was shown by Pozegic et al. to lead to hierarchical CFRCs with even more pronounced in-plane and out-of-plane electrical conductivities, namely 330% and 510%, respectively [51]. In another study, Fogel et al. tried to increase the homogenise the through-thickness electrical conductivity of CFRCs by dispersing CNTs into the polymeric matrix by a calendaring process and then spraying this mixture with an airbrush onto dry CF plies. This approach resulted in CFRCs with only a small improvement in the transverse (2.1 over 0.8 S m⁻¹), and longitudinal (13.8 over 9.3 S m⁻¹) electrical conductivities [161].

In this chapter, the mechanical response of hierarchical laminated composites where the CF-CNT reinforcements were produced by the wet chemical protocols and dip coating was evaluated by short-beam shear tests. The reference CF/epoxy composites were also assessed for comparison. A fractographic investigation accompanied the mechanical tests and provided valuable insight into the failure process of the interlaminar regions of the hierarchical and the reference composites. Furthermore, the electrical characteristics of the hierarchical CF-CNT/epoxy composites and the reference CF/epoxy composites were assessed.

6.2 Materials and Methods

6.2.1. Manufacturing of composite laminates

CF tows were carefully aligned one next to the other in order to form unidirectional plies. These plies were subsequently stacked by the hand lay-up method for the manufacturing of composite laminates. Vacuum was applied upon completion of the lamination process in order to remove the excess of resin. Two composite laminates were manufactured, a reference and a hierarchical, using the M40 sized CFs and CF-CNT_60_50, respectively. Both laminates were balanced and symmetric with a quasi-isotropic lamination sequence, $[90/\pm 45/0]_s$. A two-part epoxy resin MY750/HY951 with a ratio of 100:25 was used as the matrix. The curing cycle was performed at 60°C for 2 hours under vacuum, while post curing took place at 120°C for 1.5 hours.

6.2.2. Mechanical characterisation

Specimens with the desired dimensions were then cut from both laminates according to the ASTM D 2344 standard for short-beam strength measurements [231]. This mechanical characterisation technique is a three-point bending experiment, whereby the loading is preferentially guided to the interlaminar regions of the composite. Hence the ILSS is evaluated.

The specimens were tested at a Universal Testing Machine WDW-100 by Jinan S.A. according to the procedure described by ASTM D 2344 standard. Only specimens which failed in the interlaminar shear mode were used for the calculation of the short-beam strength.

Short-beam Shear Strength for the reference CF/S and the hierarchical CF-CNT_60_50 composite laminates were calculated according to equation (12) for at least five specimens in each case.

$$F^{sbs} = 0.75 \times \frac{P_m}{b \times h} \quad (12)$$

where

$$F^{sbs} = \text{short-beam strength [MPa];}$$

P_m = maximum load observed during the test [N];

b = measured specimen width [mm]

h = measured specimen thickness [mm]

6.2.3. Evaluation of the fracture surfaces with SEM

After fracture, all specimens were observed with a JEOL JSM 6510 LV SEM/Oxford Instruments Scanning Electron Microscope in order to study the fracture process. The fractured specimens were placed on a double-sided carbon adhesive tape to be stabilised and coated with a thin layer of Au/Pd (5 nm) prior to the SEM analysis to avoid charging effects.

6.2.4. Measurement of the electrical properties of the hierarchical laminates

The electrical resistance, R , of the reference and the hierarchical composite laminates was measured using an Agilent34401A Digital Multimeter. The hierarchical CF-CNT_60_50 and the reference CF/S laminates were evaluated during this study. Five specimens from each category with fixed rectangular geometry (Length (L): 21mm, Width (w): 9mm and Thickness (t): 3.65mm) were used for the evaluation of the CFRP electrical conductivity.

All specimens were engraved on specific spots at 16mm geometrical distance in order to remove the resin and prepare a suitable electrical contact between the surface fibres and the measuring electrodes. Then, proper ohmic metallic contacts were formed by filling the etched epoxy regions with silver paint droplets (Ag paint by Agar Scientific).

The electrical resistance, R , of the specimens, was measured with the multimeter, and the electrical conductivity was calculated by the use of the equation (13) and equation (14), respectively,

$$R = \rho \frac{L}{A} \quad (13)$$

where ρ is the electrical resistivity of the specimens [Ωm], L is the length [m], and A is the area of the rectangular specimens [m^2] calculated by multiplying the length by the width.

Rearrangement of equation (13) gives us the value of the electrical resistivity which is subsequently used in order to calculate the electrical conductivity of the specimens by the equation (14)

$$\sigma = \frac{1}{\rho} \quad (14).$$

6.3 Results and Discussion

6.3.1. Mechanical response of hierarchical composite laminates

The mechanical response of the hierarchical CF-CNT/S_60_50 and the reference CF/S composite laminates was evaluated by short-beam strength measurements. The hierarchical composites outperformed the reference CF/epoxy composites by 21.5%, exhibiting ILSS values of 29.00 ± 2.49 MPa in comparison to the 23.87 ± 2.26 MPa (Figure 68). The observed enhancement was more pronounced by many values reported in the literature. For instance, Li et al. measured a 13% improvements in the ILSS of the CF-CNT/epoxy composites produced by the deposition of CNT-COOH on sized CFs by an aqueous suspension immersion method [91]. Awan et al. who used the same test and measured an 18% improvement in the ILSS for hierarchical composites produced by the EPD method [151], while a 10.5% enhancement was presented by Sui et al. for hierarchical composites also produced by EPD [130].

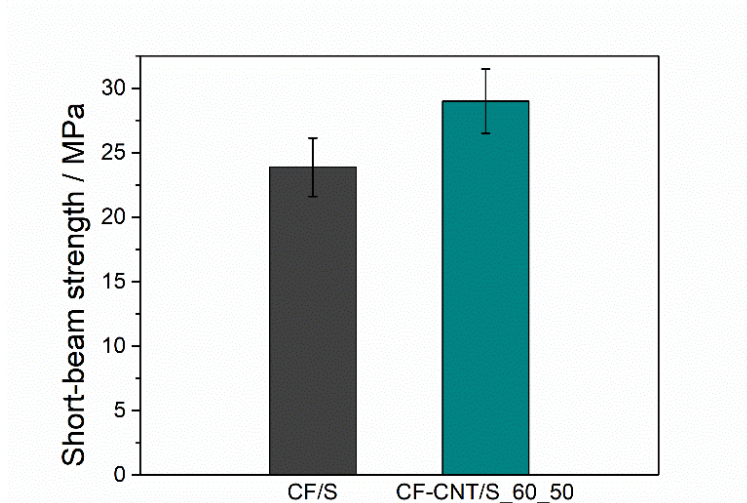


Figure 68. Bar-chart summarising the short-beam strength values of the hierarchical and the reference composites.

As can be seen from the characteristic load-displacement curves (Figure 69), both the load and the extension of the hierarchical composites were increased in comparison to the reference CF/S laminates.

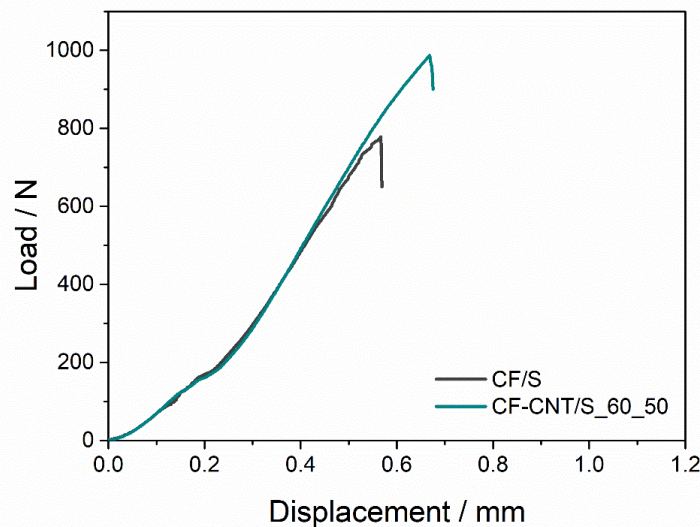


Figure 69. Representative load-displacement curve as recorded for the hierarchical and the reference laminated composites.

A fractographic study was also performed in order to identify possible differences in the failure process of the hierarchical CF-CNT/epoxy composites in comparison to the reference CF/epoxy composites. In general, a brittle fracture was observed for both the reference and the hierarchical composite specimens, but the fracture surfaces of the hierarchical CF-CNT/epoxy specimens were much rougher (Figure 70f) than the fracture surfaces of the reference CF/epoxy specimens (Figure 70b). Furthermore, many more CF-CNTs were still covered/bonded with the epoxy matrix after the failure process (Figure 70g and Figure 70h), while excessive debonding was observed for the reference composites where the exposed CFs exhibited a rather clean surface (Figure 70c and Figure 70d).

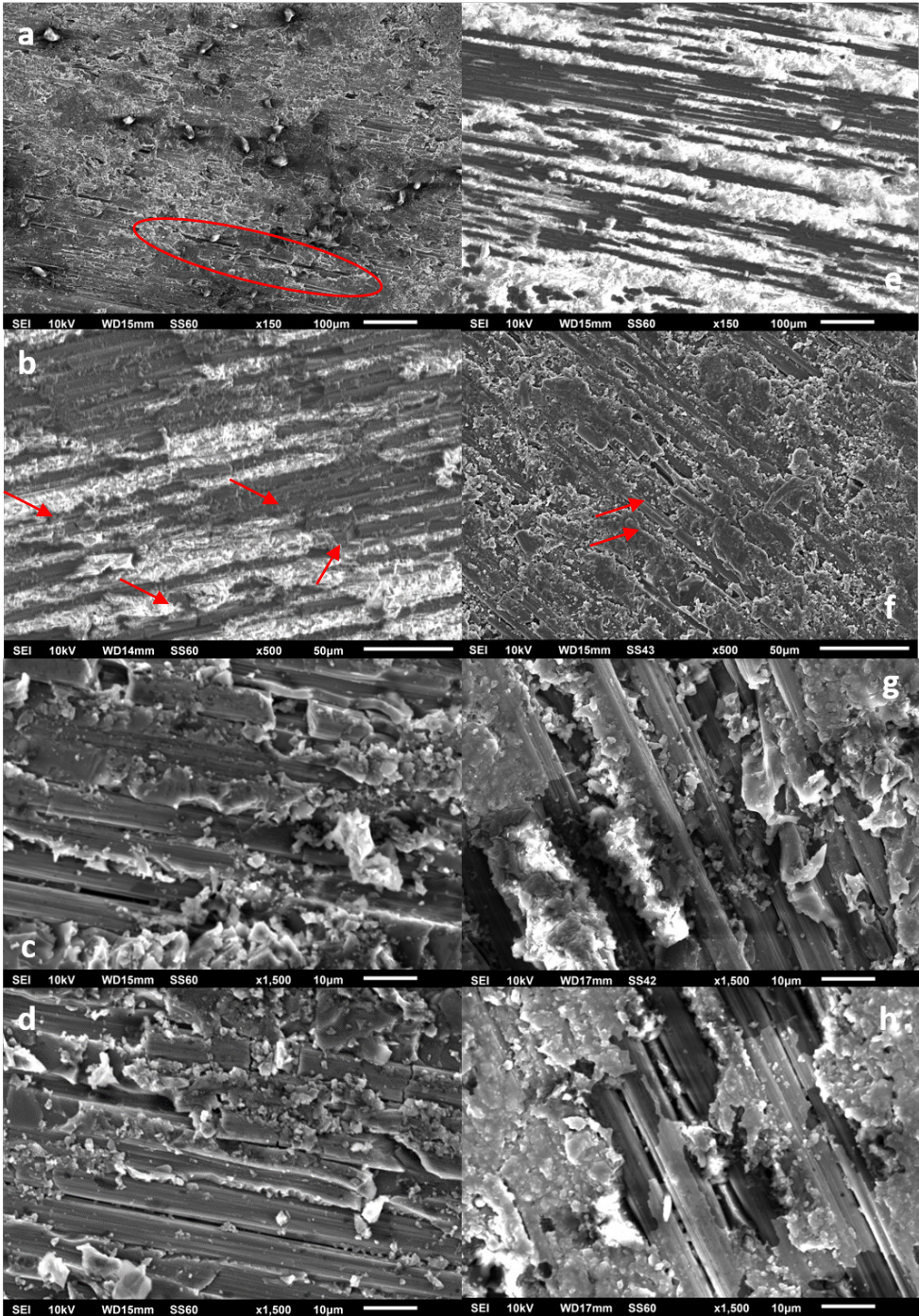


Figure 70. SEM micrographs from fractured ILSS specimens. (a, b, c, d) Reference CF/epoxy specimens and (e, f, g, h) hierarchical CF-CNT/epoxy specimens.

Intralaminar delaminations were observed for the reference CF/epoxy composites (marked with a red circle in Figure 70a), while no delaminations were observed for the hierarchical CF-CNT/epoxy composites (Figure 70e). Furthermore, several broken CFs were observed

in the fracture surface of the reference CF/epoxy composites (indicated by red arrows in Figure 70b), while CF fracture was restricted in the hierarchical CF-CNT fracture surfaces (indicated by the red arrow in Figure 70f).

Moreover, a closer examination of the fracture surface of the hierarchical CF-CNT/epoxy composites (Figure 71) revealed that some CNTs were still present after the failure process on the CF surfaces and covered by the host matrix material (Figure 71a and Figure 71b). While, in some cases resin enriched with CNTs was detached from the CF surface and bridged adjacent CFs (Figure 71b), indicating that efficient stress transfer was present among the CFs.

Based on the analysis mentioned above, the improvement on short-beam shear strength can be attributed to the increased adhesion and mechanical interlocking caused by the CNTs which acted as an interconnected nano-reinforcement which improved the load transfer from the matrix to the CFs in the laminated composites [151].

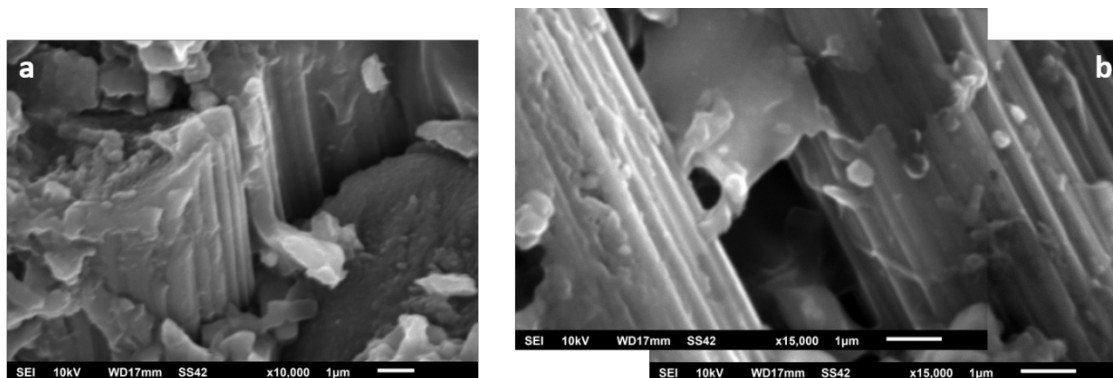


Figure 71. High magnification SEM micrographs from the hierarchical CF-CNT/epoxy composites.

6.3.2. Evaluation of the electrical properties of the hierarchical composites

The electrical response of the hierarchical laminated composites was also evaluated in comparison to the reference CF/epoxy composites. The electrical conductivity was calculated according to equations (13) and (14). In the longitudinal direction, the hierarchical CF-CNT/epoxy composites exhibited improved values of $148.54 \pm 35.25 \text{ S m}^{-1}$ in comparison to the $98.58 \pm 77.48 \text{ S m}^{-1}$ measured for the reference CF/epoxy

composites. This enhancement can be attributed to the CNT induced bridging effects among adjacent fibres in the in-plane direction.

Conversely, in the through-thickness direction, the average electrical conductivity of the hierarchical CF-CNT/epoxy composites slightly decreased to $0.39 \pm 0.07 \text{ S m}^{-1}$ from the average value of $0.42 \pm 0.02 \text{ S m}^{-1}$ which was measured for the reference CF/epoxy composites. However, the standard deviation of the measured values considerably increased for the hierarchical composites when compared to the reference indicating that both higher and lower conductivities were measured. This could further indicate that the CNTs were not equally distributed in the interlaminar regions and therefore further optimisation could lead to even more pronounced changes in the electrical properties of the hierarchical composites.

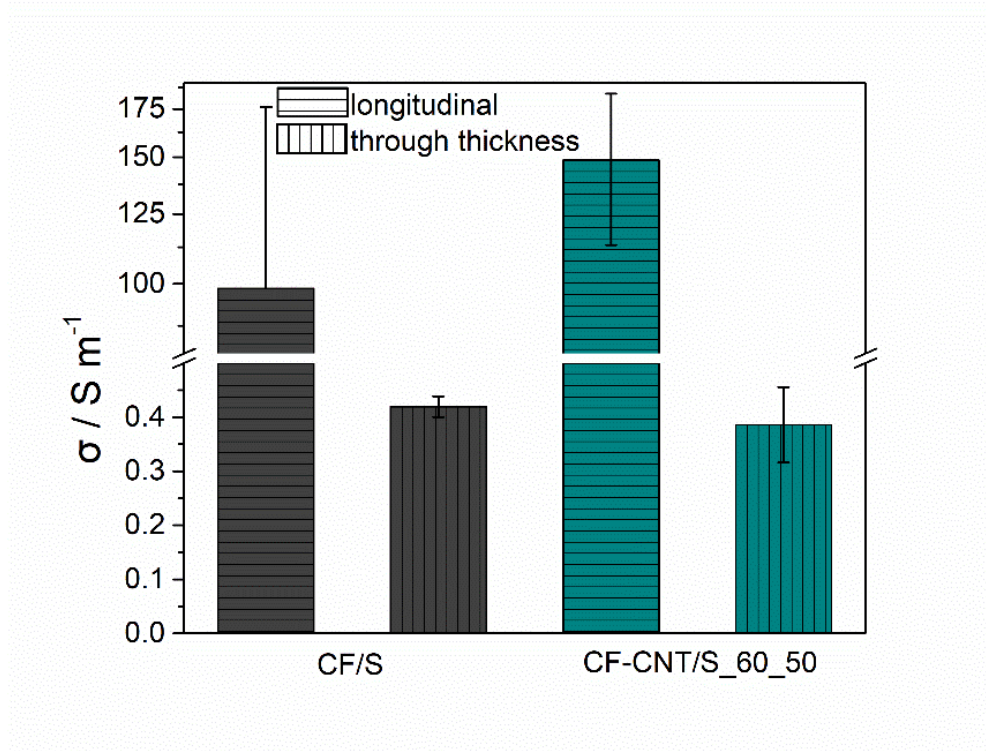


Figure 72. The electrical conductivity of the hierarchical CF-CNT/epoxy laminates and the reference CF/epoxy laminated composites in both the in-plane and the through-thickness directions.

6.4 Conclusions

The hierarchical approach was shown in this chapter to result in significantly improved out-of-plane mechanical properties for the CF-CNT/epoxy laminated composites in comparison to the reference CF-epoxy laminates. Specifically, the short-beam shear strength of the CF-CNT/epoxy composites exhibited a 21.5% improvement in comparison to the reference CF/epoxy laminates, due to the presence of the CNTs on the CF surface.

A fractography study corroborated the enhanced interlaminar properties of the hierarchical composites, where delamination phenomena and fibre fracture were restricted in comparison to the reference CF/epoxy composites. Furthermore, CNTs were still present on the surface of the CFs after failure but also were found in the intralaminar regions bridging adjacent CFs. This finding indicated a strong bonding/anchorage of the CNTs with both the primary reinforcement (CFs) as well as the epoxy matrix.

Furthermore, the in-plane electrical conductivity of the hierarchical CF-CNT/epoxy composites increased by 51% in comparison to the reference CF/epoxy composites indicating that the CNTs effectively bridged the adjacent fibres not only for the transferring of stresses but also for the easier flow of currents.

Chapter 7

Conclusions and Suggestions for future research

7.1 Conclusions

The current thesis focused on the study of advanced hierarchical fibre reinforced composites. This work targeted on the parallel investigation of two commonly used methods for the production of hierarchical reinforcements, namely CVD and wet chemical treatments. The CVD growth process was implemented as a commonly used technique for the production of hierarchical reinforcements. Conversely, the wet chemical treatments and the dip-coating procedure were developed and optimised as a straightforward and scalable process for the manufacturing of hierarchical laminated composites.

With regards to the CVD process, the growth of the CNTs was initially optimised on single CFs and then successfully implemented on CF tows, producing various morphologies which were subsequently evaluated regarding physicochemical and mechanical properties. The hierarchical reinforcements produced by CVD were used for the benchmarking study of the structural and mechanical properties at the single fibre (Chapter 4) or model composite level (Chapter 5), while the thesis focused mainly on the production of CF-CNTs by attaching commercial CNTs onto the surface of CFs by wet chemical modifications and grafting for the characterization of the mechanical properties of hierarchical laminated CF-CNT/epoxy composites (Chapter 6).

In relation to the wet chemical protocol, a systematic approach was followed during this study whereby the studied parameters (oxidation duration, concentration of CNTs in acids and mechanical aiding of the dispersion) were evaluated and ranked via an algorithmic process which was based on the experimental evidence provided by various analytical techniques (Raman, IR, TGA, XPS, EIS). The CNT INK with the best combination of properties was selected, among the several INKs that were produced, based on the aforementioned methodology, to be used as a coating on oxidised carbon fibres. SEM micrographs revealed that the formation of a thin homogeneous veil of CNTs onto the CF surface was feasible while thicker coatings could also be produced in a controllable manner. The viability and validity of the process were verified by confirming the INK choice in relation to the rest of the produced INKs.

Furthermore, valuable conclusions on the mechanisms acting during oxidation of the nanostructures were drawn, and the factors affecting the homogeneity and thickness of the

CNTs veil onto the CF surface were identified. Combined experimental findings suggested that two competing mechanisms were simultaneously present during oxidation, i.e. (i) the introduction of oxygen-based functional moieties and (ii) the purification of the CNTs. The governing conditions for the optimisation of this procedure were identified as (i) the moderate oxidation of CNTs by stirring which facilitated (ii) the production of a homogeneous, electrically percolated INK by sufficient sonication and a final (iii) systematically controlled dip coating process of the CFs in the produced INK. Additionally, the developed and optimised CNT INKs are suitable as printing materials for implementation in various processes other than dip-coating, i.e. spraying, roll-to-roll printing via screen printing technologies.

Overall, the CVD process resulted in a denser coverage of the CF surface with a porous layer of MWCNTs, which significantly altered the substrate CF diameter, in comparison to the wet chemical process. On the other hand, the wet chemical dip-coating procedure, which was developed and optimised during this study, was more efficient in controlling the thickness of the deposited CNTs onto the CFs.

A benchmarking of the hierarchical CF-CNTs produced by the CVD and the wet chemical and dip coating processes at the single-fibre level indicated that the latter reinforcements exhibited increased crystalline order and in-plane correlation lengths as well as improved thermal stability in comparison to the CVD grown CF-CNTs. With regards to the tensile properties, all the CF-CNTs exhibited decreased strength, as anticipated, along with substantially improved stiffness. The CF-CNTs produced by the wet chemical method showed lower tensile strength degradation and more notable enhancement in the elastic modulus values when compared to the CF-CNTs produced by CVD. Moreover, the Weibull modulus indicated a smaller flaw distribution for the hierarchical reinforcement produced by the wet chemical protocol (CF/S, CF-CNT/S_30_50 and CF-CNT/S_60_50) in comparison to the hierarchical reinforcements produced by the CVD process (CF/UNS and CF-CNT@850/30).

Conversely, the strain induced Raman sensitivity was higher for the CF-CNT@850/30 in comparison to the CF-CNT/S_30_50 and the CF-CNT/S_60_50, indicating that the CVD process should be used for the production of hierarchical reinforcements when more sensitive strain sensors are required.

Afterwards, the hierarchical CF-CNT reinforcements were incorporated into an epoxy matrix, and the interactions of the CNTs with the substrate CF and the epoxy in the interfacial region were evaluated. All the hierarchical reinforcements exhibited improved wettability by the epoxy resin which also affected the IFSS of the hierarchical CF-CNT/epoxy model composites, leading to notably improved adhesion and distinctly shorter fragment lengths during the SFFT. Specifically, the hierarchical reinforcements produced by CVD growth at 750°C exhibited the most pronounced IFSS enhancement, by up to 134 % in comparison to the reference CF/UNS. On the other hand, when CVD growth was performed at 850°C, the hierarchical CF-CNTs demonstrated IFSS values comparable to the hierarchical CF-CNTs produced by the wet chemical method (CF-CNT/S_60_50), exhibiting a 69-77% improvement when compared to the reference CF/UNS and CF/S, respectively.

Furthermore, valuable insight into the failure process of the hierarchical CF-CNT/epoxy model composites was provided by SEM fractography. The fracture surfaces of the hierarchical model composites were significantly altered when compared to the fracture surfaces of the reference model composites. The interphase of the hierarchical reinforcements with the epoxy matrix was significantly improved in comparison to the interphases of the reference CF/epoxy model composites, as indicated by the restricted debonding and fibre pull-out phenomena as well as the rougher imprints after the CF-CNT pull-out process from the epoxy matrix. Additional fracture phenomena related to the CNT nano-reinforcement were also observed, like CNT bridging effects and CNT rupture. These mechanisms further justified the improvements in the IFSS values for the hierarchical model composites in comparison to the reference model composites. Moreover, the fracture process was altered for some of the hierarchical reinforcements produced by the wet chemical protocol, from adhesive where the epoxy matrix at the interfacial regions failed during fracture of the specimens, to cohesive where the CF reinforcement failed during the fracture of the specimens.

Additionally, the residual thermal stresses accumulated onto the CF/epoxy and the CF-CNT/epoxy model composites during the polymerisation process due to the differences in the thermal expansion coefficients of the CFs, the CNTs and the epoxy matrix were for the first time to the author's knowledge assessed by Raman spectroscopy. The presence of the

CNTs was found to radically alter the stress field at the vicinity of the interface for the hierarchical reinforcements via an anchoring mechanism between the CF-CNT surface and the surrounding matrix. The incorporation of the CNTs onto the CFs changed the residual stress profiles from compressive for the CF/epoxy model composites, to tensile for the CF-CNT/epoxy model composites.

Finally, the hierarchical reinforcements with the optimal physicochemical and mechanical characteristics (CF-CNT/S_60_50) produced by the developed and optimised wet chemical and dip-coating protocol were selected for the manufacturing of laminated composites for the evaluation of the mechanical properties and electrical response. The hierarchical CF-CNT/epoxy laminates exhibited significantly improved out-of-plane mechanical properties in comparison to the reference CF/epoxy laminates. Specifically, the ILSS of the CF-CNT/epoxy composites, which was measured by the short-beam shear method, exhibited a 21.5% improvement in comparison to the reference CF/epoxy laminates, due to the presence of the CNTs on the CF surface. The measured ILSS for the hierarchical CF-CNT/epoxy composites is higher in comparison to the available literature results on hierarchical composites produced by wet chemical treatments or the EPD method as detailed in Chapter 6. This enhancement was also corroborated by a fractography study, which indicated that the delamination phenomena and fibre fracture were restricted in the hierarchical CF-CNT/epoxy composites in comparison to the reference CF/epoxy composites. Furthermore, CNTs were still present on the surface of the CFs after failure but were also found in the intralaminar regions bridging adjacent CFs. This finding indicated a strong bonding/anchorage of the CNTs with both the primary reinforcement (CFs) as well as the epoxy matrix. Moreover, the in-plane electrical conductivity of the hierarchical CF-CNT/epoxy composites increased by 51% in comparison to the reference CF/epoxy composites indicating that the CNTs effectively bridged the adjacent fibres not only for the transferring of stresses but also for the undisturbed flow of currents.

7.2 Suggestions for future research

Within the scope of this study, the developed wet chemical and dip-coating process led to the production of hierarchical reinforcements with improved ILSS and electrical properties in comparison to the reference CF/epoxy composites. The measured ILSS values were also higher in comparison to the available literature results on hierarchical composites produced by wet chemical treatments or the EPD method as detailed in Chapter 6. However, there is ample space for further enhancement of the out-of-plane mechanical properties as well as the improvement of additional functionalities of the hierarchical composites by further optimizing the coating process of the CFs with CNTs.

Therefore, an ongoing experimental campaign is already focused on implementing the optimised INKs in a spray coating process as well as in a roll-to-roll line for the continuous production of hierarchical reinforcements. The automation of the coating process by either of the above coating methods is anticipated to offer even better control of the coating thickness as well as the opportunity to use other carbon-based nanostructures.

Along these lines, the development of additional INKs in order to target specific functionalities of the final composites is an open research topic. These INKs will also contain other NPs than CNTs in order to improve the thermoelectric response, the electromagnetic shielding effectiveness as well as further enhance the out-of-plane mechanical properties of the hierarchical composites.

For this reason, an extensive testing campaign is already underway which will evaluate the fracture toughness, the impact resistance, the compression-after-impact and the open hole compression of the hierarchical composites. These tests are anticipated to establish structure-property relations by experimentally verifying the optimisation of the CNT or other NP deposition processes using either spray coating or roll-to-roll printing methods.

Additionally, during this thesis, the residual stress profiles of individual hierarchical CFs at the locus of the interphase with the epoxy matrix were evaluated by Raman spectroscopy. This study will be extended in order to determine the IFSS of model hierarchical composites under external loading with Raman spectroscopy. For this to be achieved a precisely measured external load will be applied to model composite specimens which will cause a certain amount of strain to both the epoxy matrix and the impregnated hierarchical

reinforcements. The shift of characteristic Raman active vibrational modes will be simultaneously monitored by Raman spectroscopy measurements and then translated to stress values by using the micromechanical analytical equations presented in Chapter 5. These results will contribute to a better understanding of the stress distributions accumulated on the hierarchical CFs under tensile or compressive loads.

Another open field of research is related to the evaluation of the chemical interactions and type of bonds which are present between the CFs and the CNTs as well as the CNTs and the epoxy matrix in the hierarchical composites. Some initial experimental evidence was presented in this thesis, while a further study is underway which includes the use of several characterisation methods like XPS, titration measurements, EDS measurements during SEM observations as well as measurements of the grafting strength of individual CNTs with the CF substrates with an AFM nano-manipulator under SEM observation. Additionally, dynamic contact angle measurements are under completion which will assist in evaluating the surface energy of the hierarchical and reference reinforcements. The results of these measurements will provide a complete picture of the chemical interactions at the interphases and contribute to the determination of relations between the selected process parameters and the resulting hierarchical reinforcements characteristics.

A database of all the aforementioned results will be created which will serve as a source of information for the further development of hierarchical reinforcements and composites with pre-estimated physicochemical and mechanical properties and additional functionalities.

Finally, the recyclability of the hierarchical composites is of great interest for the author since the minimisation of the environmental impact due to the use, and the disposal of such advanced materials is of great concern if the hierarchical composites are going to enter a wide market chain. For these reasons, a detailed Life Cycle Analysis of the hierarchical composites is also under development in order to assess and minimise possible effects on the environment.

Literature

-
- [1] R. Bacon, C.T. Moses, Carbon Fibers, from Light Bulbs to Outer Space, in: R.B. Seymour, G.S. Kirshenbaum (Eds.), High Perform. Polym. Their Orig. Dev., Springer Netherlands, Dordrecht, 1986: pp. 341–353.
- [2] J. Gorss, High Performance Carbon Fibers, American Chemical Society, Maryland, 2003.
- [3] H.W. Zhou, L. Mishnaevsky, H.Y. Yi, Y.Q. Liu, X. Hu, A. Warriier, G.M. Dai, Carbon fiber/carbon nanotube reinforced hierarchical composites: Effect of CNT distribution on shearing strength, *Compos. Part B Eng.* 88 (2016) 201–211. doi:10.1016/j.compositesb.2015.10.035.
- [4] H. Kim, E. Oh, H.T. Hahn, K.H. Lee, Enhancement of fracture toughness of hierarchical carbon fiber composites via improved adhesion between carbon nanotubes and carbon fibers, *Compos. Part A Appl. Sci. Manuf.* 71 (2015) 72–83. doi:10.1016/j.compositesa.2014.12.014.
- [5] J. Karger-Kocsis, H. Mahmood, A. Pegoretti, Recent advances in fiber/matrix interphase engineering for polymer composites, *Prog. Mater. Sci.* 73 (2015) 1–43. doi:10.1016/j.pmatsci.2015.02.003.
- [6] D.B. Anthony, X.M. Sui, I. Kellersztein, H.G. De Luca, E.R. White, H.D. Wagner, E.S. Greenhalgh, A. Bismarck, M.S.P. Shaffer, Continuous carbon nanotube synthesis on charged carbon fibers, *Compos. Part A Appl. Sci. Manuf.* 112 (2018) 525–538. doi:10.1016/j.compositesa.2018.05.027.
- [7] S. Khan, H. Singh Bedi, P.K. Agnihotri, Augmenting mode-II fracture toughness of carbon fiber/epoxy composites through carbon nanotube grafting, *Eng. Fract. Mech.* 204 (2018) 211–220. doi:10.1016/j.engfracmech.2018.10.014.
- [8] E. Kalfon-Cohen, R. Kopp, C. Furtado, X. Ni, A. Arteiro, G. Borstnar, M.N. Mavrogordato, I. Sinclair, S.M. Spearing, P.P. Camanho, B.L. Wardle, Synergetic effects of thin plies and aligned carbon nanotube interlaminar reinforcement in composite laminates, *Compos. Sci. Technol.* 166 (2018) 160–168. doi:10.1016/j.compscitech.2018.01.007.
- [9] L. Zhang, N. De Greef, G. Kalinka, B. Van Bilzen, J.P. Locquet, I. Verpoest, J.W. Seo, Carbon nanotube-grafted carbon fiber polymer composites: Damage

- characterization on the micro-scale, *Compos. Part B Eng.* 126 (2017) 202–210. doi:10.1016/j.compositesb.2017.06.004.
- [10] A.P. Mouritz, K.H. Leong, I. Herszberg, A review of the effects of stitching on the in-plane mechanical properties of fibre-reinforced polymer composites, *Compos. Part A.* 28A (1997) 979–991. doi:10.2307/3546618.
- [11] K.A. Dransfield, L.K. Jain, Y. Mai, ON THE EFFECTS OF STITCHING IN CFRPs-I . DELAMINATION TOUGHNESS, *Compos. Sci. Technol.* 58 (1998). doi:10.1016/S0266-3538(97)00229-7.
- [12] L. Lee, S. Rudov-Clark, A.P. Mouritz, M.K. Bannister, I. Herszberg, Effect of weaving damage on the tensile properties of three-dimensional woven composites, *Compos. Struct.* 57 (2002) 405–413. doi:10.1016/S0263-8223(02)00108-3.
- [13] D.D.R. Cartie, M. Troulis, I.K. Partridge, Delamination of Z-pinned carbon fibre reinforced laminates, *Compos. Sci. Technol.* 66 (2006) 855–861. doi:10.1001/jama.291.1.112-b.
- [14] A.P. Mouritz, M.K. Bannister, P.J. Falzon, K.H. Leong, Review of applications for advanced three-dimensional fibre textile composites, 30 (1999) 1445–1461. doi:10.1016/S1359-835X(99)00034-2.
- [15] H. Qian, E.S. Greenhalgh, M.S.P. Shaffer, A. Bismarck, Carbon nanotube-based hierarchical composites: a review, *J. Mater. Chem.* 20 (2010) 4751–4762. doi:10.1039/c000041h.
- [16] M.C.L. McCrary-Dennis, O.I. Okoli, A review of multiscale composite manufacturing and challenges, *J. Reinf. Plast. Compos.* 31 (2012) 1687–1711. doi:10.1177/0731684412456612.
- [17] J. Qiu, C. Zhang, B. Wang, R. Liang, Carbon nanotube integrated multifunctional multiscale composites, *Nanotechnology.* 18 (2007) 275708–275719. doi:10.1088/0957-4484/18/27/275708.
- [18] R. Zeiler, U. Khalid, C. Kuttner, M. Kothmann, D.J. Dijkstra, A. Fery, V. Altstadt, Liquid composite molding-processing and characterization of fiber-reinforced composites modified with carbon nanotubes, *AIP Conf. Proc.* 1593 (2014) 503–507. doi:10.1063/1.4873831.

-
- [19] Z. Fan, K.T. Hsiao, S.G. Advani, Experimental investigation of dispersion during flow of multi-walled carbon nanotube/polymer suspension in fibrous porous media, *Carbon N. Y.* 42 (2004) 871–876. doi:10.1016/j.carbon.2004.01.067.
- [20] K. Tsirka, L. Tzounis, A. Avgeropoulos, M. Liebscher, V. Mechtcherine, A.S. Paipetis, Optimal synergy between micro and nano scale: Hierarchical all carbon composite fibers for enhanced stiffness, interfacial shear strength and Raman strain sensing, *Compos. Sci. Technol.* (2018). doi:10.1016/j.compscitech.2018.07.003.
- [21] F. Inam, D.W.Y. Wong, M. Kuwata, T. Peijs, Multiscale Hybrid Micro-Nanocomposites Based on Carbon Nanotubes and Carbon Fibers, *J. Nanomater.* 2010 (2010) 1–12. doi:10.1155/2010/453420.
- [22] Y. Wang, S.K. Raman Pillai, J. Che, M.B. Chan-Park, High Interlaminar Shear Strength Enhancement of Carbon Fiber/Epoxy Composite through Fiber- and Matrix-Anchored Carbon Nanotube Networks, *ACS Appl. Mater. Interfaces.* (2017) acsami.6b13197. doi:10.1021/acsami.6b13197.
- [23] G. Chatzigeorgiou, G.D. Seidel, D.C. Lagoudas, Effective mechanical properties of “fuzzy fiber” composites, *Compos. Part B Eng.* 43 (2012) 2577–2593. doi:10.1016/j.compositesb.2012.03.001.
- [24] M. Kumar, Y. Ando, Chemical vapor deposition of carbon nanotubes: a review on growth mechanism and mass production, *J. Nanosci. Nanotechnol.* 10 (2010) 3739–3758. doi:10.1166/jnn.2010.2939.
- [25] H. O. PIERSON, M.L. LIEBERMAN, THE CHEMICAL VAPOR DEPOSITION OF CARBON ON CARBON FIBERS, *Carbon N. Y.* 13 (1975) 159–166. doi:10.1046/j.1523-1739.1993.07040874.x.
- [26] W.B. Downs, R.T.K. Baker, Novel carbon fiber-carbon filament structures, *Carbon N. Y.* 29 (1991) 1173–1179. doi:10.1016/0008-6223(91)90035-H.
- [27] W. Li, D. Wang, S. Yang, J. Wen, Z. Ren, Controlled growth of carbon nanotubes on graphite foil by chemical vapor deposition, *Chem. Phys. Lett.* 335 (2001) 141–149. doi:10.1016/S0009-2614(01)00032-X.
- [28] E.T. Thostenson, W.Z. Li, D.Z. Wang, Z.F. Ren, T.W. Chou, Carbon nanotube/carbon fiber hybrid multiscale composites, *J. Appl. Phys.* 91 (2002) 6034–

6037. doi:10.1063/1.1466880.
- [29] S.A. Steiner, *Carbon Nanotube Growth on Challenging Substrates: Applications for Carbon-Fiber Composites*, 2004.
- [30] V.P. Veedu, A. Cao, X. Li, K. Ma, C. Soldano, S. Kar, P.M. Ajayan, M.N. Ghasemi-Nejhad, Multifunctional composites using reinforced laminae with carbon-nanotube forests., *Nat. Mater.* 5 (2006) 457–462. doi:10.1038/nmat1650.
- [31] S. Zhu, C.-H. Su, S.L. Lehoczky, I. Muntele, D. Ila, Carbon nanotube growth on carbon fibers, *Diam. Relat. Mater.* 12 (2003) 1825–1828. doi:10.1016/S0925-9635(03)00205-X.
- [32] T.D. Makris, R. Giorgi, N. Lisi, L. Pilloni, E. Salernitano, M.F. De Riccardis, D. Carbone, Carbon Nanotube Growth on PAN- and Pitch-Based Carbon Fibres by HFCVD, *Fullerenes, Nanotub. Carbon Nanostructures.* 13 (2005) 383–392. doi:10.1081/FST-200039380.
- [33] Z.-G. Zhao, L.-J. Ci, H.-M. Cheng, J.-B. Bai, The growth of multi-walled carbon nanotubes with different morphologies on carbon fibers, *Carbon N. Y.* 43 (2005) 663–665. doi:10.1016/j.carbon.2004.10.013.
- [34] Q.J. Gong, H.J. Li, X. Wang, Q.G. Fu, Z. wei Wang, K.Z. Li, In situ catalytic growth of carbon nanotubes on the surface of carbon cloth, *Compos. Sci. Technol.* 67 (2007) 2986–2989. doi:10.1016/j.compscitech.2007.05.002.
- [35] C. Veríssimo, S. a. Moshkalyo, A.C.S. Ramos, J.L. Gonçalves, O.L. Alves, J.W. Swart, Different carbon nanostructured materials obtained in catalytic chemical vapor deposition, *J. Braz. Chem. Soc.* 17 (2006) 1124–1132. doi:10.1590/S0103-50532006000600009.
- [36] A.C. Dupuis, The catalyst in the CCVD of carbon nanotubes-a review, *Prog. Mater. Sci.* 50 (2005) 929–961. doi:10.1016/j.pmatsci.2005.04.003.
- [37] S.P. Sharma, S.C. Lakkad, Morphology study of carbon nanospecies grown on carbon fibers by thermal CVD technique, *Surf. Coatings Technol.* 203 (2009) 1329–1335. doi:10.1016/j.surfcoat.2008.10.043.
- [38] M. Al-Haik, C.C. Luhrs, M.M. Reda Taha, A.K. Roy, L. Dai, J. Phillips, S. Doorn, Hybrid carbon fibers/carbon nanotubes structures for next generation polymeric

- composites, *J. Nanotechnol.* 2010 (2010). doi:10.1155/2010/860178.
- [39] K.J. Kim, J. Kim, W.R. Yu, J.H. Youk, J. Lee, Improved tensile strength of carbon fibers undergoing catalytic growth of carbon nanotubes on their surface, *Carbon N. Y.* 54 (2013) 258–267. doi:10.1016/j.carbon.2012.11.037.
- [40] W. Fan, Y. Wang, C. Wang, J. Chen, Q. Wang, Y. Yuan, F. Niu, High efficient preparation of carbon nanotube-grafted carbon fibers with the improved tensile strength, *Appl. Surf. Sci.* 364 (2016) 539–551. doi:10.1016/j.apsusc.2015.12.189.
- [41] R. Samsur, V.K. Rangari, S. Jeelani, L. Zhang, Z.Y. Cheng, Fabrication of carbon nanotubes grown woven carbon fiber/epoxy composites and their electrical and mechanical properties, *J. Appl. Phys.* 113 (2013). doi:10.1063/1.4808105.
- [42] G. Lee, J.H. Youk, J. Lee, I.H. Sul, W.R. Yu, Low-temperature grafting of carbon nanotubes on carbon fibers using a bimetallic floating catalyst, *Diam. Relat. Mater.* 68 (2016) 118–126. doi:10.1016/j.diamond.2016.06.012.
- [43] K.J. Kim, W.R. Yu, J.H. Youk, J. Lee, Degradation and healing mechanisms of carbon fibers during the catalytic growth of carbon nanotubes on their surfaces, *ACS Appl. Mater. Interfaces.* 4 (2012) 2250–2258. doi:10.1021/am3002499.
- [44] T. Susi, A.G. Nasibulin, H. Jiang, E.I. Kauppinen, CVD synthesis of hierarchical 3D MWCNT/carbon-fiber nanostructures, *J. Nanomater.* 2008 (2008) 37–42. doi:10.1155/2008/425195.
- [45] K. Naito, Y. Tanaka, J.M. Yang, Y. Kagawa, Tensile properties of carbon nanotubes grown on ultrahigh strength polyacrylonitrile- based and ultrahigh modulus pitch-based carbon fibers, *Carbon N. Y.* 46 (2008) 189–195. doi:10.1016/j.carbon.2007.11.001.
- [46] F. An, C. Lu, J. Guo, H. Lu, Preparation of CNT-hybridized carbon fiber by aerosol-assisted chemical vapor deposition, *J. Mater. Sci.* 47 (2012) 3327–3333. doi:10.1007/s10853-011-6172-6.
- [47] H. Qian, A. Bismarck, E.S. Greenhalgh, M.S.P. Shaffer, Carbon nanotube grafted carbon fibres: A study of wetting and fibre fragmentation, *Compos. Part A Appl. Sci. Manuf.* 41 (2010) 1107–1114. doi:10.1016/j.compositesa.2010.04.004.
- [48] P. Lv, Y.Y. Feng, P. Zhang, H.M. Chen, N. Zhao, W. Feng, Increasing the

- interfacial strength in carbon fiber/epoxy composites by controlling the orientation and length of carbon nanotubes grown on the fibers, *Carbon N. Y.* 49 (2011) 4665–4673. doi:10.1016/j.carbon.2011.06.064.
- [49] F. An, C. Lu, Y. Li, J. Guo, X. Lu, H. Lu, S. He, Y. Yang, Preparation and characterization of carbon nanotube-hybridized carbon fiber to reinforce epoxy composite, *Mater. Des.* 33 (2012) 197–202. doi:10.1016/j.matdes.2011.07.027.
- [50] N. Lachman, H. Qian, M. Houllé, J. Amadou, M.S.P. Shaffer, H.D. Wagner, Fracture behavior of carbon nanotube/carbon microfiber hybrid polymer composites, *J. Mater. Sci.* 48 (2013) 5590–5595. doi:10.1007/s10853-013-7353-2.
- [51] T.R.R. Pozegic, I. Hamerton, J.V. V Anguita, W. Tang, P. Balocchi, P. Jenkins, S.R.P.R.P. Silva, Low temperature growth of carbon nanotubes on carbon fibre to create a highly networked fuzzy fibre reinforced composite with superior electrical conductivity, *Carbon N. Y.* 74 (2014) 319–328. doi:10.1016/j.carbon.2014.03.038.
- [52] H. Qian, A. Bismarck, E.S. Greenhalgh, G. Kalinka, M.S.P. Shaffer, Hierarchical composites reinforced with carbon nanotube grafted fibers: The potential assessed at the single fiber level, *Chem. Mater.* 20 (2008) 1862–1869. doi:10.1021/cm702782j.
- [53] R.J. Sager, P.J. Klein, D.C. Lagoudas, Q. Zhang, J. Liu, L. Dai, J.W. Baur, Effect of carbon nanotubes on the interfacial shear strength of T650 carbon fiber in an epoxy matrix, *Compos. Sci. Technol.* 69 (2009) 898–904. doi:10.1016/j.compscitech.2008.12.021.
- [54] Q. Zhang, J. Liu, R. Sager, L. Dai, J. Baur, Hierarchical composites of carbon nanotubes on carbon fiber: Influence of growth condition on fiber tensile properties, *Compos. Sci. Technol.* 69 (2009) 594–601. doi:10.1016/j.compscitech.2008.12.002.
- [55] K. Tanaka, Y. Hinoue, Y. Okumura, T. Katayama, Effect of the cnt growth temperature on the tensile strength of carbon fiber, *WIT Trans. Eng. Sci.* 116 (2017) 273–279. doi:10.2495/MC170281.
- [56] S.A. Steiner, R. Li, B.L. Wardle, Circumventing the mechanochemical origins of strength loss in the synthesis of hierarchical carbon fibers, *ACS Appl. Mater. Interfaces.* 5 (2013) 4892–4903. doi:10.1021/am4006385.
- [57] W. Fan, Y. Wang, C. Wang, J. Chen, Y. Yuan, Communication—Catalyst Study on

- the Large-Scale Preparation of Carbon Nanotube-Grafted Carbon Fibers with High Tensile Strength, *ECS J. Solid State Sci. Technol.* 5 (2016) M35–M37. doi:10.1149/2.0131606jss.
- [58] V. Gonzara de Resende, E.F. Antunes, A. de O. Lobo, D.A.L. Oliveira, V.J. Trava-Airoldi, E.J. Corat, Growth of carbon nanotube forests on carbon fibers with a silicon interface, *Carbon N. Y.* 48 (2010) 3635–3658. doi:10.1557/opl.2012.1338.
- [59] R. Li, N. Lachman, P. Florin, H.D. Wagner, B.L. Wardle, Hierarchical carbon nanotube carbon fiber unidirectional composites with preserved tensile and interfacial properties, *Compos. Sci. Technol.* 117 (2015) 139–145. doi:10.1016/j.compscitech.2015.04.014.
- [60] M. Felisberto, L. Tzounis, L. Sacco, M. Stamm, R. Candal, G.H. Rubiolo, S. Goyanes, Carbon nanotubes grown on carbon fiber yarns by a low temperature CVD method: A significant enhancement of the interfacial adhesion between carbon fiber / epoxy matrix hierarchical composites, *Compos. Commun.* 3 (2017) 33–37. doi:10.1016/j.coco.2017.01.003.
- [61] N. De Greef, A. Magrez, E. Couteau, J.P. Locquet, L. Forró, J.W. Seo, Growth of carbon nanotubes on carbon fibers without strength degradation, *Phys. Status Solidi Basic Res.* 249 (2012) 2420–2423. doi:10.1002/pssb.201200148.
- [62] N. De Greef, L. Zhang, A. Magrez, L. Forró, J.P. Locquet, I. Verpoest, J.W. Seo, Direct growth of carbon nanotubes on carbon fibers: Effect of the CVD parameters on the degradation of mechanical properties of carbon fibers, *Diam. Relat. Mater.* 51 (2015) 39–48. doi:10.1016/j.diamond.2014.11.002.
- [63] D.B. Anthony, H. Qian, A.J. Clancy, E.S. Greenhalgh, A. Bismarck, M.S.P. Shaffer, Applying a potential difference to minimise damage to carbon fibers during carbon nanotube grafting by chemical vapour deposition., *IOP Nanotechnol.* at press (2017) 1–24. doi:https://doi.org/10.1088/1361-6528/aa783f.
- [64] A. Mathur, S. Wadhwa, M. Tweedie, K.S. Hazra, C. Dickinson, S.S. Roy, S.K. Mitra, D.S. Misra, J.A. McLaughlin, A comparative study of the growth, microstructural and electrical properties of multiwall CNTs grown by thermal and microwave plasma enhanced CVD methods, *Phys. E Low-Dimensional Syst.*

- Nanostructures. 44 (2011) 29–36. doi:10.1016/j.physe.2011.06.035.
- [65] C. Wang, Y. Li, L. Tong, Q. Song, K. Li, J. Li, Q. Peng, X. He, R. Wang, W. Jiao, S. Du, The role of grafting force and surface wettability in interfacial enhancement of carbon nanotube/carbon fiber hierarchical composites, *Carbon N. Y.* 69 (2014) 239–246. doi:10.1016/j.carbon.2013.12.020.
- [66] P. Agnihotri, S. Basu, K.K. Kar, Effect of carbon nanotube length and density on the properties of carbon nanotube-coated carbon fiber/polyester composites, *Carbon N. Y.* 49 (2011) 3098–3106. doi:10.1016/j.carbon.2011.03.032.
- [67] C. Su, F. Xue, T. Li, Y. Xin, M. Wang, J. Tang, Y. Ma, Fabrication and multifunctional properties of polyimide based hierarchical composites with in situ grown carbon nanotubes, *RSC Adv.* 7 (2017) 29686–29696. doi:10.1039/c7ra00436b.
- [68] H.S. Bedi, M. Tiwari, P.K. Agnihotri, Quantitative determination of size and properties of interphase in carbon nanotube based multiscale composites, *Carbon N. Y.* 132 (2018) 181–190. doi:10.1016/j.carbon.2018.02.059.
- [69] K. Tsirka, L. Tzounis, A. Avgeropoulos, M. Liebscher, V. Mechtcherine, A.S. Paipetis, Optimal synergy between micro and nano scale: Hierarchical all carbon composite fibers for enhanced stiffness, interfacial shear strength and Raman strain sensing, *Compos. Sci. Technol.* (2018). doi:10.1016/j.compscitech.2018.07.003.
- [70] H. Rong, K.H. Dahmen, H. Garmestani, M. Yu, K.I. Jacob, Comparison of chemical vapor deposition and chemical grafting for improving the mechanical properties of carbon fiber/epoxy composites with multi-wall carbon nanotubes, *J. Mater. Sci.* 48 (2013) 4834–4842. doi:10.1007/s10853-012-7119-2.
- [71] S. Rahmanian, K.S. Thean, A.R. Suraya, M.A. Shazed, M.A. Mohd Salleh, H.M. Yusoff, Carbon and glass hierarchical fibers: Influence of carbon nanotubes on tensile, flexural and impact properties of short fiber reinforced composites, *Mater. Des.* 43 (2013) 10–16. doi:10.1016/j.matdes.2012.06.025.
- [72] M.F. De Riccardis, D. Carbone, T.D. Makris, R. Giorgi, N. Lisi, E. Salernitano, Anchorage of carbon nanotubes grown on carbon fibres, *Carbon N. Y.* 44 (2006) 671–674. doi:10.1016/j.carbon.2005.09.024.

-
- [73] O. Boura, E.K.K. Diamanti, S. a. Grammatikos, D. Gournis, a. S. Paipetis, Carbon nanotube growth on high modulus carbon fibres: Morphological and interfacial characterization, *Surf. Interface Anal.* 45 (2013) 1372–1381. doi:10.1002/sia.5292.
- [74] J. Hu, S. Dong, Q. Feng, M. Zhou, X. Wang, Y. Cheng, Tailoring carbon nanotube/matrix interface to optimize mechanical properties of multiscale composites, *Carbon N. Y.* 69 (2014) 621–625. doi:10.1016/j.carbon.2013.12.005.
- [75] H.S. Bedi, S.S. Padhee, P.K. Agnihotri, Effect of carbon nanotube grafting on the wettability and average mechanical properties of carbon fiber/polymer multiscale composites, *Polym. Compos.* 39 (2018) E1184–E1195. doi:10.1002/pc.24714.
- [76] F. An, C. Lu, J. Guo, S. He, H. Lu, Y. Yang, Preparation of vertically aligned carbon nanotube arrays grown onto carbon fiber fabric and evaluating its wettability on effect of composite, *Appl. Surf. Sci.* 258 (2011) 1069–1076. doi:10.1016/j.apsusc.2011.09.003.
- [77] S.P. Sharma, S.C. Lakkad, Effect of CNTs growth on carbon fibers on the tensile strength of CNTs grown carbon fiber-reinforced polymer matrix composites, *Compos. Part A Appl. Sci. Manuf.* 42 (2011) 8–15. doi:10.1016/j.compositesa.2010.09.008.
- [78] R.B. Mathur, S. Chatterjee, B.P. Singh, Growth of carbon nanotubes on carbon fibre substrates to produce hybrid/phenolic composites with improved mechanical properties, *Compos. Sci. Technol.* 68 (2008) 1608–1615. doi:10.1016/j.compscitech.2008.02.020.
- [79] K.L. Kepple, G.P. Sanborn, P.A. Lacasse, K.M. Gruenberg, W.J. Ready, Improved fracture toughness of carbon fiber composite functionalized with multi walled carbon nanotubes, *Carbon N. Y.* 46 (2008) 2026–2033. doi:10.1016/j.carbon.2008.08.010.
- [80] S. V Lomov, L. Beyers, L. Gorbatikh, I. Verpoest, Permeability and compressibility of CNT/CNF-grafted reinforcements, in: *10th Int. Conf. Flow Process. Compos. Mater.*, 2010: pp. 9–13.
- [81] S. V. Lomov, L. Gorbatikh, Z. Kotanjac, V. Koissin, M. Houille, O. Rochez, M. Karahan, L. Mezzo, I. Verpoest, Compressibility of carbon woven fabrics with

- carbon nanotubes/nanofibres grown on the fibres, *Compos. Sci. Technol.* 71 (2011) 315–325. doi:10.1016/j.compscitech.2010.11.024.
- [82] S. V. Lomov, V. Koissin, M. Karahan, A. Godara, L. Gorbatikh, I. Verpoest, Compressibility of CNT-grafted fibrous reinforcements: A theory, *Int. J. Mater. Form.* 3 (2010) 627–630. doi:10.1007/s12289-010-0848-3.
- [83] S. V. Lomov, L. Gorbatikh, M. Houille, Z. Kotanjac, V. Koissin, K. Vallons, I. Verpoest, Compression resistance and hysteresis of carbon fibre tows with grown carbon nanotubes/nanofibres, *Compos. Sci. Technol.* 71 (2011) 1746–1753. doi:10.1016/j.compscitech.2011.08.007.
- [84] R. Li, E.F. Antunes, A.H. Liotta, C. Parschau, M. Payne, B.L. Wardle, Woven Hierarchical Aerospace Composite Laminates with Aligned Carbon Nanotube Bulk Reinforcement, 57th AIAA/ASCE/AHS/ASC Struct. Struct. Dyn. Mater. Conf. (2016) 1–9.
- [85] E.J. Garcia, B.L. Wardle, A. John Hart, Joining prepreg composite interfaces with aligned carbon nanotubes, *Compos. Part A Appl. Sci. Manuf.* 39 (2008) 1065–1070. doi:10.1016/j.compositesa.2008.03.011.
- [86] R. Guzman de Villoria, P. Hallander, L. Ydrefors, P. Nordin, B.L. Wardle, In-plane strength enhancement of laminated composites via aligned carbon nanotube interlaminar reinforcement, *Compos. Sci. Technol.* 133 (2016) 33–39. doi:10.1016/j.compscitech.2016.07.006.
- [87] X. He, F. Zhang, R. Wang, W. Liu, Preparation of a carbon nanotube/carbon fiber multi-scale reinforcement by grafting multi-walled carbon nanotubes onto the fibers, *Carbon N. Y.* 45 (2007) 2559–2563. doi:10.1016/j.carbon.2007.08.018.
- [88] F.H. Zhang, R.G. Wang, X.D. He, C. Wang, L.N. Ren, Interfacial shearing strength and reinforcing mechanisms of an epoxy composite reinforced using a carbon nanotube/carbon fiber hybrid, *J. Mater. Sci.* 44 (2009) 3574–3577. doi:10.1007/s10853-009-3484-x.
- [89] A. Laachachi, A. Vivet, G. Nouet, B. Ben Doudou, C. Poilane, J. Chen, J.B. Bai, M. Ayachi, A Chemical Method to Graft Carbon Nanotubes onto a Carbon Fiber, *Mater. Lett.* 62 (2008) 394–397. doi:10.1016/j.matlet.2007.05.044.

-
- [90] A. Vivet, B. Ben Doudou, C. Poilâne, J. Chen, M. Ayachi, A method for the chemical anchoring of carbon nanotubes onto carbon fibre and its impact on the strength of carbon fibre composites, *J. Mater. Sci.* 46 (2010) 1322–1327. doi:10.1007/s10853-010-4919-0.
- [91] M. Li, Y. Gu, Y. Liu, Y. Li, Z. Zhang, Interfacial improvement of carbon fiber/epoxy composites using a simple process for depositing commercially functionalized carbon nanotubes on the fibers, *Carbon N. Y.* 52 (2013) 109–121. doi:10.1016/j.carbon.2012.09.011.
- [92] K. Tsirka, G. Foteinidis, K. Dimos, L. Tzounis, D. Gournis, A.S. Paipetis, Production of hierarchical all graphitic structures: A systematic study, *J. Colloid Interface Sci.* 487 (2017) 444–457. doi:10.1016/j.jcis.2016.10.075.
- [93] L. Lavagna, D. Massella, M. Pavese, Preparation of hierarchical material by chemical grafting of carbon nanotubes onto carbon fibers, *Diam. Relat. Mater.* 80 (2017) 118–124. doi:10.1016/j.diamond.2017.10.013.
- [94] Y. Li, Y. Li, Y. Ding, Q. Peng, C. Wang, R. Wang, T. Sritharan, X. He, S. Du, Tuning the interfacial property of hierarchical composites by changing the grafting density of carbon nanotube using 1,3-propodiamine, *Compos. Sci. Technol.* 85 (2013) 36–42. doi:10.1016/j.compscitech.2013.05.016.
- [95] M. Zhao, L. Meng, L. Ma, L. Ma, X. Yang, Y. Huang, J.E. Ryu, A. Shankar, T. Li, C. Yan, Z. Guo, Layer-by-layer grafting CNTs onto carbon fibers surface for enhancing the interfacial properties of epoxy resin composites, *Compos. Sci. Technol.* 154 (2018) 28–36. doi:10.1016/j.compscitech.2017.11.002.
- [96] L. Mei, X. He, Y. Li, R. Wang, C. Wang, Q. Peng, Grafting carbon nanotubes onto carbon fiber by use of dendrimers, *Mater. Lett.* 64 (2010) 2505–2508. doi:10.1016/j.matlet.2010.07.056.
- [97] L. Mei, Y. Li, R. Wang, C. Wang, Q. Peng, X. He, Multiscale carbon nanotube-carbon fiber reinforcement for advanced epoxy composites with high interfacial strength, *Polym. Polym. Compos.* 19 (2011) 107–112. doi:10.1021/la062743p.
- [98] Q. Peng, X. He, Y. Li, C. Wang, R. Wang, P. Hu, Y. Yan, T. Sritharan, Chemically and uniformly grafting carbon nanotubes onto carbon fibers by poly(amidoamine)

- for enhancing interfacial strength in carbon fiber composites, *J. Mater. Chem.* 22 (2012) 5928–5931. doi:10.1039/c2jm16723a.
- [99] B. Chen, X. Li, J. Yang, H. Huang, W. Peng, C. Li, Z. Zhang, Enhancement of the tribological properties of carbon fiber/epoxy composite by grafting carbon nanotubes onto fibers, *RSC Adv.* 6 (2016) 49387–49394. doi:10.1039/C6RA05081F.
- [100] Z. Wu, L. Meng, L. Liu, Z. Jiang, L. Xing, D. Jiang, Y. Huang, Chemically grafting carbon nanotubes onto carbon fibers by poly(acryloyl chloride) for enhancing interfacial strength in carbon fiber/unsaturated polyester composites, *Fibers Polym.* 15 (2014) 659–663. doi:10.1007/s12221-014-0659-0.
- [101] Y. Lv, C. Peng, Chemically grafting carbon nanotubes onto carbon fibers for enhancing interfacial strength in carbon fiber/HDPE composites, *Surf. Interface Anal.* 50 (2018) 552–557. doi:10.1002/sia.6425.
- [102] G. Wu, L. Ma, L. Liu, Y. Wang, F. Xie, Z. Zhong, M. Zhao, B. Jiang, Y. Huang, Interfacially reinforced methylphenylsilicone resin composites by chemically grafting multiwall carbon nanotubes onto carbon fibers, *Compos. Part B Eng.* 82 (2015) 50–58. doi:10.1016/j.compositesb.2015.08.012.
- [103] H. Rong, K. Han, S. Li, Y. Tian, Muhuoyu, A novel method to graft carbon nanotube onto carbon fiber by the use of a binder, *J. Appl. Polym. Sci.* 127 (2012) 2033–2037. doi:10.1002/app.37699.
- [104] F. Zhao, Y. Huang, Preparation and properties of polyhedral oligomeric silsesquioxane and carbon nanotube grafted carbon fiber hierarchical reinforcing structure, *J. Mater. Chem.* 21 (2011) 2867. doi:10.1039/c0jm03919e.
- [105] F. Zhao, Y. Huang, L. Liu, Y. Bai, L. Xu, Formation of a carbon fiber/polyhedral oligomeric silsesquioxane/carbon nanotube hybrid reinforcement and its effect on the interfacial properties of carbon fiber/epoxy composites, *Carbon N. Y.* 49 (2011) 2624–2632. doi:10.1016/j.carbon.2011.02.026.
- [106] R.L. Zhang, C.G. Wang, L. Liu, H.Z. Cui, B. Gao, Polyhedral oligomeric silsesquioxanes/carbon nanotube/carbon fiber multiscale composite: Influence of a novel hierarchical reinforcement on the interfacial properties, *Appl. Surf. Sci.* 353

- (2015) 224–231. doi:10.1016/j.apsusc.2015.06.156.
- [107] T. Kamae, L.T. Drzal, Carbon fiber/epoxy composite property enhancement through incorporation of carbon nanotubes at the fiber-matrix interphase - Part I: The development of carbon nanotube coated carbon fibers and the evaluation of their adhesion, *Compos. Part A Appl. Sci. Manuf.* 43 (2012) 1569–1577. doi:10.1016/j.compositesa.2012.02.016.
- [108] Y.T. Liu, G.P. Wu, C.X. Lu, Grafting of carbon nanotubes onto carbon fiber surfaces by step-wise reduction of in-situ generated diazonium salts for enhancing carbon/epoxy interfaces, *Mater. Lett.* 134 (2014) 75–79. doi:10.1016/j.matlet.2014.07.053.
- [109] Y. Wang, L. Meng, L. Fan, G. Wu, L. Ma, Y. Huang, Preparation and properties of carbon nanotube/carbon fiber hybrid reinforcement by a two-step aryl diazonium reaction, *RSC Adv.* 5 (2015) 44492–44498. doi:10.1039/C5RA04117A.
- [110] X. Chen, H. Xu, D. Liu, C. Yan, Y. Zhu, A novel and facile fabrication of polyphosphazene nanotube/carbon fiber multi-scale hybrid reinforcement and its enhancing effect on the interfacial properties of epoxy composites, *Appl. Surf. Sci.* 169 (2018) 34–44. doi:10.1016/j.apsusc.2017.03.104.
- [111] L. Dong, Y. Li, L. Wang, Z. Wan, F. Hou, J. Liu, Combination effect of physical drying with chemical characteristic of carbon nanotubes on through-thickness properties of carbon fiber/epoxy composites, *J. Mater. Sci.* 49 (2014) 4979–4988. doi:10.1007/s10853-014-8200-9.
- [112] Y. Deng, M.S. Islam, L. Tong, Effects of grafting strength and density on interfacial shear strength of carbon nanotube grafted carbon fibre reinforced composites, *Compos. Sci. Technol.* 168 (2018) 195–202. doi:10.1016/j.compscitech.2018.09.025.
- [113] M.S. Islam, Y. Deng, L. Tong, S.N. Faisal, A.K. Roy, A.I. Minett, V.G. Gomes, Grafting carbon nanotubes directly onto carbon fibers for superior mechanical stability: Towards next generation aerospace composites and energy storage applications, *Carbon N. Y.* 96 (2016) 701–710. doi:10.1016/j.carbon.2015.10.002.
- [114] X. He, C. Wang, L. Tong, R. Wang, A. Cao, Q. Peng, S. Moody, Y. Li, Direct

- measurement of grafting strength between an individual carbon nanotube and a carbon fiber, *Carbon N. Y.* 50 (2012) 3782–3788. doi:10.1016/j.carbon.2012.03.053.
- [115] A.R. Boccaccini, J. Cho, J.A. Roether, B.J.C. Thomas, E. Jane Minay, M.S.P. Shaffer, Electrophoretic deposition of carbon nanotubes, *Carbon N. Y.* 44 (2006) 3149–3160. doi:10.1016/j.carbon.2006.06.021.
- [116] E. Bekyarova, E.T. Thostenson, A. Yu, H. Kim, J. Gao, J. Tang, H.T. Hahn, T.-W. Chou, M.E. Itkis, R.C. Haddon, Multiscale carbon nanotube-carbon fiber reinforcement for advanced epoxy composites, *Langmuir.* 23 (2007) 3970–4. doi:10.1021/la062743p.
- [117] J. Guo, C. Lu, Continuous preparation of multiscale reinforcement by electrophoretic deposition of carbon nanotubes onto carbon fiber tows, *Carbon N. Y.* 50 (2012) 3101–3103. doi:10.1016/j.carbon.2012.02.044.
- [118] J. Guo, C. Lu, F. An, Effect of electrophoretically deposited carbon nanotubes on the interface of carbon fiber reinforced epoxy composite, *J. Mater. Sci.* 47 (2012) 2831–2836. doi:10.1007/s10853-011-6112-5.
- [119] J. Guo, C. Lu, F. An, S. He, Preparation and characterization of carbon nanotubes/carbon fiber hybrid material by ultrasonically assisted electrophoretic deposition, *Mater. Lett.* 66 (2012) 382–384. doi:10.1016/j.matlet.2011.09.022.
- [120] Q. An, A.N. Rider, E.T. Thostenson, Electrophoretic deposition of carbon nanotubes onto carbon-fiber fabric for production of carbon/epoxy composites with improved mechanical properties, *Carbon N. Y.* 50 (2012) 4130–4143. doi:10.1016/j.carbon.2012.04.061.
- [121] J.J. Jiang, F. Liu, C. Deng, L.C. Fang, D.J. Li, Influence of deposited CNTs on the surface of carbon fiber by ultrasonically assisted electrophoretic deposition, *IOP Conf. Ser. Mater. Sci. Eng.* 87 (2015) 012103–012107. doi:10.1088/1757-899X/87/1/012103.
- [122] S. Zhang, W.B. Liu, L.F. Hao, W.C. Jiao, F. Yang, R.G. Wang, Preparation of carbon nanotube/carbon fiber hybrid fiber by combining electrophoretic deposition and sizing process for enhancing interfacial strength in carbon fiber composites,

- Compos. Sci. Technol. 88 (2013) 120–125.
- [123] E. Moaseri, M. Karimi, M. Maghrebi, M. Baniadam, Fabrication of multi-walled carbon nanotube-carbon fiber hybrid material via electrophoretic deposition followed by pyrolysis process, *Compos. Part A Appl. Sci. Manuf.* 60 (2014) 8–14. doi:10.1016/j.compositesa.2014.01.009.
- [124] E. Moaseri, M. Karimi, M. Maghrebi, M. Baniadam, Two-fold enhancement in tensile strength of carbon nanotube-carbon fiber hybrid epoxy composites through combination of electrophoretic deposition and alternating electric field, *Int. J. Solids Struct.* 51 (2014) 774–785. doi:10.1016/j.ijsolstr.2013.11.007.
- [125] A. Battisti, D. Esqué-de los Ojos, R. Ghisleni, A.J. Brunner, Single fiber push-out characterization of interfacial properties of hierarchical CNT-carbon fiber composites prepared by electrophoretic deposition, *Compos. Sci. Technol.* 95 (2014) 121–127. doi:10.1016/j.compscitech.2014.02.017.
- [126] H. Mei, S. Zhang, H. Chen, H. Zhou, X. Zhai, L. Cheng, Interfacial modification and enhancement of toughening mechanisms in epoxy composites with CNTs grafted on carbon fibers, *Compos. Sci. Technol.* 134 (2016) 89–95. doi:10.1016/j.compscitech.2016.08.010.
- [127] H. Mei, J. Xia, D. Zhang, H. Li, Q. Bai, L. Cheng, Mechanical properties of carbon fiber reinforced bisphenol A dicyanate ester composites modified with multiwalled carbon nanotubes, *J. Appl. Polym. Sci.* 134 (2017) 45100. doi:10.1002/app.45100.
- [128] E. Moaseri, M. Karimi, M. Baniadam, M. Maghrebi, Enhancement in mechanical properties of multi-walled carbon nanotube–carbon fiber hybrid epoxy composite: effect of electrostatic repulsion, *Appl. Phys. A Mater. Sci. Process.* 122 (2016) 1–8. doi:10.1007/s00339-016-9600-2.
- [129] E. Moaseri, M. Karimi, B. Bazubandi, M. Baniadam, M. Maghrebi, Remarkable enhancements in mechanical properties of epoxy composites through double reinforcing structure: Integrated structure of carbon fiber-carbon nanotube instead of conventional reinforcing methods, *Polym. Compos.* 39 (2017) E1099–E1108. doi:10.1002/pc.24572.
- [130] X. Sui, J. Shi, H. Yao, Z. Xu, L. Chen, X. Li, M. Ma, L. Kuang, H. Fu, H. Deng,

- Interfacial and fatigue-resistant synergetic enhancement of carbon fiber/epoxy hierarchical composites via an electrophoresis deposited carbon nanotube-toughened transition layer, *Compos. Part A Appl. Sci. Manuf.* 92 (2017) 134–144. doi:10.1016/j.compositesa.2016.11.004.
- [131] H. Xue, N. A, Y. Xiao, J. Che, Preparation of hierarchical carbon nanotube-carbon fiber composites with coordination enhancement, *Adv. Polym. Technol.* (2017) 1–9. doi:10.1002/adv.21930.
- [132] W. Lee, S.B. Lee, O. Choi, J.W. Yi, M.K. Um, J.H. Byun, E.T. Thostenson, T.W. Chou, Formicary-like carbon nanotube/copper hybrid nanostructures for carbon fiber-reinforced composites by electrophoretic deposition, *J. Mater. Sci.* 46 (2011) 2359–2364. doi:10.1007/s10853-010-5082-3.
- [133] F. Yan, L. Liu, M. Li, M. Zhang, L. Xiao, Y. Ao, Preparation of carbon nanotube/copper/carbon fiber hierarchical composites by electrophoretic deposition for enhanced thermal conductivity and interfacial properties, *J. Mater. Sci.* 53 (2018) 8108–8119. doi:10.1007/s10853-018-2115-9.
- [134] K. Almuhammadi, M. Alfano, Y. Yang, G. Lubineau, Analysis of interlaminar fracture toughness and damage mechanisms in composite laminates reinforced with sprayed multi-walled carbon nanotubes, *Mater. Des.* 53 (2014) 921–927. doi:10.1016/j.matdes.2013.07.081.
- [135] H. Zhang, Y. Liu, M. Kuwata, E. Bilotti, T. Peijs, Improved fracture toughness and integrated damage sensing capability by spray coated CNTs on carbon fibre prepreg, *Compos. Part A Appl. Sci. Manuf.* (2015). doi:10.1016/j.compositesa.2014.11.029.
- [136] G. Lee, K.D. Ko, Y.C. Yu, J. Lee, W.-R. Yu, J.H. Youk, A facile method for preparing CNT-grafted carbon fibers and improved tensile strength of their composites, *Compos. Part A Appl. Sci. Manuf.* 69 (2015) 132–138. doi:10.1016/j.compositesa.2014.11.015.
- [137] M.S. Chaudhry, A. Czekanski, Z.H. Zhu, Characterization of carbon nanotube enhanced interlaminar fracture toughness of woven carbon fiber reinforced polymer composites, *Int. J. Mech. Sci.* 131–132 (2017) 480–489. doi:10.1016/j.ijmecsci.2017.06.016.

-
- [138] H. Yao, G. Zhou, W. Wang, M. Peng, Effect of polymer-grafted carbon nanofibers and nanotubes on the interlaminar shear strength and flexural strength of carbon fiber/epoxy multiscale composites, *Compos. Struct.* 195 (2018) 288–296. doi:10.1016/j.compstruct.2018.04.082.
- [139] Q. Li, J.S. Church, M. Naebe, B.L. Fox, A systematic investigation into a novel method for preparing carbon fibre – carbon nanotube hybrid structures, *Compos. Part A.* 90 (2016) 174–185. doi:10.1016/j.compositesa.2016.05.004.
- [140] Q. Li, J.S. Church, M. Naebe, B.L. Fox, Interfacial characterization and reinforcing mechanism of novel carbon nanotube – Carbon fibre hybrid composites, *Carbon N. Y.* 109 (2016) 74–86. doi:10.1016/j.carbon.2016.07.058.
- [141] X. Du, H.-Y. Liu, C. Zhou, S. Moody, Y.-W. Mai, On the flame synthesis of carbon nanotubes grafted onto carbon fibers and the bonding force between them, (2012). doi:10.1016/j.carbon.2012.01.003.
- [142] C. Guignier, M.-A. Bueno, B. Camillieri, M. Tournalias, B. Durand, Tribological behaviour and wear of carbon nanotubes grafted on carbon fibres, *Compos. Part A Appl. Sci. Manuf.* 71 (2015) 168–175. doi:10.1016/j.compositesa.2015.01.013.
- [143] C. Guignier, M.A. Bueno, B. Camillieri, T. Le Huu, H. Oulanti, B. Durand, Tribological behaviour and adhesion of carbon nanotubes grafted on carbon fibres, *Tribol. Int.* 100 (2016) 104–115. doi:10.1016/j.triboint.2015.12.007.
- [144] C. Guignier, M.A. Bueno, B. Camillieri, B. Durand, Influence of composite processing on the properties of CNT grown on carbon surfaces, *Appl. Surf. Sci.* 428 (2018) 835–843. doi:10.1016/j.apsusc.2017.09.221.
- [145] B. Yu, Z. Jiang, X.Z. Tang, C.Y. Yue, J. Yang, Enhanced interphase between epoxy matrix and carbon fiber with carbon nanotube-modified silane coating, *Compos. Sci. Technol.* 99 (2014) 131–140. doi:10.1016/j.compscitech.2014.05.021.
- [146] H. Yao, X. Sui, Z. Zhao, Z. Xu, L. Chen, H. Deng, Y. Liu, X. Qian, Optimization of interfacial microstructure and mechanical properties of carbon fiber/epoxy composites via carbon nanotube sizing, *Appl. Surf. Sci.* 347 (2015) 583–590. doi:http://dx.doi.org/10.1016/j.apsusc.2015.04.146.
- [147] G. Carley, V. Geraldo, S. de Oliveira, A.F. Avila, Nano-engineered composites:

- interlayer carbon nanotubes effect, *Mater. Res.* 16 (2013) 628–634. doi:10.1590/S1516-14392013005000034.
- [148] M. Tehrani, A.Y. Boroujeni, C. Luhrs, J. Phillips, M.S. Al-Haik, Hybrid composites based on carbon fiber/carbon nanofilament reinforcement, *Materials (Basel)*. 7 (2014) 4182–4195. doi:10.3390/ma7064182.
- [149] L. Gorbatikh, S. V. Lomov, I. Verpoest, Nano-engineered composites: A multiscale approach for adding toughness to fibre reinforced composites, *Procedia Eng.* 10 (2011) 3252–3258. doi:10.1016/j.proeng.2011.04.537.
- [150] Z. Zhao, K. Teng, N. Li, X. Li, Z. Xu, L. Chen, J. Niu, H. Fu, L. Zhao, Y. Liu, Mechanical, thermal and interfacial performances of carbon fiber reinforced composites flavored by carbon nanotube in matrix/interface, *Compos. Struct.* 159 (2017) 761–772. doi:10.1016/j.compstruct.2016.10.022.
- [151] F.S. Awan, M.A. Fakhar, L.A. Khan, U. Zaheer, A.F. Khan, T. Subhani, F. Abdul, Interfacial mechanical properties of carbon nanotube-deposited carbon fiber epoxy matrix hierarchical composites, *Compos. Interfaces*. 25 (2018) 681–699. doi:10.1080/09276440.2018.1439620.
- [152] K. Naito, Effect of Hybrid Surface Modifications on Tensile Properties of Polyacrylonitrile- and Pitch-Based Carbon Fibers, *J. Mater. Eng. Perform.* 25 (2016) 2074–2083. doi:10.1007/s11665-016-2028-1.
- [153] V. Lutz, J. Duchet-Rumeau, N. Godin, F. Smail, F. Lortie, J.F. Gérard, Ex-PAN carbon fibers vs carbon nanotubes fibers: From conventional epoxy based composites to multiscale composites, *Eur. Polym. J.* 106 (2018) 9–18. doi:10.1016/j.eurpolymj.2018.06.023.
- [154] L. Qu, Y. Zhao, L. Dai, Carbon microfibers sheathed with aligned carbon nanotubes: Towards multidimensional, multicomponent, and multifunctional nanomaterials, *Small*. 2 (2006) 1052–1059. doi:10.1002/sml.200600097.
- [155] S.T. Patton, Q. Zhang, L. Qu, L. Dai, A.A. Voevodin, J. Baur, Electromechanical characterization of carbon nanotubes grown on carbon fiber, *J. Appl. Phys.* 106 (2009). doi:10.1063/1.3253747.
- [156] K.K. Kar, Synthesis of Carbon Nanotubes on the Surface of Carbon Fiber / fabric by

- Catalytic Chemical Vapor Deposition and Their Characterization, Fullerenes , Nanotub. Carbon Nanostructures. (2009) 209–229.
- [157] K.Z. Li, Q. Song, Q. Qiang, C. Ren, Improving the oxidation resistance of carbon/carbon composites at low temperature by controlling the grafting morphology of carbon nanotubes on carbon fibres, *Corros. Sci.* 60 (2012) 314–317. doi:10.1016/j.corsci.2012.03.031.
- [158] H. Chen, Y. Li, Y. Feng, P. Lv, P. Zhang, W. Feng, Electrodeposition of carbon nanotube/carbon fabric composite using cetyltrimethylammonium bromide for high performance capacitor, *Electrochim. Acta.* 60 (2012) 449–455. doi:10.1016/j.electacta.2011.11.101.
- [159] H. Lu, W. Yin, W.M. Huang, J. Leng, Self-assembled carboxylic acid-functionalized carbon nanotubes grafting onto carbon fiber for significantly improving electrical actuation of shape memory polymers, *RSC Adv.* 3 (2013) 21484–21488. doi:10.1039/c3ra42704h.
- [160] T.R. Pozegic, J. V. Anguita, I. Hamerton, K.D.G.I. Jayawardena, J.-S. Chen, V. Stolojan, P. Balocchi, R. Walsh, S.R.P. Silva, Multi-Functional Carbon Fibre Composites using Carbon Nanotubes as an Alternative to Polymer Sizing, *Sci. Rep.* 6 (2016) 37334. doi:10.1038/srep37334.
- [161] M. Fogel, P. Parlevliet, P. Olivier, É. Dantras, Manufacturing of conductive structural composites through spraying of CNTs/epoxy dispersions on dry carbon fiber plies, *Compos. Part A Appl. Sci. Manuf.* 100 (2017) 40–47. doi:10.1016/j.compositesa.2017.04.020.
- [162] M. Zou, W. Zhao, H. Wu, H. Zhang, W. Xu, L. Yang, S. Wu, Y. Wang, Y. Chen, L. Xu, A. Cao, Single Carbon Fibers with a Macroscopic-Thickness, 3D Highly Porous Carbon Nanotube Coating, *Adv. Mater.* 1704419 (2018) 1704419. doi:10.1002/adma.201704419.
- [163] Z. Wu, C.U. Pittman, S.D. Gardner, Nitric acid oxidation of carbon fibers and the effects of subsequent treatment in refluxing aqueous NaOH, *Carbon N. Y.* 33 (1995) 597–605. doi:10.1016/0008-6223(95)00145-4.
- [164] G. Zhang, S. Sun, D. Yang, J.-P. Dodelet, E. Sacher, The surface analytical

- characterization of carbon fibers functionalized by H₂SO₄/HNO₃ treatment, *Carbon N. Y.* 46 (2008) 196–205. doi:10.1016/j.carbon.2007.11.002.
- [165] S.Y. Jin, R.J. Young, S.J. Eichhorn, Hybrid carbon fibre-carbon nanotube composite interfaces, *Compos. Sci. Technol.* 95 (2014) 114–120. doi:10.1016/j.compscitech.2014.02.015.
- [166] M. Sharma, S. Gao, E. Mäder, H. Sharma, L.Y. Wei, J. Bijwe, Carbon fiber surfaces and composite interphases, *Compos. Sci. Technol.* 102 (2014) 35–50. doi:10.1016/j.compscitech.2014.07.005.
- [167] Y.-C. Chiang, C.-C. Lee, C.-Y. Lee, Surface characterization of acid-oxidized multi-walled carbon nanotubes, *Toxicol. Environ. Chem.* 91 (2009) 1413–1427. doi:10.1080/02772240902751647.
- [168] I. V. Pavlidis, T. Tsoufis, A. Enotiadis, D. Gournis, H. Stamatis, Functionalized multi-wall carbon nanotubes for lipase immobilization, *Adv. Eng. Mater.* 12 (2010) 179–183. doi:10.1002/adem.200980021.
- [169] L. Tzounis, M. Kirsten, F. Simon, E. Mäder, M. Stamm, The interphase microstructure and electrical properties of glass fibers covalently and non-covalently bonded with multiwall carbon nanotubes, *Carbon N. Y.* 73 (2014) 310–324. doi:10.1016/j.carbon.2014.02.069.
- [170] Y.T. Shieh, G.L. Liu, H.H. Wu, C.C. Lee, Effects of polarity and pH on the solubility of acid-treated carbon nanotubes in different media, *Carbon N. Y.* 45 (2007) 1880–1890. doi:10.1016/j.carbon.2007.04.028.
- [171] K. Balasubramanian, M. Burghard, Chemically functionalized carbon nanotubes, *Small.* 1 (2005) 180–192. doi:10.1002/sml.200400118.
- [172] A.G. Osorio, I.C.L. Silveira, V.L. Bueno, C.P. Bergmann, H₂SO₄/HNO₃/HCl—Functionalization and its effect on dispersion of carbon nanotubes in aqueous media, *Appl. Surf. Sci.* 255 (2008) 2485–2489. doi:10.1016/j.apsusc.2008.07.144.
- [173] M. Deborah, A. Jawahar, T. Mathavan, M.K. Dhas, A.M. Franklin, Preparation and Characterization of Oxidized Multi-Walled Carbon Nanotubes and Glycine Functionalized Multi-Walled Carbon Nanotubes, 4046 (2015) 37–41. doi:10.1080/1536383X.2014.899212.

-
- [174] Y.C. Chiang, W.H. Lin, Y.C. Chang, The influence of treatment duration on multi-walled carbon nanotubes functionalized by H₂SO₄/HNO₃ oxidation, *Appl. Surf. Sci.* 257 (2011) 2401–2410. doi:10.1016/j.apsusc.2010.09.110.
- [175] D.G. Bekas, A.S. Paipetis, Study of the effect of damage on the electrical impedance of carbon nanotube reinforced epoxy nanocomposites, *J. Sensors*. 2015 (2015) 1–7. doi:10.1155/2015/805303.
- [176] A. Policicchio, T. Caruso, G. Chiarello, E. Colavita, V. Formoso, R.G. Agostino, T. Tsoufis, D. Gournis, S. La Rosa, Electronic, chemical and structural characterization of CNTs grown by acetylene decomposition over MgO supported Fe-Co bimetallic catalysts, *Surf. Sci.* 601 (2007) 2823–2827. doi:10.1016/j.susc.2006.12.051.
- [177] M. Guigon, A. Oberlin, G. Desarmot, Microtexture and structure of some high tensile strength, PAN-base carbon fibres, *Fibre Sci. Technol.* 20 (1984) 55–72. doi:10.1016/0015-0568(84)90057-5.
- [178] R. Fuge, M. Liebscher, C. Schröfl, S. Oswald, A. Leonhardt, B. Büchner, V. Mechtcherine, Fragmentation characteristics of undoped and nitrogen-doped multiwalled carbon nanotubes in aqueous dispersion in dependence on the ultrasonication parameters, *Diam. Relat. Mater.* 66 (2016) 126–134. doi:10.1016/j.diamond.2016.03.026.
- [179] L. Lavagna, D. Massella, M.F. Pantano, F. Bosia, N.M. Pugno, M. Pavese, Grafting carbon nanotubes onto carbon fibres doubles their effective strength and the toughness of the composite, *Compos. Sci. Technol.* (2018). doi:10.1016/j.compscitech.2018.03.015.
- [180] X.Z. Liao, A. Serquis, Q.X. Jia, D.E. Peterson, Y.T. Zhu, H.F. Xu, Effect of catalyst composition on carbon nanotube growth, *Appl. Phys. Lett.* 82 (2003) 2694–2696. doi:10.1063/1.1569655.
- [181] Z. Wang, M.D. Shirley, S.T. Meikle, R.L.D. Whitby, S. V. Mikhalovsky, The surface acidity of acid oxidised multi-walled carbon nanotubes and the influence of in-situ generated fulvic acids on their stability in aqueous dispersions, *Carbon N. Y.* 47 (2009) 73–79. doi:10.1016/j.carbon.2008.09.038.
- [182] S. Osswald, M. Havel, Y. Gogotsi, Monitoring oxidation of multiwalled carbon

- nanotubes by Raman spectroscopy, *J. Raman Spectrosc.* 38 (2007) 728–736. doi:10.1002/jrs.
- [183] G. Socrates, *Infrared and Raman characteristic group frequencies*, 2004. doi:10.1002/jrs.1238.
- [184] R. Kumar, G. Sahu, S.K. Saxena, H.M. Rai, P.R. Sagdeo, Qualitative Evolution of Asymmetric Raman Line-Shape for NanoStructures, *Silicon*. (2014) 1–5. doi:10.1007/s12633-013-9176-9.
- [185] M.S. Dresselhaus, G. Dresselhaus, R. Saito, A. Jorio, Raman spectroscopy of carbon nanotubes, *Phys. Rep.* 409 (2005) 47–99. doi:10.1016/j.physrep.2004.10.006.
- [186] S. Costa, Borowiak-Palen E, Raman Study on Doped Multiwalled Carbon Nanotubes, *Acta Phys. Pol. A.* 116 (2009) 32–35.
- [187] V. Datsyuk, M. Kalyva, K. Papagelis, J. Parthenios, D. Tasis, A. Siokou, I. Kallitsis, C. Galiotis, Chemical oxidation of multiwalled carbon nanotubes, *Carbon N. Y.* 46 (2008) 833–840. doi:10.1016/j.carbon.2008.02.012.
- [188] N. Liaros, J. Tucek, K. Dimos, A. Bakandritsos, K.S. Andrikopoulos, D. Gournis, R. Zboril, S. Couris, The effect of the degree of oxidation on broadband nonlinear absorption and ferromagnetic ordering in graphene oxide, *Nanoscale*. 8 (2016) 2908–2917. doi:10.1039/C5NR07832F.
- [189] D.G. Bekas, G. Gkikas, G.M. Maistros, A.S. Paipetis, On the use of dielectric spectroscopy for the real time assessment of the dispersion of carbon nanotubes in epoxy, *RSC Adv.* 6 (2016) 78838–78845. doi:10.1039/C6RA15594D.
- [190] D.G. Bekas, A.S. Paipetis, Damage monitoring in nanoenhanced composites using impedance spectroscopy, *Compos. Sci. Technol.* 134 (2016) 96–105. doi:10.1016/j.compscitech.2016.08.013.
- [191] K.S. Park, J.R. Youn, Dispersion and aspect ratio of carbon nanotubes in aqueous suspension and their relationship with electrical resistivity of carbon nanotube filled polymer composites, *Carbon N. Y.* 50 (2012) 2322–2330. doi:10.1016/j.carbon.2012.01.052.
- [192] K.L. Lu, R.M. Lago, Y.K. Chen, M.L.H. Green, P.J.F. Harris, S.C. Tsang, Mechanical damage of carbon nanotubes by ultrasound, *Carbon N. Y.* 34 (1996)

- 814–816. doi:10.1016/0008-6223(96)89470-X.
- [193] J. Li, P.C. Ma, W.S. Chow, C.K. To, B.Z. Tang, J.K. Kim, Correlations between percolation threshold, dispersion state, and aspect ratio of carbon nanotubes, *Adv. Funct. Mater.* 17 (2007) 3207–3215. doi:10.1002/adfm.200700065.
- [194] G. Gkikas, C. Saganas, S.A. Grammatikos, G.M. Maistros, N.-M. Barkoula, A.S. Paipetis, Dispersion monitoring of carbon nanotube modified epoxy systems, in: *Sensors Smart Struct. Technol. Civil, Mech. Aerosp. Syst.*, 2012: p. 83454R–1–8. doi:10.1117/12.915486.
- [195] S.L. Gao, R.C. Zhuang, J. Zhang, J.W. Liu, E. Mäder, Glass fibers with carbon nanotube networks as multifunctional sensors, *Adv. Funct. Mater.* 20 (2010) 1885–1893. doi:10.1002/adfm.201000283.
- [196] L. Tzounis, M. Liebscher, S. Petinakis, A.S. Paipetis, E. Mäder, M. Stamm, CNT-grafted glass fibers as a smart tool for the epoxy cure monitoring, UV-sensing and thermal energy harvesting in model composites, *RSC Adv.* (2016) 2–4. doi:10.1039/C6RA09800B.
- [197] Q. Zhao, H.D. Wagner, Raman spectroscopy of carbon-nanotube-based composites, *Phil. Trans. R. Soc. Lond.* 362 (2004) 2407–2424. doi:10.1098/rsta.2004.1447.
- [198] A.S. Paipetis, Stress induced changes in the Raman Spectrum of Carbon Nanostructures and Their Composites, in: A. Paipetis, V. Kostopoulos (Eds.), *Solid Mech. Its Appl.*, Springer Netherlands, 2013: pp. 185–217. doi:10.1007/978-94-007-4246-8.
- [199] K. Carron, R. Cox, Qualitative analysis and the answer box: A perspective on portable Raman spectroscopy, *Anal. Chem.* 82 (2010) 3419–3425. doi:10.1021/ac901951b.
- [200] A. Paipetis, C. Vlattas, C. Galioitis, Remote Laser Raman Microscopy (ReRaM). 1- Design and Testing of a Confocal Microprobe, *J. Raman. Spectrosc.* 27 (1996) 519–526. doi:10.1002/(SICI)1097-4555(199607)27:7<519::AID-JRS994>3.0.CO;2-4.
- [201] L. Liu, P.C. Ma, M. Xu, S.U. Khan, J.K. Kim, Strain-sensitive Raman spectroscopy and electrical resistance of carbon nanotube-coated glass fibre sensors, *Compos. Sci. Technol.* 72 (2012) 1548–1555. doi:10.1016/j.compscitech.2012.06.002.

- [202] ASTM C 1557, Standard Test Method for Tensile Strength and Young's Modulus of Fibers, Astm. (2014) 1–10. doi:10.1520/C1557-14.2.
- [203] S. van der Zwaag, The Concept of Filament Strength and Weibull Modulus, *J. Test. Eval.* 17 (1989) 292–298. doi:10.1520/JTE11131J.
- [204] F. Tuinstra, L. Koenig, Raman Spectrum of Graphite, *J. Chem. Phys.* 53 (1970) 1126–1130. doi:10.1063/1.1674108.
- [205] S. Santangelo, G. Messina, G. Faggio, M. Lanza, C. Milone, Evaluation of crystalline perfection degree of multi-walled carbon nanotubes: Correlations between thermal kinetic analysis and micro-Raman spectroscopy, *J. Raman Spectrosc.* 42 (2011) 593–602. doi:10.1002/jrs.2766.
- [206] D.S. Knight, W.B. White, Characterization of diamond films by Raman spectroscopy, *J. Mater. Res.* 4 (1989) 385–393. doi:10.1557/JMR.1989.0385.
- [207] A. Ferrari, J. Robertson, Interpretation of Raman spectra of disordered and amorphous carbon, *Phys. Rev. B.* 61 (2000) 14095–14107. doi:10.1103/PhysRevB.61.14095.
- [208] L. Tzounis, S. Debnath, S. Rooj, D. Fischer, E. Mäder, A. Das, M. Stamm, G. Heinrich, High performance natural rubber composites with a hierarchical reinforcement structure of carbon nanotube modified natural fibers, *Mater. Des.* 58 (2014) 1–11. doi:10.1016/j.matdes.2014.01.071.
- [209] T.A. Langston, R.D. Granata, Influence of nitric acid treatment time on the mechanical and surface properties of high-strength carbon fibers, *J. Compos. Mater.* 0 (2012) 1–18. doi:10.1177/0021998312470471.
- [210] J.L. Thomason, On the application of Weibull analysis to experimentally determined single fibre strength distributions, *Compos. Sci. Technol.* 77 (2013) 74–80. doi:10.1016/j.compscitech.2013.01.009.
- [211] O. Frank, G. Tsoukleri, I. Riaz, K. Papagelis, J. Parthenios, A.C. Ferrari, A.K. Geim, K.S. Novoselov, C. Galiotis, Development of a universal stress sensor for graphene and carbon fibres., *Nat. Commun.* 2 (2011) 255. doi:10.1038/ncomms1247.
- [212] A.H. Barber, Q. Zhao, H.D. Wagner, C.A. Baillie, Characterization of E-glass-

-
- polypropylene interfaces using carbon nanotubes as strain sensors, *Compos. Sci. Technol.* 64 (2004) 1915–1919. doi:10.1016/j.compscitech.2004.02.004.
- [213] Q. Zhao, M.D. Frogley, H.D. Wagner, The use of carbon nanotubes to sense matrix stresses around a single glass fiber, *Compos. Sci. Technol.* 61 (2001) 2139–2143. doi:10.1016/S0266-3538(01)00166-X.
- [214] P. Ladevèze, D. Néron, H. Bainier, *The Structural Integrity of Carbon Fiber Composites*, 2017. doi:10.1007/978-3-319-46120-5.
- [215] W. Szmyt, S. Vogel, A. Diaz, M. Holler, J. Gobrecht, M. Calame, C. Dransfeld, Protective effect of ultrathin alumina film against diffusion of iron into carbon fiber during growth of carbon nanotubes for hierarchical composites investigated by ptychographic X-ray computed tomography, *Carbon N. Y.* 115 (2017) 347–362. doi:10.1016/j.carbon.2016.12.085.
- [216] A. Paipetis, C. Galiotis, Modelling the stress-transfer efficiency of carbon – epoxy interfaces, *Proc. R. Soc. A.* (2001) 1555–1577. doi:10.1098/rspa.2000.0774.
- [217] C. Galiotis, D.N. Batchelder, Strain dependences of the first-and second-order Raman spectra of carbon fibres, *J. Mater. Sci. Lett.* 7 (1988) 545–547. <http://www.springerlink.com/index/P214J7X71116787H.pdf>.
- [218] I. Robinson, M. Zakikhani, R. Day, Strain dependence of the Raman frequencies for different types of carbon fibres, *J. Mater.* 6 (1987) 1212–1214. doi:10.1007/BF01729187.
- [219] S.Y. Jin, R.J. Young, S.J. Eichhorn, Controlling and mapping interfacial stress transfer in fragmented hybrid carbon fibre-carbon nanotube composites, *Compos. Sci. Technol.* 100 (2014) 121–127. doi:10.1016/j.compscitech.2014.05.034.
- [220] A. Paipetis, C. Galiotis, Y.C. Liu, J.A. Nairn, Stress Transfer from the Matrix to the Fibre in a Fragmentation Test: Raman Experiments and Analytical Modeling, *J. Compos. Mater.* 33 (1999) 377–399. doi:10.1177/002199839903300404.
- [221] V.G. Hadjiev, G.L. Warren, L. Sun, D.C. Davis, D.C. Lagoudas, H.J. Sue, Raman microscopy of residual strains in carbon na[1] V.G. Hadjiev, G.L. Warren, L. Sun, D.C. Davis, D.C. Lagoudas, H.J. Sue, Raman microscopy of residual strains in carbon nanotube/epoxy composites, *Carbon N. Y.* 48 (2010) 1750–1756., *Carbon N.*

- Y. 48 (2010) 1750–1756. doi:10.1016/j.carbon.2010.01.018.
- [222] C.A. Schneider, W.S. Rasband, K.W. Eliceiri, NIH Image to ImageJ: 25 years of image analysis, *Nat. Methods*. 9 (2012) 671. <https://doi.org/10.1038/nmeth.2089>.
- [223] J.-K. Kim, Y.-W. Mai, Y.-W. Mai, *Engineered Interfaces in Fiber Reinforced Composites*, 1998. doi:10.1016/B978-0-08-042695-2.X5000-3.
- [224] A. Kelly, W.R. Tyson, Tensile properties of fibre-reinforced metals: Copper/tungsten and copper/molybdenum, *J. Mech. Phys. Solids*. 13 (1965) 329–350. doi:10.1016/0022-5096(65)90035-9.
- [225] A. Paipetis, *A study of Carbon Fibre / Epoxy Interface using Remote*, Queen Mary and Westfield College, University of London, 1997.
- [226] H. Vašková, V. Křesálek, Quasi real-time monitoring of epoxy resin crosslinking via Raman microscopy, *Int. J. Math. Model. Methods Appl. Sci*. 5 (2011) 1197–1204.
- [227] F.N. Alhabill, R. Ayoob, T. Andritsch, A.S. Vaughan, Effect of resin/hardener stoichiometry on electrical behavior of epoxy networks, *IEEE Trans. Dielectr. Electr. Insul*. 24 (2017) 3739–3749. doi:10.1109/TDEI.2017.006828.
- [228] A. Paipetis, C. Galiotis, Effect of fibre sizing on the stress transfer efficiency in carbon/epoxy model composites, *Compos. Part A Appl. Sci. Manuf*. 27 (1996) 755–767. doi:10.1016/1359-835X(96)00054-1.
- [229] R.S. Ruoff, D. Qian, W.K. Liu, Mechanical properties of carbon nanotubes: Theoretical predictions and experimental measurements, *Comptes Rendus Phys*. 4 (2003) 993–1008. doi:10.1016/j.crhy.2003.08.001.
- [230] M.-F. Yu, *Fundamental Mechanical Properties of Carbon Nanotubes: Current Understanding and the Related Experimental Studies*, *J. Eng. Mater. Technol*. 126 (2004) 271–278. doi:10.1115/1.1755245.
- [231] A.S. for T. and Materials, *ASTM D2344 Standard Test Method for Short-Beam Strength of Polymer Matrix Composite Materials and Their Laminates*, ASTM, 100 Barr Harb. Drive, West Conshohocken, PA 19428-2959, United States. (2000). doi:10.1520/D2344.

Appendix

Additional details on the vibrational spectroscopies (IR and Raman)

A.1 Quantification of the functionalization degree of CNTs through FT-IR

The FT-IR spectra of the CNTs (Figure 28 of the main text) were further processed in order to quantify the relative changes induced in each sample due to the oxidation process. The processing consisted of a normalization of the intensity of each spectrum by dividing with the intensity value at the lowest measured wavenumber. Then, a linear baseline was subtracted from each dataset, and subsequently, a fitting procedure was applied using a single Gaussian distribution for each of the encountered vibrational modes. No constraints were applied to the characteristics of the distributions (Intensity, Area, FWHM).

The fitting procedure for a characteristic spectrum is presented in Figure A1.

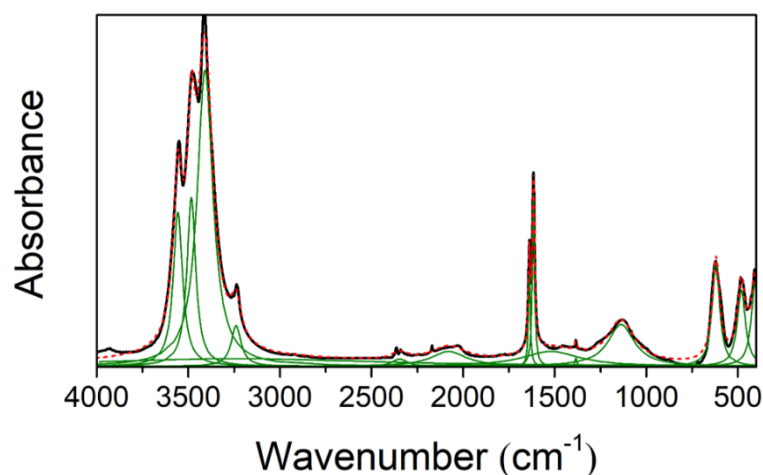


Figure A 1. The fitted spectrum of the as received CNTs. Underlying black line: raw data, green lines: fitting distributions for each vibrational mode, red line: cumulative fitting curve.

A.2 Evaluation of oxidized CFs via FTIR spectroscopy

Both the unsized and the sized CFs were evaluated via FTIR measurements before and after their oxidation in nitric acid for 30, 60 or 90 min. The spectra of the as-received CF/S and CF/UNS did not present any substantial differences (Figure A2). A literature-based assignment for those peaks reveals that the 3435 cm^{-1} and the 1634 cm^{-1} vibrational modes can be attributed to oxygen-hydrogen bonds in water, while the absorption at 1716 cm^{-1} was assigned to carbonyl groups [1]. Regarding the rest of the vibrations which presented lower absorbance intensities, the 1510 cm^{-1} and the 1371 cm^{-1} vibrations were due to the C-C

stretching motions [2], the 1438 cm^{-1} emerged due to the combination of the C-O stretching and O-H deformation vibrations in carboxyl moieties [3] and the 1229 cm^{-1} and the 1120 cm^{-1} bands were assigned to the stretching of the C-O bond of ether moieties or the same bond stretching vibration in carboxylic groups [4].

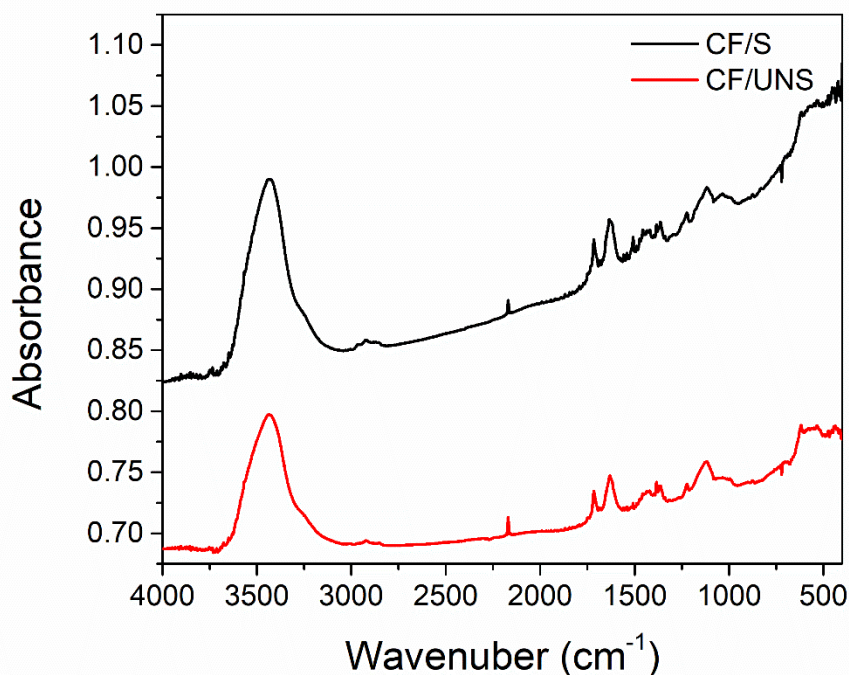


Figure A 2. FT-IR spectra of the sized (black line) and unsized (red line) as received CFs.

Additionally, all the spectra, including those from the oxidized CFs, were baseline subtracted using a 5th order polynomial baseline in an attempt to find any possible differences in the intensities of the encountered vibrational modes (Figures A3 and A4). The most prominent difference among the as received and the oxidized CFs, in both the CF/S and the CF/UNS, was the amount of water present in the sample, which although heated for 12 hours before the measurements was not eliminated entirely. Another small difference regarding the CF/UN_30 was found in the 1120 cm^{-1} vibration which might imply that more ether moieties carboxylic groups were present in those CFs.

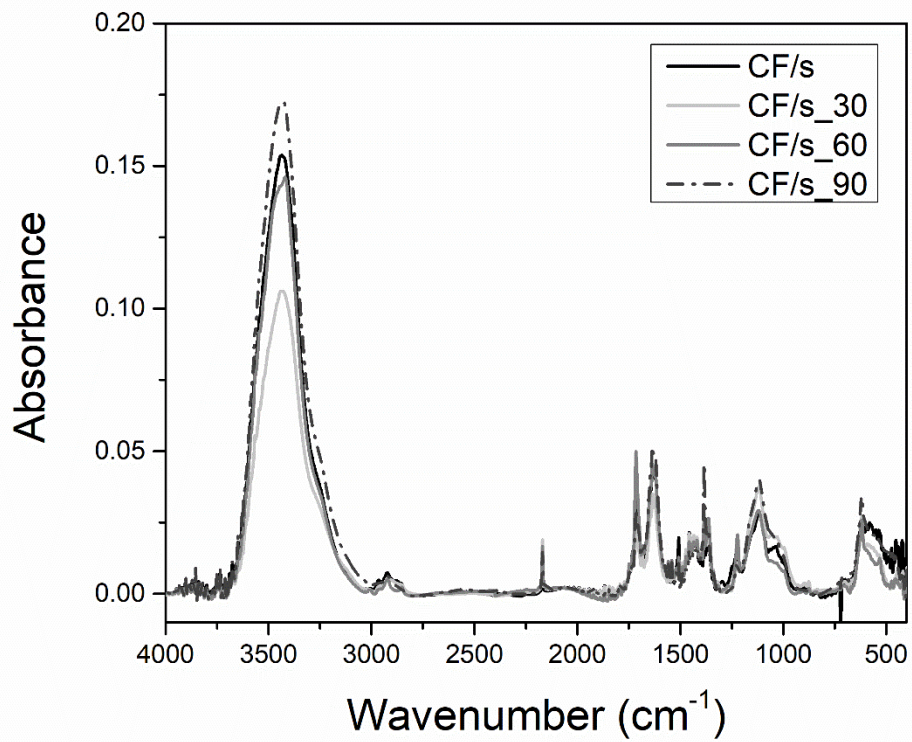


Figure A 3. FT-IR spectra of the as received and the oxidized sized CFs.

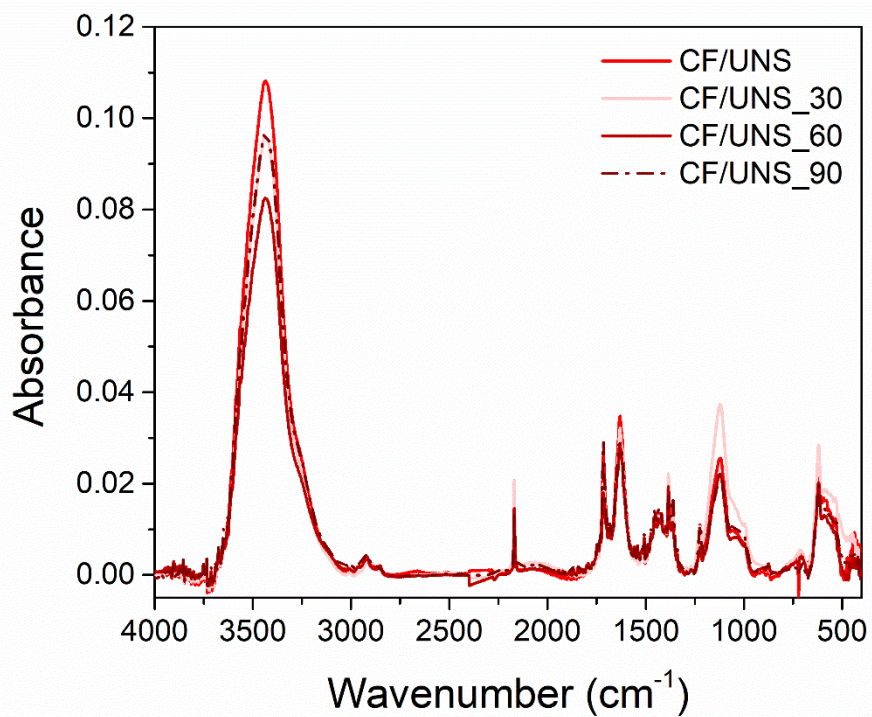


Figure A 4. FT-IR spectra of the as received and the oxidized unsized CFs.

A.3 Details about Raman vibrational spectroscopy studies

Raman spectroscopy is a non-destructive characterization method which can provide invaluable information about the structural properties of carbon-based materials. This technique has been used in several instances throughout this thesis, and thus it was considered vital to include a detailed analysis of the origins of each of the vibrational modes encountered into the spectrum of carbonaceous materials. Moreover, this section includes additional details for the experimental procedures followed in each case for the treatment of the raw Raman spectra.

A.3.1 Origins of the Raman active vibrational modes in graphitic substances

The most prominent band of the spectrum of carbon located at about 1580 cm^{-1} is the Graphitic or G vibration. The G band is common in well-ordered graphitic structures consisting of sp^2 carbon atoms and corresponds to the in-plane lattice vibrations of the plane graphitic crystal. The aforementioned band is the E_{2g} vibrational Raman active mode for graphite [5]. The other two strongly interrelated bands in the first order spectrum of the CNTs are the disorder induced (D band) and the D' band appearing at about 1350 cm^{-1} and 1620 cm^{-1} , respectively. Both these bands were active by double resonance. D band, as an intervalley process, came from the transverse optical phonons around the Brillouin zone boundary K [6]. D' band usually appeared as a shoulder of the G band representing an intravalley process, connecting two points belonging to the same Dirac cone (representing electronic dispersion) around K [7]. Both these defect-induced bands were generally associated with lattice defects and finite crystal size which induce a breaking of the 2D translational symmetry [8]. Finally, the 2D or G' band dominates the second-order spectrum of carbon at about 2700 cm^{-1} . Another double resonance process, the second order 2D or G' band, was found at approximately 2700 cm^{-1} . This band was characterized as the first overtone of the D band (2D) [9], but as it did not require disorder to be activated, it was instead a symmetry-allowed band (G') [10].

For all the Raman measurements in each of the following studies a batch fitting procedure was used, and then the goodness of fitting was evaluated by checking the coefficient of

determination (R^2) value for each individual spectrum. Only spectra with R^2 higher than 0.95 were considered for the average values in each case.

A.3.2 Evaluation of the oxidized CFs and CNTs

The Raman spectra of the as received and oxidized CFs and CNTs were further treated in order to evaluate the characteristics (see below) of each vibrational mode. A linear baseline subtraction adjacent to the minimum intensity was initially applied in each spectrum. Then, a fitting procedure using Lorentzian (D, G and 2D vibrational modes) and Gaussian (D' vibrational mode) distributions was implemented. No other constraints applied during the integration for the evaluation of the parameters of interest. These parameters were the Position [cm^{-1}], the Intensity [a.u.] and the Full Width at Half Maximum (FWHM), or in other words the width of each distribution at the half of its maximum intensity [cm^{-1}].

A.3.3 Evaluation of the hierarchical CF-CNTs

Additionally, several other bands existed in the spectra of the produced CNTs. Not all of these features were easily noticed in the normalized data of Figure 29 until the spectra were fitted by Lorentzian bands, as presented in Figure A 5 and Figure A 6. All bands were normalized with respect to the G band, which is a material property.

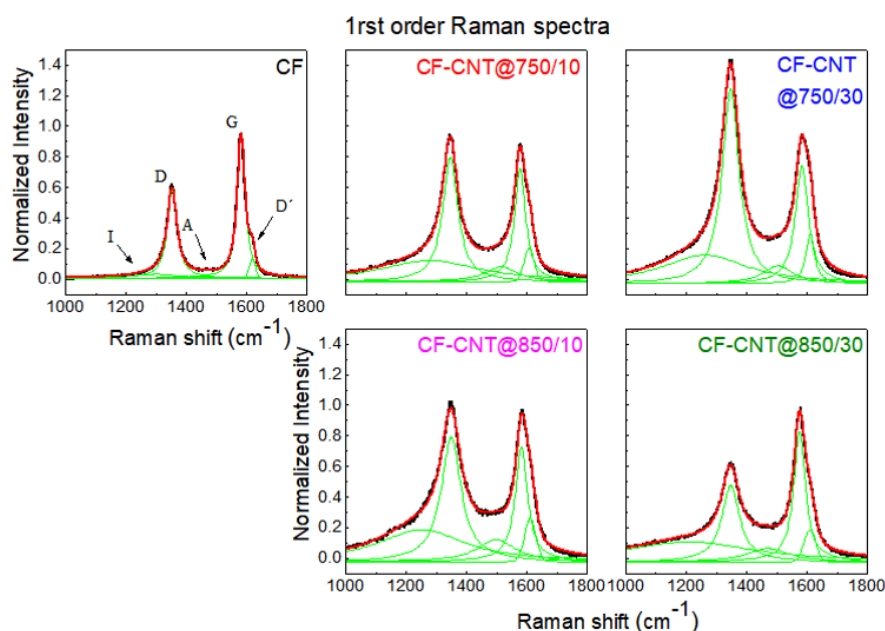


Figure A 5. First order Raman spectra of CF and CF-CNT from different growth conditions. The green curves are the fitting curves of each Raman band, and the red curve represents the cumulative fitting curve.

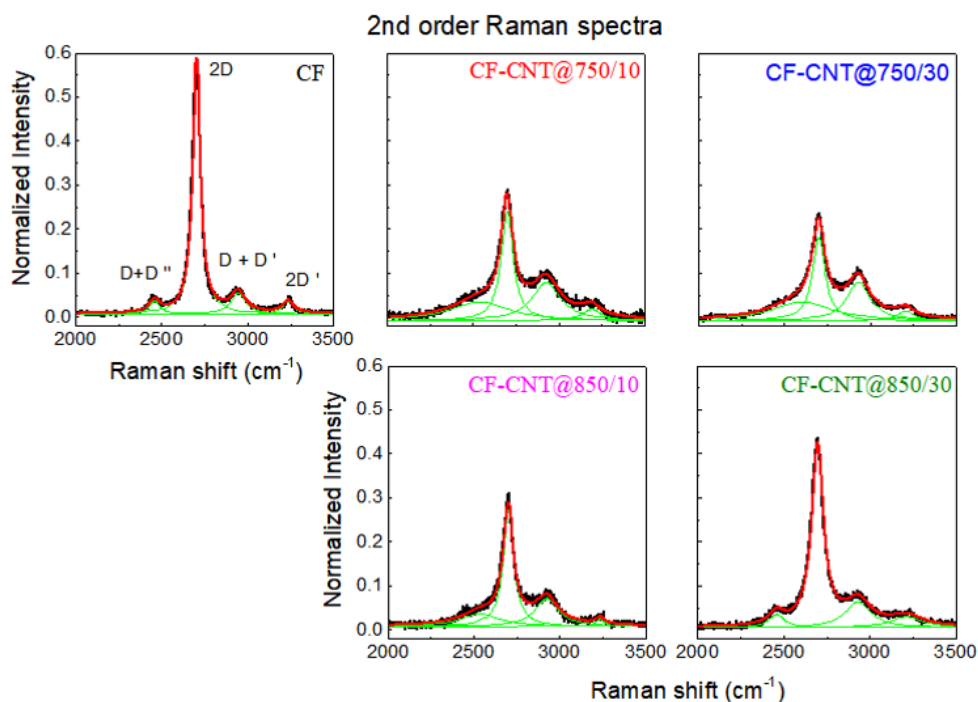


Figure A 6. Second-order Raman spectra of CF and CF-CNT from different growth conditions. The green curves are the fitting curves of each Raman band. The red curve represents the cumulative fitting curve.

These additional bands included the I band ($1200\text{--}1300\text{ cm}^{-1}$) and A or D'' band ($1465\text{--}1530\text{ cm}^{-1}$) in the first order region of the spectra, and the $D+D''$ band ($2450\text{--}2600\text{ cm}^{-1}$), the $D+D'$ band ($2920\text{--}2945\text{ cm}^{-1}$) and the $2D'$ band ($3190\text{--}3240\text{ cm}^{-1}$) in the second order region of the spectra. The I band was attributed to impurity ions or $C=C$, and $C-C$ stretching modes of polyene like structures and the A band was assigned to amorphous carbon. The $D + D''$ and $D + D'$ were combination bands as implied by their names, and the $2D'$ band was an overtone of D' band. The fitted parameters of the acquired and treated spectra of interest for this study were the I_x and A_x which stand for the intensity and the area of the utilized distributions describing each encountered peak. It has to be noted at this point that, all measurements presented below from CF-CNTs come solely from the CNTs and not the underlying fibre. This statement is supported by the fact that the penetration depth of Raman measurements in graphite as reported by Tuinstra and Koenig, as early as 1970, is only 50 nm due to the graphite high extinction coefficient [11].

A.3.4 Quantification of strain induced Raman sensitivity

For the strain sensing measurements, the response of the 2D peak, ($\sim 2700 \text{ cm}^{-1}$), of the reference CFs and the CNTs from the hierarchical CF-CNTs to externally applied strain was monitored with an acquisition time of 20 sec. Individual CFs and CF-CNTs, with gauge lengths of 15 mm, were bonded to the jaws of a custom designed straining rig ($\pm 1 \mu\text{m}$ precision), with their longitudinal axes aligned parallel to the stretching direction to $\pm 5^\circ$. The CFs were tensioned at distinct levels of strain, and the response of the 2D graphitic vibrational mode was monitored. Five Raman spectra were acquired at each straining level.

In order to obtain accurate frequency position determination, spectral analysis was performed which involved a linear baseline subtraction and the fitting of the 2D vibrational mode with Lorentzian distributions. Frequent calibration values of unstressed fibres in air, ν_{ref} , were obtained for the 2D vibrational mode and used as a reference for zero stress. Subsequently, these values, ν_{ref} , were subtracted from the measured Raman shift values, ν , in order to calculate the relative shift of the 2D band, $\nu - \nu_{ref}$, at each strain level.

Literature

- [1] Osswald S, Havel M, Gogotsi Y. Monitoring oxidation of multiwalled carbon nanotubes by Raman spectroscopy. *J Raman Spectrosc* 2007;38:728–36. doi:10.1002/jrs.
- [2] Jiang JJ, Liu F, Deng C, Fang LC, Li DJ. Influence of deposited CNTs on the surface of carbon fiber by ultrasonically assisted electrophoretic deposition. *IOP Conf Ser Mater Sci Eng* 2015;87:012103–7. doi:10.1088/1757-899X/87/1/012103.
- [3] Socrates G. Infrared and Raman characteristic group frequencies. 2004. doi:10.1002/jrs.1238.
- [4] Wu Z, Meng L, Liu L, Jiang Z, Xing L, Jiang D, et al. Chemically grafting carbon nanotubes onto carbon fibers by poly(acryloyl chloride) for enhancing interfacial strength in carbon fiber/unsaturated polyester composites. *Fibers Polym* 2014;15:659–63. doi:10.1007/s12221-014-0659-0.
- [5] Paipetis AS. Stress induced changes in the Raman Spectrum of Carbon Nanostructures and Their Composites. In: Paipetis A, Kostopoulos V, editors. *Solid*

- Mech. Its Appl., vol. 188, Springer Netherlands; 2013, p. 185–217. doi:10.1007/978-94-007-4246-8.
- [6] Martins Ferreira EH, Moutinho MVO, Stavale F, Lucchese MM, Capaz RB, Achete CA, et al. Evolution of the Raman spectra from single-, few-, and many-layer graphene with increasing disorder. *Phys Rev B - Condens Matter Mater Phys* 2010;82. doi:10.1103/PhysRevB.82.125429.
- [7] Ferrari AC, Basko DM. Raman spectroscopy as a versatile tool for studying the properties of graphene. *Nat Nanotechnol* 2013;8:235–46. doi:DOI 10.1038/nnano.2013.46.
- [8] Velasquez M, Batiot-Dupeyrat C, Gallego J, Santamaria A. Chemical and morphological characterization of multi-walled-carbon nanotubes synthesized by carbon deposition from an ethanol-glycerol blend. *Diam Relat Mater* 2014;50:38–48. doi:10.1016/j.diamond.2014.08.015.
- [9] Bokobza L, Bruneel JL, Couzi M. Raman spectroscopy as a tool for the analysis of carbon-based materials (highly oriented pyrolytic graphite, multilayer graphene and multiwall carbon nanotubes) and of some of their elastomeric composites. *Vib Spectrosc* 2014;74:57–63. doi:10.1016/j.vibspec.2014.07.009.
- [10] Dresselhaus MS, Dresselhaus G, Hofmann M. Raman spectroscopy as a probe of graphene and carbon nanotubes. *Philos Trans R Soc A* 2008;366:231–6. doi:10.1098/rsta.2007.2155.
- [11] Tuinstra F, Koenig L. Raman Spectrum of Graphite. *J Chem Phys* 1970;53:1126–30. doi:10.1063/1.1674108.

